Targeting glial cells as a therapeutic approach for the treatment of chemotherapy-induced neuropathic pain

Sheila Piedra Barrull

DOCTORAL THESIS UPF / 2021

Thesis director:

Dr. Miguel Ángel Martín Sánchez

Departament de ciències experimentals i de la salut

Universitat Pompeu Fabra Barcelona

Abstract

Chemotherapy-induced peripheral neuropathy (CIPN) is the most common adverse effect of many first-line antineoplastic agents, which negatively affects the quality of life and clinical outcome. Current clinical management of this condition provides unsatisfactory efficacy and unwanted side effects, highlighting the urgent need for the identification and development of novel effective therapeutic strategies that can prevent or mitigate this debilitating disease. Accumulating evidence have revealed that glial cells are powerful contributors to pathological pain of different etiologies; however, relatively little is known about their role in CIPN. In the present Thesis we have first characterized the involvement of glial cells, especially astrocytes, in the pathophysiology of CIPN by using a mouse model of vincristine-induced neuropathic pain together with a cell-specific transcriptomic approach. Bioinformatic analysis revealed predominant effects on genes associated with important astrocyte homeostatic functions after vincristine treatment, producing a strong downregulation indicating widespread astrocyte dysfunction. Alternatively, we have demonstrated the analgesic efficacy of a novel compound antagonist of sigma-1 receptors (σ1R) on this disease model and described its modulatory role in astrocytes. Overall, we provided unique insights to advance in the understanding of the complexity of CIPN and identified astrocytes as potential therapeutic targets for a better management of this pathology.

Resumen

La neuropatía periférica inducida por quimioterapia (NIQ) es el efecto adverso más común de muchos antineoplásicos de primera línea, afectando negativamente la calidad de vida y los resultados clínicos. Los tratamientos actuales proporcionan resultados insatisfactorios y producen efectos secundarios, lo que pone de relieve la necesidad de identificar y desarrollar nuevas estrategias terapéuticas para prevenir o mitigar esta enfermedad tan debilitante. Existen cada vez más pruebas de la contribución de las células gliales en el dolor patológico de diferente etiología; sin embargo, se sabe relativamente poco sobre su papel en la NIQ. En la presente tesis hemos caracterizado por primera vez la implicación de las células gliales, especialmente de los astrocitos, en la fisiopatología de la NIQ. Para ello, hemos utilizado un modelo de ratón de dolor neuropático inducido por vincristina combinado con un enfoque transcriptómico específico de tipo celular. El análisis de los datos reveló efectos predominantes en genes asociados con importantes funciones homeostáticas de los astrocitos tras el tratamiento con vincristina, concretamente una baja expresión, indicando una disfunción generalizada de los astrocitos. Por otra parte, hemos demostrado la eficacia analgésica de un nuevo compuesto antagonista de los receptores sigma-1 (σ1R) en este modelo de enfermedad, y hemos descrito su función moduladora en los astrocitos. En general, hemos aportado una visión única para avanzar en la comprensión de la complejidad de la NIQ e identificado los astrocitos como potenciales dianas terapéuticas para un mejor tratamiento de esta patología.

Abbreviations

ACC	Anterior cingulate cortex
ALDH1L1	Aldehyde dehydrogenase 1 light chain 1
AMPA	α-amino-3-hydroxy-5-methyl-4-isoxazeloproprionic acid receptor
AQP4	Aquaporin 4
BDNF	Brain-derived neurotrophic factor
BiP	Binding immunoglobulin protein
CIPN	Chemotherapy-induced peripheral neuropathy
CNS	central nervous system
CX	Connexins
CX3CR1	CX3C chemokine receptor 1 or fractalkine (CX3CL1) receptor
CXCL1	Chemokine (C-X-C motif) ligand 1 or fractalkine
DAMPs	Endogenous damage-associated molecular patterns
DE	Differential gene expression
DEG	Differentially expressed genes
DRG	Dorsal root ganglia
EMPs	Erythromyeloid progenitors
ER	Endoplasmic reticulum
FACS	Fluorescence-activated cell sorting
FC	Fold-change
GABA	Gamma-aminobutyric acid
GFAP	Glial fibrillary acidic protein
GFP	Green fluorescent protein
GSEA	Gene Set Enrichment Analysis
HA	Hemagglutinin
Hb	Hemoglobin
HPMC	Hydroxypropylmethyl cellulose

IASP	International Association for the Study of Pain
IFN-γ	Interferon-γ
IGF-1	Insulin-like growth factor 1
IP	Immunoprecipitation
IP_3	Inositol-1,4,5-trisphosphate
IPC	Intermediate progenitor cell
LPS	Lipopolysaccharides
MAM	Mitochondrion-associated endoplasmic reticulum membranes
mDNA	Mitochondrial DNA
mGluR	Glutamate metabotropic receptors
MHC	Major histocompatibility complex
NeuPSIG	Neuropathic Pain Special Interest group
NF-κβ	Nuclear factor-kappa B
NMDA	N-methyl-D-aspartate
NO	Nitric oxide
OPC	Oligodendrocyte progenitor cells
PAG	Periaqueductal gray
PAMPs	Pathogen-associated molecular patterns
PCA	Principal component analysis
PFC	Prefrontal cortex
PGE	Prostaglandins
PNS	Peripheral nervous system
RG	Radial glia
RNA-seq	RNA sequencing
ROS	Reactive oxygen species
RPL22	Ribosomal protein L22
RVM	Rostroventral medulla

SNRIs	Serotonin-norepinephrine reuptake inhibitors ()
SS	Somatosensory cortex
SSRIs	Serotonin-specific reuptake inhibitors
SVZ	Subventricular zone
TAM	Tamoxifen
TCAs	Tricyclic antidepressants
TLR4	Toll-like receptor 4
TNF-α	Tumor necrosis factor-α
TRAP	Translating ribosome affinity purification
TRPV1	Transient receptor potential vanilloid type-1
VCR	Vincristine
σ1R	Sigma-1 receptor

INDEX

INTRODUCTION

1 Glial cells

Glial cells, also called glia or neuroglia, represent a diverse population of non-neuronal cells in the nervous systems. In 1846, Rudolph Virchow first introduced the concept of neuroglia, which he referred to as an in-between tissue into "which the nervous system elements are embedded" (Virchow, 1856). Following Virchow's observations, Camillo Golgi first demonstrated that glia represents a cellular population distinct from nerve cells (Golgi, 1870). Using the silver-chromate staining technique (*reazione nera*), he described a remarkable diversity of glial cells in the brain, reported glial networks, and identified glial endfeet plastering blood vessels (Golgi, 1903) **(Figure 1).** Other important researchers such as Santiago Ramón y Cajal or Pío del Río Hortega continued to characterize the cellular nature of glial cells and their functional role in the brain. (Ramón y Cajal, 1895; Del Rio-Hortega, 1919).

Neuroglia is classified as peripheral or central depending on whether they are located in the peripheral or central nervous system, respectively. **Peripheral glial cells** originate from the neural crest and include Schwann cells, satellite cells, olfactory ensheathing cells, and enteric glia. By contrast, **central glia** is subdivided into macroglia, which have a neuroepithelial origin and include astrocytes, oligodendrocytes, and oligodendrocyte progenitor cells (OPC), also known as NG2 glia, and microglia, which originates from the mesoderm. In terms of numbers, at the level of the central nervous system (CNS), the most abundant glial cells are oligodendrocytes and NG2 cells combined (40–60%), followed by astrocytes (20-40%), and microglia being the least abundant (less than 10%), which on a whole represent about half of the volume of the human brain, although this volumetric ration not only varies between animal

species but also between the regions of a single brain (Herculano-Houzel, 2014; Tay *et al.*, 2019).

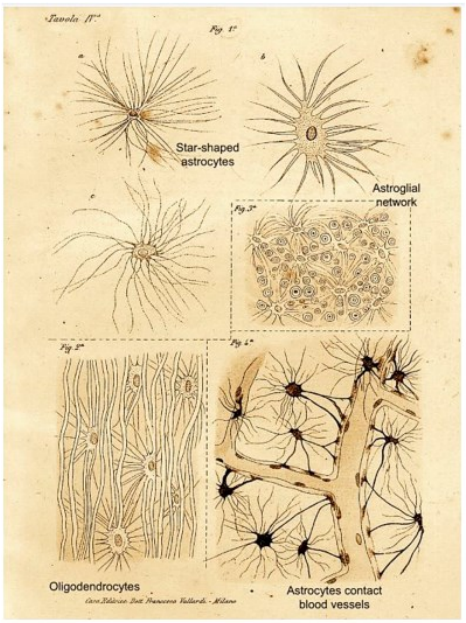

Figure 1. Neuroglial cells stained by the silver-chromate technique and drawn by Camillo Golgi. Top panels show individual star-shaped astrocytes and astroglial networks. At the bottom right, astrocytes forming numerous contacts (the end feet) with brain capillaries are drawn. The bottom left panel shows the drawing of white matter with multiple cellular processes oriented parallel to axons, which most likely represent oligodendrocytes. Extracted from (Golgi, 1903).

In terms of their basic functional roles, neuroglia can be defined as **homeostatic** and **defensive** cells of the nervous system (Verkhratsky and Butt, 2013). In this sense, neuroglia are the supportive cells of the nervous system, keeping it in a functional state. This capability underlies its fundamental role in neuropathology, which is generally defined as a homeostatic failure of the nervous system. On one hand, environmental stress and pathological insults trigger glial homeostatic response and reactivity. On the other hand, glial asthenia or atrophy, which is seen in many neurological conditions, favors the development of the disease due

to impaired homeostatic and defensive capabilities of the glia (Tay *et al.*, 2019). Apart from these essential functions, recent studies have shown an important role of neuroglial populations, especially astrocytes, in regulating complex neuronal processes including cognitive functions such as memory and learning (Gao *et al.*, 2016; Adamsky *et al.*, 2018; Kol *et al.*, 2020), or emotional states (Cao *et al.*, 2013).

Although evidences suggest that oligodendrocytes also play an important role in many neurological disorders, this thesis will focus largely on the characterization of **astrocytes** and **microglia** in order to better understand their activities in the healthy and disturbed nervous systems.

1.1 Microglia

1.1.1 Overview of microglial cells

Microglial cells are the resident innate immune cells of the CNS, where they represent around 10% of adult CNS cells in rodents and between 0.5% to 16.6% in humans, with high variability depending on the brain area (Lawson *et al.*, 1990; Herculano-Houzel, 2014). They are distributed over the entire CNS parenchyma with variable density across distinct CNS regions, ranging from 5% in the cortex to 12% in the substantia nigra (Lawson *et al.*, 1990), and being more abundant in gray matter than in white matter (Kofler and Wiley, 2011).

Microglia are considered tissue-resident macrophage-like cells of the CNS that arise from early colonization of mesodermal progenitors of the embryonic yolk sac **(Figure 2)** (Alliot *et al.*, 1999). Precisely, microglial cells originate from immature erythromyeloid progenitors (EMPs), that is, primitive hematopoietic stem cells that migrate into the neuroectoderm in a single colonization wave around embryonic day 9.5 (E9.5, in mice) and

differentiates into matured microglia through a stepwise developmental program (Ginhoux *et al.*, 2010; Matcovitch-Natan *et al.*, 2016). Therefore, unlike the other CNS glial cells with a neuroepithelial lineage, microglial cells have a myeloid origin and derive from mesodermal progenitors. By the time of birth, an important number of microglial cells are present in the CNS, forming a dense network along the parenchyma. A stabilized number of mature microglia is maintained throughout life via a tightly controlled process of self-renewal (Bruttger *et al.*, 2015). Furthermore, in some circumstances involving microglial loss, depleted microglia can be replaced with peripherally derived macrophages that maintain their own unique molecular identity and have distinct functional roles in the progression or resolution of neurological diseases **(Figure 2).**

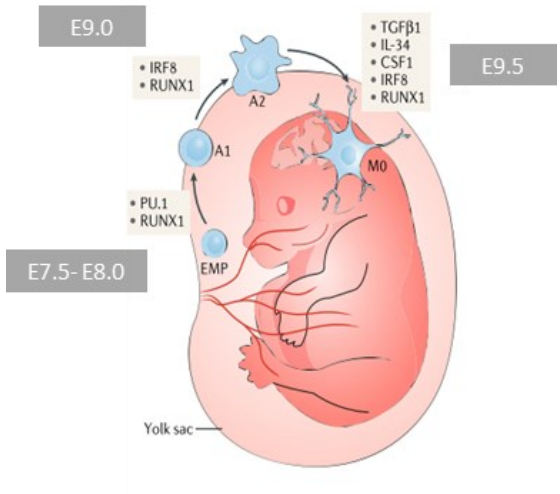

Figure 2. Key features of microglial mammalian development. Microglial derive from uncommitted erythromyeloid progenitors (EMP) originated from primitive hematopoiesis at embryonic days 7.5-8 (E7.5-E8.0). Specific transcriptional regulation drives the differentiation of these cells through following immature states (A1 and A2) and its migration to populate the CNS parenchyma around embryonic day 9.5 (E9.5), where it finally differentiates into mature (homeostatic) microglia (M0). Once established in the CNS, they sustain the microglial pool via local clonal expansion throughout life. Adapted from (Butovsky and Weiner, 2018).

1.1.2 Physiological functions

As resident immune cells of the CNS, microglia are pivotal players in immune surveillance by acting as the first line of defense in the CNS. Beyond this well-accepted function, microglia also play critical roles during the development of CNS and for the maintenance of its homeostasis throughout all life (Butovsky and Weiner, 2018; Prinz *et al.*, 2019) **(Figure 3).**

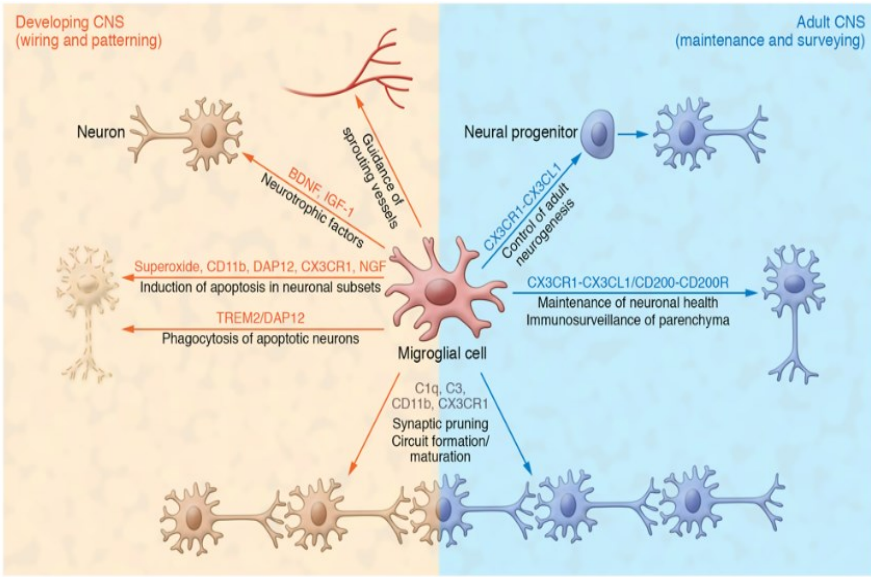

Figure 3. Homeostatic function of microglia in the developing and adult CNS. In addition to their task as resident immune cells in the CNS, microglia display a variety of other functions in maintaining tissue homeostasis. Microglia modulate wiring and patterning in the developing CNS by regulating apoptosis of neuronal subpopulations, releasing neurotrophic factors, and guiding sprouting vessels in the parenchyma. They are also crucial for circuit formation and neuronal network maturation, as well as for regulating adult neurogenesis and maintaining neuronal health in the adult CNS. Extracted from (Kierdorf and Prinz, 2017).

In the **developing CNS**, microglial cells are critically involved in the modulation of the neuronal architecture and connectivity of the CNS

(Figure 3). In this context, microglia act as **regulators of neuronal cell number** by actively phagocytosing progenitor cells and inducing programmed cell death via release of superoxide ion or nerve growth factor (NGF) (Dekkers and Barde, 2013). They also support and promote neuronal survival in a region-specific manner via the secretion of different neurotrophic factors. For instance, the microglial release of insulin-like growth factor 1 (IGF-1) is critical for the survival of cortical layer V neurons in the somatosensory cortex during the first postnatal week (Ueno *et al.*, 2013). Similarly, subsets of microglial cells also regulate oligodendrocyte precursors differentiation and myelinization via the release of IGF-1 (Wlodarczyk *et al.*, 2017). Microglia are also involved in **synaptic development and reorganization**, with a well-described role as mediators in synaptic and axonal pruning during the development and postnatal phase by phagocytizing inappropriate presynaptic inputs. This function relies on activity-dependent and complement tagging (C1q, C3), as well as on the CX3CR1-CX3CL1 (fractalkine) pathway, which altogether is closely regulated by neuronal activity and the contribution of astrocytes (Schafer *et al.*, 2012). In this line, recent studies have revealed that microglia are required for the promotion and proper maturation of excitatory synapses in the neocortex, either by promoting the formation of spines or regulating synaptic transmission through establishing direct contact with pre- and post- synaptic structures (Wake *et al.*, 2009). In parallel with their roles in early neuronal development, microglia also play an essential role in **vascular networking** by modulating sprouting vessel tip fusion via secretion of soluble guidance factors in a bidirectional communication manner (Rymo *et al.*, 2011).

In the healthy **adult CNS**, microglial cells present a resting surveillant phenotype characterized by a small soma and highly ramified and long motile branches through which they actively monitor the surroundings to maintain tissue homeostasis and function (Kettenmann et al., 2011; Prinz and Priller, 2014; Kierdorf and Prinz, 2017) **(Figure 3)**. In this regard, microglia play a critical role in maintaining **synaptic plasticity** and regulating synaptic properties, particularly during learning and circuit maturation (Tremblay et al., 2011). In fact, the depletion of microglia at various postnatal stages and early adulthood resulted in a reduction in both synapse elimination and formation during learning, suggesting that microglia retain the ability to regulate learning-induced synapse modification in young adult animals (Parkhurst et al., 2013). Additionally, microglia shape **adult neurogenesis** in the hippocampus and subventricular zone (SVZ) through apoptosis-coupled phagocytosis (Sierra et al., 2010). Neuronal progenitors continuously proliferate in these two areas, but only a few of them become integrated into functional neuronal circuits. These remanent cells upregulate apoptotic markers leading to recognition by microglia for phagocytosis, which is mainly dependent on the expression of the TAM-receptor kinases AXL and MER. Several studies revealed that regulation of adult neurogenesis is mediated by the interaction of microglial CX3CR1 receptor with chemokine fractalkine (CX3CL1), expressed by neurons, which suppresses microglial activation (Bachstetter et al., 2011). Lastly, and concerning its best known and studied function, microglia act as local sentinels of the CNS, playing a pivotal role in **innate immune responses** by detecting disruptions caused by injury, pathology, or aging (Nimmerjahn et al., 2005; Kettenmann et al., 2011). As noted below, upon detection of neurophysiological alterations, microglial cells become activated and move to the site of injury to

efficiently phagocyte pathogens and cell debris, and release proinflammatory mediators to attract and stimulate other cells for the resolution of the damage.

In summary, the growing understanding of the many physiological roles of microglia in both the developing and mature CNS suggests that aberrations in these functions may contribute to disease processes in the CNS, fueling a surge in scientific interest in the role of microglia in disease. In fact, microglia are considered to have significant contributions to some neurodegenerative disorders such as Alzheimer's disease, neuropsychiatric disorders like anxiety and depression, neurodevelopmental diseases such as autism, and ischemia and neuropathic pain (Salter and Stevens, 2017).

1.1.3 Microglial activation process: steps and main features

Under physiological conditions, microglial cells occupy distinct, nonoverlapping territories and display a ramified morphology with motile processes through which they constantly scan the surroundings to detect any insult or disturbance (Del Rio-Hortega, 1919; Kettenmann *et al.*, 2011; Kierdorf and Prinz, 2017). Upon brain injury or inflammatory stimuli, microglia respond through a process of **"activation"** defined by both physical and biochemical changes including a shift in cell shape from a highly branched morphology to an amoeboid-like form, and the production of inflammatory mediators necessary to stimulate other CNS cells and immune cells to resolve the damage. During this process, microglial cells move to the site of pathology following chemotactic gradients (Salter and Stevens, 2017). This transition has been classically simplified into a bimodal linear scheme involving an initial M1 (proinflammatory) state that is shifted to an M2 (immunoregulatory) state

over time (Orihuela *et al.*, 2016). However, beyond this oversimplified conception of reactive microglia, there is a heterogeneous population with different phenotypes and properties rather than a single-cell type that uniformly responds to extrinsic factors. Thus, a diversity of reactive microglial phenotypes is generated depending on the features of the stimulus detected and the environmental factors that produced their activation (Gosselin *et al.*, 2017; Hammond *et al.*, 2019; Masuda *et al.*, 2020a).

Microglial activation processes are tightly controlled by different signals that can either trigger or inhibit the transition of microglial cells from a resting surveillant state to an altered and activated state. The sudden appearance of "On/activating" signals or loss or downregulation of constitutively "Off/calming" inputs may result in activation of microglia (Biber *et al.*, 2007) **(Figure 4).** Multiple **"On/activating" signals** have been described to activate microglial cells, including pathogen-associated molecular patterns (PAMPs) such as bacterial wall lipopolysaccharides (LPS) or bacterial and viral RNA/DNA, and endogenous damage-associated molecular patterns (DAMPs) like intracellular elements released from necrotic cells, among others **(Figure 4).** Other molecules such as interferon-γ (IFN-γ) and tumor necrosis factor-α (TNF-α) released from astrocytes and lymphocytes may also trigger the activation of microglial cells, which then produce pro-inflammatory cytokines through transcriptional activation mediated by nuclear factor kappa B (NF-κβ) (Kettenmann *et al.*, 2011). In addition, injured neurons and astrocytes release ATP and UTP that stimulate the purinergic receptors expressed on microglial cells, predominantly the P2X ionotropic receptors P2X4 and P2X7, and the P2Y metabotropic receptors P2Y2, P2Y6 and P2Y12. These receptors are important for the role of microglia in surveillance, synaptic

plasticity and response to injury (Inoue, 2019; Tozaki-Saitoh and Tsuda, 2019). Other important receptors expressed by microglial cells are the α-amino-3-hydroxy-5-methyl-4-isoxazeloproprionic acid receptors (AMPA) and glutamate metabotroic receptors (mGluR), both activated by glutamate, as well as cytokine, adenosine, cholinergic, adrenergic, and dopamine receptors, which altogether may modulate microglial activity and proliferation (Kettenmann *et al.*, 2011).

In contraposition, microglial cells are maintained in a "resting/surveillant" state through interactions with soluble and membrane-bound factors from surrounding cells **(Figure 4).** Some of these **"Off/calming" signals** are the fractalkine (CX3CL1) and glycoprotein CD200, found on the cell surface of healthy neurons, which interact with their respective receptors on microglia (CX3CR1 and CD200R) (Sheridan and Murphy, 2013; Dentesano *et al.*, 2014). Additional ligand-receptor interactions that regulate microglial activation include CD22, HSP60, and CD47 on neurons, binding to CD45, TREM2, and SIRPα, respectively, on microglia (Biber *et al.*, 2007). Neurons also release neurotrophic factors such as brain-derived neurotrophic factor (BDNF) that contribute to the immunosuppressed state of microglia by inhibiting the expression of major histocompatibility complex (MHC) class II genes. Various neurotransmitters and neuropeptides, such as gamma-aminobutyric acid (GABA) and dopamine, also bind to their respective receptors on microglia and suppress the production of proinflammatory cytokines. Additionally, the interaction of the anti-inflammatory cytokines IL-4, IL-10, IL-13, and the transforming growth factor-β (TGF-β) with their respective receptors expressed on microglial cells also reduces the microglial activated phenotype (Kettenmann *et al.*, 2011). Interestingly, reactive microglia (M2 state) can

also release these anti-inflammatory mediators, thus influencing the shift back to a resting homeostatic state.

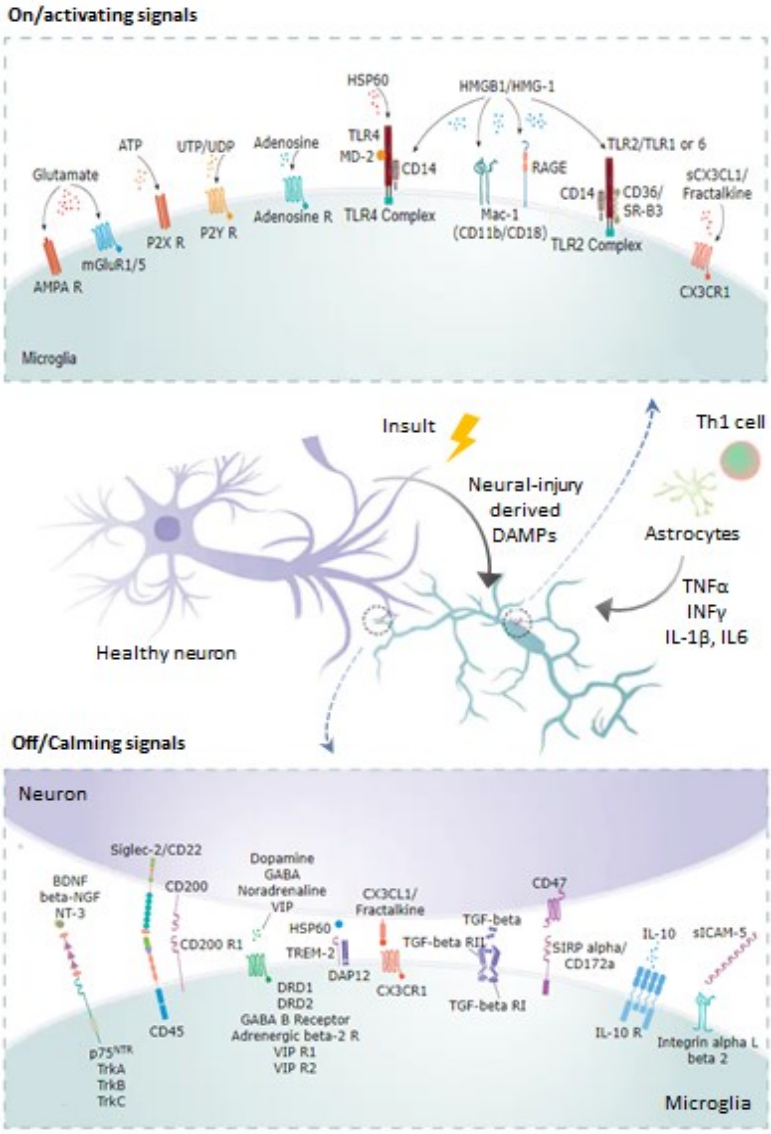

Figure 4. Microglial activation regulatory signals. Microglia activation is initiated through both removal of the inhibitory neuronal signaling (Off signals) and activation of pattern-recognition receptors, such as Toll-like receptors (TLRs) and RAGE, by PAMPs and DAMPs, as well as detection of ATP or UTP, glutamate, and proinflammatory cytokines (On signals) (top panel). Microglia are maintained or shift to a resting/surveillance state through interactions with membrane-bound

factors, such as CD47, CD200, CX3CL1, or soluble molecules like anti-inflammatory cytokines (IL-4, IL-10, IL-13, TGF-β) and neurotrophic factors (BDNF) (bottom panel). Adapted from R&D Systems resources (www.rndsystems.com/pathways).

Microglial activation occurs rapidly after most disturbances of CNS homeostasis, and the intensity to which it occurs corresponds to the severity of the disruption. Although microglial activation is initially directed to damage resolution and restoration of homeostasis, the persisting microglial reaction is harmful and has been involved in pathological conditions ranging from traumatic injuries, infectious diseases, tumors, and neurodegenerative disorders (Stratoulias et al., 2019).

1.2 Astrocytes

1.2.1 Overview of astroglia

Astrocytes, or astroglia, account for approximately 20-40% of the total number of cells in mammalian brains and are principal cells responsible for sustaining homeostasis and providing a defense of the CNS (Herculano-Houzel, 2014; Verkhratsky and Nedergaard, 2018). Astrocytes are a class of neural cells that originate from the neuroepithelium-derived radial glia (RG), that are the universal neural progenitors **(Figure 5). Astrogliogenesis** proceeds in two distinct phases: during embryogenesis (1), RG undergo a gliogenic switch by which neurogenesis is taken over by gliogenesis. Astrocytes may originate by the direct transformation of glial-committed precursors but also through an intermediate progenitor (IPC) stage that arises from the asymmetric division of these RG (Kriegstein and Alvarez-Buylla, 2009). During early postnatal stages (2), a second wave of astrogliogenesis occurs by direct transformation of RG and symmetrical division of differentiated astrocytes. This postnatal wave of glia generation

is much larger, leading to an increase from 4 million to over 140 million glial cells in mice, and accounts for the ≈ 50% of all astrocytes (Molofsky and Deneen, 2015; Verkhratsky and Nedergaard, 2018). Thus, astrocytes can develop from intermediate progenitors, through the direct transformation of radial glia, and from the proliferation of differentiated astrocytes. In addition, neurogenesis and gliogenesis also persist in the adult brain at specific locations such as the SVZ. In adult SVZ, it is mediated by quiescent neural stem cells (NSCs) expressing astrocytic markers, thereby sometimes described as SVZ astrocytes, that give rise to IPCs, producing immature neuroblasts and oligodendrocytes. Indeed, another possible source of astroglia is suggested to be associated with NG2 glial cells (Nishiyama *et al.*, 2016) **(Figure 5)**.

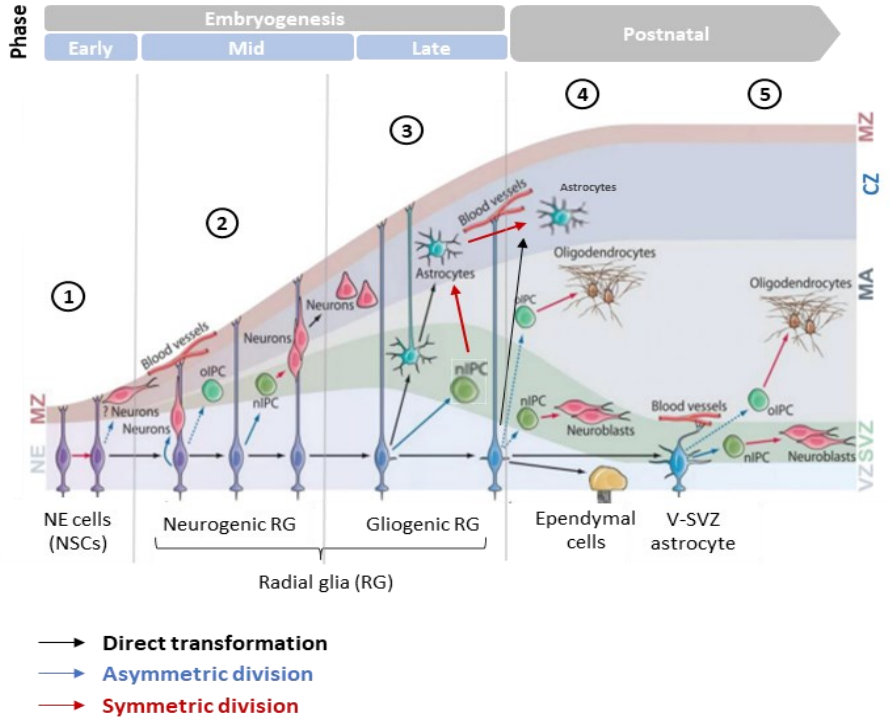

Figure 5. Generation of neural cell types during development. Early neuroepithelial cells (NE) give rise to radial glial cells (RG) (1), which in turn

generate first neurons (2), and then become glial committed (3), giving rise to both astrocytes and oligodendrocytes in late embryogenesis and during early postnatal stage. Later in the adult stage, neurogenesis and gliogenesis persist in the SVZ. n/oIPC= neurogenic/oligodendrytic intermediate progenitor cell, NE= neuroepithelium, MZ= marginal zone, CZ= cortical zone, MA= mantle, V-SVZ= ventricular-subventricular zone. Adapted from (Kriegstein and Alvarez-Buylla, 2009; Bayraktar *et al.*, 2015).

1.2.2 Astrocyte diversity and heterogeneity

Astrocytes are highly heterogeneous in form and function across different brain structures, and this heterogeneity is intimately tied to astrocyte development timing. According to this, two major subtypes of astrocytes have been well established: the protoplasmic and fibrous astrocytes **(Figure 6),** although many other types are described in the mammalian brain (Tay *et al.*, 2019). **Protoplasmic** astrocytes are the most abundant astrocyte subtype, mainly residing in deep cortical layers (layers 2-6) in the grey matter and thus the firsts in developmental origin. In rodents, these astrocytes have small round somata (10 μm in diameter) from which emanate 5-10 primary processes that branch to form highly elaborated and dense peripheral arborization, conforming to a spongiform morphology. Even so, the overall morphological appearances of protoplasmic astrocytes differ between and within anatomical structures (Bushong *et al.*, 2002). Besides this high complexity, these cells are in close contact with each other, exhibiting nonoverlapping domain organization and neuronal synapses via gap junctions, thus participating in synaptic communication in a variety of indirect and direct ways (Tabata, 2015). Moreover, protoplasmic astrocytes send processes to blood vessels where it forms perivascular endfeet. These cells are generally characterized by very low or almost negligible expression of the glial fibrillary acidic protein (GFAP).

On the other hand, **fibrous** astrocytes are mainly located in the white matter and have fewer, thicker, and longer processes than protoplasmic astrocytes. In addition, the processes of fibrous astrocytes overlap, reflecting the absence of domain organization. By contrast, fibrous astrocytes have higher levels of the astrocyte intermediate filament GFAP. They fit into the classical role of astrocytes by providing metabolic support to the neurons, but other functions are not yet clear. In humans, protoplasmic and fibrous astrocytes exhibit unique structures: they have a 2 to 2.5-fold larger domain than that in rodents and human protoplasmic astrocytes have about 10 times more primary processes and a more complex arborization **(Figure 6**¡Error! No se encuentra el origen de la referencia.**)** (Oberheim *et al.*, 2009). Besides protoplasmic and fibrous astrocytes, the brain of higher primates (including humans) contains several more types of specialized astrocytes, including interlaminar, polarized, and varicose projection astrocytes **(Figure 6)** (Oberheim *et al.*, 2009). **Interlaminar** astrocytes have small somata localized in layer I and one or two long processes that penetrate through the cortex and end in layers II to IV. **Polarized** astrocytes are uni-or-bipolar cells located in cortical layers V and VI, displaying one or two long and thin processes penetrating superficial layers. **Varicose projection** astrocytes only exist in the brain of humans and are characterized by several exceptionally long unbranched processes that extend in all directions through the deep cortical layers. These cells are similar to atypical protoplasmic astrocytes, described in adult human brains (Oberheim *et al.*, 2009).

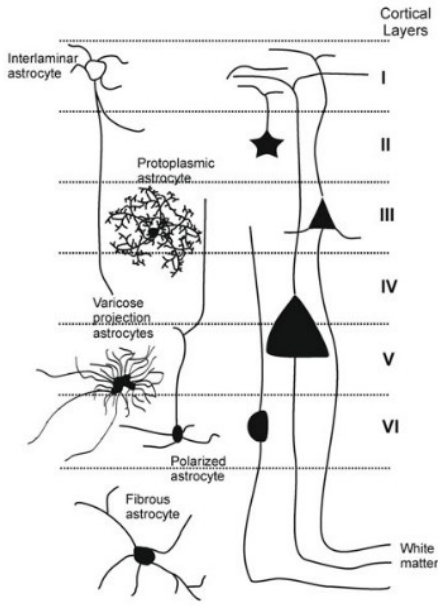

Figure 6. Morphological heterogeneity and subtypes of astrocytes in the cortex of higher primates and humans. Protoplasmic, polarized and varicose projection astrocytes reside in deep cortical layers (layers II-VI), whereas somata of interlaminar astrocytes are located superficial, and their processes penetrate deeper layers. Fibrous astrocytes, by contrast, are found in the white matter (WM). Extracted from (Verkhratsky and Butt, 2013).

The remarkable morphological heterogeneity of astrocytes coincides with substantial **molecular diversity**. A universal marker that may stain and reveal all astrocytes subtypes in the CNS does not exist, but several molecular markers which target a broad range of astrocytes have been identified and can be used with varying success. In this sense, **GFAP** is often regarded as the prototypical astrocyte marker, but closer examination reveals that not all astrocytes are uniformly labeled with this marker. As noted above, white matter fibrous astrocytes constitutively express high levels of GFAP, in contrast with grey matter astrocytes, which are poorly stained by this marker (Khakh and Sofroniew, 2015). On the other hand, GFAP is expressed by different cell types in the CNS, such as in

radial glia during late development and radial astrocytes in the adult SVZ (V-SVZ astrocytes) (Bayraktar *et al.*, 2015). Thus, detectable GFAP expression is neither required nor sufficient to identify a cell as a mature differentiated astrocyte. In addition, GFAP expression is upregulated in reactive astrocytes. Despite all these limitations and disputable use as a "prototypical" astrocytic marker, GFAP labeling is still widely used for immunohistochemistry and cell-specific transcriptional studies (Waller *et al.*, 2016). The glycoprotein **S100β** is a Ca^{2+}-binding protein expressed in high levels in astrocytes and thus universally used as a marker for this cell type, both in physiology and pathology. However, the specificity of its expression to astrocytes alone is highly disputed as it has been found not only in astroglia but also in oligodendrocytes, radial glia, lymphocytes, and mature neurons in adult mice (Steiner *et al.*, 2007). The key enzyme of foliate metabolism, aldehyde dehydrogenase 1 light chain 1 **(ALDH1L1),** was found to be expressed explicitly in astrocytes, thereby being recently promoted as a highly specific astrocytic marker (Cahoy *et al.*, 2008a). Later analysis showed that *Aldh1l1* gene expression changes with age and is also expressed in a subpopulation of oligodendrocytes (Yang *et al.*, 2011). Other examples of astrocyte molecular diversity are in glutamate transporters **EAAT1** and **2** (known as **GLAST** and **GLT1**, respectively, in rodents), and glutamine synthase **(GLUL)**, which have been also found in some neurons and oligodendrocytes (Northington *et al.*, 1998; Robinson, 2001).

There are many other reported markers for astrocytes, such as the water channel aquaporin 4 **(AQP4),** with a highly polarized expression concentrated in the endfeet, and connexins (CX), through which they form

gap junctions, with predominant expression of **CX43** and, to a lesser extent, of **CX30** (Freitas-Andrade and Naus, 2016).

1.2.3 Physiological functions of astroglia

Astrocytes are responsible to maintain homeostasis of the CNS at all levels of organization, from molecular and metabolic (ion, water, and neurotransmitter homeostasis, regulation of pH, metabolic support), cellular and network (neuronal guidance, synaptogenesis and synaptic maturation and extinction), organ (regulation of the blood-brain barrier) to systemic (chemosensing, sleep homeostasis) level (Verkhratsky and Nedergaard, 2018) **(Figure 7)**. These numerous functions of astrocytes are possible since they are integrated into cellular networks (known as astroglial syncytium) through gap junctional coupling, providing for intercellular transport of ions, second messengers, and other biological molecules. Moreover, astroglial syncytium are tightly coupled into neural networks and act within the context of neural tissue (Giaume *et al.*, 2010; Kiyoshi and Zhou, 2019). Indeed, this close structural and functional partnership of astrocytes and neurons gave rise years ago to the **"tripartite synapse"** concept, where astrocytes actively participate and exchange information with neurons (Araque *et al.*, 1999).

Astrocytes are thus of vital importance for all aspects of CNS function, including its development, experience-dependent adaptation and aging. In the following sections, we briefly review the major astrocytic functions to control homeostasis of the CNS **(Figure 7)**.

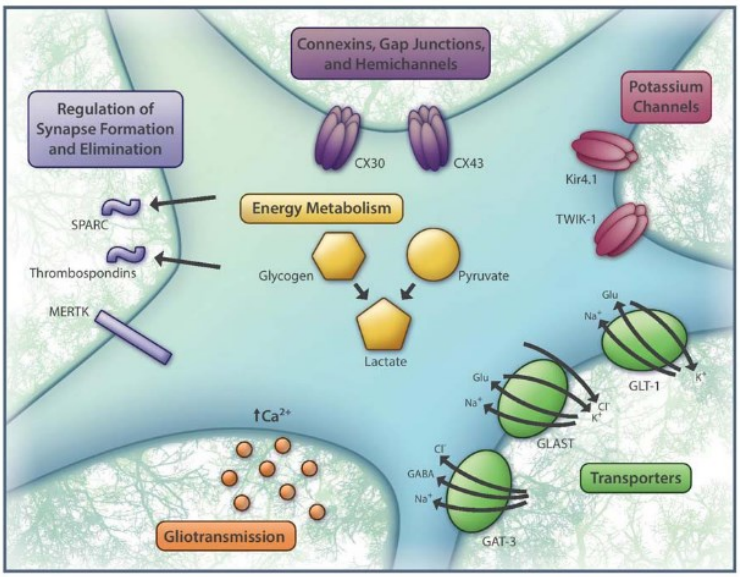

Figure 7. Basic physiological functions of astrocytes involved in homeostatic control. In the healthy CNS, astrocytes maintain the molecular homeostasis through control of extracellular amounts of ions (K^+), water, pH, and neurotransmitter via specialized membrane transporters, modulate synaptic activity directly via release of "gliotransmitters", regulate energy metabolism and offer energy support to neurons, and take part in the formation and pruning of synapses. Adapted from (Xin and Bonci, 2018).

Synapse formation, elimination and function

During late developmental stages, astrocytes regulate neuronal migration and **synapse formations and maturation** by providing guidance cues in the form of membrane-bound, cytoplasmic, or secreted proteins (Ullian *et al.*, 2001). To date, several astrocytic molecules have been proven to be responsible for mediating this synaptogenic effect, including thrombospondins, SPARC, Hevin, and Glypicans (Chung *et al.*, 2015) **(Figure 7)**. In fact, these molecules continue to be expressed by astrocytes into adulthood and at significantly different levels across regions (Boisvert *et al.*, 2018), thus suggesting parallels with the formation and plasticity of synapses in the adult stage as a result of learning, environmental changes,

or pathology. Astrocytes also play an important role in **synapse elimination**, together with microglia, during development, facilitating synaptic pruning and, participating in synaptic plasticity in adulthood (Chung *et al.*, 2015). Astrocytes mediate synapse elimination by releasing signals that induce the expression of complement C1q, which in turn tag synapses for elimination by microglia **(Figure 8 a).** In addition, astrocytes can directly eliminate silent synapses by phagocytosis dependent on MEGF10 and MERTK phagocytic receptors **(Figure 8 b)** (Chung *et al.*, 2013). Therefore, astrocytes share with microglia the ability to actively engulf and eliminate synapses in response to neural activity during the development and adult stage. Furthermore, astrocytes have the potential to exert powerful and long-term influences on **synaptic function** by releasing both positive and negative signals to finely tune synaptic strength. Some of these molecules are BDNF and cholesterol, which act as positive signals that induce glutamatergic synapse formation and increase presynaptic strength and release probability, respectively (Chung *et al.*, 2015).

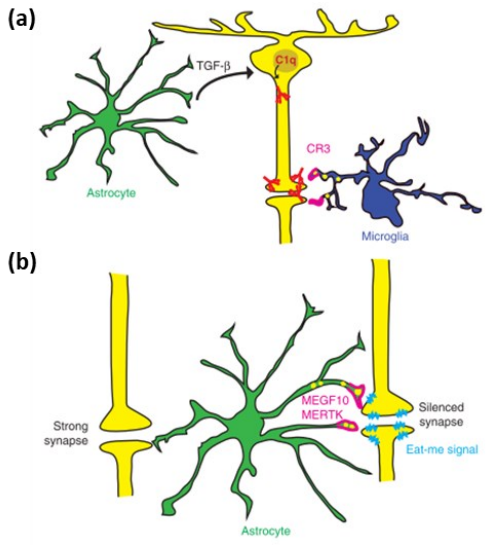

Figure 8. Astrocytes mediate synapse elimination through indirect (a) and direct (b) mechanisms. (a) Astrocytes (green) induce C1q expression (red) in radial glial

cells (RG; yellow) through TGF-β signaling. C1q-labeled synapses can be recognized by complement component-3 receptors (C3R, magenta) in microglia (dark blue) and eliminated through complement-dependent phagocytosis. (b) Astrocytes (green) directly eliminate synapses by recognizing "eat-me signals" (light blue) presented in the silent synapses and phagocytosing them through MEGF10 and MERTK phagocytic pathways (magenta). Adapted from (Chung et al., 2015).

Energy support and metabolism

Astrocytes processes contact with blood vessels and neuronal axons and synapses, thereby being well-positioned to regulate blood flow and molecules efflux from the circulatory system to neurons. Compelling evidence indicates that brain activity is linked to local circulation and that astrocytes may have a specific role in neurovascular coupling and regulation of regional blood flow. In response to enhanced neuronal activity, astrocytes produce and release molecular mediators such as prostaglandins (PGE), nitric oxide (NO), and arachidonic acid, which in turn produce vasodilatation to enhance the delivery of oxygen and glucose to the active brain region (Gordon *et al.*, 2007).

Regarding energy needs, astrocytes use glycogen to continuously synthesize lactate to supply neuronal energy demand **(Figure 7)**. In fact, astrocytes are the principal storage of glycogen in the CNS, with the highest levels observed in areas of high synaptic density, such as the hippocampus (Oe *et al.*, 2016). Apart from glycogen, astrocytes are considered to be the main net producer and storage of cholesterol and various lipid derivatives in the adult CNS. Conversely, neurons are considered to be the net consumers, and they synthesize lipids less efficiently than astrocytes (Nieweg *et al.*, 2009). Therefore, metabolic supplies from astrocytes to neurons are required to assure a correct synaptic transmission and proper brain function (Deijk *et al.*, 2017).

Several messengers like glutamate, K^+, NO, and ammonia signals the metabolic demands of neurons to astrocytes. Thus, neurons rely on astrocytes for energetic and metabolic supply.

Molecular homeostasis

Astrocytes exert essential functions in maintaining the ion, pH, water, and neurotransmitters homeostasis of the extracellular space, critical for healthy neuronal excitability and synaptic connectivity (Verkhratsky and Nedergaard, 2018). **Ionic homeostasis** of the CNS is of paramount importance for nervous function because it defines overall excitability and major signaling processes. For example, astrocytes exhibit spatial buffering for K^+ within seconds of neuronal activity, which is mediated by astrocyte-specific $K_{ir}4.1$ channels **(Figure 7)**, thereby maintaining its extracellular concentration constantly low (Hertz and Chen, 2016). Moreover, cytosolic and extracellular pH regulation is of great importance as even mild acidosis or alkalinization significantly affects brain function. Aquaporins and other membrane transporters mediate the flux of water and gases like O_2, CO_2, or NO. Precisely, astrocyte processes are rich in the AQP4 water channel and $K_{ir}4.1$ channels, which together play a role in fluid homeostasis (Seifert *et al.*, 2006). Astrocytes are also accountable for fighting against reactive oxygen species **(ROS)**, to which neurons are highly susceptible. The antioxidant system of the CNS mainly relies on glutathione and ascorbic acid, which are both synthesized and accumulated in astrocytes (Makar *et al.*, 1994). Astrocytes are also fundamental for **neurotransmitter turnover** by expressing high levels of transporters for neurotransmitters such as glutamate, GABA, and glycine, which serve to remove them from the synaptic space (Sofroniew and Vinters, 2010). Glutamate clearance from the extracellular space is an

important task to protect neurons from excitotoxicity. This task is accomplished by glia-specific transporters EAA1 and 2 (GLAST and GLT1, in rodent). Once inside astrocytes, the neurotransmitters are converted by enzymes like glutamine synthase into precursors such as glutamine (in the case of glutamate) that are recycled back to neurons for reconversion into active neurotransmitters (Verkhratsky and Nedergaard, 2018) **(Figure 9)**.

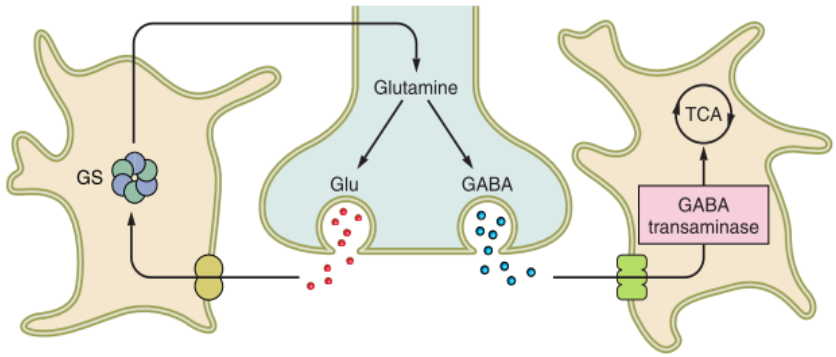

Figure 9. Neurotransmitter homeostasis in astrocytes. Astrocytes take up glutamate, GABA, and other neurotransmitters through membrane transporters. In the case of glutamate, it is converted to glutamine (by glutamine synthetase, GS), which is shuttled to neurons for subsequent conversion into glutamate and GABA. GABA accumulated by astrocytes is mainly consumed by the tricarboxylic acid cycle. Adapted from (Verkhratsky and Nedergaard, 2018).

On the other hand, astrocytes can also release neuroactive agents, including the neurotransmitters glutamate, ATP, GABA, and glycine, through which they play direct roles in synaptic transmission. **Gliotransmission** occurs in response to changes in neuronal synaptic activity through an increase in astroglial Ca^{2+} **(Figure 7).** It might modulate the strength of inhibitory and excitatory synaptic transmission by activating receptors in neurons. For example, astrocytes in the spinal dorsal horn secrete ATP that is hydrolyzed to produce adenosine, which suppresses nociception by activating adenosine A1 receptors expressed by

sensory neurons, suggesting that gliotransmission may inhibit pain under normal physiological conditions. (Foley *et al.*, 2011). In addition, astrocytes have refined terminal processes with which they reach thousands of synapses simultaneously, thus leading to the synchronization of neuronal firing patterns through the release of gliotransmitters (Volterra and Meldolesi, 2005). Overall, such evidence supports the 'tripartite synapse' hypothesis (introduced earlier), which postulates astrocytes as direct and interactive players with neurons during synaptic activity in an essential manner for information processing by neural circuits (Araque *et al.*, 1999). Indeed, there is accumulating evidence that astrocytes are directly involved in complex phenomena such as memory processing (Adamsky *et al.*, 2018; Kol *et al.*, 2020) or the development of mood disorders like depression (Cao *et al.*, 2013) and obsessive-compulsive disorder (Aida *et al.*, 2015).

1.2.4 Reactive astrogliosis and pathophysiology of astrocytes

Besides their many functions in brain physiology, astrocytes are involved in many brain pathologies. In response to CNS damage and disease, astrocytes undergo cellular, molecular, and functional changes commonly referred to as **reactive astrogliosis,** involving transcriptional regulation, as well as biochemical, morphological, metabolic, and physiological remodeling. These changes ultimately lead to both gain and loss of functions, which may be both detrimental and beneficial to neurons and non-neuronal cells (Escartin *et al.*, 2021). In addition, a disruption of normal astrocyte functions in healthy tissue may be the direct cause of neurological dysfunction and disease, which gives rise to the concept of astrocytopathies (Sofroniew and Vinters, 2010). Overall pathological changes in astroglia are thus complex and diverse. A better understanding

of this diversity of changes could be useful to gain insight into the specific involvement of these cells in the initiation and progression of different CNS pathologies, thus offering new pharmacological targets for their treatment. The following chapters briefly describes the process of astrocyte reactivity or astrogliosis and their functional implications.

1.2.4.1 Morphological and molecular changes involved in astrogliosis and glial scar formation

Astrogliosis is not a simple stereotypical response but a finely tuned spectrum of progressive potential changes ranging from reversible alterations in gene expression and cellular hypertrophy to compact scar formation involving marked cell proliferation and permanent tissue rearrangement (Khakh and Sofroniew, 2015) **(Figure 10 a)**. In addition, astrogliosis does not occur in isolation. Still, it is part of a coordinated multicellular response involving multiple types of glia, neurons, and non-neural cells intrinsic to the CNS, such as endothelial and pericytes, or entering the bloodstream like leukocytes and platelets. Astrocytes take part in this process by receiving and sending instructive signals that influence the onset, progression, and resolution (Sofroniew, 2014) **(Figure 10 b-c)**. Thus, astrogliosis is a complex mixture of events that occur in a context-specific manner as determined by multiple interactions and signaling events that vary with the nature and severity of specific CNS insults.

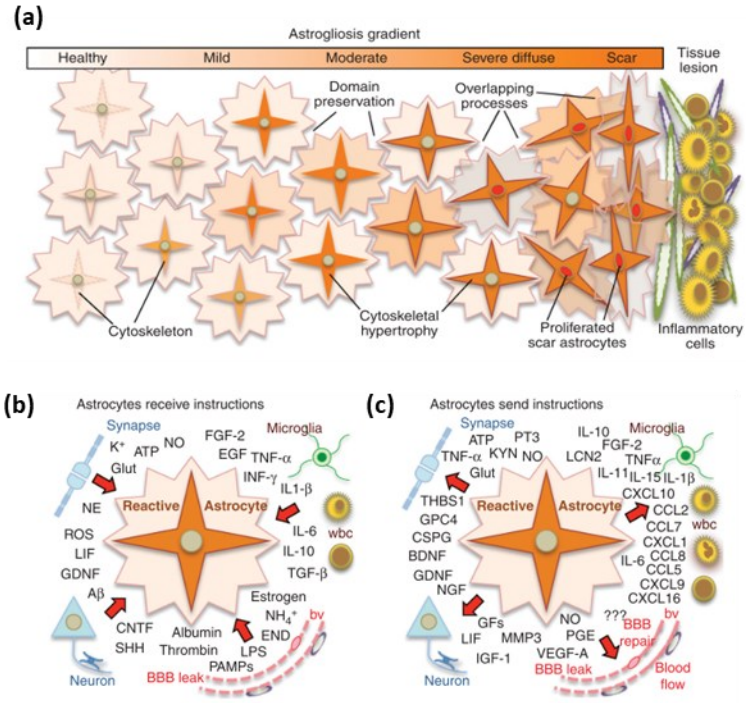

Figure 10. Morphological and molecular signature involved in reactive astrogliosis. (a) Astrogliosis gradient from mild to moderate and scar formation involve progressive morphological changes, including hypertrophy of astrocytic cytoskeleton, increased proliferation (represented by red nuclei), and overlapping domains. Compact astroglial scars consist of newly proliferated astrocytes with tightly overlapping projections that form boundaries to damaged tissue and inflammation. **(b-c)** Reactive astrocytes receive and send diverse molecular instructions that instruct themselves and other cells, respectively. Adapted from (Sofroniew, 2014)**.**

Morphological changes are linked to the severity of the insult and progression of astrogliosis. They include increasing levels of cellular hypertrophy, astrocyte proliferation, and tissue reorganization with substantial intermingling and overlapping of astrocytes processes that form dense, narrow, and compact glial scars **(Figure 10 a).** According to tissue reorganization, the first stages (mild to moderate astrogliosis) have the potential for resolution. In contrast, in more severe stages (severe

diffuse astrogliosis), this capacity is reduced, and there is even a high tendency toward long-lasting tissue remodeling (Sofroniew, 2009; Sofroniew and Vinters, 2010). The glial scar persists for a long time even after triggering insult may have resolved but serve as a mechanism to confine lesions to prevent the spread of inflammation and thus preserve function after CNS traumatic injury, stroke, infection, and degenerative disease (Khakh and Sofroniew, 2015).

The triggering and regulation of the different changes and effects of astrogliosis are specifically controlled by many inter- and intra-cellular molecular signals that can be released by both reactive astrocytes and all cell types of CNS tissue **(Figure 10 b-c)** and reflect the specific contexts of the stimuli. Such molecular mediators include regulation of particular functions or effects of astrogliosis, including regulators of cell proliferation (endothelin-1), extracellular matrix proteins (Laminin, Metalloproteases, Ephrins), structural filaments (GFAP, vimentin, nestin), neurotransmitters (glutamate, ATP, noradrenaline), ROS, metabolites (lactate), and cytokines (IL6, TNFα, INFγ, IL10, TGFβ), proteins of the antigen presentation and complement pathway (Sofroniew, 2009). Therefore, the response of astrocytes to injury is not uniform, and it varies in a context-specific manner as determined by the specific molecular signature associated with specific insults and the environment in which they occur (Hamby *et al.*, 2012; Zamanian *et al.*, 2012). Currently, a study analyzing the transcriptional profile of reactive astroglia from adult mice following brain injury (either ischemic stroke causing cell death or LPS injection causing neuroinflammation) reported that at least 50% of the altered genes were specific to the type of injury, which may also suggest the occurrence of different subtypes of reactive astrocytes (Zamanian *et al.*, 2012).

1.2.4.2 Dysfunctional astrogliosis and its implication in neurological disorders

Although reactive astrogliosis is initiated as an adaptive and beneficial process directed at tissue protection, it also has the potential to exert detrimental effects as determined by dysfunctional signaling mechanisms caused by either genetic defects or chronic exposure to inflammatory stimuli, thus contributing to, or even being the primary cause of many CNS diseases (Verkhratsky and Butt, 2013). Hence, reactive astrocytes can play either neuroprotective or detrimental roles depending on the pathological context. It is well documented that dysfunctional astrocytes have the potential to exert a variety of damaging effects, such as exacerbating inflammation via cytokine production (Hamby *et al.*, 2012; Zamanian *et al.*, 2012), producing neurotoxic levels of ROS (Zamanian *et al.*, 2012), releasing potentially excitotoxic glutamate and compromising blood-brain barrier function (Sofroniew and Vinters, 2010). Therefore, a persistent or altered astrogliosis may underlie neural dysfunction and pathology in various conditions, including trauma, stroke, or multiple sclerosis.

1.3 Genetic targeting of glial cells

Given the now-recognized potential contribution of glial cells to CNS-associated disorders, interest has grown in studying fundamental glial biology and evaluating their causal and correlative roles in the neural circuit activity, as well as its role in disease-related phenotypes. To conduct hypothesis-driven studies, complete gene or protein expression profiles are helpful to shed light on complex phenomena. In this context, several methods have been developed to target and manipulate both astrocytes and microglia and uncover their transcriptional and translational profiles.

The transcriptome of defined cell populations can be assessed using **cell isolation** methods such as fluorescence-activated cell sorting (FACS) and magnetic-bead based cell sorting in combination with **reporter mouse lines** and antibodies against cell-type specific molecules. Transgenic mice overexpressing green fluorescent protein (GFP) under the control of several cell-specific promoters have been widely used for this purpose. **Astrocytes** from various brain regions, developmental stages, and disease conditions have been studied this way by using gene promoters *Gfap* (Lovatt *et al.*, 2007)*, S100β* (Cahoy *et al.*, 2008a) or *Aldh1l1* (Zamanian *et al.*, 2012; Orre *et al.*, 2014; Zhang *et al.*, 2014). On the other hand, the fractalkine receptor CX3CR1 has been the basis of reporter mouse lines for **microglia** (Jung *et al.*, 2000). Nonetheless, recently described reporter mice have taken advantage of microglia-specific signature genes identified in bulk RNA sequencing (RNA-seq) studies (Hickman *et al.*, 2013; Bennett *et al.*, 2016; Butovsky and Weiner, 2018; van der Poel *et al.*, 2019). These genes include *Tmem119, Sall1,* and *Hexb,* and have been used as promoters together with the expression of GFP or dTomato fluorescent reporter proteins (Buttgereit *et al.*, 2016; Kaiser and Feng, 2019; Masuda *et al.*, 2020b; Ruan *et al.*, 2020).

However, there is no transgenic mouse line that exclusively targets astrocytes or microglia cells; every available line has its limitations, mainly regarding the efficiency and the specificity of the cell marker through the lifespan of the mice. For instance, transgene expression driven by the *Gfap* promoter does not occur for all astrocytes and it is often detected in large numbers of neurons, since the *Gfap* promoter is also active in embryonic radial glia (Sofroniew, 2012). Similarly, *Cx3cr1* is also expressed by peripheral monocytes, dendritic cells, and natural killer cells (Jung *et al.*, 2000). In this context, when choosing a genetic strategy to express or

delete genes in specific cells, it is vital to consider the efficiency and specificity of the targeted cell marker. In this context, the establishment of Cre-loxP system opened new avenues in the genetic manipulation of cells (Orban *et al.*, 1992). In particular, tamoxifen (TAM)-inducible Cre lines (CreER) allow the insertion or deletion of genes in a cell-type specific and temporally inducible manner, thus avoiding expression to other cell types during embryonic development. Accordingly, the best available transgenic model for targeting **astrocytes** across the entire brain is the TAM-inducible **Aldh1l1-CreERT2** mouse line, which allows temporal regulation of gene expression and has proven high astrocyte selectivity and efficiency when induced in adulthood (Srinivasan *et al.*, 2016; Winchenbach *et al.*, 2016). Likewise, the TAM-inducible **Cx3cr1-CreERT2** lines provide excellent tools to selectively target **microglia** with high frequency and allow long-term genetic alteration over months (Goldmann *et al.*, 2013; Yona *et al.*, 2013). Additionally, several other TAM-inducible Cre lines now also exist for microglia with the above-mentioned novel markers, among which Hexb-CreERT2 mice are reported to have the highest microglia specificity (Masuda *et al.*, 2020b).

The isolation of defined cells from tissue relies on enzymatic digestion to achieve single-cell suspensions, a manipulation that bears the inherent risk of artifacts and is often inefficient and likely to induce bias. To circumvent the need for cell retrieval, newer strategies were introduced to isolate cell-specific **translatomes**. One approach is bacterial artificial chromosome (BAC) translating ribosome affinity purification **(TRAP),** by which ribosomes from genetically accessible cell populations are isolated, allowing for sequencing the associated actively translated mRNAs (Doyle *et al.*, 2008; Heiman *et al.*, 2008, 2014). Multiple BAC-TRAP mouse lines exist to target astrocytes (Sun *et al.*, 2015; Boisvert *et al.*, 2018; Clarke *et*

al., 2018), but none for microglia. A similar method is the **RiboTag approach** (Sanz *et al.*, 2009), in which cell-type specific expression of Cre recombinase is used to activate expression of hemagglutinin (HA) tag in the ribosomal protein L22 (RPL22) by deletion of a 'floxed' wild-type exon. This RiboTag mouse line has been crossed with TAM-inducible Aldh1l1-CreERT2 mice for transcriptome profiling of mature astrocytes from different brain regions (Srinivasan *et al.*, 2016; Chai *et al.*, 2017) and with Gfap-Cre mice to investigate molecular alterations in astrocytes after spinal cord injury (Anderson *et al.*, 2016), in a mouse model of multiple sclerosis (Itoh *et al.*, 2017), and to compare adult and aged astrocyte transcriptomes (Boisvert *et al.*, 2018). Similarly, constitutive Cre and TAM-inducible Cx3cr1-Cre/CreERT2 mouse lines were also crossed with RiboTag mice in several different studies (Haimon *et al.*, 2018; Chappell-Maor *et al.*, 2019; Chucair-Elliott *et al.*, 2020).

Overall, currently available tools allow a better experimental design to explore astrocyte and microglial biology from molecules to systems.

2 Pain

2.1 Definition

Many efforts are constantly made to develop a clear, concise, and unambiguous statement that better describes the concept of pain while recognizing its diversity and complexity. The latest revised definition of pain by the International Association for the Study of Pain (IASP) was published in 2020, and pain is defined as "an unpleasant sensory and emotional experience associated with, or resembling that associated with, actual or potential tissue damage" (Raja *et al.*, 2020). This definition highlights that pain is always a subjective experience; thus, the inability to verbally communicate pain sensation does not preclude its existence.

Describing pain as an "experience" separates it from nociception. Therefore, pain is a complex phenomenon comprising the integration of both sensory and emotional components (Talbot *et al.*, 2019). The sensorial or nociceptive element involves the transduction and transmission of noxious stimuli from peripheral sensory nerves to the central nervous system and provides information about the features of the stimuli (location, duration, modality, and intensity). The emotional component comprises the unpleasant character of pain perception, and it is influenced to varying degrees by the previous experience and several psychological and social factors.

Pain has a clear protective role under physiological conditions aimed at alerting external or internal stimuli that can potentially induce damage. However, pain can also represent a disastrous condition when it loses its warning purpose (Scholz and Woolf, 2002).

2.2 Classification

Pain has been classified according to duration, intensity, anatomical localization, etiology, or the underlying pathophysiological mechanisms. However, it is important to consider these different classifications as one-dimensional to provide a comprehensive assessment and a multimodal approach.

2.2.1 According to duration

Pain can be described as acute or chronic depending on the time that a patient experiences it. However, the distinction of these states is not only due to a temporal issue but also to the different pathophysiological mechanisms of the two modalities (Basbaum *et al.*, 2009; Price and Ray, 2019).

Acute pain is an immediate, short-lasting response to a noxious stimulus. It has a biological function as a warning mechanism, and it resolves with the healing of the injured tissue. By contrast, **chronic pain** is defined as pain that persists or recurs for more than three months. It remains beyond the damage, so it does not serve a biological function in most cases, and it is not considered a symptom but rather a disease itself (Treede *et al.*, 2019). Moreover, persistent pain is accompanied by physical, emotional, social, or cognitive alterations that diminish the patient's quality of life (Nicholas *et al.*, 2019). Chronic pain is not simply a temporal extension of acute pain but an expression of functional and structural changes at different anatomical levels of the neuronal nociceptive pathway as well as the immune and glia participation, that finally leads to the progression from acute to chronic pain (Scholz and Woolf, 2007; Price and Ray, 2019).

2.2.2 According to pathophysiological mechanisms

Pain can be divided into nociceptive, inflammatory, and neuropathic pain, according to the pathophysiological mechanisms involved (Cervero and Laird, 1991; Costigan *et al.*, 2009) **(**

Figure 11).

Nociceptive pain is described as pain arising from actual or threatened damage to non-neural tissue occurring with a normally functioning somatosensory nervous system by activating specialized high-threshold sensory fibers **(**

Figure 11 a). The painful sensation is proportional to the intensity of the stimulus and continues as long as the noxious stimulus is present (Treede, 2018). Nociceptive pain is an early-warning physiological protective system aimed to detect and avoid contact with damaging or harmful stimuli (Basbaum *et al.*, 2009).

Inflammatory pain occurs as a result of an inflammatory process triggered by tissue injury or damage. Here the imperative shifts from a protective to an adaptative function by promoting healing and repairing the damage. The inflammatory response induces the release of several mediators that directly activate and sensitize nociceptive fibers (Woolf, 2011) **(**

Figure 11 b). Due to this sensitization process, inflammatory pain causes sensory abnormalities that alter the relationship between stimulus intensity and painful sensation. Once the healing process has finished, inflammatory pain usually disappears, although in some cases, it may persist, leading to chronic pain, thereby losing its physiological purpose (Costigan et al., 2009).

Neuropathic pain is caused by a lesion or disease of the somatosensory nervous system, including peripheral fibers and central neurons (Colloca *et al.*, 2017). Conditions such as trauma, infections, diabetes, chemotherapy treatments, or chronic inflammatory diseases are examples of disorders that may cause neuropathic pain **(**

Figure 11 c). This pathological pain is maladaptive since it neither protects nor supports healing and repair, and it lengthens beyond the injury and remains once the lesion disappears (Costigan *et al.*, 2009). Moreover, the relationship between the intensity of the stimulus and the painful response is disproportional, becoming in some cases extremely severe and disabling for the individual. Further details on this concept are in **section 2.4 below.**

In some conditions, such as fibromyalgia, irritable bowel syndrome, and interstitial cystitis, there is no identifiable noxious stimulus nor any detectable inflammation or damage to the nervous system. These clinical syndromes can best be called dysfunctional pain or **nociplastic pain (**

Figure 11 d). This new mechanistic descriptor was recently proposed to describe pain states characterized by clinical and psychophysical findings that suggest altered nociception despite the absence of clear evidence of actual or threatened damage (Kosek *et al.*, 2016).

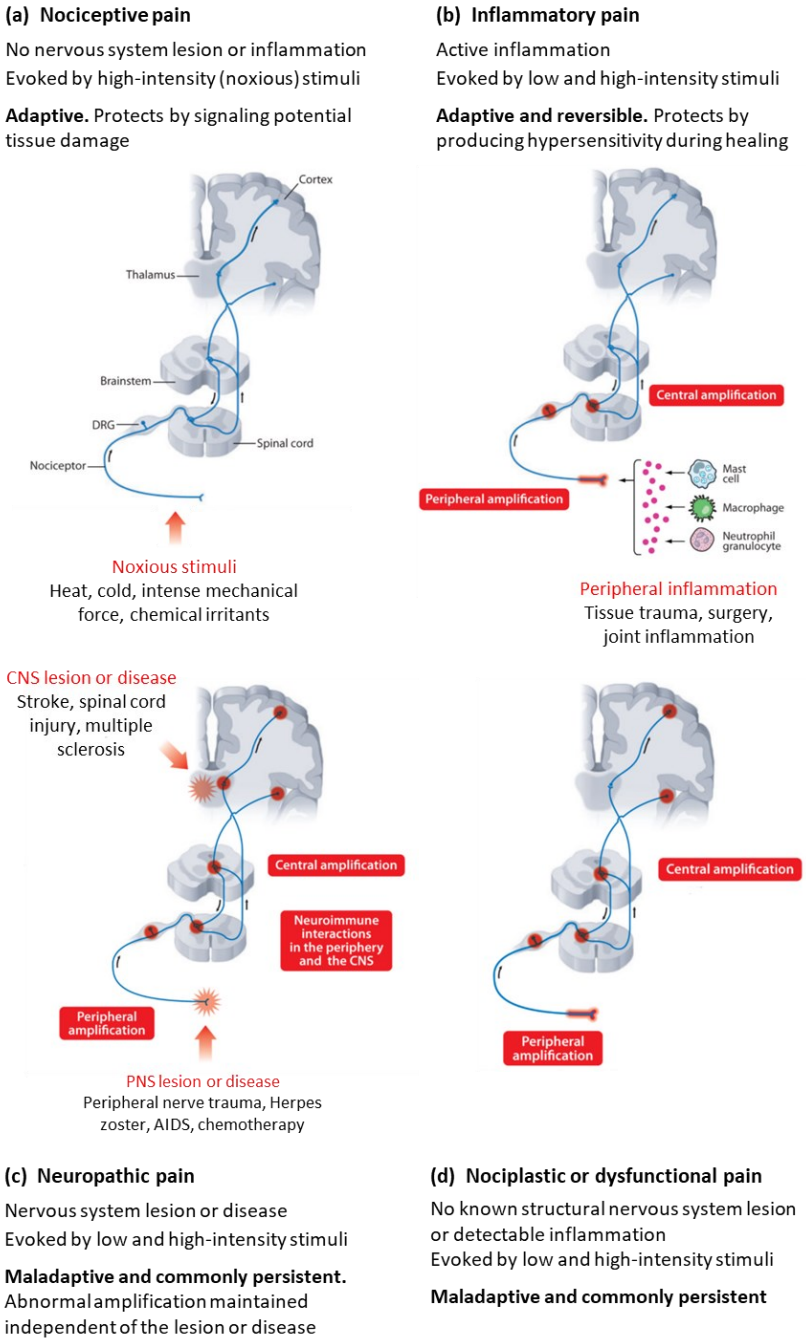

Figure 11. Pain classification. Pain can be broadly divided into four classes: (a) Nociceptive pain, (b) inflammatory pain, (c) neuropathic pain, and (d) nociplastic pain. Adapted from (Costigan et al., 2009).

2.3 The route of pain transmission

2.3.1 Detection of noxious stimuli from the periphery

The route for the pain sensation involves a complex series of mechanisms starting in the periphery with the potential presence of noxious stimuli, which are encoded as nociceptive messages and progressively transmitted to higher nervous centers, where it is processed.

Nociceptors are high-threshold sensory receptors specialized in detecting different modalities of noxious stimuli and transducing them into action potentials (Serra Catafau, 2007; Grace *et al.*, 2014). They are located in the peripheral terminals of primary afferent neurons, which have the cellular body in dorsal root ganglia (DRG) or the trigeminal ganglion, detecting stimuli from the body or the face, respectively. Primary afferent neurons are pseudo-unipolar neurons that have both a peripheral axonal branch that innervates the target tissue or organ and a central axon that synapses with second-order neurons in the dorsal horn of the spinal cord or the trigeminal nucleus caudalis (Basbaum *et al.*, 2009; Dubin and Patapoutian, 2010).

Primary sensory fibers are classified into four major groups (Aα, Aβ, Aδ, and C fibers) considering different characteristics such as myelinization, diameter, information, and speed, with the main types conveying pain signals being Aδ and C fibers **(Table 1)**. Thus, nociceptors are the free nerve endings of these fibers, and, unlike other sensory fibers transmitting innocuous information, they show high activation thresholds and multimodal stimuli detection (Serra Catafau, 2007). **Aδ fibers** are thinly myelinated, medium (2 - 5 µm), and fast driving (5 - 30 m/s) fibers conducting well-localized immediate pain signals (Serra Catafau, 2007;

Yam *et al.*, 2018). These fibers can be further divided into two main classes: type I (high-threshold mechanical receptors), which respond to intense mechanical stimuli, and type II, which mediate first acute response to noxious heat (Basbaum *et al.*, 2009). By contrast, **C fibers** are small diameter (< 2 µm) unmyelinated fibers related with slow (2 m/s), diffuse, and long-lasting pain. In terms of cytochemical content, they can be classified as either peptidergic or non-peptidergic, regarding their synthesized and released neuroactive substances (Usoskin *et al.*, 2015). Moreover, peptidergic C fibers mediate noxious thermal information, whereas non-peptidergic C fibers are polymodal (Basbaum *et al.*, 2009).

Table 1. Primary afferent axons arriving at the spinal cord. Adapted from (Serra Catafau, 2007)

Fiber	Myelin	Diameter (µm)	Velocity (m/s)	Function	Dorsal horn lamina
Aα	Yes	13-20	80-120	Proprioception of skeletal muscle	III-IV
Aβ	Yes	6-12	35-75	Touch, low threshold mechanoreceptors	III, IV, V
Aδ	Yes	2-5	5-30	Touch and temperature	I, IIo, V
				Pain: mechanical and cold nociceptors	I, IIo, V
C	No	< 2	0.5-2	Polymodal nociceptors (Non-peptidergic C-fibers)	IIi
				Thermal nociceptors (Peptidergic C-fibers)	I-IIo

Under physiological conditions, Aβ fibers conduct low threshold mechanosensitivity without eliciting pain sensation. If noxious stimuli are of sufficient intensity, Aδ fibers immediately transmit localized pain signals followed by diffuse pain signals conducted by C fibers. In the setting of an

injury, activated nociceptors and non-neural cells release inflammatory mediators, including peptides, neurotransmitters, and cytokines, that lead to the development of **peripheral sensitization** (Schaible, 2007). In these sensitizing conditions, there is a decrease in threshold to stimulation and an increase in firing rate of primary afferent nociceptors, provoking an exaggerated stimulus-evoked painful sensation such as **hyperalgesia** phenomenon **(Figure 12)** (Gold and Gebhart, 2010). Furthermore, there is an abnormal growth of both Aβ and Aδ fibers to innervate the neurons receiving the lost signal from the C fibers, which ultimately changes the characteristics of response to tactile stimuli that will be perceived as painful. This phenomenon is known as mechanical **allodynia,** and it also appears as a result of the sensitization conditions (Woolf, 2011) **(Figure 12)**.

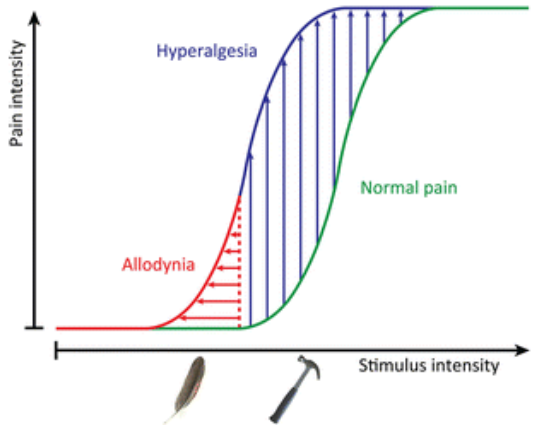

Figure 12. Sensitization to pain. Graphical representation of the shift from a normal pain sensation [green] to altered thresholds during pathological conditions. Hyperalgesia [blue] emerges from the sensitization of Aδ fibers and C fibers that become activated by low-threshold stimuli leading to an amplification of the pain signal. Allodynia [red] results from abnormal sprouting of Aβ-afferents that form new connections with nociceptive neurons, changing the response to tactile stimuli that will be perceived as painful. Adapted from (Lolignier *et al.*, 2015a).

2.3.2 Sensory transmission to the spinal cord

The central terminals of primary afferent fibers transmitting nociceptive information from the periphery enter the spinal cord through the dorsal root and project to second-order neurons located in different layers of spinal grey matter, organized into **laminae**. Most Aδ and C fibers project superficially to laminae I, II, with a smaller number reaching deeper layers (laminae V). By contrast, low-threshold Aβ fibers predominantly innervate laminae III, IV, and V **(Figure 13)** (D'Mello and Dickenson, 2008; Basbaum *et al.*, 2009). Thus, depending on the specific synaptic inputs received, second-order neurons can be distinguished in nociceptive-specific neurons, which are found mainly in laminae I and II and are generally responsive to noxious stimulation (via Aδ and C fibers), wide dynamic range neurons (WDR) located in laminae V and VI and respond to a range of sensory stimuli and intensities, and low-threshold non-noxious neurons in laminae III and IV, which respond solely to innocuous stimulation (via Aβ).

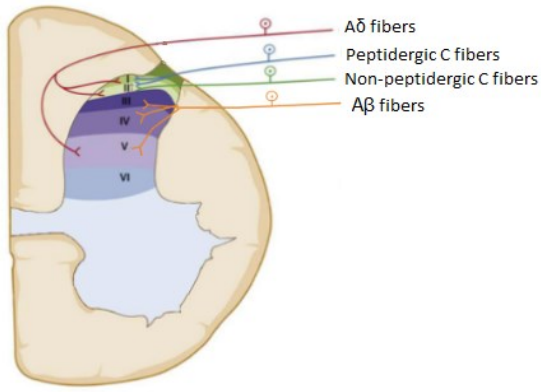

Figure 13. Termination sites of Aδ, peptidergic, and non-peptidergic C fibers in the spinal cord. Primary afferent fibers (Aβ, Aδ, and C) transmit impulses from the periphery, through the dorsal root ganglia, and into the dorsal horn of the spinal cord.

Excitatory amino acids such as glutamate and aspartate are the principal neurotransmitters involved in these first relays, but neuropeptides (substance P and calcitonin gene-related peptide) and purines (ATP) act as co-transmitters in peptidergic and non-peptidergic C fibers, respectively, to enhance pain transmission (Basbaum *et al.*, 2009). In **pathological pain**, these neuromodulators are overexpressed in response to persistent nociceptive inputs, contributing to the generation and maintenance of **central sensitization** at the spinal level. Consequently, there is a state of hyperexcitability established in the central nervous system, leading to the amplification of nociceptive signals, generating allodynia and hyperalgesia phenomena (Latremoliere and Woolf, 2009).

Besides neuronal modulation, **microglia and astrocytes** are also recognized as potent modulators of pain transmission, particularly under pathological conditions (further details in **section 2.4.4 below).** There is substantial evidence that strong activation of glial cells leads to proinflammatory responses with pathological effects such as neuronal hyperexcitability and neurotoxicity, thus contributing to central sensitization and transition from acute to chronic pain (Ji *et al.*, 2013).

2.3.3 Ascending pain pathways and supraspinal integration

The nociceptive signals received in the spinal cord ascend to supraspinal areas through different ascending pathways **(Figure 14).** Axons of second-order neurons decussate to the contralateral side of the spinal cord and project directly to thalamic structures (spinothalamic tract) or indirectly in brainstem nuclei, including the reticular formation (spinoreticular tract) or the parabrachial nucleus and periaqueductal gray matter (PAG; spinomesencephalic tract) (McCarberg and Peppin, 2019). These three tracts constitute the **anterolateral system**, the main ascendant pathway

that transmits nociceptive information to higher brain areas (Patestas and Gartner, 2016).

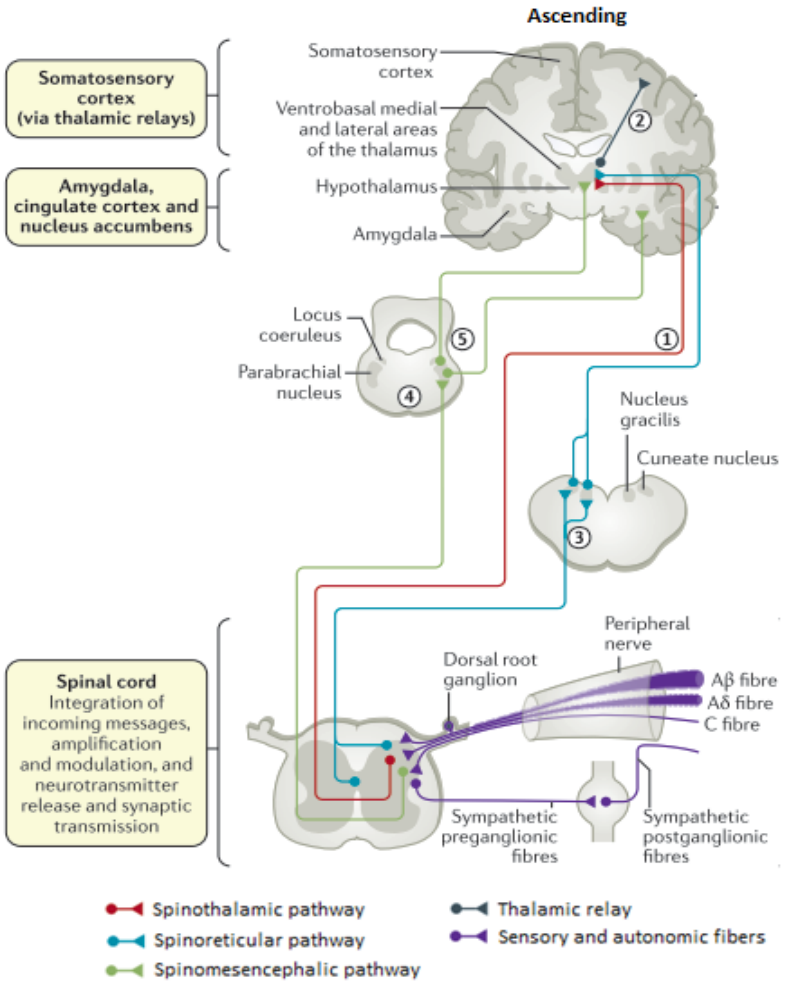

Figure 14. Ascending pain transmission pathways. Primary afferent nociceptors (namely, Aβ, Aδ, and C fibers) convey noxious information to projection neurons within the dorsal horn of the spinal cord. A subset of these projection neurons transmits the sensory components of pain via the spinothalamic pathway (1), which then projects to the somatosensory cortex (2). The spinal cord also has spinoreticular projections to the cuneate nucleus and nucleus gracilis (3). Other projection neurons relay in the parabrachial nucleus, through the spinomesencephalic tract (4-5), before contacting the hypothalamus and amygdala, contributing to the affective component of the pain experience. Adapted from (Colloca *et al.*, 2017).

At the supraspinal level, the **thalamus** is a key relay station for the transmission of nociceptive signals to other supraspinal areas where the different components of pain are integrated, but it is also crucial for the first conscious perception of pain (Ab Aziz and Ahmad, 2006). Thalamic projections from the direct ascending pathway (spinothalamic tract) mainly conduct tactile, proprioceptive, and nociceptive signals to **primary and secondary somatosensory cortices (SS)**, which integrate the sensory discriminative aspects of pain such as location, intensity, and duration of the stimulus (Thompson and Neugebauer, 2019) **(Figure 15)**. Additionally, recent findings revealed that, besides its predominant role in somatosensory processing, the SS contributes to emotional states in pain, but emotions influence pain processing in the SS (Tan and Kuner, 2021). Other projections from the thalamus to cortical areas include the prefrontal cortex (PFC), the anterior cingulate cortex (ACC), and the insular cortex, mediating cognitive-evaluating, attentional orienting, and the aversive quality of the pain percept, but also limbic structures, such as the amygdala, which is critically involved in the emotional-affective dimensions of pain **(Figure 15).** The amygdala also receives nociceptive inputs from the parabrachial nucleus, providing a direct pathway into the limbic system. Altogether constitute two significant aspects of the cortical pain percept: the cognitive and discriminative features of painful sensation and the emotional aspects generating an aversive state and triggering motor responses (Bushnell *et al.*, 2013; Groh *et al.*, 2018; Thompson and Neugebauer, 2019). On the other hand, the indirect ascending pain pathways (spinoreticular and spinomesencephalic tracts) send collaterals to several areas related to vegetative and homeostatic processes, such as the reticular formation, PAG, superior colliculus

(tectum), and hypothalamus, involving the autonomic and endocrine responses secondary to pain (Patestas and Gartner, 2016) **(Figure 15)**.

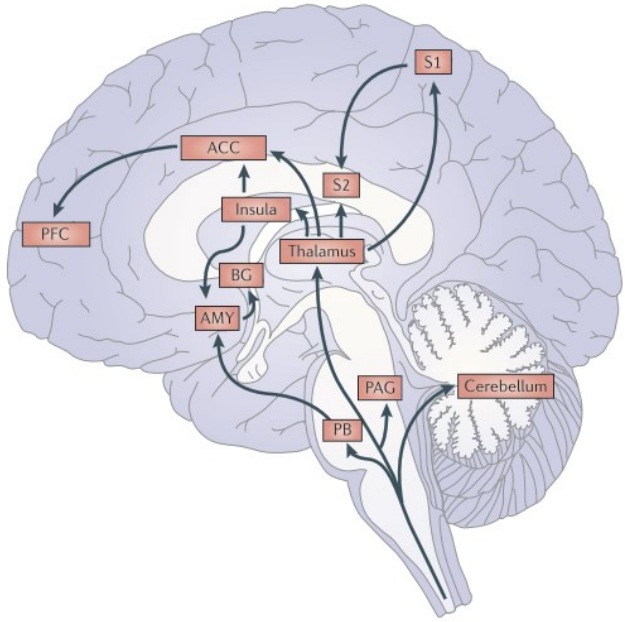

Figure 15. Supraspinal pain processing areas and connections. Nociceptive information from the thalamus is projected to several cortical and subcortical regions that encode sensory-discriminative (somatosensory cortex – S1, primary; S2, secondary), cognitive and emotional (anterior cingulate cortex, ACC; insula; amygdala, AMY) aspects of pain. BG, basal ganglia; PAG, periaqueductal gray; PB, parabrachial nucleus; PFC, prefrontal cortex. Adapted from (Bushnell *et al.*, 2013).

It is important to emphasize that these regions are not selectively or exclusively activated by nociception or restricted solely to pain perception. Indeed, areas serving several neurological functions, including cognition, emotion, motivation, and sensation, are functionally connected and give rise to the whole experience of pain. The interactions among these sites also provide a means whereby emotional and motivational cues can alter the experience and perception of pain through interactions with the descending pain modulatory system (Ossipov *et al.*, 2014).

Additionally, there is rising evidence showing functional and structural adaptative changes of these supraspinal structures during **chronic pain** states, affecting and increasing painful sensation and experience.

2.3.4 Descending modulatory control of pain

As a result of the processing and integration of nociceptive information in corresponding supraspinal areas, a physiological response to the painful sensation is built by a descending modulatory circuit **(Figure 16).** This descending control of pain underlies changes in pain thresholds as a response to both "bottom-up" (sensory information) and "top-down" (cognitive and emotional factors) inputs, allowing a quick adaptation to the environmental circumstances (Bushnell *et al.*, 2013; Colloca *et al.*, 2017).

The classical descending pain modulation system involves projections from the midbrain PAG to brainstem nuclei, including the rostroventral medulla (RVM) and the locus coeruleus, to the dorsal horn of the spinal cord **(Figure 16).** The **PAG** receives impulses from higher brain regions such as the thalamus, hypothalamus, amygdala, and PFC. Neurons in the PAG project downstream to the **RVM**, which also receive nociceptive information from the thalamus, the parabrachial area, the locus coeruleus, and the parabrachial tract. The RVM is the top output node in descending modulation of nociception and the final common relay before sending bilateral projections to the spinal dorsal horns and trigeminal nucleus caudalis. Neurons projecting from the RVM are called OFF/ON-cells since they exert a bidirectional modulatory effect by inhibiting and facilitating pain perception, respectively (Chen and Heinricher, 2019). These pathways mainly produce serotonin, and noradrenaline, conforming two primary monosynaptic descending routes **(Figure 16)**. Compelling

evidence shows that an imbalance or dysfunction in descending control systems that favor facilitation over inhibition may underlie persistent pain states (Basbaum *et al.*, 2009; Denk *et al.*, 2014; Yarnitsky, 2015).

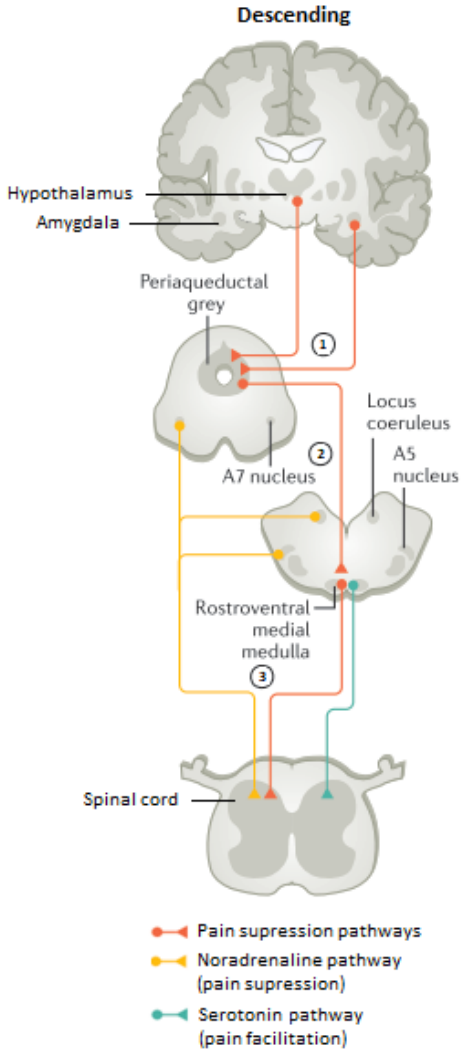

Figure 16. Descending modulation of pain. Descending efferent pathways from supraspinal areas (amygdala and hypothalamus) drive (1) the periaqueductal gray (1), the locus coeruleus, A5 and A7 brainstem nuclei, and rostroventral medial medulla (2). Thence, descending noradrenaline inhibition (yellow) or serotonin excitation (blue) modulates spinal cord activity (3).

Moreover, local circuits within the dorsal horn also play a role in modulating pain perception. In 1965, Melzack and Wall conceptualized in their "Gate Control Theory" the inhibitory role of non-nociceptive Aβ fibers over signals from pain fibers (C fibers), which could thereby inhibit pain (Melzack and Wall, 1965). Subsequently, Le Bars et al. demonstrated the inhibition inflicted on the response to one nociceptive stimulus by a concomitant another one, administered remotely from the first (Le Bars *et al.*, 1979). It may explain how a mechanical stimulus, such as scratching or pressing the injured area, can temporarily ease the pain sensation.

2.4 Neuropathic pain

2.4.1 Definition and classification

Neuropathic pain is defined as "pain caused by a lesion or disease of the somatosensory nervous system", according to the IASP's Neuropathic Pain Special Interest group (NeuPSIG) (Treede *et al.*, 2008; Jensen *et al.*, 2011). Neuropathic pain may result from etiologically diverse lesions or disorders affecting the peripheral or the central nervous system. Thus, it can be classified according to both the etiology and the presumed location (peripheral, central, or generalized) of the insult to the nervous system (Baron *et al.*, 2010; Cousins *et al.*, 2010; Scholz *et al.*, 2019) **(Table 2).**

Not all patients with peripheral or central neuropathy develop neuropathic pain, and the same condition can be painful in some patients and painless in others. The presence of a neurological lesion or disease is, thus, clearly not sufficient for the development of neuropathic pain. It appears to be the secondary changes, the induced dysfunctions of the peripheral and central nociceptive systems rather than the lesion itself (Bouhassira and Attal, 2019).

Table 2. Disease-based and anatomy-based classification of neuropathic pain. Adapted from (Baron *et al.*, 2010; Scholz *et al.*, 2019).

Peripheral neuropathic pain
Focal, multifocal
Trigeminal neuralgia Peripheral nerve lesion (posttraumatic or post-surgical) Post-herpetic neuralgia (herpes zoster) Painful radiculopathy (lesions or disease involving cervical, thoracic, lumbar, or sacral nerve roots) Phantom pain, stump pain
Generalized (polyneuropathies)
Metabolic or nutritional (diabetes, hypothyroidism) Infectious, inflammatory, or immune disease (HIV infection, Guillain-Barré syndrome) Neurotoxic (chemotherapy, antiretroviral, thalidomide, acrylamide, arsenic) Hereditary (Charcot-Marie-Tooth disease, erythromelalgia) Malignant (carcinoma-associated, myeloma)
Central neuropathic pain (associated or caused by):
Spinal cord injury (posttraumatic or post-surgical) Brain injury (posttraumatic or post-surgical) Central post-stroke pain (cerebrovascular lesion, infarct, or hemorrhage) Multiple sclerosis Inflammatory diseases other than multiple sclerosis (syphilis) Neurodegenerative diseases (Parkinson's disease) Other (syringomyelia and syringobulbia, epilepsy, tumors)

2.4.2 Epidemiology

Neuropathic pain affects millions of people worldwide, although it is usually underdiagnosed and undertreated (Colloca *et al.*, 2017). This clinical entity has pathogenic mechanisms that remain largely unknown, and current treatments are limited by the lack of efficacy and significant side effects (Bouhassira and Attal, 2018). Thus, neuropathic pain represents a challenge to health care and an enormous economic burden

for society, estimating a cost of billions of euros costs for the European population (Breivik *et al.*, 2013).

Estimating the exact incidence and prevalence of neuropathic pain has been difficult because of the lack of simple diagnostic criteria and the heterogeneity of clinical characteristics. According to general European population studies, the prevalence of chronic pain with neuropathic characteristics has been estimated to be in the range of 7–10% (Bouhassira *et al.*, 2008; Van Hecke *et al.*, 2014), however, taking into account specific subpopulations suffering other pathological conditions, such as diabetes (20-30%) (Abbott *et al.*, 2011) HIV infection (50%) (Schütz and Robinson-Papp, 2013), or cancer (30-40%) (Bennett *et al.*, 2019), the incidence is much higher.

2.4.3 Clinical characteristics

Nociceptive and sensorial manifestations

Clinically, neuropathic pain is characterized by altered sensations comprising negative and positive symptoms **(Table 3). Negative symptoms** indicate reduced impulse conduction in the neural tissues producing deficits in different somatosensory qualities, which are uncomfortable but not painful. These include hypoesthesia, anesthesia, and hypoalgesia. Conversely, **positive symptoms** refer to abnormal painful sensations, which can be spontaneous or evoked by stimulation, reflecting an enhanced level of excitability in the nervous system (Baron *et al.*, 2010). Spontaneous positive symptoms include paresthesia and dysesthesia, as well as paroxysmal and ongoing superficial pain. The classic stimulus-evoked positive symptoms are **allodynia and hyperalgesia**, two of the most typical clinical sensory alterations manifested in patients with neuropathic pain (Scholz *et al.*, 2019)**.** Other symptoms and clinical

findings (e.g., motor paresis, muscle cramps, and autonomic nervous symptoms) may also appear depending on the injury site. (Merskey H *et al.*, 1994).

Table 3. Definition and classification of common symptoms suggestive of neuropathic pain. Adapted from (Merskey H *et al.*, 1994; Baron *et al.*, 2010).

Negative symptoms	
Hypoesthesia	Reduced sensation to non-painful stimuli
Anesthesia	Lack of stimulation or loss of sensation
Hypoalgesia	Reduced sensation to normally painful stimuli
Positive symptoms	
Spontaneous pain	
Paresthesia	Non-painful ongoing sensation
Dysesthesia	Unpleasant sensation
Paroxysmal pain	Intermittent spontaneous pain (shooting electrical attacks)
Stimulus-evoked pain	
Hyperalgesia	Increased response to a normally painful stimulus

Apart from sensory alterations, neuropathic pain often associates with other problems, such as loss of function, anxiety, depression, disturbed sleep, and impaired cognition. These comorbid symptoms could be caused by the persistence of pain experience *per se* or by the original etiologies of chronic pain. They can negatively affect the life quality of patients on the one hand and further aggravate the sensory abnormalities of chronic pain on the other hand.

Cognitive manifestations

Cognitive impairment is commonly associated with the persistence of pathological pain experience (Moriarty *et al.*, 2011). Dysfunction of a wide range of cognitive domains, including attention, concentration, memory, decision-making, and executive function, have been reported in

individuals suffering from neuropathic pain (Apkarian *et al.*, 2004; Muñoz and Esteve, 2005), as well as in preclinical animal (La Porta *et al.*, 2016; Martínez-Navarro *et al.*, 2020). Several theories have arisen regarding the mechanisms that mediate cognitive impairment in persistent pain, suggesting a reciprocal modulation since some neuroanatomical substrates involved in cognition, such as the medial PFC and the hippocampus, also participate in pain processing. Precisely, it is suggested that chronic pain-induced cortical and hippocampal plasticity may underlie cognitive impairments through central sensitization (Woolf, 2011) and long-term potentiation-dependent mechanisms (D. Liu *et al.*, 2014).

Emotional manifestations

Emotional alterations frequently accompanied neuropathic pain in a prevalence ranging from 33% to 42% (Langley *et al.*, 2013). Clinical studies consistently report that patients with neuropathic pain are afflicted with depression and anxiety disorder, a pattern also seen in animal models (Liu and Chen, 2014; Doan *et al.*, 2015; Descalzi *et al.*, 2017). A variety of animal studies have been conducted to assess **anxiety-like behavior** in multiple types of preclinical models of pathological pain, such as partial-sciatic nerve ligation (La Porta *et al.*, 2016; Martínez-Navarro *et al.*, 2020), postherpetic neuralgia (Hasnie *et al.*, 2007) or chemotherapy (Toma *et al.*, 2017), showing enhanced anxiety-related symptoms. Depression represents another comorbid symptom frequently suffered by chronic pain patients (Nicolson *et al.*, 2009). The development of **depressive-like behavior** was reported by extensive preclinical research in animals following a nerve injury (Gonçalves *et al.*, 2008; Leite-Almeida *et al.*, 2009; Wang *et al.*, 2011) or chemotherapy treatment (Toma *et al.*, 2017), shown

by a prolonged immobility time in the forced swimming test and decreased sucrose preference (indicative of anhedonia).

There is a complex reciprocal relationship between persistent pain and emotional alteration since chronic pain can induce negative affective states, contributing to worsening pain perception (Bushnell *et al.*, 2013) **(Figure 17).**

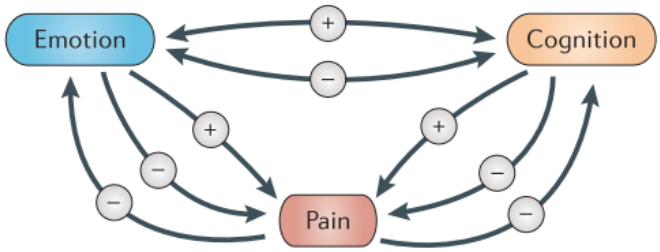

Figure 17. Feedback loop between pain, emotions and cognition. Pain can have adverse effects on emotions and cognitive function. Conversely, a negative emotional or cognitive state can increase pain, whereas a positive condition can reduce it. Naturally, emotions and cognition can also reciprocally interact. Adapted from (Bushnell *et al.*, 2013).

2.4.4 Pathophysiology of neuropathic pain: focus on the role of glial cells

Our knowledge of pathological pain has revolved around neuronal mechanisms. However, a great body of evidence has shown that the processes underlying pathological pain, notably neuropathic pain, are not limited to an aberrant neuronal activity, as previously thought. In this context, glial cells have emerged as powerful contributors to pathological and chronic pain processes (Milligan and Watkins, 2009). Microglia and astrocytes generate signaling molecules upon activation, which can have

either neuroprotective or pathogenic effects. Glial activation in the spinal cord is a common underlying mechanism that leads to pathological pain in several pain syndromes with widely different etiologies, including diabetic neuropathy, chemotherapy-induced neuropathy, peripheral nerve inflammation, and trauma (Watkins *et al.*, 2006).

2.4.4.1 Role of glia in pathological pain processing

After repeated synaptic communication, which occurs in response to persistent noxious stimuli such as following peripheral nerve injury, primary afferent neurons overexpress neurotransmitters such as glutamate, ATP, and substance P, resulting in long-term central sensitization, which leads to transcriptional changes and altered function of dorsal horn neurons **(Figure 18)**. **Astrocytes** and **microglia** both express different receptors for these neurotransmitters and are so activated under certain conditions. For instance, resident microglia express a variety of purinergic receptors, which are triggered by ATP produced by injured neurons or astrocytes (or both). The activation of these receptors stimulates microglia to release BDNF, which activates its neuronal receptors (Tsuda and Inoue, 2016). In particular, $P2X_4R$ and $P2X_7R$ purinoreceptors have been implicated in neuropathic pain by experiments that inhibited receptor activity pharmacologically and genetically (Ulmann *et al.*, 2008; Sorge *et al.*, 2012). Once activated, astrocytes and microglia exert their influence on neural pain processing circuitry via soluble mediators. Notably, ongoing excitation induces the activation of mitogen-activated protein kinases (MAPK) signaling pathways such as those involving ERK, p38, and JNK in both glial cells, leading to the activation of NF-κB transcription factor that promotes the synthesis of **pro-inflammatory factors** such as IL1β, IL6, TNFα, CCL2 and PGE2, and other

factors such as ROS and NO **(Figure 18)** (Milligan and Watkins, 2009). These immune mediators can directly modulate excitatory synaptic transmission at central terminals, principally by enhancing glutamate release. In this context, with continuous exposure to high amounts of synaptic glutamate, the astrocyte glutamate transporters EAA1 and 2 (GLT1 and GLAST in rodents) become dysregulated or are persistently downregulated, leading to excitotoxicity (Sung *et al.*, 2003) **(Figure 18)**. Similarly, such immune mediations also decrease inhibitory signaling in the spinal dorsal horn by reducing the release of GABA and glycine from interneurons and descending inhibitory projections (Kawasaki *et al.*, 2008). Overall, the ultimate consequence is an increase in nociceptive hypersensitivity and an unmasking of responses to innocuous peripheral inputs.

Although astrocytes and microglia are comparable in certain aspects of local immunological signaling, their roles are likely to differ in terms of activation patterns and the transition from acute to chronic stages. Microglia are thought to be the first to respond to injury-induced factors released from damaged neurons by promoting the initial production and secretion of pro-inflammatory cytokines, whereas astrocytes are activated with a slower onset and longer time course, reflecting their primary role in maintaining chronic pain hypersensitivity rather than initiating it (Ji *et al.*, 2013).

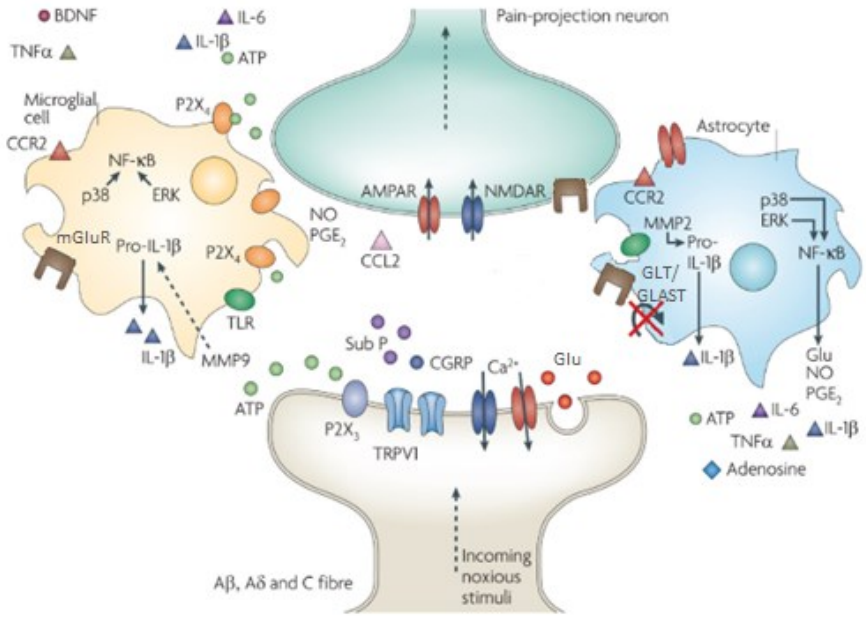

Figure 18. Glia activation and molecules involved under pathological pain processing. After intense stimulation or persistent injury, activated C and Aδ nociceptors release a variety of neurotransmitters, including glutamate (Glu), substance P (Sub P), calcitonin gene-related peptide (CGRP), and ATP, onto pain-projection neurons in the dorsal horn. As a result, a sustained central sensitization is produced, leading to maladaptive changes and altered neuronal function. Astrocytes and microglia respond to this ongoing synaptic activity by releasing excitatory neurotransmitters such as glutamate (Glu) and ATP, and pro-inflammatory factors like TNFα, IL-1β, IL-6, NO, and PGE2. These factors promote increased excitability and enhanced pain in response to both noxious and innocuous stimulation. Adapted from (Milligan and Watkins, 2009).

2.4.4.2 Protective roles of glia

A reactive phenotype does not imply a pro-inflammatory or pro-nociceptive phenotype. In fact, a fast, well-regulated immune response to neuronal insult is critical for regulating gliosis and clearing tissue debris to enable neuroregeneration. For example, studies with transgenic TNFα-knockout animals demonstrated that endogenous microglial TNFα was crucial for the resolution of an inflammatory response and excitotoxic cell

death in a model of NO-induced neurotoxicity (Blais and Rivest, 2004). Furthermore, while a lack of TNFα reduced microglial activation within 6 hours in these mice, it was exacerbated 4 days later. Hence, the timing of TNFα activity may be critical for neuroprotection, and the early reactive cascade may be crucial for such control.

Both astrocytes and microglia can also release **anti-inflammatory factors** such as IL-10 and IL-4. On the one hand, these molecules may facilitate the clearance of apoptotic cells and tissue debris by inducing the expression of several receptors that recognize surface proteins of altered cells to phagocyte them and, on the other hand, they may indirectly inhibit the synthesis of pro-inflammatory cytokines and chemotactic factors by microglia and T cells (Milligan and Watkins, 2009).

Overall, these mechanisms help to dampen and halt continued pro-inflammatory actions. However, under chronic pathological conditions, these immune-regulatory processes often become dysfunctional, generating an imbalance between the protective and harmful effects of activated glial cells.

2.4.4.3 Glia and sex differences in pain

Most patients with chronic pain are women; yet, most preclinical studies have been conducted in male rodents, making it hard to establish whether this bias translates to genuine sex differences in pain sensitivity (Mogil, 2012). Nonetheless, pain-related sex differences have been receiving increased attention in recent years. In this context, a growing body of data suggests that immune cells, particularly microglial cells, exhibit sex dimorphism in pain processing. An interesting suggestion is that microglia only play a role in males, while in females, infiltrating T lymphocytes mediate neuropathic pain signaling in the spinal cord (Sorge *et al.*, 2011,

2015). First, Sorge et al. found that pain resulting from inflammation or nerve injury depends on spinal Toll-like receptor 4 (TLR4) in male, but not female, mice (Sorge *et al.*, 2011). Moreover, interruption of microglial activity, either pharmacologically or genetically, relieved allodynia in male mice only (Sorge *et al.*, 2015). Interestingly, this sex-specific microglial response was testosterone-dependent since minocycline (microglia inhibitor) did not alleviate allodynia in castrated males but did in testosterone-treated females (Sorge *et al.*, 2015). In contrast, female mice exhibited increased T cell infiltration after nerve injury, relative to males, suggesting that T cells might promote allodynia in females, as microglia do in males (Sorge *et al.*, 2015). Notably, microglial hypertrophy and proliferation did not differ between sexes, as shown by comparable microgliosis and expression of CX3CR1and IBA-1 (Sorge *et al.*, 2015; Taves *et al.*, 2016). However, nerve injury induced phosphorylated p38 (p-p38) in spinal microglia predominantly in male mice (Taves *et al.*, 2016). Nonetheless, other authors found an increase of p-p38 in both microglia and astrocytes in female mice following nerve injury (Vacca *et al.*, 2014), indicating that spinal p38 activation is not necessarily male-specific.

Interestingly, whereas sex appears to govern the role of microglia to pain etiology, inhibiting astrocyte activation attenuates pain equally in males and females in preclinical models, indicating that astrocytes may participate similarly (Chen *et al.*, 2018; Ji *et al.*, 2019), although more investigation is needed to draw conclusive affirmations. It's worth noting that clinical studies in humans have yet to show that microglia play a sex-specific role in pain, and both microglia and astrocytes have been reported to be activated in both sexes (Mapplebeck *et al.*, 2017).

2.4.5 Therapeutic approaches for neuropathic pain

Neuropathic pain is widely recognized as one of the most difficult pain syndromes to manage. Nowadays, there is no fully effective treatment to palliate all neuropathic pain symptoms despite the many approaches available. Moreover, there is evidence of inappropriate drug use in treating this condition (Attal *et al.*, 2011; Torrance *et al.*, 2013), which is partly because neuropathic pain is often underdiagnosed. This difficulty in diagnostic and treatment might result from the heterogeneity of neuropathic pain mechanisms, the inter-individual variability of neuropathic pain symptoms, and the frequently coexisting psychological and emotional comorbidities. In addition, treatments available so far are often directed to diminish pain and help patients cope with their symptoms rather than suppress pain (Woolf and Mannion, 1999). Thus, in clinical practice, this complexity is considered by an interdisciplinary therapeutic approach, including pharmacological and non-pharmacological therapies, to provide the greatest pain relief with the fewest side effects.

Regarding **pharmacological therapies**, neuropathic pain is usually refractory to traditional pain therapies (Costigan *et al.*, 2009). Recommended pharmacotherapy for neuropathic pain is listed and detailed in **Table 4** below, based on the latest guidelines published by the NeuPSIG (Finnerup *et al.*, 2015; Attal, 2019). **First-line** therapy mainly includes non-opioid medications such as tricyclic antidepressants (TCAs), dual serotonin-norepinephrine reuptake inhibitors (SNRIs), and gabapentanoids. TCAs and SNRIs exert a pain-relieving effect by inhibiting the reuptake of serotonin and noradrenaline, thereby increasing inhibitory control. Besides their analgesic effects, TCAs and SNRIs are considered

first-line therapy due to their antidepressant properties, which may also benefit the emotional comorbidities associated with chronic neuropathic pain (Baron *et al.*, 2010; Bates *et al.*, 2019). Gabapentanoids include gabapentin and pregabalin, and are a group of anticonvulsants that act by blocking presynaptic α2δ calcium channels at the level of the spinal dorsal horn, thus inhibiting neurotransmitter release, reducing excitability of afferent neurons and facilitating descending inhibitory control of pain (Patel and Dickenson, 2016), which altogether contribute to ameliorate neuropathic pain symptoms. **Second-line** treatments include topical agents and tramadol. Topical medications include lidocaine patches and capsaicin, and are topically administered to relieve focal peripheral neuropathic pain (Attal, 2019; Bates *et al.*, 2019), although their therapeutic gain is modest compared with placebo (Demant *et al.*, 2015). Lidocaine works by decreasing ectopic firing of peripheral nerves through nonspecific block of Na^+ channels on ectopic peripheral afferent fibers, whereas capsaicin acts by activating and desensitizing transient receptor potential (TRP) vanilloid type-1 (TRPV1) receptors in the nociceptors, thus reducing peripheral sensitization and alleviating neuropathic pain (Attal *et al.*, 2010). Tramadol is a weak opioid agonist with serotonin and norepinephrine reuptake inhibition, which has been found beneficial mainly in peripheral neuropathic pain (Attal, 2019). However, it should be used with caution in association with first-line medications such as antidepressants (Finnerup *et al.*, 2015).

The analgesic effects of opioid agonists in neuropathic pain are mediated by reducing the excitability of afferent neurons, modulating pain integration in supraspinal areas, and increasing descending inhibition of pain transmission into the dorsal horn (Nadal *et al.*, 2013). Strong opioids, particularly oxycodone and morphine, have been reported to be

moderately effective in peripheral neuropathic pain (Finnerup *et al.*, 2015; Attal, 2019). However, these compounds have the potential to develop tolerance and dependence, as well as significant side effects. For this reason, the clinical use of opioids is restricted to **third-line** therapy (Finnerup *et al.*, 2015; Attal, 2019), even though current guidelines suggest that opioids should be firmly considered **fifth-line**, due to their dependence/side effect profile, after a trial of neurostimulation has been attempted first (Bates *et al.*, 2019).

Finally, since opioids should be relegated to the last option, for patients who do not tolerate or do not achieve sufficient pain relief from first- or second-line therapy, it may be considered the use of serotonin-specific reuptake inhibitors (SSRIs), other anticonvulsants, such as carbamazepine or topiramate, and N-methyl-D-aspartate (NMDA) antagonists, although with an inconclusive level of evidence (Finnerup *et al.*, 2015; Attal, 2019).

Non-pharmacological treatments are also important to consider in the treatment plan for managing neuropathic pain to address depression, anxiety, sleep disturbance, or social interactions. It is worth mentioning the benefits of exercise, massage, and supportive psychotherapy (Evans *et al.*, 2003; Bates *et al.*, 2019).

Table 4. Evidence-based recommendations for pharmacotherapy of neuropathic pain. Adapted from (Finnerup *et al.*, 2015; Attal, 2019).

Drug	Mechanism of action
Strong recommendations for use	
First-line therapy	
Antidepressants	
Tricyclic antidepressants (TCAs)	Monoamine reuptake inhibition; sodium channel blocking; anticholinergic effects
Serotonin–norepinephrine reuptake inhibitors (SNRIs)	Serotonin and norepinephrine reuptake inhibition
Anticonvulsives	
Gabapentin Pregabalin	Act on α2δ subunit of voltage-gated calcium voltage-gated calcium channels
Weak recommendations for use	
Second-line therapy	
Topical agents	
Lidocaine (5% patches)	Sodium channel blockade
Capsaicin (high concentration patches – 8%)	TRPV1 agonist
Opioids (weak)	
Tramadol	μ-receptor agonist and inhibition of monoamine reuptake
Third-line therapy	
Opioids (strong) – Low dose	
Morphine, Oxycodone	μ-receptor agonists; oxycodone may also act as kappa receptor agonist
Inconclusive recommendations for use	
Tapentadol NMDA antagonists Serotonin-selective reuptake inhibitors (SSRI) Other anticonvulsives (Carbamazepine, Topiramate)	

It is important to note that no one drug works for all patients, pain relief is usually partial, and side effects often limit the ability to achieve

adequate pain control with a single agent, leading either to discontinuation of the treatment or to use of more than one drug to optimize pain control. Indeed, a combination of two or more drugs is often used in clinical practice to achieve satisfactory pain relief (Namaka *et al.*, 2009). Moreover, current therapeutic strategies for neuropathic pain mainly target neuronal components to finally modulate neural activity. Therefore, considering that the involvement of glial cells in the development of neuropathic pain is now well established, the targeting of these cells may provide an exceptional opportunity to progress to a new disease-modifying therapeutic approach. In this regard, this thesis offers the tools and preliminary findings to further validate potential targets within the transcriptome of glial cells exposed to (drug-related) polyneuropathy.

2.4.6 Experimental models for neuropathic pain evaluation

Animal models of neuropathic pain have been crucial in the last decades to study the mechanisms underlying the pathophysiology of this disease and to design novel therapeutic strategies for clinical use (Bridges *et al.*, 2001). Several successful models have been developed to mimic neuropathic pain evoked by damage to the central or peripheral nervous system and different etiologies. They can be classified in many ways, but there are five main categories, namely central pain models, peripheral nerve injury models, drug-induced neuropathic pain, disease-induced neuropathic pain, and miscellaneous (Colleoni and Sacerdote, 2010; Kumar *et al.*, 2018). **Table 5** summarizes the main neuropathic pain experimental models.

Table 5. Classification of main neuropathic pain models. Adapted from (Colleoni and Sacerdote, 2010; Kumar *et al.*, 2018).

Central pain
• ***Spinal cord injury***
Excitotoxins, contusion, photochemical model
• ***Spinal hemisection***
• ***Thalamic syndrome***
Peripheral nerve injury
• ***Complete lesion***
Sciatic nerve transection (neuroma model)
Brachial plexus avulsion
• ***Partial lesion***
Sciatic nerve chronic constriction injury (CCI)
Partial sciatic nerve ligation (PSNL)
Spinal nerve ligation (SNL)
Spared nerve injury (SNI)
Drug-induced neuropathy
• ***Chemotherapeutic agents***
Vincristine, Cisplatin, Taxanes
• ***Anti-retroviral drugs***
Didanosine, Zalcitabine, Stavudine
Disease-induced neuropathy
Diabetes (streptozotocin-induced peripheral diabetic neuropathy)
Cancer pain model
HIV-induced
Post herpetic neuralgia model
Miscellaneous
Inherited-induced neuropathies (Charcot-Marie-Tooth)
Ethanol consumption/withdrawal-induced neuropathy
Pyridoxine (vitamin B6)-induced neuropathy
Uremic peripheral neuropathy (end-stage kidney disease)

Among the available models, drug-induced neuropathic pain models are helpful to study the specific causes producing the neuropathic phenotype, but also the prevention and treatment of their neurotoxicity (Colleoni and Sacerdote, 2010). In this context, chemotherapeutic agents used to treat

cancer often produce peripheral neuropathy as a severe side effect being a limiting factor for achieving effective doses to treat the underlying pathology. Predictable and uniform neurotoxicity is produced by these agents inducing a neuropathy that can occur as early as the first treatment and may last indefinitely (Boyette-Davis *et al.*, 2013), which suggests its potential use to study the specific alterations involved in the onset, progression, and chronification of pain.

3 Chemotherapy-induced peripheral neuropathy

3.1 Epidemiology and risk factors

Cancer is currently a leading cause of mortality worldwide. Fortunately, thanks to advances in medicine and modern technology, the number of cancer survivors is rising. Estimates for 2020 suggested that, of all new cases, 66% will survive for at least five years, and 40% will be alive more than ten years after the diagnosis (Glare *et al.*, 2014). Although these patients may survive cancer, many have poor outcomes that reduce their quality of life because of cancer treatment. Indeed, between 19% to more than 85% of patients receiving chemotherapy suffer from moderate to intense pain, which may persist for months or even years after the cessation of chemotherapy (Fallon and Colvin, 2013). This common condition is known as **chemotherapy-induced peripheral neuropathy (CIPN)**, and it is a severe and dose-limiting adverse effect of most chemotherapeutic agents. CIPN can result in dose interruptions and subtherapeutic dosing, or even discontinuation of therapy, in turn negatively impacting cancer progression (Cavaletti and Marmiroli, 2010; Carozzi *et al.*, 2015; Zajaczkowską *et al.*, 2019).

Painful CIPN can begin after the first dose of chemotherapy and is often related to cumulative dose. Once CIPN develops, there is a high likelihood that it will become a chronic condition. Indeed, persistent symptoms are observed in 68% and 30% of patients within the first month and six months after cessation of chemotherapy (Seretny *et al.*, 2014). Several predisposing risk factors of CIPN have been identified, including patient age, pre-existing neuropathy before starting chemotherapy, lifestyle, and genetic factors (Seretny *et al.*, 2014; Flatters *et al.*, 2017). Nevertheless, the development, the incidence, and the severity of CIPN depend not only

on individual risk factors but also on the cumulative dose, treatment duration, and drug used (Carozzi *et al.*, 2015).

3.2 Clinical characteristics

The effects of chemotherapy on the nervous system vary among the different drugs, depending on the specific physical and chemical properties of the drug used and its single or cumulative doses (Banach *et al.*, 2017). Generally, clinical signs of CIPN involve deficits in sensory, motor, and autonomic functions of varying intensity. **Sensory symptoms** usually develop first and are commonly presented in a "stocking and glove" type distribution, progressing from the distal to the proximal regions (Carozzi *et al.*, 2015). These symptoms comprise numbness, tingling, paresthesia, dysesthesia, and more painful sensations such as spontaneous pain, mechanical or thermal allodynia/hyperalgesia, and even sensory loss in severe cases. **Motor and autonomic symptoms** occur less frequently and involve distal weakness, gait and balance disturbances, as well as orthostatic hypotension, constipation and altered sexual or urinary function, respectively (Argyriou *et al.*, 2012; Cavaletti and Marmiroli, 2015; Zajaczkowską *et al.*, 2019). These symptoms have a marked and often underappreciated impact on quality of life and safety.

3.3 Pathophysiology of chemotherapy

3.3.1 Antineoplastic mechanisms

Chemotherapeutic drugs that cause CIPN are, however, used as standard, routine medications against the most common types of cancer. The most neurotoxic groups of antineoplastic drugs are the platinum derivatives (oxaliplatin and cisplatin), the taxanes (paclitaxel), and thalidomide and its analogs. However, other less neurotoxic but also commonly used drugs

are bortezomib and vinca alkaloids (vincristine) (Starobova and Vetter, 2017) **(Table 6)**. Indeed, paclitaxel, oxaliplatin, and vincristine are the three most used chemotherapeutic drugs. The mechanisms of action of chemotherapeutic agents that lead to potent antimitotic effects are well-described **(Table 6)** and are often linked to the development of their neurotoxicity, implying the apparent difficulty in reducing toxicity without diminishing their anticancer efficacy.

Table 6. Characteristics of CIPN-inducing drugs routinely used in cancer treatment. Incidence and antineoplastic mechanism of action. Adapted from (Velasco and Bruna, 2010).

Drug	Mechanism of action	Neuropathy incidence
Platinum-based drugs Oxaliplatin Cisplatin	DNA-cross-linking (formation of platinum-DNA adducts)	70-100%
Taxanes Paclitaxel Decetaxel	Microtubule formation impairment and cell-cycle arrest	11-87%
Thalidomide and analogues	Antiangiogenesis immunomodulation	20-60%
Bortezomib	Proteasome inhibition	20-30%
Vinka alkaloids Vincristine Vinblastine	Microtubule formation impairment and cell-cycle arrest	Up to 20%

The platinum-based chemotherapeutic agents **oxaliplatin and cisplatin** are used for the treatment of various solid tumors. Oxaliplatin is used first-line and adjuvant colorectal cancer therapy, while cisplatin is one of the most effective treatments for small cell lung cancer, testicular, ovarian, brain, and bladder cancer. These compounds exert chemotherapeutic effects by binding to cellular DNA and creating intra-strand crosslinks, also

called platinum (Pt)-DNA adducts. These Pt-DNA adducts, in turn, inhibit DNA replication and transcription, finally leading to apoptosis cell death of cancer cells (Carozzi *et al.*, 2015; Ibrahim and Ehrlich, 2020).

Paclitaxel belongs to the family of taxanes, widely used to treat breast, prostate, lung, pancreatic, gynecological, and other solid tumors. These drugs act by inhibiting the disassembly of tubulin from the microtubule polymer, leading to disturbance of interphase processes and cell death (Starobova and Vetter, 2017).

Vincristine, a type of vinca alkaloid, is one of the most common anticancer drugs clinically employed in pediatric and adult hematologic cancers such as acute lymphoblastic leukemia and Hodgkin's lymphoma, but also in a range of other adult tumors, including non-small cell lung cancer and testicular cancer. Its primary mechanism of action is through binding to tubulin to disrupt polymerization and microtubular assembly, leading to aborted cell division and cell death. As with taxanes, the disruption of microtubule assembly and disassembly results in severe alterations on nervous fibers, including loss of intact axonal microtubules and changes in their length, arrangement, and orientation. These effects lead to the impairment of neuronal transport and axonal degeneration (Carozzi *et al.*, 2015; Fumagalli *et al.*, 2021).

3.3.2 Pathological mechanisms of CIPN

Chemotherapy treatments result in numerous changes to cellular structure and function, including alterations to membrane receptors and ion channels, neurotransmission, and intracellular signaling and organelles, all of which can negatively influence neuronal and glial cell phenotypes, thereby contributing to CIPN (Flatters *et al.*, 2017; Starobova

and Vetter, 2017; Zajaczkowską *et al.*, 2019). Here, we review the state-of-art of these previously cited mechanisms involved in CIPN and the contribution of the different chemotherapeutic agents **(Figure 19)**.

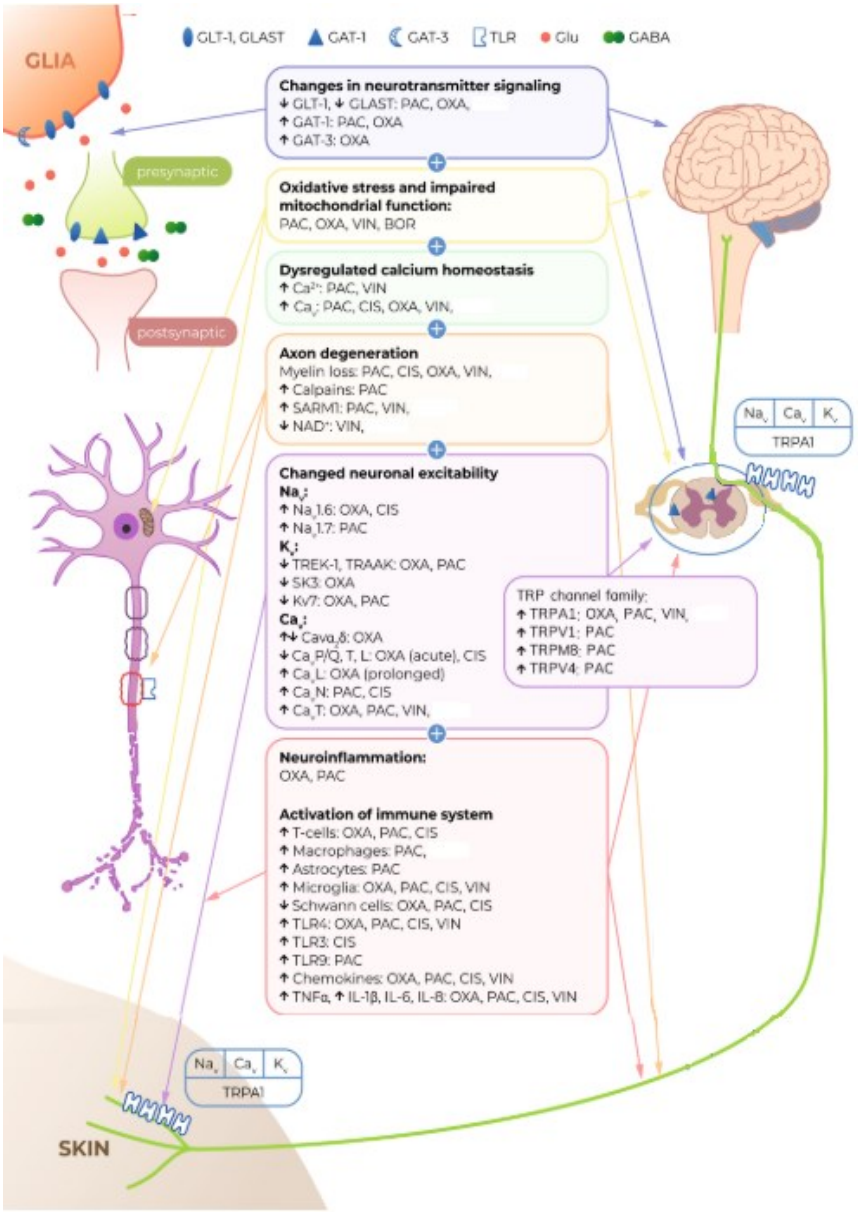

Figure 19. Main mechanisms underlying CIPN induced by most common chemotherapeutic agents. CIPN is a multifactorial disorder with many common

pathological mechanisms, including altered ion channel functions, oxidative stress, mitochondrial dysfunction, axonal degeneration, neuroinflammation, and activation of immune and glial cells. PAC: paclitaxel, VIN: vincristine, OXA: oxaliplatin, CIS: cisplatin. Adapted from (Sałat, 2020).

Changes in ion channels and receptors

Chemotherapeutic agents cause changes to peripheral nerve excitability that contribute to the development of peripheral sensory neuropathy. It is likely caused by altered expression and function of a range of ion channels, including sodium (NaV), potassium (KV), and calcium (CaV)-voltage-gated channels, as well as the transient receptor potential (TRP) channels **(Figure 19)**. The **NaV channels** are among the most abundant voltage-gated ion channels and are strongly implicated in CIPN development and maintenance for agents. Experimental studies *in vivo* confirmed the involvement of Na_v 1.7 and Na_v 1.9 channels in oxaliplatin (Ghelardini *et al.*, 2010; Lolignier *et al.*, 2015b) and paclitaxel-involved CIPN (Li *et al.*, 2018). Alterations in **KV channel's** function have also been noted at several levels. These channels are downregulated in cortical and DRG neurons of rats treated with oxaliplatin (Descoeur *et al.*, 2011; Thibault *et al.*, 2012) and in the DRG of rats with paclitaxel-related CIPN (Zhang and Dougherty, 2014), resulting in spontaneous activity of nociceptors that corresponds to the development of neuropathic pain. In addition, increased levels of **CaV channel** mRNA have been reported in DRG following paclitaxel treatment in mice (Li *et al.*, 2017), thus probably contributing to CIPN. The **TRP channels**, especially the TRP vanilloid (TRPV) family, have been widely studied regarding CIPN. The TRPV1, TRPA1 (TRP ankyrin), and TRPM8 (TRP melastatin) channels are expressed in DRG neurons. A few preclinical studies have shown that they play a crucial role in thermal and mechanical sensitivity induced by cisplatin, oxaliplatin,

bortezomib, and paclitaxel (Flatters *et al.*, 2017; Boyette-Davis *et al.*, 2018; Zajaczkowską *et al.*, 2019).

Numerous studies have also documented alterations in processes involved primarily in **neurotransmitter signaling** following chemotherapy treatment **(Figure 19)**. The contribution of **glutamate** to CIPN has been revealed by pharmacological inhibition of glutamate receptors and production, improving nerve conduction deficits following cisplatin and paclitaxel (Carozzi *et al.*, 2015). Moreover, glutamate transporters GLT1 and GLAST are diminished following treatment with paclitaxel and vincristine in spinal astrocytes (Robinson and Dougherty, 2015), thereby reducing glutamate clearance by astrocytes can lead to increased responses of spinal neurons to nociceptive input (Matute *et al.*, 2006). In addition to decreased glutamate reuptake, increased synaptic **GABA** reuptake resulting from the enhanced GABA receptors GAT-1 and GAT-3 function should also be considered a phenomenon implicated in CIPN development (Sałat, 2020). There is also evidence for the involvement of **serotonin** receptors and transporters in CIPN, with 5HT2A knockout mice showing protection against the development of vincristine-induced CIPN (Thibault *et al.*, 2008). Changes to other neurotransmitter receptors have also been observed in animal models of CIPN, including cannabinoid receptors (Uhelski *et al.*, 2015; King *et al.*, 2017) and A3 adenosine receptors (Janes *et al.*, 2014), proving potential avenues for new treatments.

Mitochondrial damage and oxidative stress

Mitochondria are involved in many critical cellular processes, including energy production, storage of intracellular calcium and calcium signaling, apoptosis, and cell metabolism. In physiological conditions, mitochondria

produce small amounts of ROS such as peroxide, superoxide, and hydroxyl radicals as a product of oxygen metabolism, which carries out essential functions in cell signaling.

Most chemotherapeutic agents can cause **mitochondrial damage and dysfunction.** The impairment of the mitochondrial physiological function leads to increased production of ROS and thus to increased **oxidative stress**, which can worsen mitochondrial function in a feedback loop **(Figure 19)**. Some in vivo preclinical studies suggest that mitochondrial ROS is causal to the development and maintenance of CIPN. Paclitaxel and oxaliplatin have been reported to increase mitochondrial production of ROS (Hui *et al.*, 2013; Toyama *et al.*, 2014). The pathological increase in ROS production can cause damage to intracellular enzymes, proteins, and lipid molecules, which in turn leads to demyelination and disruption of the cytoskeleton of peripheral nerves, resulting in altered signal transduction (H. Zheng *et al.*, 2011).

Furthermore, ROS can activate the apoptotic and proinflammatory pathways, thus further contributing to chronic CIPN (Areti *et al.*, 2014). To understand how ROS are managed endogenously, several studies examined the activity of different antioxidant enzymes in the DRG and peripheral sensory neurons, showing either an enhanced activity of these enzymes (Duggett *et al.*, 2016) or an impaired mitochondrial antioxidant response after paclitaxel, oxaliplatin and bortezomib (Janes *et al.*, 2013). In this regard, supplementation with acetyl-L-carnitine (ALC), which has antioxidant properties, showed initial promising results in preventing the development of these alterations (Flatters *et al.*, 2006). However, subsequent trials found that ALC not only fails to have a significant ameliorating effect but can worsen CIPN (Hershman *et al.*, 2013).

Damage to DNA due to the direct effect of chemotherapeutics and ROS production has also strongly been implicated in CIPN (Areti *et al.*, 2014). Through binding to mitochondrial DNA (mDNA), oxaliplatin and cisplatin form mDNA adducts, which cannot be repaired since mitochondria do not express DNA repair systems. These mDNA adducts lead to the synthesis of abnormal proteins, resulting in the impairment of the respiratory chain in mitochondria and thus, mitochondrial dysfunction and cell death (Canta *et al.*, 2015). Contrary to platinum-based agents action, the effects of vincristine likely involve altered mitochondrial Ca^{2+} signaling (Canta *et al.*, 2015; Carozzi *et al.*, 2015), leading to activation of apoptotic pathways, alteration in neuronal excitability, and dysfunction of glial cells. Like vincristine, paclitaxel does not directly affect mDNA but induces swollen and vacuolated mitochondria in C fibers and A-fibers (Flatters and Bennett, 2006), as well as a significantly decreased activity in mitochondrial respiratory chain complexes I and II. These changes were also observed following treatment with oxaliplatin and bortezomib (H. Zheng *et al.*, 2011; Zheng *et al.*, 2012).

Immune system and glial cells alterations

Chemotherapy agents are well known to cause profound effects on the immune system, mainly transient immunosuppression due to cytotoxic activity targeting rapidly dividing immune cells. Conversely, many chemotherapeutics can also activate the immune system, an effect that is suggested as a key contributor to support the destruction of tumor cells (Westbom *et al.*, 2015), but also the development of CIPN through the induction of a neuroinflammatory process **(Figure 19)**. Accordingly, the immune response induced by chemotherapeutics varies significantly in nature, with paclitaxel and vincristine involving a robust inflammatory

component that seems to be less severe during oxaliplatin-induced CIPN (Sisignano *et al.*, 2014). Indeed, it was recently shown that vincristine dysregulates genes associated with immunological processes, while oxaliplatin causes dysregulation of genes associated with neuronal function (Starobova *et al.*, 2020). Animal models have implicated the effects of chemotherapeutics on the innate and adaptive immune system (Kiguchi *et al.*, 2008a; X. J. Liu *et al.*, 2014), as well as on peripheral and central glial cells (Robinson *et al.*, 2014; Lee and Kim, 2020; Qin *et al.*, 2020) **(Figure 19)**.

Paclitaxel increases the activity and infiltration of macrophages and pro-inflammatory T cells into the DRG (X. J. Liu *et al.*, 2014; Zhang *et al.*, 2016). Similarly, macrophages activity in the DRG is also elevated in other models of neuropathy induced by oxaliplatin and vincristine (Kiguchi *et al.*, 2008a). In fact, it has been shown that vincristine induces the migration of macrophages expressing CX3CR1 receptor into the nervous system through enhanced expression of integrin on the surface of endothelial cells. Activating these macrophages by the chemokine CX3CL1 leads to ROS production and subsequent activation of TRPA1 in sensory nerves, resulting in pain signaling (Old *et al.*, 2014).

Moreover, the inflammatory response triggered by immune and glial cells under chemotherapy treatment is indicated as a key driver of neuroinflammation and sensitization of the nervous system, thereby playing a crucial role in the progression of CIPN. Most studies demonstrated an increased production and release of pro-inflammatory cytokines (TNFα, IL-1b, and IL-6, IFN-γ) and chemokines (CCL2, CXCL12, CCL11, CCL3, and CCL4), accompanied by a decreased expression of anti-inflammatory cytokines (IL-10 and IL-4) within the DRG and spinal cord

after the administration of several chemotherapeutics including paclitaxel, cisplatin, and vincristine (Lees *et al.*, 2017; Makker *et al.*, 2017). For instance, a study using vincristine treatment confirmed that TNFα was released by activated spinal glial cells since this marker colocalized with the glial markers Iba-1 and GFAP for microglia and astrocytes, respectively (Kiguchi *et al.*, 2008b). On the contrary, neither microglia hypertrophy nor an increase of Iba-1 levels was detected in the study of other authors (F. Y. Zheng *et al.*, 2011).

In line with these findings, differential results are reported following treatment with varied chemotherapeutic agents concerning microglia and astrocytes activity. For example, paclitaxel causes activation of astrocytes in the spinal dorsal horn, which was observed in the absence of microglial activation (Zhang *et al.*, 2012). Conversely, several studies report increased microglia activation following paclitaxel treatment (Ruiz-Medina *et al.*, 2013). Another model showed an absence of astrocyte activation in oxaliplatin-treated mice (Makker *et al.*, 2017), suggesting that, unlike paclitaxel, astrocyte activation may be a contributing factor but not a critical phenotypic change for the development of pain hypersensitivity after oxaliplatin treatment. In this regard, different studies report transient activation (Di Cesare Mannelli *et al.*, 2014), significant increases in activation (Burgos *et al.*, 2012), or no change (Robinson *et al.*, 2014) in activated spinal microglial cells. In many other types of neuropathic pain, a primary role is assigned to microglia that does not appear to be involved in CIPN. Such contrasting findings between studies indicate the broader issues within neuropathic pain research regarding the comparison of preclinical data from diverse animal models.

Moreover, peripheral pathology seen in CIPN can lead to maladaptive responses in the brain that contribute to CIPN even if chemotherapy drugs do not enter the brain, as discussed above. Indeed, astrocytes are reportedly activated in higher brain areas due to paclitaxel treatment, whereas both astrocytes and microglia were activated following oxaliplatin treatment. These areas include the ACC, thalamus, somatosensory cortex, dorsolateral PAG, and other brain regions associated with chronic pain and nociceptive processing (Pacini *et al.*, 2016). Therefore, the knowledge of both peripheral and brain-based mechanisms can better advance the study of CIPN.

3.4 Treatment strategies for CIPN

The development of CIPN is likely multifactorial and involves several mechanisms (discussed above). Despite apparent similarities in both the pathological mechanisms and clinical symptomatology of CIPN, the pathophysiology of CIPN nonetheless is thought to be compound-specific, with mechanism-specific prevention or treatment being the overarching clinical aim. In addition to providing targeted neuroprotection and relief from symptoms, any putative treatment for CIPN must not interfere with the anti-tumor effects of the causative chemotherapeutic agent.

There have been numerous clinical trials for CIPN prevention, but consistent beneficial effects have not yet been shown for any single agent. Current treatment strategies are predominantly based on modifying the chemotherapy regimen and symptomatic management using a range of pharmacological and non-pharmacological approaches. **Pharmacological** management of CIPN is multifaceted and includes treatments targeting the neuropathic component in CIPN (described above in section 2.4.5), featuring SSRIs, anticonvulsants, and analgesics. In fact, the only

recommended treatment is the SSRI duloxetine (Loprinzi *et al.*, 2020) which only mildly improves CIPN pain (Smith *et al.*, 2013). However, since many patients also suffer from anxiety, depression, and sleeping disturbances, adjuvant antidepressants would improve these psychological symptoms, aside from pain control. Gabapentin and pregabalin alone or in combination with opioids have also been used to treat CIPN, with minimal effectiveness (Kim *et al.*, 2018; Magnowska *et al.*, 2018). Intravenous lidocaine was recently tested in patients with CIPN with promising results, although small sample size (van den Heuvel et al., 2017). Related to topicals, in the latest guideline of the American Society of Clinical Oncology (ASCO), there is a weak recommendation for a topical gel containing baclofen (10 mg), amitriptyline (40 mg), and ketamine (20 mg), based on one study (Barton *et al.*, 2011; Loprinzi *et al.*, 2020). Targeting the endocannabinoid system has also shown a certain level of efficacy and limited adverse effects in alleviating CIPN in preclinical and clinical studies and gives rise to considerations for future research (Burgos *et al.*, 2012; Romero-Sandoval *et al.*, 2015). Additionally, several nutraceuticals have demonstrated selective efficacy for preventing/treating CIPN. There are promising reports using glutathione for oxaliplatin (Milla *et al.*, 2009), vitamins E and B6 for cisplatin (Kottschade *et al.*, 2011; Schloss *et al.*, 2017), and omega-3 fatty acids for taxanes-induced CIPN (Ghoreishi *et al.*, 2012), although with a moderate recommendation by the ASCO because of not sufficient evidence-based benefit (Loprinzi *et al.*, 2020). As **non-pharmacological** approaches, there are also several promising yet unproven interventions to treat or prevent CIPN, such as exercise (Kleckner *et al.*, 2018), acupuncture, scrambler therapy (peripheral nerve stimulation), or cryotherapy (Loprinzi *et al.*, 2020).

Given the current lack of effective treatments for CIPN, research needs a paradigm shift to focus on novel mechanisms. It is time to utilize new hypotheses that lead to a deeper understanding of the many cellular and biological processes causing CIPN to develop better treatment options.

3.5 Animal models of CIPN

Most of the chemotherapeutics agents that cause peripheral neuropathy in human patients have been used to develop animal models of CIPN. However, there are some issues with modeling CIPN in animals. First, there is little consistency in the **homogeneity** of animals used across studies; regarding rodents, mice and rats of different sex, age, mass, and genetic backgrounds have all been used. These variables are likely to play a role in the discrepancies found between studies. For instance, Taxol studies have shown significant variation in the severity of peripheral neuropathy based on the genetic background of mice and the age of animals used. A pivotal study with paclitaxel established DBA/2 strain as high-allodynic and C57BL/6 strain as low-allodynic, although both had comparable cold allodynia and did not display any thermal hyperalgesia. It (Smith *et al.*, 2004). Another study involving paclitaxel administration to young (31-day-old), adult (3- to 4-month-old), and aged (12- to 13-month-old) CD1 mice showed that young mice, followed by aged mice, had more severe impairment of mechanical allodynia and thermal hyperalgesia. Thus, the age of the animals used affects the level of neuropathy and needs to be standardized. Another major issue is the matter of **chemotherapy regimen**: route of administration, dosage, and duration. These vary significantly between studies, so even attempting exact dosing reports different results. In fact, in mice models of vincristine-induced CIPN there

is even less consistency in dosing, with a dosage ranging from 0.1 mg/kg to 2 mg/kg (Apfel *et al.*, 1993; Saika *et al.*, 2009).

In some cases with this same model, the intermittent schedule commonly used in rat models (two cycles of 5 days, with a skip of 2 days) is used (Old *et al.*, 2014), while others deviate from this, dosing twice each week for a period of 8 to 10 weeks or daily for 7 days (Apfel *et al.*, 1993; Saika *et al.*, 2009). For new studies, it is encouraged to use the intermittent systemic administration schedule (noted above) to mimic cycles of chemotherapy as opposed to daily dosing. As for the route of administration, intraperitoneal drug delivery predominates in rodent models because it is safe for the animals and a more straightforward method. However, it is not the best method to model the human disease, where such a route results in local toxic effects. Instead, the ideal mode of administration would be intravenously by tail vein injection, despite the difficulty and limitations such as the deterioration of the tail vein.

On the other hand, although rodent models of CIPN with a tumor might be considered more clinically relevant, the practical/ethical problems should be considered. Therefore, since chemotherapy is often administered after surgical removal of the tumor to eliminate possible micrometastases, modeling CIPN by administering chemotherapy alone is a good approach. Developing animal models of CIPN that replicate all patient-reported symptoms is challenging, like numbness, tingling, and persistent pain all rely on verbal reports from patients. Thus, most studies have focused on measuring evoked pain-like behaviors such as allodynia and hyperalgesia, as has been the case in preclinical studies with other chronic pain models**. Animal health** must be considered when using rodent models of CIPN for ethical reasons and practicality. Indeed, pain-

like behaviors cannot be accurately assessed when rodents are ill because of systemic toxicity, and thus, lethargic/insensitivity to hind paw stimulation. These sensory symptoms are evaluated by applying stimuli to the rodents' hind paws and then measuring withdrawal responses to these stimuli. For instance, mechanical stimuli typically used are von Frey filaments (calibrated nylon monofilaments that, when bent, produce a specific force) applied to the plantar surface of the hind paw (Chaplan *et al.*, 1994). In contrast, heat hyperalgesia is measured through latency response to radiant heat application to the hind paw plantar surface (Hargreaves *et al.*, 1988). Therefore, rigorous daily control of the weight and the general status of the animals during the experiment is fundamental to obtain reliable and consistent results.

To move the field forward and make comparisons of data from different laboratories more valid, there might be a consensus on the choice of animals (similar sex, age, and genetic background), mode and schedule of drug delivery, and outcome measures used in the evaluation.

4 Sigma-1 receptor

4.1 Overview of the sigma-1 receptor: structure, distribution and mechanism of action

Sigma-1 receptors (σ1R) are intracellular chaperone proteins that reside on mitochondrion-associated endoplasmic reticulum membranes (MAM), forming a globular complex enriched in cholesterol and neutral lipids (Hayashi and Su, 2007; Zamanillo *et al.*, 2013). The human gene for the σ1R is located on chromosome 9 (chromosome 4 in mice) and encodes a 24 kDa molecular mass protein of 223 amino acids (Hayashi and Su, 2007). It has two alpha-helical transmembrane segments with the NH2 and COOH termini on the cytoplasmic side of the plasma membrane or in the lumen of the endoplasmic reticulum (ER) (Aydar *et al.*, 2002; Hayashi and Su, 2007; Almansa and Vela, 2014) **(Figure 20).** Additionally, two other hydrophobic regions form the "steroid-binding domain like" (SBDL), which is involved in the formation of the ligand-binding site (Pal *et al.*, 2007, 2008). Therefore, the binding site of the σ1R is located in the inner surface of the membrane, thus enabling hydrophobic molecules to associate with the receptor.

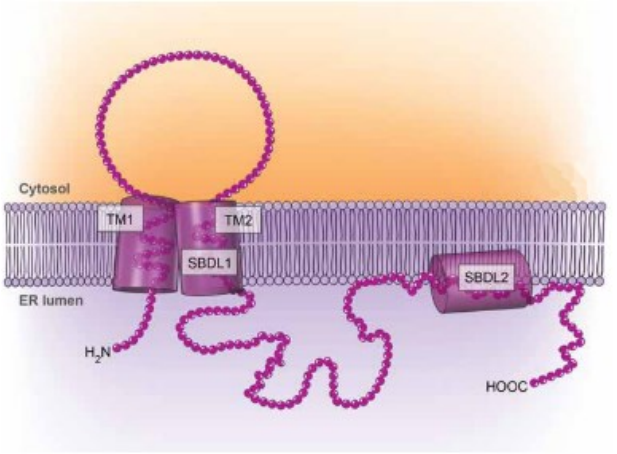

Figure 20. Structure of sigma-1 receptors. σ1R contains two hydrophobic transmembrane regions (TM1/2) with the N- and C- terminals in the intracellular side of the plasma membrane or in the endoplasmic reticulum (ER) lumen. Two additional hydrophobic regions form the steroid-binding domain like (SBDL1/2). Extracted from (Davis, 2015).

At the **anatomical level**, σ1R is ubiquitously expressed in mammalian tissues and is widely distributed in peripheral organs, such as the digestive tract, liver, kidney, heart, and skin (Samovilova and Vinogradov, 1992; Hellewell *et al.*, 1994; Sánchez-Fernández *et al.*, 2013). It is also extensively present in the central and peripheral **nervous system**, where it is expressed both in neurons and glia (Alonso *et al.*, 2000; Maurice and Su, 2009; Bangaru *et al.*, 2013; Moon *et al.*, 2014). In the PNS, σ1R is highly expressed in primary sensory neurons of the DRG (Sánchez-Fernández *et al.*, 2013; Shin *et al.*, 2020), highlighting the potential role of σ1 receptors in the control of the sensory transmission. Within the CNS, σ1R is abundantly expressed in the spinal cord, mainly in the superficial layers of the dorsal horn (Alonso *et al.*, 2000; Bangaru *et al.*, 2013). At the supraspinal level, it is concentrated in specific brain areas involved in pain modulation, particularly in the PAG, locus coeruleus, and RVM, but also in other areas involved in memory and emotion, such as the hippocampus, hypothalamus, olfactory bulb, and PFC (McCann *et al.*, 1994; Alonso *et al.*, 2000).

At a **cellular level**, the location of σ1R in the subcellular compartment is dynamic. Under physiologic non-stressed conditions, σ1R are bound to the binding immunoglobulin protein (BiP) and ankyrin at the MAM, where they are responsible for Ca^{2+} flux from the ER into the mitochondria through stabilization of inositol-1,4,5-trisphosphate ($IP3_3$) receptors (Maurice and Su, 2009). With cellular stress, when the IP_3 concentration is

too high, there is a dramatic drop of Ca^{2+} concentration in the ER, and the σ1R becomes activated. It dissociates from BiP and ankyrin and interacts with IP_3 receptors, thus preventing IP_3 degradation and increasing Ca^{2+} into mitochondrion (Hayashi and Su, 2007; Zamanillo *et al.*, 2013). Once dissociated, σ1R can translocate to the plasma membrane to interact with various ion channels, receptors, and kinases. Similarly, it can also migrate to the nuclear envelope, thus playing a role in regulating gene transcription (Su *et al.*, 2016). This relocation possibly increases the number or type of proteins targeted by this receptor (Zamanillo et al., 2013).

Once σ1R is located in the **plasma membrane**, it direcly interacts with ion channels, such as voltage-gated Ca^{2+} channels and K^+ channels, leading to a decreased influx of Ca^{2+} and efflux of K^+ (Aydar *et al.*, 2002). Moreover, it also stimulates phospholipase C (PLC), which finally increases IP_3 and thus an efflux of Ca^{2+} into the cytosol that indirectly activates other kinases. Activated σ1R directly interacts with G-protein-coupled receptors (GPR), mainly dopamine and opioids, but also cannabinoid CB1 receptors (Kim *et al.*, 2010; Sánchez-Blázquez *et al.*, 2014).

At the **nucleus**, σ1R activation has been proposed to directly or indirectly modulate several transcription factors, such as the ROS-induced NF-κβ, cAMP response element-binding protein (CREB), and c-fos. As a result, σ1R transcriptionally regulates the gene expression of several proteins related to inflammation, nociception, neuronal survival, synaptogenesis, and neurogenesis, including the antiapoptotic protein Bcl-2, the BDNF, and interleukins 8/10 (Meunier and Hayashi, 2010; Hayashi *et al.*, 2011).

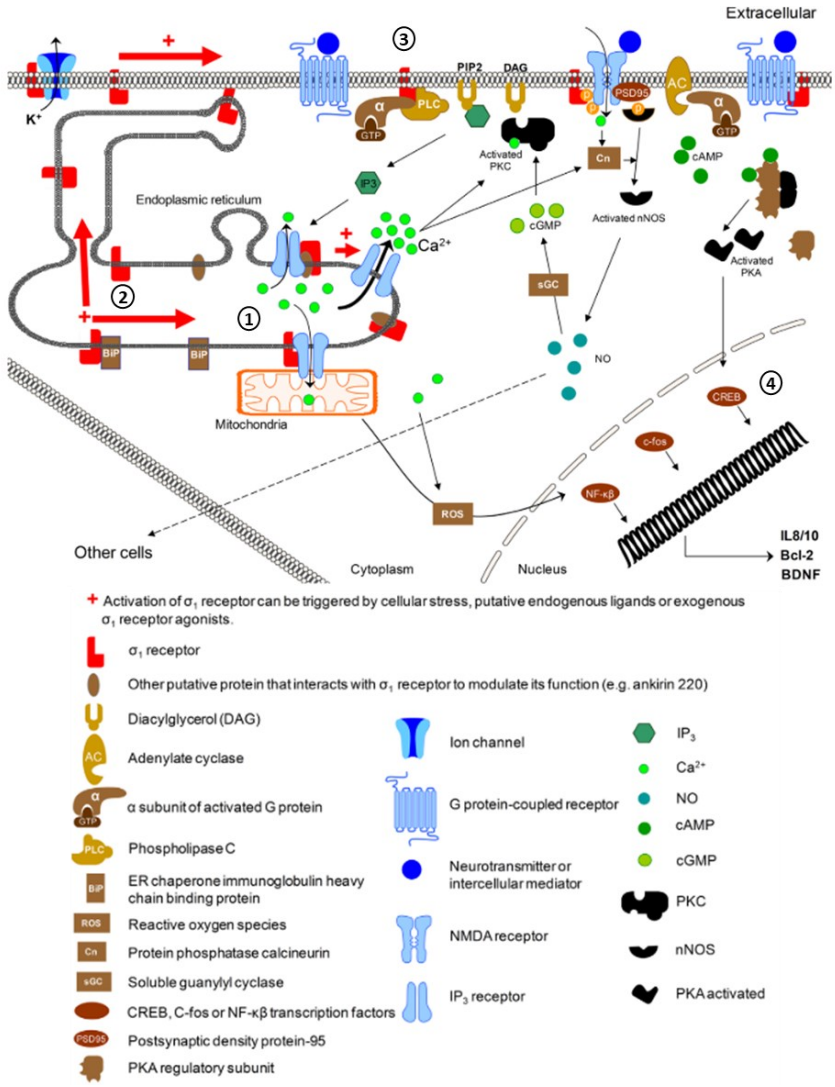

Figure 21. Signal transduction pathways modulated by σ1R activation. (1) At the endoplasmic reticulum (ER), σ1R binds IP_3 receptors to enhance Ca^{2+} signaling from the ER into the mitochondria to increase ATP production. (2) Activation of σ1R in the ER allows itself to dissociate from the chaperone binding immunoglobulin protein (BiP), which promotes the redistribution to peripheral endoplasmic membranes to bind ion channels, receptors, or protein kinases. (3) At the plasma membrane, σ1R regulates the activity of components of the plasma membrane-bound signal transduction, such as phospholipase C (PLC) and protein kinase C (PKC). It also modulates the activity of neurotransmitter receptors and ion channels, including K^+, Ca^{2+} channels, and NMDA receptors. σ1R also interacts

with G protein-coupled receptors such as dopamine receptor and mu-opioid receptor. (4) At the nucleus, σ1R activation controls transcriptional regulation of gene expression of the antiapoptotic protein Bcl-2, brain-derived neurotrophic factor (BDNF) or interleukins 8/10 (IL8/10) by the reactive oxygen species (ROS)-induced nuclear factor-κB (NF-κB), cAMP response element-binding protein (CREB) or c-fos, respectively. Adapted from (Zamanillo et al., 2013).

These pleiotropic modulatory effects, as well as their widespread expression throughout the nervous system, have elevated this receptor to the forefront of research for the treatment of a wide range of neurodegenerative diseases and neuropathic pain conditions (Su *et al.*, 2016).

4.2 Modulation of the sigma-1 receptor

The characterization of σ1R ligands has been hampered by the vast range of compounds with different structures that exhibit affinity for this receptor. Furthermore, while ligands affect σ1R activity, they can also be active in the absence of ligands (Aydar *et al.*, 2002), implying that the conventional idea of agonist and antagonist may not be entirely relevant to substances that interact with σ1R.

Although the **endogenous ligands** for the σ1R have yet to be definitively identified, currently neurosteroids, such as dehydroepiandrosterone (DHEA), pregnenolone, progesterone, and its sulfate esters are presently thought to be the most plausible naturally-occurring σ1R endogenous ligands (Su *et al.*, 1988; Maurice *et al.*, 2001). Other potential endogenous ligands have been discovered, including the natural hallucinogen N,N-Dimethyltryptamine (DMT) (Fontanilla *et al.*, 2009), sphingosine (Ramachandran *et al.*, 2009), and the endogenous peptide NPY (Roman *et al.*, 1989).

Similarly, many **exogenous ligands** have shown moderate/low to high affinity for σ1R, albeit with limited selectivity. These ligands include compounds with a broad range of therapeutic and pharmacological applications, comprising antipsychotics (e.g., haloperidol), antidepressants (e.g., sertraline), antitussive (e.g., dextromethorphan), and drugs of abuse (e.g., cocaine), among others. Moreover, more selective and high-affinity σ1R drugs have been produced, which are now considered archetypal σ1R ligands. Some examples of σ1R agonists are (+)-pentazocine and PRE084, whereas antagonists include BD1063, BD1047, or NE100 (reviewed by Cobos *et al.*, 2008; Zamanillo *et al.*, 2012). It is worth mentioning the σ1R antagonist S1RA (also named E-52862 or MR309), which was recently developed (Díaz *et al.*, 2012; Romero *et al.*, 2012) and is the most advanced drug candidate under clinical development (Bruna *et al.*, 2018). Indeed, six patents claim the effectiveness of S1RA for CNS diseases, including diabetic neuropathies, chemotherapy-induced peripheral neuropathy, and postherpetic neuralgia, established both *in vitro* and *in vivo* (Gris *et al.*, 2016b).

The number of reported σ1R ligands is rapidly increasing as these ligands provide valuable research tools to investigate the characteristics and function of the σ1R. Of special interest for this thesis is the σ1R antagonist EST, a new compound synthesized by Esteve Pharmaceuticals, S.L. Data from radioligand binding assay show that EST binds to σ1Rs with high affinity (Ki=78 nM in humans). Moreover, EST is a highly selective compound, lacking significant affinity for sigma-2 receptors (σ2R) (Ki > 1000 nM for the human σ1R) and a panel of more than 180 other receptors, enzymes, transporters and ion channels. Antagonist activity has been shown using several *in vitro* tests (Phenytoin test, σ1R-NR1

interaction test and σ1R-BiP interaction assay) and confirmed *in vivo* in mouse models of pain (capsaicin test). Altogether, this makes EST suitable to selectively antagonize σ1R and to study its potential as an analgesic compound.

4.3 Therapeutic interest of the sigma-1 receptor

The diversity of compounds that bind to σ1R suggested that this receptor has relevant contribution and pharmacological significance in many diseases. Moreover, given the wide range of modulatory effects described for σ1R ligands, as well as the extensive distribution of this receptor in the CNS and peripheral organs, drugs interacting with σ1R appear to be beneficial in a large number of therapeutic areas. Many of the proposed indications are in the neurological field, such as in psychotic disorders, the area with most patents, although interest in pain therapies based on σ1R interaction has steadily increased (Zamanillo *et al.*, 2012).

4.3.1 Sigma-1 receptor in pain

The knowledge of σ1R distribution in several areas of the nervous system with great importance in pain control (Alonso *et al.*, 2000) has provided a solid basis to suggest a potential role of this receptor in modulating pain mechanisms (Zamanillo *et al.*, 2013). Indeed, numerous preclinical studies demonstrate a significant function of the σ1R in the development and maintenance of pathological pain in various experimental models (Bangaru *et al.*, 2013; Moon *et al.*, 2014; Merlos *et al.*, 2017).

The genetic or pharmacological blockade of σ1R has been shown to strongly attenuate or abolish painful behaviors in different animal models of neuropathic pain, such as spinal cord injury (de la Puente *et al.*, 2009; Romero *et al.*, 2012; Castany *et al.*, 2018, 2019) or CIPN models (Nieto *et*

al., 2012, 2014; Gris *et al.*, 2016b), inflammatory pain models (Gris *et al.*, 2014), osteoarthritis (Carcolé *et al.*, 2019b), and capsaicin (Entrena *et al.*, 2009) and formalin (Cendán *et al.*, 2005) sensitization models. Moreover, σ1R blockade only exerts analgesic effects in sensitizing conditions, without altering the normal basic pain behavior (de la Puente *et al.*, 2009; Sánchez-Fernández *et al.*, 2013; Zamanillo *et al.*, 2013), thus confirming the entanglement between the putative pathophysiological mechanisms involved in nociceptive sensitization and σ1R antagonism.

Taken together, these preclinical findings well established the role of σ1R blockade for the treatment of neuropathic pain and supported the progress to further studies in humans. In this context, it is worth mentioning that the efficacy of the σ1R antagonists S1RA in alleviating chemotherapy-induced neuropathic pain observed in preclinical studies was yet validated in Phase II clinical trials (Bruna *et al.*, 2018). Moreover, in almost all clinical trials, no serious adverse events were observed in the patients treated with S1RA. Therefore, targeting σ1R is a new efficacious and safe strategy to approach neuropathic pain.

4.3.1.1 Role of Sigma-1 receptor in the neuroimmune and neuroglial interactions in pain

The importance of the interactions between sensory neurons and non-neuronal cells in producing and maintaining pain has been firmly established (Ji *et al.*, 2018). A great body of evidence support that σ1R plays a crucial role in these interactions at several critical steps in painful neurotransmission **(Figure 22)**. For instance, after peripheral tissue damage, immune cells are immediately recruited to target tissue and start producing a wide range of inflammatory factors, coordinating the inflammatory response as a whole (Pinho-Ribeiro *et al.*, 2017) **(Figure 22)**.

In this situation, immune cells also produce endogenous opioid peptides such as β-endorphin and enkephalins, which bind to the opioid receptors, albeit exerting insufficient analgesic effect (Przewlocki *et al.*, 1992). In this regard, σ1R can bind opioid receptors acting as a regulatory subunit, thus attenuating opioids analgesic effect (Chien and Pasternak, 1993). Several studies demonstrated that the inhibition of σ1R potentiated the opioid analgesia induced by both opioid drugs and endogenous opioids, selectively in the painful area (Sánchez-Fernández *et al.*, 2017).

Other cells become activated after nerve damage, including the Schwann cells at the site of the injury, and neurons and satellite cells in the DRG, producing several factors that promote both axonal regeneration (e.g., BDNF) and recruitment of immune cells (e.g., CCL2, IL6), together contributing to nociceptive sensitization **(Figure 22)**. In this connection, and noting that these cells highly express σ1R (Palacios *et al.*, 2004; Sánchez-Fernández *et al.*, 2013) (except for satellite cells), the blocking of σ1R showed decreased sensory hypersensitivity and neuroinflammation in models of peripheral nerve injury (Bravo-Caparrós *et al.*, 2020) and osteoarthritis (Carcolé *et al.*, 2019b).

At the CNS level, **microglia and astrocytes** play a pivotal role in pathological pain. Regarding σ1R expression in these cells, there is conflicting evidence on the precise location of these receptors in the spinal cord (Alonso *et al.*, 2000; Moon *et al.*, 2014); however, the results aiming at determining their involvement in central pain regulation are highly consistent. A decrease in microgliosis, and subsequent decrease in pro-inflammatory cytokines such TNF or IL-1β, was seen in the spinal cord dorsal horn after repeated early treatment with σ1R antagonist S1RA in a model of osteoarthritis (Carcolé *et al.*, 2019b) and in σ1R-knockout mice

after spinal cord injury (Castany *et al.*, 2018) **(Figure 22)**. Similarly, the repeated early administration of the σ1R antagonist BD-1047 also prevented astrocytosis in the spinal cord dorsal horn in several pathological pain models (Moon *et al.*, 2014; Choi *et al.*, 2016) **(Figure 22)**. In all these studies, a decrease in sensory hypersensitivity was also seen, indicating that the reduction of microglia and astrocyte activity by σ1R antagonism had functional repercussions.

In addition to the effects in the spinal cord, it is known that glial activity increases in supraspinal areas during chronic pain (Blaszczyk *et al.*, 2018; Carcolé *et al.*, 2019a). In this context, administration of σ1R antagonist S1RA in animals with experimental osteoarthritis was reported to decrease microglial proliferation in the medial PFC (Carcolé *et al.*, 2019a) **(Figure 22)**, which is relevant for the modulation of pain perception, but also emotional processing and cognitive function (Etkin *et al.*, 2011).

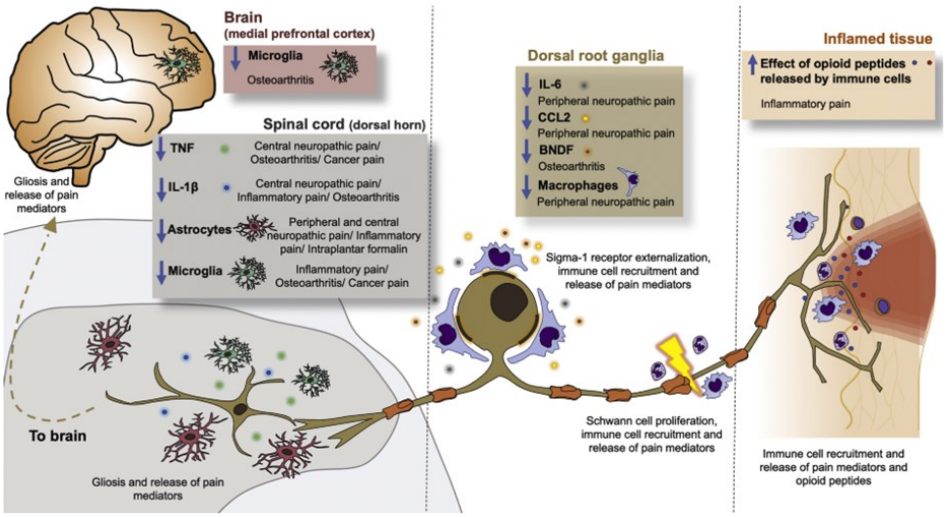

Figure 22. Effect of sigma-1 receptor inhibition on neuroimmune and neuroglial interactions in pain. Neurons and non-neuronal cells interact through chemical signals at several steps of nociceptive transmission: target tissue (right),

peripheral (middle), and central (left) nervous system. Colored boxes summarize the effects of σ1R inhibition and the preclinical pain models in which they have been described. Adapted from (Ruiz-Cantero et al., 2021).

Overall, these results suggest that σ1R play a critical role in painful transmission, acting as a connection between the modulation of neuron-immune/glial cells interactions during pathological pain. In this scenario, σ1R antagonists may constitute a new class of analgesics with a novel mode of action, representing an intriguing therapeutic potential.

OBJECTIVES

Objective 1

To investigate the participation of glial cells in the initiation and progression of CIPN and in the analgesic effects of a σ1R antagonist on this pathology.

Study 1

Astrocyte-specific transcriptomics in a mouse model of vincristine-induced neuropathy: therapeutic potential of a novel sigma-1 receptor antagonist

Supplementary results

Characterization of Cx3cr1-CreERT2:RiboTag mouse line for microglia-specific transcriptomics: focus on the analgesic effects of a selective σ1R antagonist on CIPN

Objective 2

To explore the region and sex-specific genetic properties of glial cells in relevant regions for pain modulation.

Study 2

Molecular and functional heterogeneity of regional astrocytes in physiological state

MATERIALS & METHODS

Animals

Mice were purchased from the Jackson Laboratory (Bar Harbor, ME), bred, and housed in the animal facility of Universitat Pompeu Fabra - Barcelona Biomedical Research Park (UPF-PRBB; Barcelona, Spain) under SPF conditions in a HEPA barrier environment. In separate breeding strategies, tamoxifen-inducible *Aldh1l1-CreERT2*$^{+/wt}$ (JAX stock #29655) (Srinivasan *et al.*, 2016) and *Cx3cr1-CreERT2*$^{+/+}$(JAX stock #20940) (Yona *et al.*, 2013) males were mated with *RiboTag*$^{loxP/loxP}$ females (JAX stock #011029) (Sanz *et al.*, 2009) to generate the desired progeny: *Aldh1l1-CreERT2*$^{+/wt}$*:RiboTag*$^{loxP/wt}$ and *Cx3cr1-CreERT2*$^{+/+}$*:RiboTag*$^{loxP/wt}$. Resulting offspring were genotyped to confirm the presence of the Cre recombinase gene and the RiboTag allele using PCR conditions described elsewhere (Sanz *et al.*, 2019). Male and female *Aldh1l1-CreERT2*$^{+}$*:RiboTag*$^{+}$ (referred as Astrocyte-RiboTag) and *Cx3cr11-CreERT2*$^{+}$*:RiboTag*$^{+}$ (referred as Microglia-RiboTag) mice were used to perform this study.

Mice were 8-10 weeks old at the beginning of experimental testing and they were housed in groups of 3-4 with *ad libitum* access to water and food. The housing conditions were maintained at 21 ± 1°C and 55 ± 10% relative humidity in a controlled 12-12-hour light/dark cycle (light on between 8:00 A.M. and 8:00 P.M.). Animals were habituated to housing conditions and handled for 1 week before the start of the experiment. All experimental procedures and animal husbandry were conducted following the ARRIVE guidelines and according to the ethical principles of the International Association for the Study of Pain (IASP) for the evaluation of pain in conscious animals (Zimmermann, 1986) and the European Communities Council Directive (2010/63/EU), and were approved by autonomic (Generalitat de Catalunya, Departament de Territori i

Sostenibilitat) and local (Comitè Ètic d'Experimentació Animal - Parc de Recerca Biomèdica de Barcelona) ethical committees. Animals were randomly allocated to experimental groups and all experiments were performed under blinded conditions.

Experimental procedure

To induce Cre recombination for cell-type specific HA-tag expression on ribosomes, all mice (6-8 weeks old) were first treated i.p with tamoxifen (100 mg/kg) for 3 times every other day (Ceolin *et al.*, 2017). Behavioral experiments and treatment schedules started 2 weeks after the last tamoxifen injection.

Peripheral neuropathy was induced by repeated injections of VCR (0.5 mg/kg, i.p) in two cycles of 5-days each, leaving a rest period between cycles of 2 days (Old *et al.*, 2014; Starobova *et al.*, 2019). A last challenge injection was performed on day 15 (11 injections, cumulative dose: 5.5 mg/Kg, i.p). Saline injections were used to reproduce conditions in a control group. In order to assess a possible preventive effect of EST on the development of VCR-induced neuropathic pain, EST was co-administered with VCR. For this purpose, EST was administered repeatedly once a day at 25 mg/kg p.o., starting 1 days before the first injection of VCR and during the entire VCR-treatment period (last VCR injection on day 15). Similarly, a control group of animals were administered with vehicle solution (0.5% HPMC) following identical schedules **(Figure 23).**

Nociceptive sensitivity to mechanical and heat stimuli was assessed using the Von Frey and Hargreaves test, respectively. Animals were habituated three times to the environment of nociceptive tests and two baseline measurements (alternative days) were made prior to treatments, the

average of which is presented. Nociception was assessed again on days 2, 5, 8, 11 and 15 after first VCR injection **(Figure 23).** Mechanical allodynia was assessed before (PRE) and 30 min after (POST) EST (or vehicle) administration, while thermal hyperalgesia was evaluated around 60 minutes afterwads **(Figure 23).** On the days of testing, VCR (or saline) was administered at the end of behavioral evaluation. Finally, mice were euthanized on days 3 or 16 for tissue sample collection. Tissue was extracted 12 ± 1 h after the last drug administrations. Specifically, the somatosensory cortex, periaqueductal gray region and whole dorsal spinal cord were rapidly isolated, frozen in liquid nitrogen and stored at -80°C for subsequent mRNA extraction to perform transcriptomic analysis by RNA sequencing. This experimental procedure was conducted in parallel for Astrocyte-RiboTag and Microglia-RiboTag mice, with males and females tested on alternative days to avoid interferences in data interpretation.

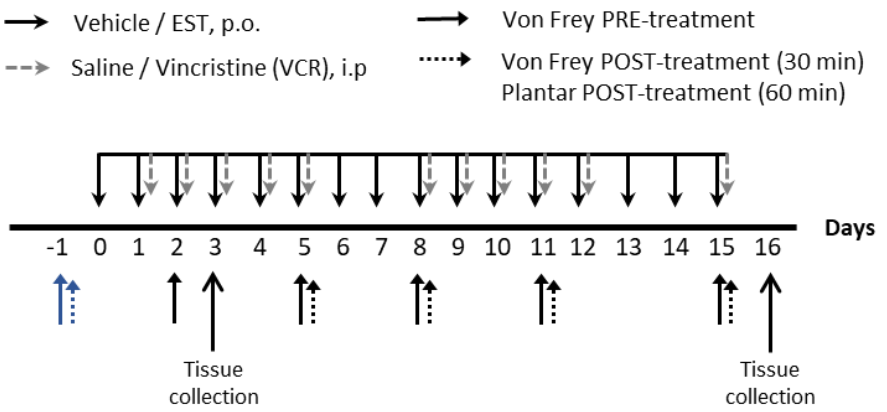

Figure 23. Experimental procedure (behavior). Mice were treated with either saline or vincristine (0.5 mg/Kg) with a 5-day-on, 2-day off schedule over 14 days, and with a last injection on day 15 (grey dashed arrows). Chronic EST (25 mg/Kg) or vehicle (0.5% HPMC) were administered by gavage (p.o) once a day starting 1 day before the first exposure to vincristine (or saline) and for the 16 days of protocol (day 0 to 15; black upper arrows). Mechanical and heat nociception was assessed under basal conditions (blue arrows, last measurement) and on days 2,

5, 8, 11, and 15. Mechanical allodynia was evaluated with the von Frey test before (PRE) and 30 min after (POST) the daily dose of EST (or vehicle). Heat hyperalgesia was assessed in the plantar test after mechanical evaluations (POST). On testing days, VCR (or saline) was administered at the end of the behavioral evaluation. Mice were euthanized on days 3 and 16 for tissue sample collection.

Drug preparation and experimental groups

Tamoxifen (Sigma-Aldrich) was dissolved in corn oil/ethanol (10:1) by warm bath (35-40ºC) sonication to a stock concentration of 20 mg/ml and administered by intraperitoneal (i.p) route at 100 mg/Kg (Ceolin *et al.*, 2017) to all animals 2 weeks before starting treatment protocols. Vincristine Sulfate (Pfizer) was dissolved in sterile physiological saline (0.9%, sodium chloride) and injected into the peritoneal cavity (i.p) at 0.5 mg/Kg (Hansen *et al.*, 2011; Old *et al.*, 2014; Starobova *et al.*, 2019). Based on established conversion between murine and human doses based on body surface area, a dose of 0.5 mg/kg i.p. would be equivalent to 1.4 mg/m2, which is close to human doses ranging from 0.5 to 2.0 mg/m2 (Nair and Jacob, 2016). The σ1R antagonist EST (ESTEVE Pharmaceuticals S.L, Barcelona, Spain) was dissolved in an aqueous vehicle solution (0.5% hydroxypropylmethyl cellulose, HPMC; Sigma-Aldrich) and administered orally via gavage at a concentration of 25 mg/Kg. In parallel, experimental control animals were treated with either saline or vehicle (0.5% HPMC) following the same corresponding administration protocols. All compounds were administered at a volume of 10 ml/Kg. VCR preparation and injection of animals was always performed on sterile conditions in a Class II biosafety cabinet (BIO II A).

Accordingly, animals were distributed into 4 experimental groups, namely Sal-Veh (Saline 0.9% i.p.; 0.5% HPMC p.o), Sal-EST (Saline 0.9% i.p.; EST 25 mg/Kg), VCR-Veh (VCR 0.5 mg/Kg i.p.; 0.5% HPMC p.o), and VCR-EST (VCR

0.5 mg/Kg i.p.; EST 25 mg/Kg). A total of 144 Astrocyte-RiboTag mice (n = 72 per sex, n = 36 per time-point, n = 9 per group) and 207 Microglia-RiboTag mice (Male: n = 111; 12 mice per group on day 3, 15-18 mice per group on day 16; Female: n = 96; 48 mice per time-point, 12 mice per group) were used for behavioral experimentation.

Nociceptive behavior

Sensitivity to mechanical (referred as allodynia) and heat (referred as hyperalgesia) stimuli was used as outcome measures of neuropathic pain. Mice were tested in each paradigm at different time points (see experimental procedures), using the same sequence.

Mechanical allodynia was evaluated by measuring the hind paw withdrawal response to von Frey filaments stimulation following the up-down paradigm, as previously reported (Chaplan *et al.*, 1994). Briefly, animals were placed in Plexiglas cylinders (20 cm high, 9 cm diameter) on a grid surface through which the von Frey calibrated filaments (North Coast Medical, USA) were applied. Animals were habituated for 15-30 min before testing to allow an appropriate behavioral immobility. Filaments equivalent to 0.02, 0.04, 0.07, 0.16, 0.4, 0.6, 1 and 2 g were used, applying first the 0.4 g filament, and increasing or decreasing the strength of the next filament according to the response (negative or positive, respectively). The filaments were applied to the plantar surface of the hind paw of the mouse until bent and then held for 3 seconds or until the paw was withdrawn in a reflex not associated with movement or grooming. Clear paw withdrawal, shaking, or licking was considered as a nociceptive response. The mechanical threshold (in grams) was then calculated by the up-down Excel program (Dixon, 1965). Both hind paws were tested, although no differences were detected on mechanical thresholds.

Heat hyperalgesia was assessed by recording the hind paw withdrawal latency in response to radiant heat applied with the Hargreaves plantar test apparatus (Ugo Basile, Varese, Italy) as previously reported (Hargreaves *et al.*, 1988). Mice were placed in Plexiglas cylinders (20 cm high, 9 cm diameter) positioned on a glass surface and habituated to the environment for 15 min before testing. The mean paw withdrawal latencies for left and right hind paws were determined from the average of 3 separate trials, taken at 3-5 min intervals to avoid thermal sensitization. A cut-off time of 20 s was used to prevent tissue damage.

Immunofluorescence analysis

Tissue preparation for immunofluorescence

Two weeks after tamoxifen exposure, two mice per sex and transgenic mouse line (Astrocyte-RiboTag and Microglia-RiboTag) were used for immunohistochemical validation of cell-type specific Cre recombination. Animals were deeply anesthetized by i.p injection (0.2 ml/10 g of body weight) of a mixture of ketamine (100 mg/kg, Richter Pharma AG, Austria) and xylazine (20 mg/kg, Sigma-Aldrich, Saint Louis, MO, USA). Once all reflexes subsided, the animals were perfused intracardially with 30 ml of ice cold 0.1M Na2HPO4/NaH2PO4/NaCl buffer (PBS), pH 7.5, followed by 60 ml 4% paraformaldehyde (PFA) in 0.1M PBS, delivered with a peristaltic pump at 30ml/min. Brains and whole spinal cords were quickly removed.

Mouse brains were postfixed overnight at 4°C in the same fixative solution (4% PFA), rinsed twice in 0.1M PBS and then transferred in a buffered solution of 30% sucrose in 0.1M PBS at 4°C until use (for a minimum of 48h or until they sink). Coronal brain sections (30 µm) containing the somatosensory cortex and the periaqueductal gray were obtained on a

freezing microtome (Leica Biosystems) and kept in a solution of 5% sucrose with 0.02% sodium azide at 4°C until use. Spinal cords were postfixed for 4 hours in 4% PFA at 4°C, rinsed twice in 0.1M PBS, cryoprotected in 30% sucrose in 0.1M PBS and stored overnight at 4°C. The following day, tissues were immersed in O.C.T. (Sakura, Finetek, Europe B.V., Alphen aan den Rijn) and frozen at -80ºC. Spinal cords were cryosectioned coronally at 20 µm with a cryostat (Leica Biosystems) and sections were collected directly onto gelatin-coated slides in a 1:8 series, with slides stored at -20ºC until use.

Immunofluorescence

Brain sections

Immunofluorescence of brain sections was performed as described (Sanz *et al.*, 2019) with little modifications. Free-floating sections were first tempered at RT and rinsed 3 times with 0.1M PBS for 5 min each and blocked at room temperature (RT) with agitation for 2 hours in blocking buffer containing 0.1M PBS with 0.3% Triton X-100 (PBS-T) and 10% normal donkey serum (NDS; Sigma-Aldrich). The slices were then incubated overnight at 4°C with primary antibodies diluted in PBS-T with 1% NDS. Primary antibodies used were rabbit Iba1 polyclonal (1:500; Wako, Cat# 019-19741) for microglia, rabbit ALDH1L1 polyclonal (1:500; Abcam, Cat# ab87117) for astrocytes, or rabbit NeuN polyclonal (1:1000; Abcam, Cat# ab128886) for neurons, together with mouse HA monoclonal (1:500; Biolegend, Cat# 901514 - previously Covance Cat# MMS-101R) for the detection of the HA tag. The following day, sections were rinsed 3 times in PBS-T for 5 min each and incubated for 2 hours at RT with secondary antibodies Alexa Fluor 488 donkey anti-rabbit polyclonal (1:500; Thermo Fisher Scientific, Cat# A-21206) for microglia, astrocytes or

neurons staining and Alexa Fluor 555 donkey anti-mouse polyclonal (1:500; Thermo Fisher Scientific, Cat# A31570) for the HA tag detection, both diluted in the same buffer as primary antibodies. After incubation, sections were rinsed with 0.1 PBS and mounted immediately after onto glass slides coated with gelatin in Fluoromount G with DAPI (Electron Microscopy Sciences, Cat# 17984–24).

Spinal Cord

Immunostaining of spinal cord sections was performed directly onto slides as described (Martínez-Navarro *et al.*, 2020). Sections were first air-dried for 15 minutes, washed 3 x 5 min with 0.1M PBS and blocked at RT for 2 h in blocking buffer containing PBS-T and 10% NDS. Spinal cord sections were double stained with primary antibodies rabbit anti-Iba1 (1:500; Wako), anti-GFAP (1:1000; Agilent, Cat# Z0334), or anti-NeuN (1:1000; Abcam), and mouse anti-HA (1:500; mouse, Biolegend), all of them diluted in PBS-T with 1% NDS, for 2 h at RT. Sections were washed 3x 5 min in PBS-T and incubated for 2 h at RT with donkey anti-rabbit Alexa Fluor-488 (1:500; Thermo Fisher Scientific) and donkey anti-mouse Alexa Fluor-555 (1:500; Thermo Fisher Scientific), both diluted in PBS-T with 1% NDS. Finally, sections were rinsed in 0.1M PBS and let dry before cover-slipping with Fluoromount G with DAPI (Electron Microscopy Sciences).

Image analysis

The stained sections were analyzed with the oil immersion 40× objective and 1× zoom using a confocal microscope (Leica TCS SP5 inverted). All parameters were held constant for all sections from the same experiment. The images were processed using the ImageJ analysis software.

Polyribosome immunoprecipitation (IP) and RNA extraction

Mice were killed by cervical dislocation 3 or 16 days after first VCR injection. The somatosensory cortex, periaqueductal gray region, and dorsal lumbar region of the spinal cord were rapidly isolated and placed in individual tubes, flash-frozen in liquid nitrogen and stored at −80ºC until use.

Ribosome immunoprecipitation was performed as described previously (Sanz *et al.*, 2019). Tissue samples of 3 mice from the same treatment group were pooled and homogenized in an ice-cold dounce homogenizer vessel with 1 mL polysome homogenization buffer (50 mM Tris pH7.5m 100 mM KCl, 12 mM MgCl2, 1% NP-40, supplemented with 1 mM DTT, 200 U/mL Promega RNasin, 1 mg/mL heparin, 100 ug/mL cycloheximide and protease inhibitor mixture, in RNase-free water). To remove cell debris, lysates were transferred to a microtube on ice and centrifuged at 10.000 x g for 10 min at 4°C. Clear supernatants were transferred to fresh tubes on ice and a small aliquot of 50 µl was removed and kept at -80°C, serving as input fraction for subsequent analysis. Mouse anti-HA antibody (5 µl/sample; Biolegend, Cat# 901514) was then added to the remaining supernatant and incubated for 4 h at 4°C in a microtube rotator with gentle mixing. After incubation, the cleared lysates with the antibody were added to 200 µl each of protein A/G magnetic beads (Thermo Fisher Scientific, Cat# 88803), previously washed with 400 µl of homogenization buffer for 5 min in a rotator and incubated overnight at 4 °C with constant rotation. The following day, samples were placed into a magnetic stand on ice to collect supernatant (saved at −80ºC for subsequent analysis). Pellet of beads were washed 3 x 5 min with 800 µl of high salt buffer (50 mM Tris pH 7.5, 300 mM KCl, 12 mM MgCl2, 1% N P-40, 0.5 mM DTT, 100 ug/mL

cycloheximide) in a rotator at 4°C. At the end of the washes, 350 µl of RLT buffer (from Qiagen Rneasy extraction kit), supplemented with 1% β-Mercaptoethanol, was added to release mRNA from ribosomes and RNA was extracted using Rneasy Micro kit (Qiagen; Cat# 74004) followed by in-column DNAse treatment to remove genomic DNA contamination. RNA was finally eluted in 15 µl Rnase-free water and stored at -80°C until analysis. Total RNA was also extracted from the Inputs by using the same RNA extraction procedure (Rneasy Micro Kit; Qiagen).

Quality and quantity of RNA samples were both determined by NanoDrop™ One spectrophotometer (Thermo Fisher Scientific) and chip-based capillary electrophoresis using an Agilent 2100 Bioanalyzer (Agilent, Palo Alto, CA, USA). RNA integrity number (RIN) greater than 8 were used for subsequent analysis. Three biological replicates per treatment group, each one composed of a pool of 3 mice, were used for RNA-seq analysis.

Quantitative real-time PCR analysis (qRT-PCR)

Confirmation of gene expression levels was performed by qRT-PCR analysis of IP samples and Inputs. Since different levels of RNA were obtained from Astrocyte-RiboTag (> 20 ng/ul) and Microglia-RiboTag (< 10 ng/ul) mice, we use distinct qRT-PCR procedures to perform the analysis. Briefly, RNA samples from Astrocyte-RiboTag mice were reverse transcribed to cDNA using High Capacity RNA-to-cDNA kit (Applied Biosystems, Cat# 4390778) according to the manufacturer's instructions and qRT-PCR was carried out in triplicate using the SYBR Green PCR Master Mix (Roche, Cat# 04707516001) with a QuantStudio 12K Flex Real-Time PCR System (4471134, Applied Biosystems). Conversely, mRNA samples from Microglia-RiboTag mice were directly analyzed in triplicate using Power SYBR RNA-to-CT 1-Step Kit (Thermo Fisher Scientific, Cat#

4391178), following manufacturer's instructions, with same RT-PCR system. The cycle threshold (Ct) values were calculated automatically by the Expression Suite v1.3 software with default parameters. Levels of the target genes were normalized against the housekeeping gene *Actb* and compared using the comparative Ct (ΔΔCt) method (Livak & Schmittgen, 2001) to give the fold-change.

To validate the cell-type specificity of transcripts in IP RNA samples, enrichment was calculated as gene expression levels relative to Input, while confirmation of differences between treatment groups was calculated as gene expression levels relative to saline-vehicle control group. The expression of the following genes was analyzed: aldehyde dehydrogenase 1 light chain 1 (*Aldh1l1),* CX3C chemokine receptor 1 (*Cx3cr1),* UDP galactosyltransferase 8A *(Ugt8a),* RNA binding fox-1 homolog 3 *(Rbfox3),* hemoglobin subunit beta *(Hbb),* hemoglobin subunit alfa *(Hba),* 5'-aminolevulinate synthase 2 *(Alas2),* actin beta *(Actb).* Primer sequences are indicated in **Table 7**.

Table 7. Sequences of PCR primers used for qRT-PCR analysis.

Genes	Primer sequence (5' – 3')	
	Forward	*Reverse*
Aldh1l1	TGTGTTCACCATCCCAGACAA	TGACCTCCATGGGTATGAACTG
Cx3cr1	GCGTGAGACTGGGTGAGTGA	CAAATAACAGGCCTCAGCAGAA
Ugt8a	TCATAGAATGGCTGCCTCAAAA	ATGGTCTCCAAACAGTGGGATT
Rbfox3	AGGAACAGTCTATGGGCCTGAA	GAGGTGGTGCAGCTCGAAAT
Hbb	GTTGTCTACCCTTGGACCCA	ACATGCAGCTTGTCACAGTG
Hba	TGAAGCCCTGGAAAGGATGT	TGAAGTTGACGGGATCCACA
Alas2	CAGTATGGAGCCCTGACCTT	GTCCCGAGTGCTGGCTATAT
Actb	CCTTCTTGGGTATGGAATCCTGT	CACTGTGTTGGCATAGAGGTCTTTAC

Library preparation and RNA sequencing (RNA-seq)

RNA library generation and sequencing were carried out by CRG Genomics unit (PRBB, Barcelona, Spain). The NEBNext Low Input RNA Library Prep Kit for Illumina (New England Biolabs Inc, Cat# E6420) was used on 5 ng of total RNA to generate full length cDNAs, followed by conversion to sequence-ready libraries, according to manufacturer's instructions. Resulting RNA libraries were size selected to a median insert size of 380 bp. Sequencing was performed on an Illumina HiSeq2500 sequencer with paired-end 75-bp reads and minimum output of 20 million reads per sample.

RNA-seq data analysis

Raw sequencing reads in the FASTQ files were mapped with STAR version 2.7.1a (Dobin *et al.*, 2013) against the Gencode release 25 based on the mouse reference genome GRCm38.p6 (mm10) and the corresponding GTF file. The entire chromosome Y was hard-masked with Ns for a sex-informed alignment (Olney *et al.*, 2020). The table of counts was obtained with FeatureCounts function in the package subread, version 1.6.4 (Liao *et al.*, 2014) . Genes having less than 10 counts in at least 3 samples were excluded from the analysis. Raw library size differences between samples were treated with the weighted "trimmed mean method" (TMM; Robinson and Oshlack, 2010) implemented in the edgeR package (Robinson *et al.*, 2010). The normalized counts were used in order to make unsupervised analysis, PCA, clusters (Ward.D2 method with correlation distances), and heatmaps.

For the differential gene expression (DE) analysis, read counts were converted to log2-counts-per-million (logCPM) and the mean-variance relationship was modeled with precision weights using voom approach in

the limma package version 3.44.1 (Ritchie *et al.*, 2015) and using R version 4.0.0. SVA package (version 3.38.0) was used to compute surrogate variables (SV) using *svaseq* function. SVs were added to the design matrix with the primary variable. In the Study 1, differential expression was defined as p-value < 0.05 and fold-change (FC) > 2 (logFC > 1). Adjusted p-value (adj.p.val) for multiple comparisons (Benjamini and Hochberg, 1995) was also calculated and represented when necessary (ad.p < 0.05). In the Study 2, genes were filtered using an adj.p.val < 0.05 and a FC > 1.5 (logFC > 0.585) cutoff as significance level criteria for differential expression.

In both studies, pre-ranked Gene Set Enrichment Analysis (GSEA; Subramanian *et al.*, 2005) implemented in clusterProfiler (Yu *et al.*, 2012) package version 3.18.0 was used in order to retrieve enriched functional pathways. The ranked list of genes was generated using the -log(p.val)*signFC for each gene from the statistics obtained in the DE analysis mentioned. Functional annotation was brought based on the enrichment of gene sets belonging to gene set collection c5.bp (v7.2) in Molecular Signatures Database (MSigDB).

Statistical analysis

All data from behavioral and qRT-PCR evaluations were first subjected to the Shapiro-Wilk test of normality, and appropriate statistical methods were applied depending on the distribution. ANOVA with repeated measures or linear mixed model was used when required to test the evolution over time. Bonferroni *post hoc* analysis was performed when pertinent. Two or three-way ANOVA by subsequent *post hoc* analysis (Bonferroni) or Kruskall-Wallis, followed by Mann-Whitney U analysis, were used when appropriate for multiple group comparison. A probability of 0.05 or less was considered statistically significant. Detailed statistical

analyses for the data described in the figures are presented in the corresponding Supporting material section. Statistics of the RNA-seq data were performed as outlined in the “RNA-seq data analysis” section.

RESULTS

Study 1

Astrocyte-specific transcriptomics in a mouse model of vincristine-induced neuropathy: therapeutic potential of a novel sigma-1 receptor antagonist

STUDY 1

Astrocyte-specific transcriptomics in a mouse model of vincristine-induced neuropathy: therapeutic potential of a novel sigma-1 receptor antagonist

Several lines of evidence suggest that many neurological disorders may involve astrocyte dysfunction (Siracusa *et al.*, 2019). In fact, the role of astrocytes in the pathogenesis of pain is widely accepted (Ji *et al.*, 2018), especially neuropathic pain resulting from nerve injuries such as trauma. For this reason, glial cells are emerging as new pharmacological targets for drug development (Scholz and Woolf, 2007; Milligan and Watkins, 2009). However, its relevance in chemotherapy-induced neuropathies is debated, with studies showing contradictory findings (Zhang *et al.*, 2012; Makker *et al.*, 2017), but pointing to a central role of glial cells, especially astrocytes, in the pathophysiology of these conditions. Antitumoral chemotherapy tends to have long-term complications involving peripheral neuropathy that may seriously impact patients' quality of life (Cavaletti *et al.*, 2019). Treatment or prevention of the development of this condition is a goal towards improving the wellbeing of patients during and after exposure to chemotherapy. In this scenario, σ1R arises as a potential target to approach chemotherapy-induced neuropathic pain conditions, with promising results yet obtained in preclinical (Nieto *et al.*, 2012, 2014) and clinical studies (Bruna *et al.*, 2018) by using selective σ1R antagonist.

However, the specific modifications in astrocyte gene signature and functionality associated with the development of CIPN and their involvement in σ1R analgesic effects are unknown.

To address these issues, we used a mouse model of vincristine-induced neuropathic pain to evaluate the therapeutic potential of a σ1R antagonist (EST) in modulating the signs of this neuropathy and investigate the associated transcriptomic changes occurring exclusively in the astrocyte population of key CNS areas for pain control. For this purpose, we generated Aldh1l1-CreERT2:RiboTag mice (Srinivasan *et al.*, 2016) and used high-throughput RNA sequencing analysis to document astrocyte-specific transcriptomic profiles under this pathological condition.

Anatomical characterization of the Astrocyte-RiboTag mouse line

The Aldh1l1-CreERT2 mice have been reported as highly efficient and specific for temporally controlled astrocytic gene expression (Srinivasan *et al.*, 2016; Winchenbach *et al.*, 2016), and the crossing with RiboTag mice offers a useful tool to document astrocyte gene expression during disease processes and look for similarities and differences between distinct areas of the CNS. As an initial validation of the model, two Aldh1l1-CreERT2:RiboTag mice per sex were sacrificed two weeks after exposure to tamoxifen (3 x 100 mg/Kg, i.p), and brains and spinal cords were dissected for immunohistochemistry analyses. Immunostaining of the HA-epitope tag combined with specific antibodies for astrocytes (Aldh1l1 or Gfap), microglial cells (Iba1), or neurons (NeuN), revealed a widespread expression of HA-tagged ribosomes in all CNS regions examined **(Figure 24 a)** and a high colocalization with Aldh1l1 or GFAP-positive cells **(Figure 24 b, SS; Supporting Figure *1*, other regions)**, supporting that Cre-mediated recombination upon TAM induction specifically targeted astrocytes. In contrast, no colocalization of the HA-tag was observed with neither Iba1-positive microglia nor NeuN-positive neurons **(Figure 24 b, SS; Supporting Figure *1*, other regions).** In the absence of TAM exposure, Aldh1l1-

CreERT2:RiboTag mice did not display HA-tagged ribosomes expression (not shown), consistent with temporally controlled, TAM-dependent induction of Cre-recombinase under the control of the Aldh1l1 promoter.

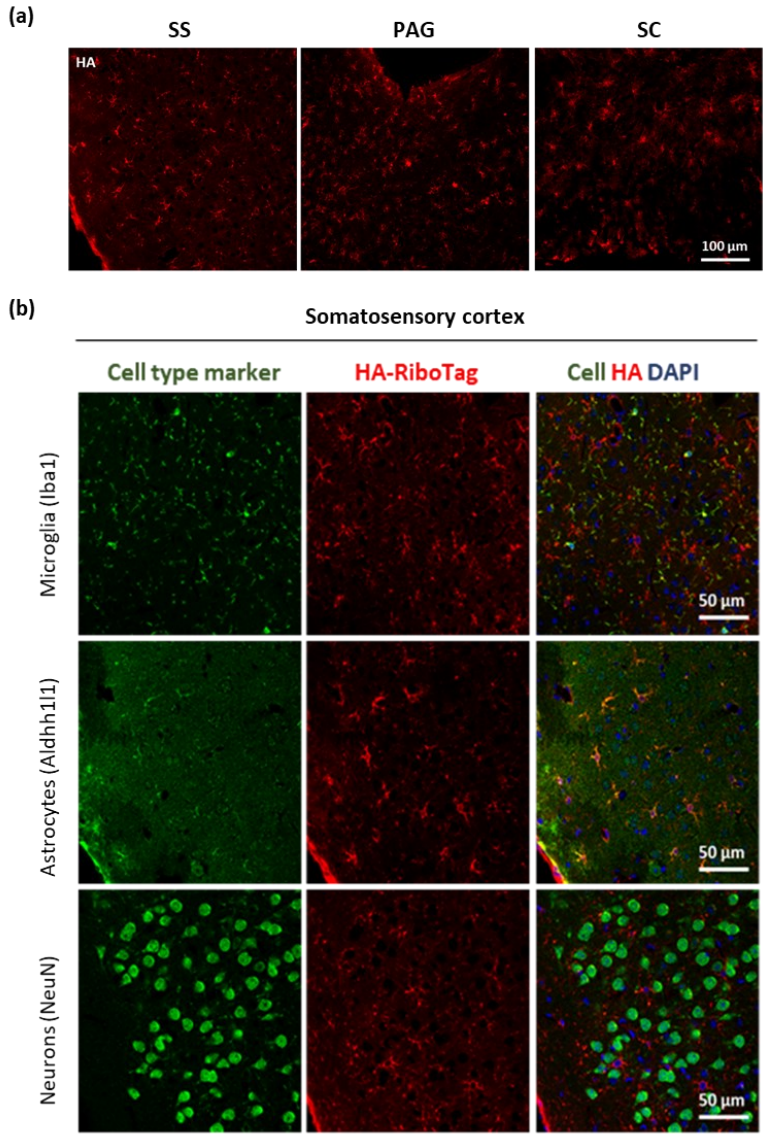

Figure 24. Immunohistochemical validation of Astrocyte-RiboTag mouse line. (a) Representative images for HA immunofluorescence showing the efficient induction of HA-tag expression in the different pain-related areas. **(b)** Double immunofluorescence for HA (red) and cell-specific markers (green),

counterstained with DAPI (blue), to determine the cell-type expression of HA-tagged ribosomes. Images showing strong co-expression between HA and Aldh1l1 (astrocytes), but no colocalization of HA with Iba1 (microglia) or NeuN (neurons). Representative images from SS (n= 2 mice x sex). See **Supporting Figure 1** for other regions. SS, somatosensory cortex; PAG, periaqueductal gray; SC, spinal cord dorsal horn.

Behavioral characterization of the CIPN mouse model on Astrocyte-RiboTag mice: effect of σ1R antagonist EST on the development of VCR-induced neuropathy

Animal welfare

Chemotherapy may directly or indirectly play a role in the development and sustainment of cachexia, which is characterized by skeletal muscle and adipose tissue wasting, and thus with substantial weight loss and fatigue (Le Bricon *et al.*, 1995). On this account, the body weight of animals was measured daily to control signs of health deterioration that may represent a potential bias on nociceptive responses. Vincristine caused a progressive reduction in the body weight in animals of both sexes ($p < 0.001$ saline vs. VCR; **Figure 25 a,b),** but especially in males, which showed significantly higher weight loss than females at the end of the treatment ($p < 0.001$; **Figure 25 c,d).** However, no animal exceeded humane endpoint criterion (≥ 20% decrease in body weight) (Talbot *et al.*, 2020), and they did not present major changes in their general wellbeing throughout the experimental procedure. The administration of EST did not produce significant changes in body weight within saline or VCR-treated animals in neither sex. Saline-treated mice did not display significant modifications in their body weight throughout the experimental sequence.

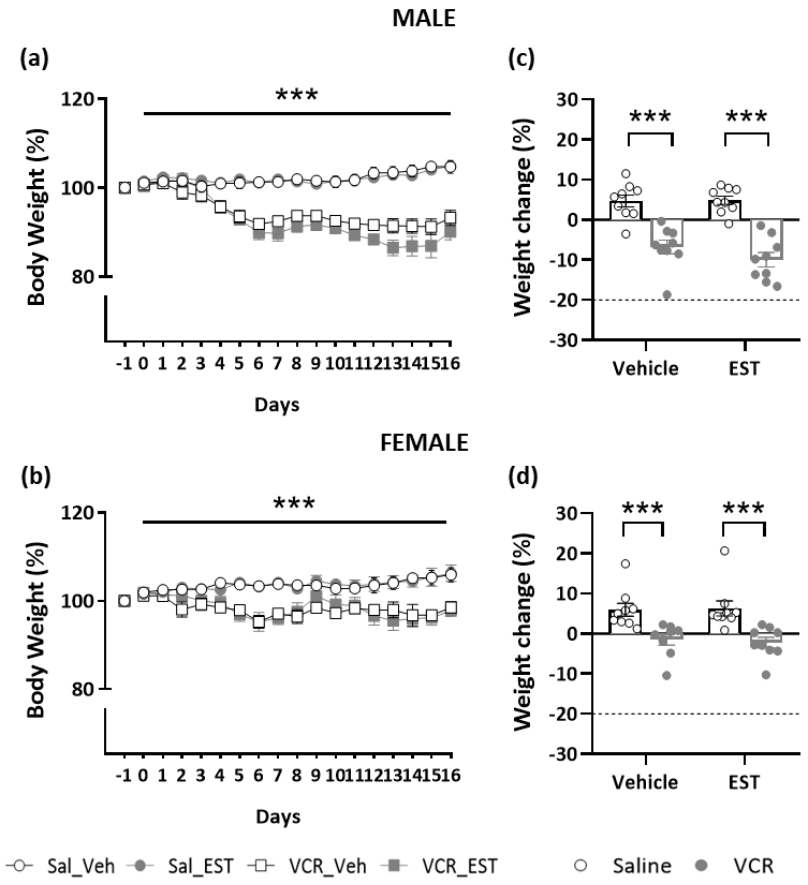

Figure 25. Effect of the treatments on the body weight of Astrocyte-RiboTag mice. Vincristine (0.5 mg/Kg i.p) induced significant but not critical weight loss in both sexes. **(a,b)** Vincristine produced a gradual reduction in the body weight in both sexes. Repeated treatment with EST did not produce significant weight variations. **(c,d)** Total weight loss was significantly higher in male than female mice treated with vincristine. No animal had to be excluded from the experiment for critical weight loss (dot lines represent humane endpoint criterion value of 20% weight reduction). Data are expressed as mean ± SEM: percentage of body weight relative to initial weight in naïve conditions (day -1; a,b); percentage of total weight change at day 16 relative to initial weight. *** $p<0.001$ Sal vs. VCR. Three-way repeated measures ANOVA + Bonferroni (a,b); Two-way ANOVA + Bonferroni (c,d). Sal, saline; Veh, vehicle; VCR, vincristine; EST, σ1R antagonist. Detailed statistical analyses are shown in **Supporting Table 1.**

Effect of vincristine and σ1R antagonist EST on nociception

Unlike other neuropathic pain conditions, chemotherapy administration to cancer patients is a planned/scheduled procedure and thus neuropathic pain can be anticipated in a short-term frame following administration of the cytostatic. In this scenario, it makes sense to investigate preventive measures that might reduce the negative effects of antineoplastics. Therefore, given the potential benefit of co-administering patients with chemotherapy drugs and drugs counteracting its undesired effects, the possible preventive effect of EST drug on the development of VCR-induced neuropathic pain was also investigated. For this purpose, EST (or vehicle) was administered p.o at 25 mg/kg starting 1 day before the first injection of VCR (or saline) and throughout the whole experimental procedure (last injection on day 16).

The von Frey test was used to assess the development of mechanical allodynia. To evaluate the acute and long-lasting analgesic effects of the σ1R antagonist EST, mechanical responses were measured before (PRE) and 30 min after (POST) the daily EST or vehicle administration **(Figure 26 a,b)**. Baseline mechanical thresholds (day -1) were similar in all experimental groups, and no differences were observed between sexes. Exposure to saline did not modify the mechanical responses during the whole experimental procedure, and EST treatment had no consequences in withdrawal thresholds in saline-treated animals **(Figure 26 a,b**). As expected, systemic exposure to vincristine (0.5 mg/kg i.p) elicited pronounced mechanical allodynia in both sexes, as evidenced by a significant decrease in the withdrawal thresholds to mechanical stimulation when compared with saline-treated mice. Mechanical allodynia developed after the first administration of this compound and

was maintained during the entire experimental protocol **(Figure 26 a,b).** We observed that EST produced mild analgesic effects after acute administration on every testing day both in male and female mice **(Figure 26 a,b *right panels*).** However, prolonged exposure to EST promoted a gradual recovery of the response in both sexes, revealed as an increase in the mechanical threshold observed in EST pre-exposure (PRE) assessments throughout the study **(Figure 26 a,b *left panels*).**

On the other hand, sensitivity to heat stimulation was also assessed in these animals in the plantar test once mechanical evaluations were completed and approximately 60 minutes after vehicle or EST administration. All mice showed similar withdrawal latencies in basal conditions (day -1), with no differences between sexes. Heat sensitivity was unaffected by exposure to saline, and EST treatment did not affect the responses of saline-treated mice **(Figure 26 c).** A single administration of VCR was sufficient to produce heat hyperalgesia in male and female mice. This sensory alteration became more pronounced throughout prolonged chemotherapy with VCR **(Figure 26 c).** Repeated administration of EST significantly attenuated thermal hyperalgesia, with both sexes reaching a total recovery of baseline levels at the end of the experimental procedure **(Figure 26 c).**

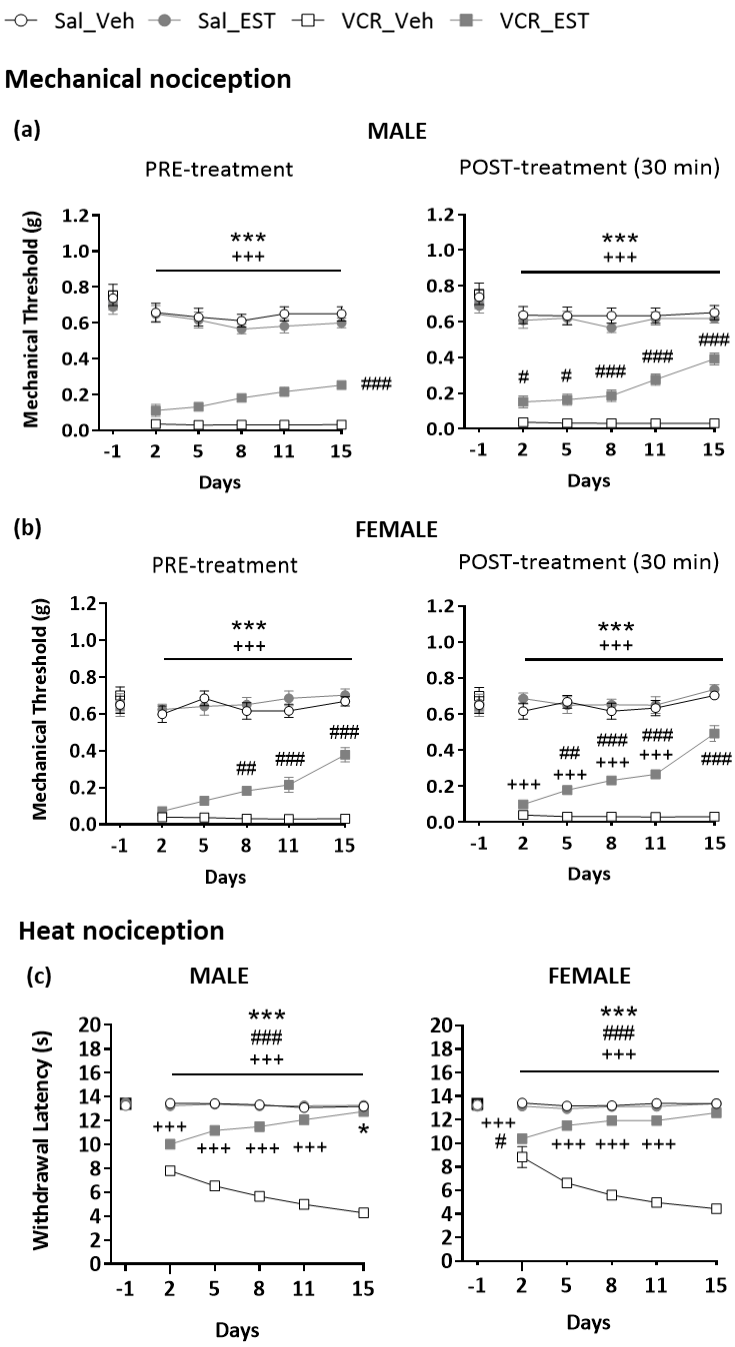

Figure 26. Effects of repeated and acute administration of EST on mechanical and heat sensitivity in vincristine-induced neuropathy in Astrocyte-RiboTag mice. Nociceptive sensitivity to mechanical and heat stimulation was evaluated

using the Von Frey and Hargreaves plantar test, respectively. **(a, b)** Vincristine causes the development of mechanical allodynia after a single injection (day 2) compared to saline-treated animals. Repeated treatment with σ1R antagonist EST 25 mg/kg produced a progressive increase of mechanical thresholds, especially in female. Acute EST administration was subeffective in alleviating mechanical hypersensitivity, as demonstrated by no significant differences between PRE and POST mechanical values. No significant differences were observed between sexes. **(c)** Heat hyperalgesia was also confirmed by significant differences in withdrawal latencies between saline and VCR-treated animals after a single dose of VCR and during whole experimental protocol. Repeated EST administration induced a gradual normalization of heat sensitivity with complete recovery of baseline values. No differences in heat nociception were observed between male and female mice. Data are expressed as mean ± SEM (n = 9/group). *** $p<0.001$ vs VCR; # $p<0.05$, ## $p<0.01$, ### $p<0.001$ vs Veh; +++$p<0.001$ vs baseline (VCR treated groups). Sal, saline; Veh, vehicle; VCR, vincristine; EST, σ1R antagonist. Kruskal-Wallis (baseline, a,b); Mixed Model Analysis + Bonferroni (a,b,c); Detailed statistical analyses are shown in **Supporting Table 2**.

To better understand the analgesic potential of EST on vincristine-induced neuropathic pain, the percentage of analgesia was also represented. The results showed that repeated EST treatment gradually increased analgesic levels for both mechanical and heat sensitivity in both sexes **(Figure 27).** Notably, almost a total analgesic efficacy was observed for heat sensitivity at the end of the experiment in both males (93.2 ± 5.2; **Figure 27 a**) and females (93.3 ± 4.3 **(Figure 27 b**), with no significant differences between sexes. In contrast, EST treatment showed a lower analgesic efficacy in alleviating mechanical allodynia. In this case, prolonged treatment with EST had significantly higher effects on alleviating mechanical allodynia in females than males ($p < 0.01$), especially at the end of the study, where females exhibited around 60% of analgesia (59.1 ± 16.8 **(Figure 27 b)** while in males it was around 35% (33.1 ± 5.5) (PRE values relative to baseline) **(Figure 4 a)**. Additionally, a significant acute analgesic effect was also revealed. Thus, an increase in analgesia was observed in POST compared to

PRE evaluations ($p < 0.001$). Again, this effect was significantly higher in females compared to males ($p < 0.01$) **(Figure 27 a,b)**.

Together, these results indicate that persistent modulation of σ1R activity by EST leads to functional changes that efficiently alleviate vincristine-induced mechanical allodynia and especially thermal hyperalgesia.

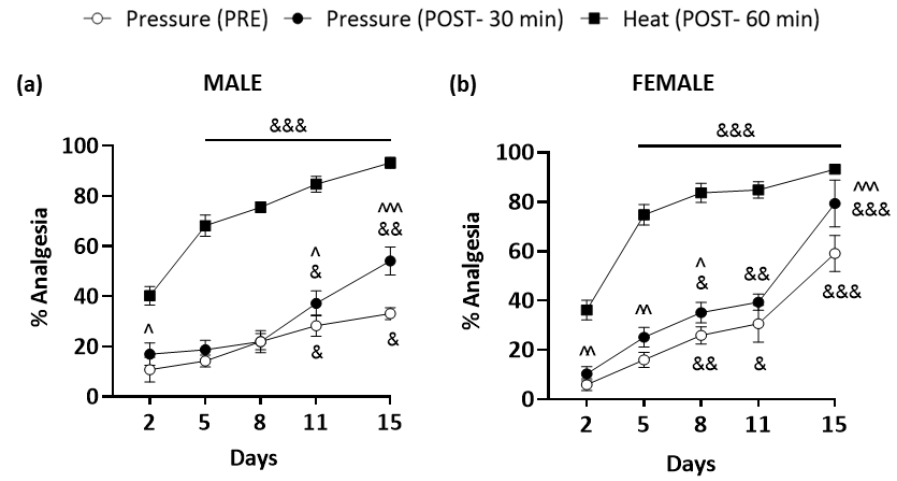

Figure 27. Analgesic efficacy of EST treatment on vincristine-induced neuropathic pain in Astrocyte-RiboTag mice. Repeated EST treatment produced different analgesic efficiency for mechanical and thermal sensitivity in both male **(a)** and female **(b)** mice. A full analgesic effect was reached for heat sensitivity in both sexes, while lower efficacy was observed in alleviating mechanical allodynia. A slight but significant analgesic effect of acute administration of EST is also observed for mechanical sensitivity, especially at the end of the experiment and in females. Data are expressed as mean ± SEM (n = 9/group). ^ $p<0.05$, ^^ $p<0.01$, ^^^ $p<0.001$ vs PRE; & $p<0.05$, && $p<0.01$, &&& $p<0.001$ vs Day 2. One or Two-way repeated measures ANOVA + Bonferroni. Detailed statistical analyses are shown in **Supporting Table 3****Supporting Figure 2**.

Purification and sequencing of Astrocyte-Enriched mRNA from diverse pain-related regions of the CNS

To evaluate the transcriptomic alterations associated with vincristine-induced neuropathic pain and the modifications involved in EST analgesic effects, specifically in astrocytes, we performed RNA-seq analysis of astrocyte-purified mRNA. After behavioral characterization, astrocyte mRNA was isolated from different CNS areas crucially involved in the transmission and processing of the nociceptive signal – the SS, PAG, and dorsal SC - by HA-tagged polysomes immunoprecipitation. Two-time points were considered: day 3 (early; after 2 VCR injections and 3 doses of EST), when symptoms of the development of neuropathic pain are first observed, and on day 16 (late; 11 doses of VCR and 16 doses of the treatment), when CIPN is fully established and maintained.

Validation of cellular specificity of isolated mRNA samples (IP samples) was first assessed by qRT-PCR analysis. As expected, this analysis revealed a clear enrichment of astrocytic marker *Aldh1l1* in immunoprecipitated (IP) samples compared to the input fraction (which contain all mRNAs from the initial homogenate) and de-enrichment of markers for other cell types, including *Cx3cr1* for microglia, *Ugt8a* for oligodendrocytes, and *Rbfox3* for neurons **(Figure 28 a,b, right insert).** Samples that presented enrichment for any of these non-astrocytic markers were excluded for sequencing analysis. Selected samples were then sequenced (RNA-seq) to identify and quantify gene expression changes. Input samples (whole tissue mRNA) from the control saline group (saline-vehicle) were also sequenced to provide a reference for astrocyte specificity.

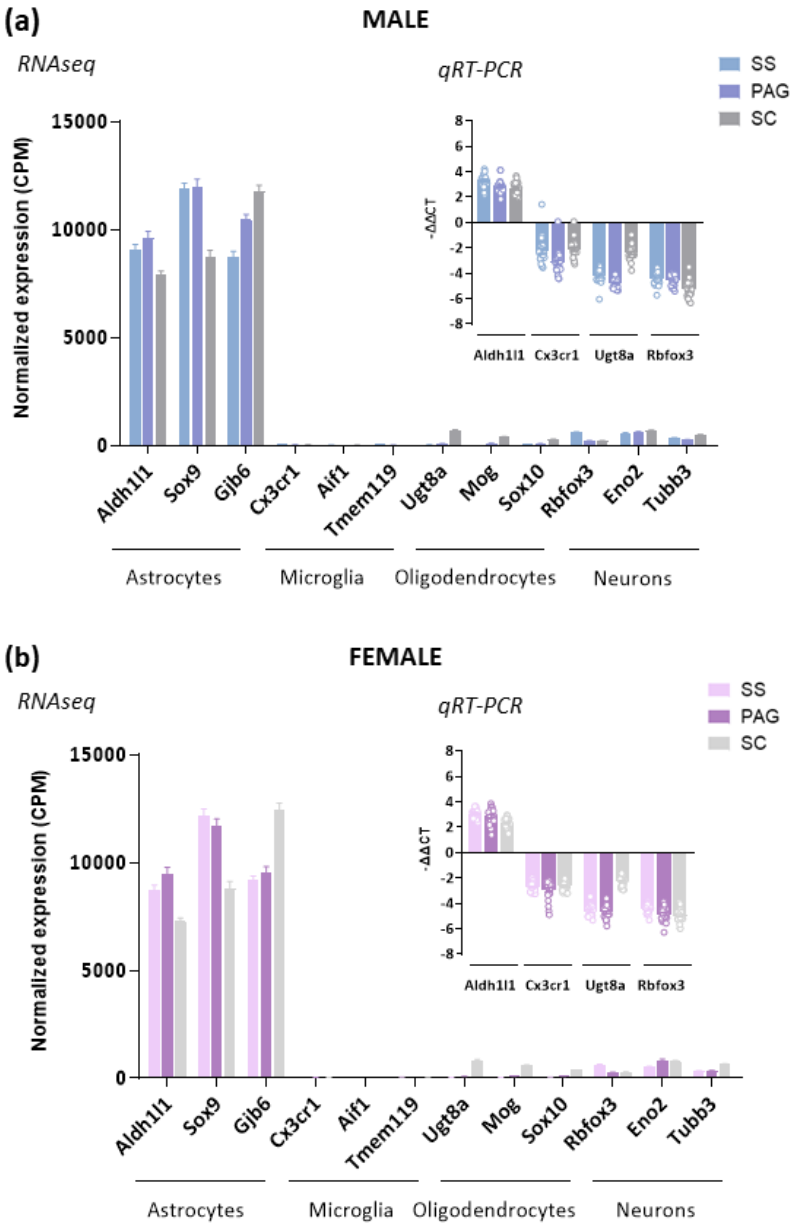

Figure 28. Isolation and cell-specificity verification of Aldh1l1-RiboTag mice mRNA from pain-related areas. (a,b) Gene expression levels (in read counts per million; CPM) of markers for astrocytes, microglia, oligodendrocytes, and neurons, in RNAseq data from male **(a)** and female **(b)** HA-immunoprecipitated (IP) samples (cell-specific mRNA) of whole somatosensory cortex (SS), periaqueductal gray (PAG) and dorsal spinal cord (SC) extracts. Data are presented

as mean values ± SEM (Male: n = 23 samples/ region; Female: n = 24 samples/ region). **(a,b, insert)** Validation by qRT-PCR (-ΔΔCt) of the enrichment of astrocyte markers (Aldh1l1) and de-enrichment of microglial (Cx3cr1), oligodendrocytes (Ugt8a), and neuronal (Rbfox) markers in IP samples compared with the input fractions (mRNAs from all cellular types). Males: one sample from each region were discarded for presenting contamination from microglial mRNA. Females: All mRNA samples showed good astrocyte specificity and were included for sequencing. Data are presented as the mean values ± SEM (n = 24 samples/ region/ sex).

To further confirm that the resultant molecular profiles reflect astrocyte-specific signatures and discard any significant contamination from other cell types not detected by *qRT-PCR*, we examined the expression of established markers for astrocytes, microglia, oligodendrocytes, and neurons (Zhang *et al.*, 2014) in our data **(Figure 28 a,b).** Together, these data indicate that we successfully isolated astrocyte-specific mRNA and profiled their transcriptomes from distinct CNS regions.

Quality control and sample distribution

All samples showed a homogeneous total number of counts and a high ratio of alignment and assignment (around 75%; not shown), indicating overall good quality and suitability for further analysis. We applied principal component analysis (PCA) using normalized counts as an unbiased approach to analyze global gene expression patterns to determine sample distribution. PCA revealed a clear separated clustering of IP samples and inputs (PC1; **Figure 29 a),** underscoring the difference between cell-specific RNA (IP) and the whole tissue (input) gene expression profile. After mRNAs isolation (IP vs. input), the origin of the mRNA (region of extraction) represented the primary source of variability (PC2; **Figure 29 a).** In this regard, PCA showed that samples cluster primarily by region **(Figure 29 b),** showing a similar clustering distribution

in males and females. The SS displayed the greatest expression pattern variation (PC1; **Figure 29 b)** compared to PAG and SC, which aggregated closer. Dendrogram of sample-to-sample correlation distances confirmed this clustering (not shown). By contrast, there was little aggregation by time point **(Figure 29 c)** and a significant variability according to the treatment group in both sexes **(Figure 29 d).** This separation between astrocytes derived from various regions of the CNS was observed in both VCR and saline controls, with this being consistent with the concept of regional heterogeneity of astrocytes (Khakh and Sofroniew, 2015) and indicating regional differences in gene expression in astrocytes during CIPN conditions.

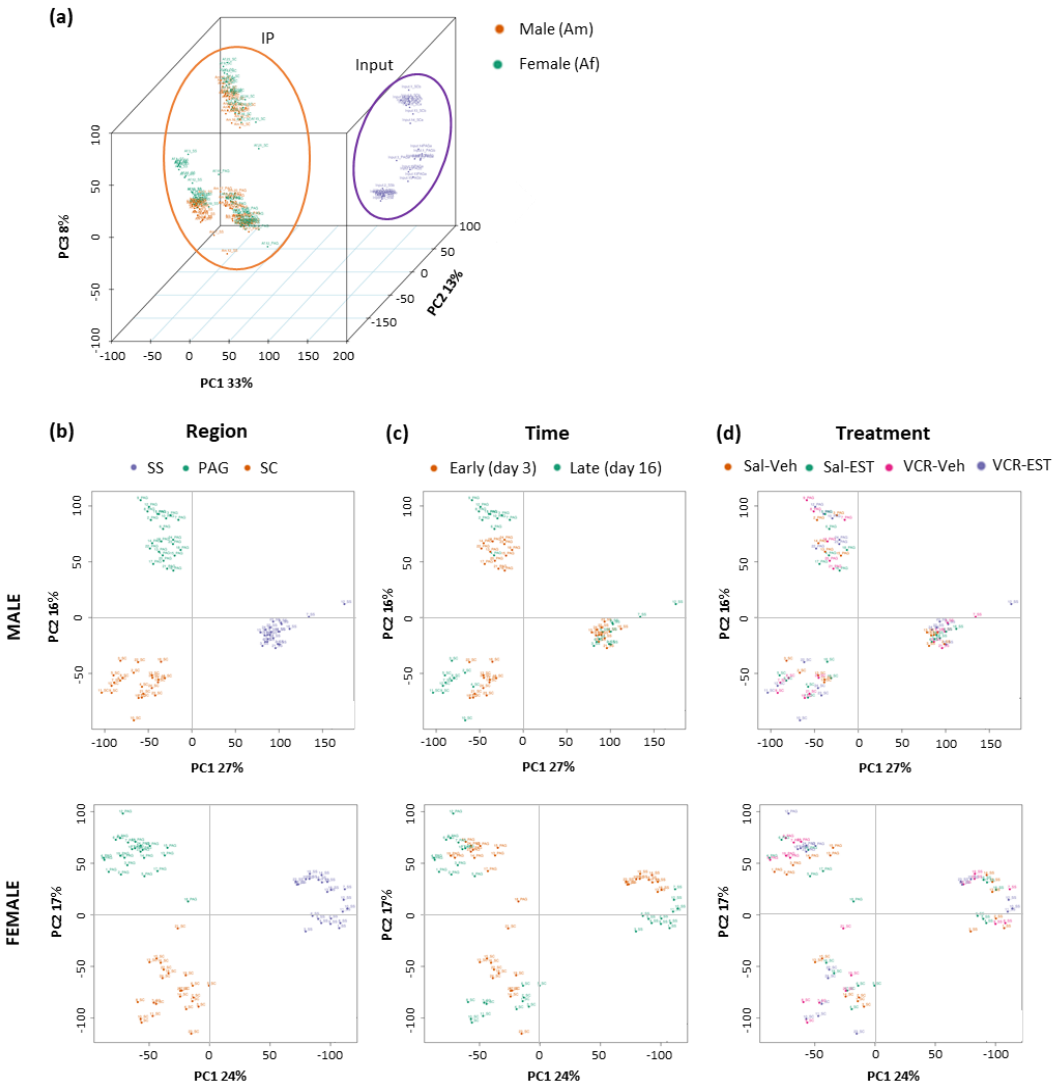

Figure 29. Principal component analysis (PCA). (a) PCA analysis of RNAseq gene expression of all astrocyte-enriched RNAs (IP samples) and control inputs (saline vehicle) from male and female Aldh1l1-RiboTag mice. IP samples are clearly separated from inputs (PC1). Within astrocyte-enriched samples (IP), they cluster primarily by **(b)** region (SS, somatosensory cortex; PAG, periaqueductal gray; SC, spinal cord dorsal horn), then by **(c)** time point, and finally according to **(d)** treatment replicates, with a similar distribution in males and females. Each number corresponds to a pool of tissues from 3 mice (IP: n = 23-24/region/sex; Input: n = 6/region/sex). Sal, saline; Veh, vehicle; VCR, vincristine; EST, σ1R antagonist.

Identification of specific gene expression changes induced by vincristine and the blockage of sigma-1 receptors in astrocytes from multiple pain-related regions

Effects of vincristine in the astrocyte transcriptome

Next, we sought to identify the gene expression changes induced after short (early) and prolonged (late) exposure to vincristine, contributing to the development and maintenance of the neuropathy by astrocytes, respectively. Towards this, we performed differential gene expression (DE) analysis by comparing VCR-vehicle to saline-vehicle treated groups for each region, time point, and sex, separately. Using a p-value < 0.05, this analysis identified 1000-2500 significantly different genes throughout the comparatives. Filtering these genes by applying a p value adjusted for multiple comparisons (Benjamini and Hochberg, 1995), the list of candidates was narrowed down to < 30 genes for the distinct conditions. Since this number was too few to extract relevant conclusions, we focused on the list of genes differentially expressed with p value < 0.05 significance level but filtering for a FC > 2 or < -2. With these criteria, the list of differentially expressed genes (DEG) was reduced to 200-350 genes for each comparative (top 20 up- and downregulated genes per region; **Supporting Table 4 -Supporting Table *5***). To determine whether the DEG are region-specific and identify core VCR-induced gene changes, we looked for overlap between regions for up (FC > 2) and downregulated (FC < -2) genes during early and late chemotherapy separately.

This analysis identified 11 downregulated genes in males and 12 in females during the short-term dose period **(Table 8; Figure 30 a),** whereas no overlap between the upregulated genes was found in neither sex. Interestingly, core downregulated genes were the same in both sexes.

Some of these genes were considerably depleted in VCR group (6-40-fold change) and significantly different expressed in this comparative (adjusted $p < 0.05$) **(Table 8; Figure 30 b).** These included two α-globin (*Hba)* and two β-globin (*Hbb)*, which together constitute the hemoglobin complex, and *Alas2*, encoding for the enzyme 5'-Aminolevulinate Synthase 2 that catalyzes the first step in the heme biosynthetic pathway. Other core downregulated genes included *Ube2l6, Rsad2,* and *Isg20,* which all play a role in immune response, the erythrocyte anion exchanger *Slc4a1*, and *Apol11b*, a lipoprotein involved in both heme metabolism and immune response. However, most of these genes were not differentially expressed ($p > 0.05$) in any area during prolonged chemotherapy with the exception of *Apol11b* and *Slc4a1,* which were significantly upregulated in astrocytes from SS and PAG in males **(Supporting Table 5)** and all three regions in females. In fact, in this time-point, neither up nor downregulated core genes were found in males but 8 upregulated genes in females, including the above mentioned **(Figure 30 c,d).**

To further investigate the specific functionality and connections of these core VCR-induced genes, we looked for their interactome network. This analysis confirmed that genes are highly interconnected and aggregate in two main domains of functionality, including (1) oxygen transport, and (2) immune system process **(Figure 30 e).** Therefore, these results indicate that changes in hemoglobin (Hb)-like molecules and immune-related coding genes in astrocytes may contribute to the early VCR sensitized phenotype observed in both male and female mice.

Overall, these data identified core VCR-induced changes that are common to all astrocytes from pain-related areas in both males and females, as well as unique region- and sex-dependent transcriptomic changes.

Table 8. List of overlapping downregulated genes between regions and between males and females by comparing VCR-vehicle to saline-vehicle groups receiving short-term chemotherapy (early).

	MALE			FEMALE		
Gene	**SS**	**PAG**	**SC**	**SS**	**PAG**	**SC**
Alas2	-3,56*	-4,42*	-4,12*	-2,95*	-3,80*	-3,16*
Apol11b	-3,20	-5,40*	-6,59*	-4,11*	-4,09*	-4,92
E2f2	X	-2,12	-2,05*	X	-1,76	-1,90
Gda	X	X	-2,14*	X	X	-1,80
Gypa	X	X	-5,37*	-3,57*	-3,90	-4,10
Hba-a1	-3,08*	-3,97*	-4,13*	-3,42*	-3,97*	-2,59*
Hba-a2	-3,00*	-4,03*	-4,21*	-3,70*	-4,21*	-2,76*
Hbb-bs	-3,29*	-4,05*	-4,08*	-3,35*	-4,03*	-2,44*
Hbb-bt	-4,29*	-5,20*	-5,40*	-4,16*	-4,95*	-3,45*
Helz2	X	X	-2,68*	X	X	-1,63
Isg15	X	X	-1,15	X	X	-1,50
Isg20	-1,24	-1,43	-2,17*	-1,85	-1,60	-2,84*
Nrap	-4,22	X	X	-2,12	X	X
Pde4c	-1,73	X	X	-2,55	X	X
Rsad2	-1,05	-2,05*	-2,80*	-1,33	-2,27*	-2,21
Sash3	X	X	-2,39	X	X	-2,66
Slc25a37	X	-1,06*	-2,07*	X	-1,29	-1,49*
Slc4a1	-3,48	-5,36*	-5,34	-3,91	-5,72*	-4,50
Snca	X	-1,10*	-1,78*	X	-1,40*	-1,34
Spta1	-2,90	X	-4,51*	X	-3,41	-5,20
Tent5c	-3,14*	-2,63*	-3,83*	-2,93*	-2,42*	-2,96*
Trim10	X	X	-2,19	-3,27	X	-4,55
Ube2c	X	X	-1,97	X	X	-2,24
Ube2l6	-1,80	-2,11*	-2,44*	-1,66	-1,85*	-1,87*
$Total_1$		11			12	
$Total_2$	13	14	22			

Data from lists of differentially expressed genes (DEG) with $p < 0.05$ and logFC < -1 in astrocyte-specific RNAs from each region. The values are logFC between VCR-vehicle and saline-vehicle groups. Negative values indicate downregulation in VCR-vehicle group. $Total_1$, genes in common between regions in the same sex; $Total_2$, genes in common between sexes in each region. SS, somatosensory cortical astrocytes; PAG, periaqueductal gray matter astrocytes; SC, spinal cord dorsal horn astrocytes. X, absent.* adjusted $p < 0.05$

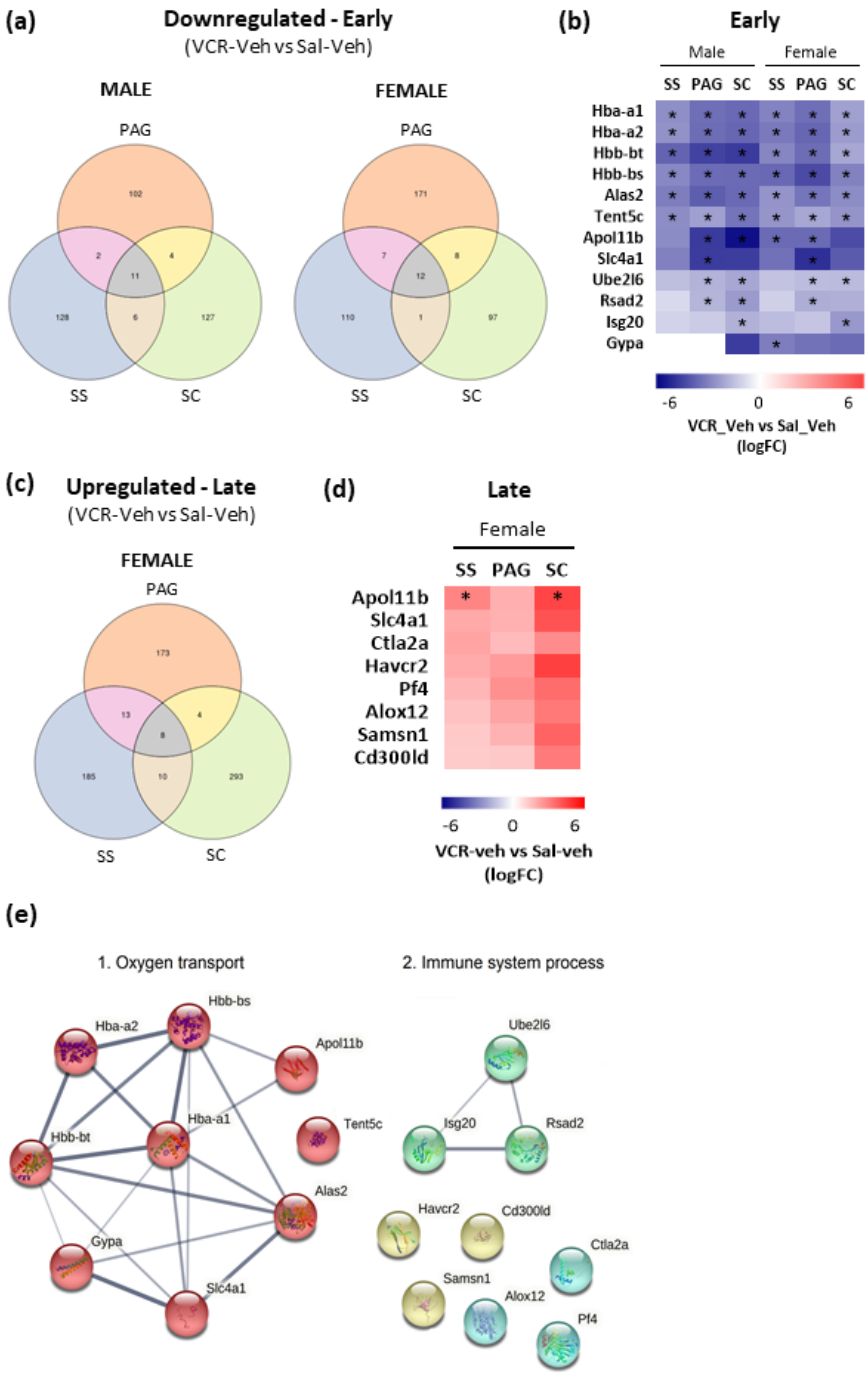

Figure 30. Relevant gene expression changes induced by VCR in astrocytes from pain-related regions. (a) Venn diagram showing overlap of genes downregulated

in astrocytes from 3 different CNS regions between vincristine-vehicle (VCR-Veh) and saline-vehicle (Sal-Veh) during early chemotherapy (day 3) in males and females ($p < 0.05$ and logFC < -1). **(b)** Heatmap of genes that are significantly downregulated in astrocytes by VCR in all regions for males and females. **(c)** Venn diagram of overlapping genes upregulated in astrocytes from 3 different CNS regions between vincristine-vehicle (VCR-Veh) and saline-vehicle (Sal-Veh) during late chemotherapy (day 16) in females ($p < 0.05$ and logFC > 1). **(d)** Heatmap of significantly upregulated genes in astrocytes by VCR in all regions in females. **(e)** STRING protein-protein interaction network for proteins encoded by core genes described. Each circle represents the protein affected by at least one variant in the list. The thickness of the grey lines represents the strength of data supporting a protein-protein interaction (Edge confidence: low, 0.150; medium, 0.4; high, 0.7; highest, 0.9). The color of circles represents aggregation on a different functional cluster. The PPI enrichment p-value for the number of identified edges (22) compared to expected (1) in a group of 20 proteins was 1 x 10-16, thus significantly more than expected. * adjusted $p < 0.05$. SS, somatosensory cortex; PAG, periaqueductal gray; SC, spinal cord dorsal horn.

Modulatory effects of sigma-1 receptor blockade on the astrocyte transcription profile under neuropathic pain induced by vincristine

To address the direct or indirect effects of the σ1R antagonist EST on astrocytic function under vincristine-induced neuropathic pain conditions, we applied DE analysis by comparing VCR-EST to its control group (Sal-EST) first, and then to VCR-vehicle group. Again, we focused on the list of genes obtained using the filtering criteria of $p < 0.05$ significance level and FC > 2 or < -2 cutoff and looked for overlapping between regions and sexes.

Short treatment with EST produced minor changes on VCR-induced transcriptomic alteration, as showed by the lack of relevant differences in gene expression patterns obtained between VCR-EST vs. Sal-EST and VCR-Veh vs. Sal-Veh comparisons. In fact, we obtained the same profile of downregulated genes, with no other relevant findings **(Table 9).** However, with prolonged exposure to EST (16 days, that produced relevant analgesic

effects), we still observed some of the VCR-induced core genes mentioned as significantly downregulated, especially in males **(Table 10).**

Table 9. List of overlapping downregulated genes between regions and between males and females by comparing VCR-EST to saline-EST groups receiving short-term treatments (early).

	MALE			FEMALE		
Gene	**SS**	**PAG**	**SC**	**SS**	**PAG**	**SC**
Adcy4	X	-1,85	X	X	-2,64	X
Alas2	-3,36*	-3,12*	-4,13*	-2,88*	-3,36*	-3,77*
Apol11b	-4,10*	-5,02*	-5,03*	-4,11*	-4,85*	-4,90*
Ctse	X	X	-2,80	-3,27	X	-3,34
E2f2	X	X	-1,26	X	-2,81	-1,81
Gda	X	-1,92	-2,11	X	X	-2,99*
Gypa	X	X	-4,08	-3,74	-2,88	-2,92
Hba-a1	-3,47*	-3,69*	-3,87*	-3,20*	-3,43*	-3,11*
Hba-a2	-3,76*	-3,85*	-4,32*	-3,54*	-3,54*	-3,44*
Hbb-bs	-3,52*	-3,82*	-3,86*	-3,11*	-3,39*	-3,09*
Hbb-bt	-4,65*	-4,66*	-5,00*	-3,55*	-3,74*	-4,04*
Hmcn1	X	X	-1,35	X	X	-1,31
Isg20	-1,93	X	-2,86*	-1,52	-2,04	-2,72
Prkag2os1	-1,12	X	X	-1,11	X	X
Rsad2	X	-2,10*	-2,27*	-1,51	-2,02	-2,70
Slc25a37	X	X	-1,78*	-1,18	-1,39	-2,16*
Slc4a1	-3,92*	-3,28	-6,17	-4,63*	-3,90*	-6,81*
Snca	X	-1,30*	-1,65*	X	-1,48	-1,77*
Spta1	-3,45	X	-4,08	X	X	-2,80
Tent5c	-3,10*	-3,02*	-3,56*	-2,62*	-2,53	-3,78*
Trim10	X	X	-4,16	-3,13	X	-3,92
Ube2l6	-2,16*	-1,62*	-2,12*	-2,31*	-1,60	-1,79*
$Total_1$		9			13	
$Total_2$	12	12	20			

Data from lists of differentially expressed genes (DEG) with $p < 0.05$ and logFC < -1 in astrocyte-specific mRNAs from each region. The values are logFC between VCR-EST and saline-EST groups. Negative values indicate downregulation in VCR-EST group. $Total_1$, genes in common between regions in the same sex; $Total_2$, genes in common between sexes in each region. SS, somatosensory cortical astrocytes; PAG, periaqueductal gray matter astrocytes; SC, spinal cord dorsal horn astrocytes. X, absent.* adjusted $p < 0.05$

Table 10. List of overlapping downregulated genes between regions and between males and females by comparing VCR-EST to saline-EST groups receiving prolonged treatments (late).

	MALE			FEMALE		
Gene	**SS**	**PAG**	**SC**	**SS**	**PAG**	**SC**
Alas2	-1,35*	-4,20*	-4,13*	X	X	X
Ccdc87	X	-2,38	X	X	-1,25	X
Cd36	X	X	-2,06	X	X	-18,38
Cntnap5c	X	X	-1,92	X	X	-3,05
Cpne7	X	X	-1,61	X	X	-3,76
Crh	-1,23	X	X	-2,60	X	
Fabp4	X	X	-3,63	X	X	-42,84
Gngt2	-2,00	-1,88	-2,05	X	X	-2,33
Hba-a1	X	-2,54*	-4,01*	X	X	-2,54
Hba-a2	X	-2,44*	-3,90*	X	X	-2,63
Hbb-bs	-1,04*	-2,58*	-4,02*	X	X	-2,97
Isg20	X	-1,18	-2,29	-2,26	X	X
Itgal	-2,00*	X	-2,00	X	X	X
Npy2r	-2,49	X	X	-3,45	X	X
Pcdha5	-2,74	X	X	-4,06	X	X
Pck1	X	X	-4,25	X	X	-13,29
Sspo	X	-1,21	3,20	X	-1,13	X
Traf1	X	-1,05*	X	X	-1,16	X
$Total_1$		4			0	
$Total_2$	3	3	9			

Data from lists of differentially expressed genes (DEG) with $p < 0.05$ and logFC < -1 in astrocyte-specific RNAs from each region. The values are logFC between VCR-EST and saline-EST groups. Negative values indicate downregulation in VCR-EST group. $Total_1$, genes in common between regions in the same sex; $Total_2$, genes in common between sexes in each region. SS, somatosensory cortical astrocytes; PAG, periaqueductal gray matter astrocytes; SC, spinal cord dorsal horn astrocytes. X, absent.* adjusted $p < 0.05$

These results were corroborated when comparations between VCR-Veh and VCR-EST-treated groups were performed (top 20 up- and downregulated genes per region; **Supporting Table 6 -Supporting Table *7*).** During early treatments, no differential expression of the described core genes was observed in any region (**Supporting Table 6**), indicating similar expression levels and thus, no relevant effect of the treatment. In contrast, these genes appeared as significantly downregulated during late period,

with overlap between regions and sexes **(Figure 31 a).** In particular, *Hba, Hbb* and *Alas2* were notably depleted in males, especially in SC astrocytes **(Figure 31 b).**

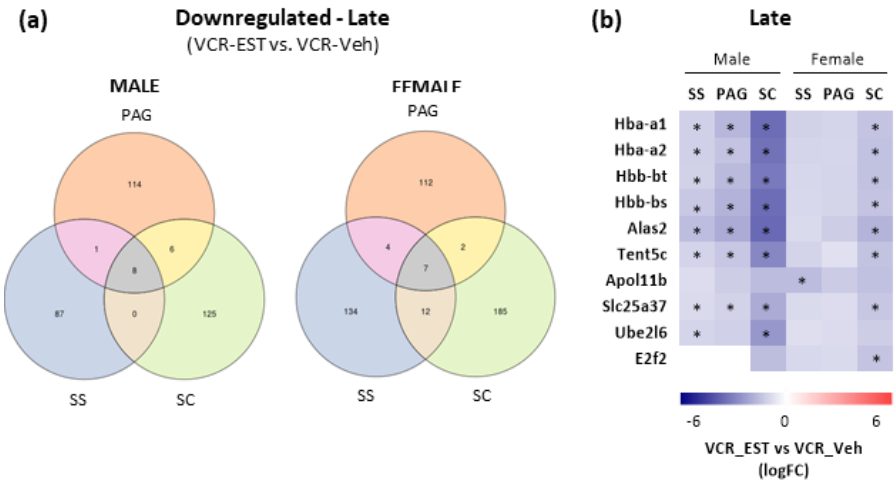

Figure 31. Relevant gene expression changes induced by σ1R blockade on astrocytes under VCR-induced effects. (a) Venn diagram showing overlap of genes downregulated in astrocytes from 3 different CNS regions between vincristine-EST (VCR-EST) and vincristine-vehicle (VCR-Veh) during late treatment (day 16) in males and females ($p < 0.05$ and logFC < -1). **(b)** Heatmap of genes that are significantly downregulated in astrocytes by EST (σ1R antagonist) in all regions for males and females. * adjusted $p < 0.05$. SS, somatosensory cortical astrocytes; PAG, periaqueductal gray matter astrocytes; SC, spinal cord dorsal horn astrocytes

Together, these results suggest that short-term σ1R blockade have minor direct influence in modulating VCR-induced alterations on astrocytes, while prolonged exposure to σ1R antagonist EST did produce some regulatory actions on astrocyte functionality under VCR influence. In this regard, it showed some efficacy in reversing VCR-induced damage in females, which is consistent with behavioral results.

Validation of vincristine-induced gene expression changes in astrocytes

To validate the changes obtained in gene expression, we first checked for astrocyte specificity by comparing their expression in IP versus input mRNAs **(Figure 32 a).** Analysis of RNA-seq data demonstrated an enrichment for astrocytes over other cell types in the pull-down (IP; astrocyte mRNA) compared to corresponding input (total mRNA) (adjusted $p < 0.05$; Figure 9 a, left). Astrocyte specificity of some genes was also confirmed by *qRT-PCR* analysis, revealing a 2 to 3-fold enrichment in all IP mRNAs compared to inputs **(Figure 32 a, right).**

Next, qRT-PCR analysis was used to evaluate gene expression levels of *Hbb, Hba* and *Alas2* genes with 2 days (early period) and 16 days (late period) of treatment **(Figure 32 b).** Fitting with RNA-seq data, the expression of all genes was significantly downregulated by VCR during short-term treatment in both sexes. With longer treatment (late period), a significant increase in gene expression was observed in VCR-Veh group compared to saline. By contrast, the depletion continued in VCR-EST group on males but not females. These results are consistent with RNA-seq data but for the increase in gene expression on VCR-Veh group (late), which is not observed as significantly different on RNA-seq data. Further analysis will be required.

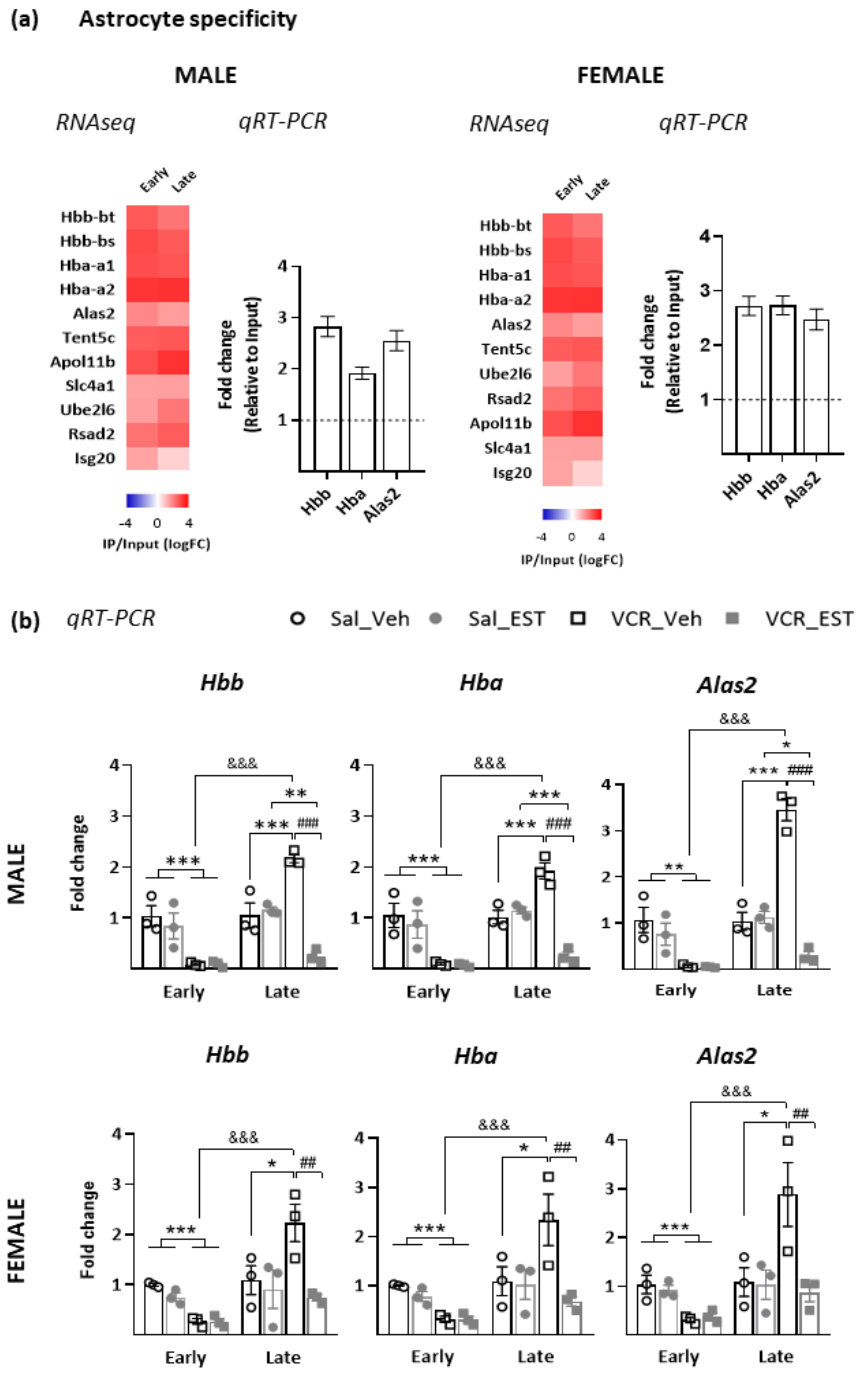

Figure 32. Validation of gene expression changes produced in spinal cord astrocytes during early (day 3) and late (day 16) CIPN. (a) Astrocyte specificity of core downregulated genes in astrocytes was validated by (left) RNA-seq data

analysis and confirmed by (right) qRT-PCR analysis in dorsal spinal cord of male and female mice. This analysis demonstrated enrichment for astrocytes over other cell types in the pull-down (IP; astrocyte mRNA) compared with input (total mRNA). The same cohort of Aldh1l1-RiboTag mice were used for both techniques. RNAseq: fold change (logFC) comparing IP vs input mRNAs of saline-vehicle control group (adjusted $p < 0.05$). Data are expressed as mean (n = 3 samples/ time point). qRT-PCR: fold change ($2^{-\Delta Ct}$) expression of Hbb, Hba and Alas2 genes relative to input. Data are expressed as mean ± SEM (n = 23-24 samples/ sex). **(b)** qRT-PCR analysis of Hbb, Hba and Alas2 gene expression levels in astrocyte-specific mRNA (IP) from dorsal spinal cord in males and females. Expression of target genes is presented as the fold-change ($2^{-\Delta Ct}$) relative to saline-vehicle control group. All target genes were first standardized to Actb endogenous control expression. Data are expressed as mean ± SEM (n = 3 samples/ group) * $p < 0.05$, ** $p < 0.01$, *** $p < 0.001$ vs saline; ## $p< 0.01$, ### $p < 0.001$ vs vehicle (two-way ANOVA + Bonferroni); &&& $p < 0.001$ vs Early (three-way ANOVA + Bonferroni). Early, short-term treatment (Day 3); Late, chronic treatment (Day 16). Detailed statistical analyses are shown in Supporting table S8.

Functional analysis of gene signatures induced by vincristine and EST treatments on astrocytes

Functional profile of VCR-induced changes on astrocyte transcriptome

As an unbiased approach to broaden insight into the biological processes affected by VCR chemotherapy in astrocytes, we carried out a functional enrichment analysis of all DEG in each pain-related region by the GSEA method (Subramanian *et al.*, 2005).

Fitting with the pattern of individual gene expression changes, during early chemotherapy, astrocytes from the three pain-related areas in both sexes showed a relevant downregulation of genes involved in oxygen transport and cellular detoxification **(Figure 33 a,b),** with the major-rate limiting genes of hemoglobin complex (*Hbb*, *Hba*) as significantly decreased, but also other genes such as the *Gpx,* encoding for the glutathione peroxidase. In addition, several immune response processes were also significantly

downregulated especially in males **(Figure 33 a),** with *Rsad2* as the first ranked gene but others such *Cd74* and *Tnf* superfamily members (not shown).

Additionally, during early chemotherapy, this analysis also identified an enrichment of genes involved in cholesterol and derivatives synthesis and metabolism in both male and female astrocytes **(Figure 33 a,b).** Concerning males, this enrichment profile was present in SS and SC astrocytes, whereas astrocytes from PAG showed a different functional enrichment pattern, with most representative gene sets involved in the regulation of synaptic transmission **(Figure 33 a).** Conversely, females showed an increase in cholesterol-related gene sets in SS and PAG but not SC astrocytes, which in turn presented an enrichment in genes involved in the immune response **(Figure 33 b).**

Regarding the effects of prolonged chemotherapy with VCR on astrocytes, the functional analysis revealed an opposite expression pattern, with a reversal on the direction of change of some of the representative processes mentioned above **(Figure 33 a,b).** Specifically, several cholesterol and lipid biosynthesis processes were significantly decreased in both sexes, but especially in females, following the same tissue-specific expression pattern commented before. In contrast, there was a mild increase in immune response-related genes, more relevant in females. Besides this, there was also a significant depletion of genes encoding for proteins of the mitochondrial respiratory chain complex, thus associated with mitochondrial dysfunction. This downregulation induced by VCR was significantly relevant in females where it was present in all pain-related regions but especially in PAG and SC astrocytes **(Figure 33 b).** In males, however, it was only relevant in PAG astrocytes **(Figure 33 a).**

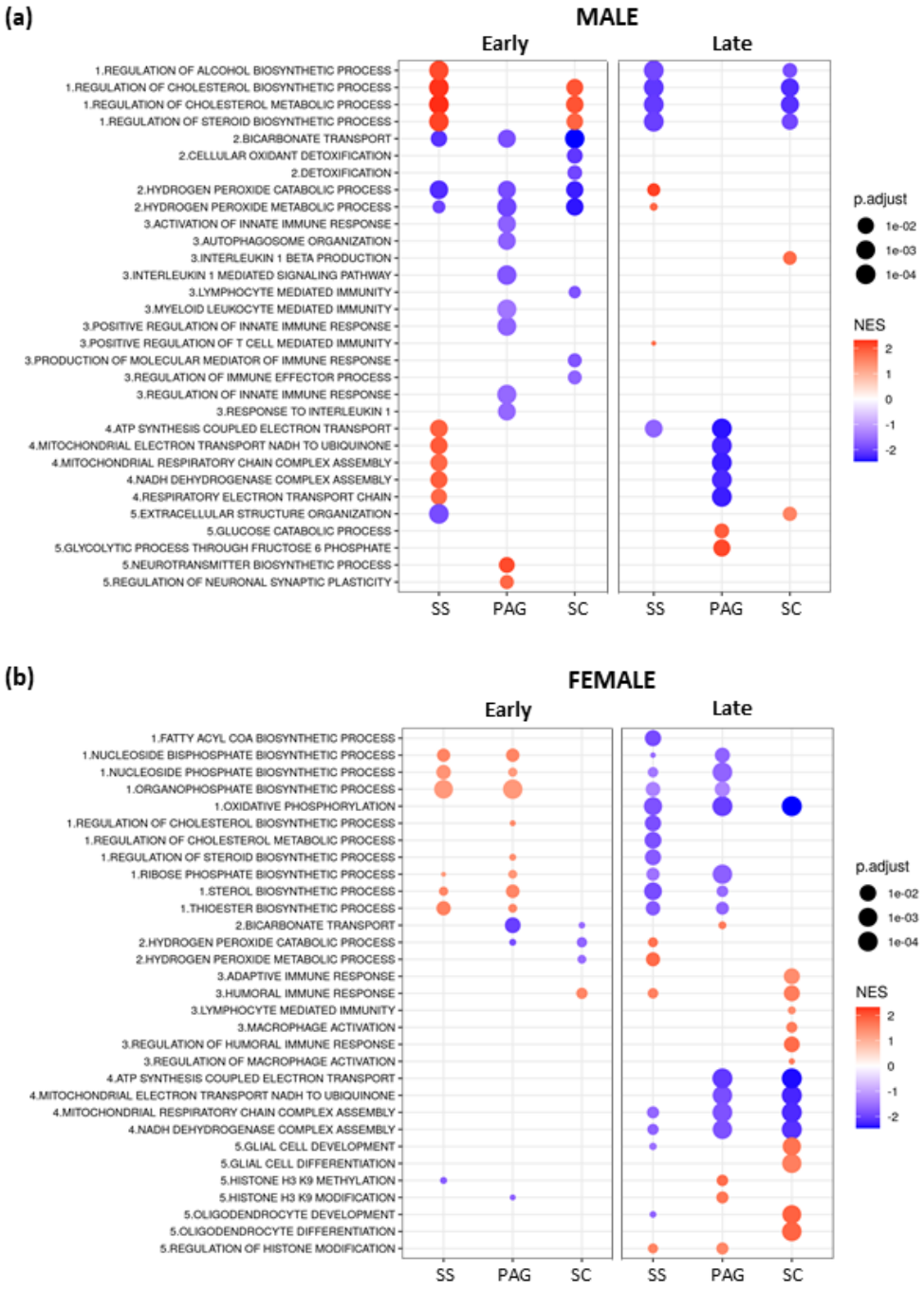

Figure 33. Identification of differentially expressed pathways between VCR and saline groups during early (day 3) and late (day 16) chemotherapy in multiple pain-related regions. Functional enrichment analysis of differentially expressed

genes (DEG) in VCR-vehicle compared to saline-vehicle group identified 4 clusters of related biological processes affected by VCR. Gene Ontology (GO) gene sets (Y-axis) are grouped in clusters of different functionalities by a number: (1) cholesterol and derivatives synthesis and metabolism, (2) cellular detoxification and oxygen transport, (3) immune response, (4) mitochondrial dysfunction, and (5) additional functional processes. NES, Normalized Enrichment Score; SS, somatosensory cortical; PAG, periaqueductal gray; SC, spinal cord dorsal horn.

Overall, functional enrichment analysis revealed that VCR chemotherapy is exerting small but coordinated changes in four major arrays of related biological processes, which were reproduced in a similar manner in both sexes. Accordingly, VCR is affecting astrocytic processes involved in (1) cholesterol and derivatives synthesis, metabolism, and transport, (2) cellular detoxification and oxygen transport, (3) immune response, and (4) mitochondrial function **(Figure 34 a-d).** In this sense, males displayed a more robust pattern of changes within and between regions, whereas females showed a more diffuse functional profile. Together, these results indicate that VCR induces a relevant dysfunction in important astrocytic biological processes, which may be contributing to the establishment of CIPN in mice.

Functional pattern of the effects of σ1R blockade on astrocytes under CIPN conditions

We applied the same functional enrichment analysis to determine whether the σ1R antagonist EST is affecting other functionalities on astrocytes under CIPN conditions. This analysis was consistent with the individual gene expression pattern, showing no significant differences in the represented pathways during early treatment when compared with previous analysis (VCR-vehicle vs saline-vehicle), but a relevant depletion of the above-mentioned genes involved in oxygen transport and cellular detoxification during chronic treatment (not shown).

Therefore, these results further confirm that short-term σ1R blockage exert minor effects on VCR-induced changes on astrocytes, but longer exposure to the σ1R antagonist influences somehow astrocyte functionality.

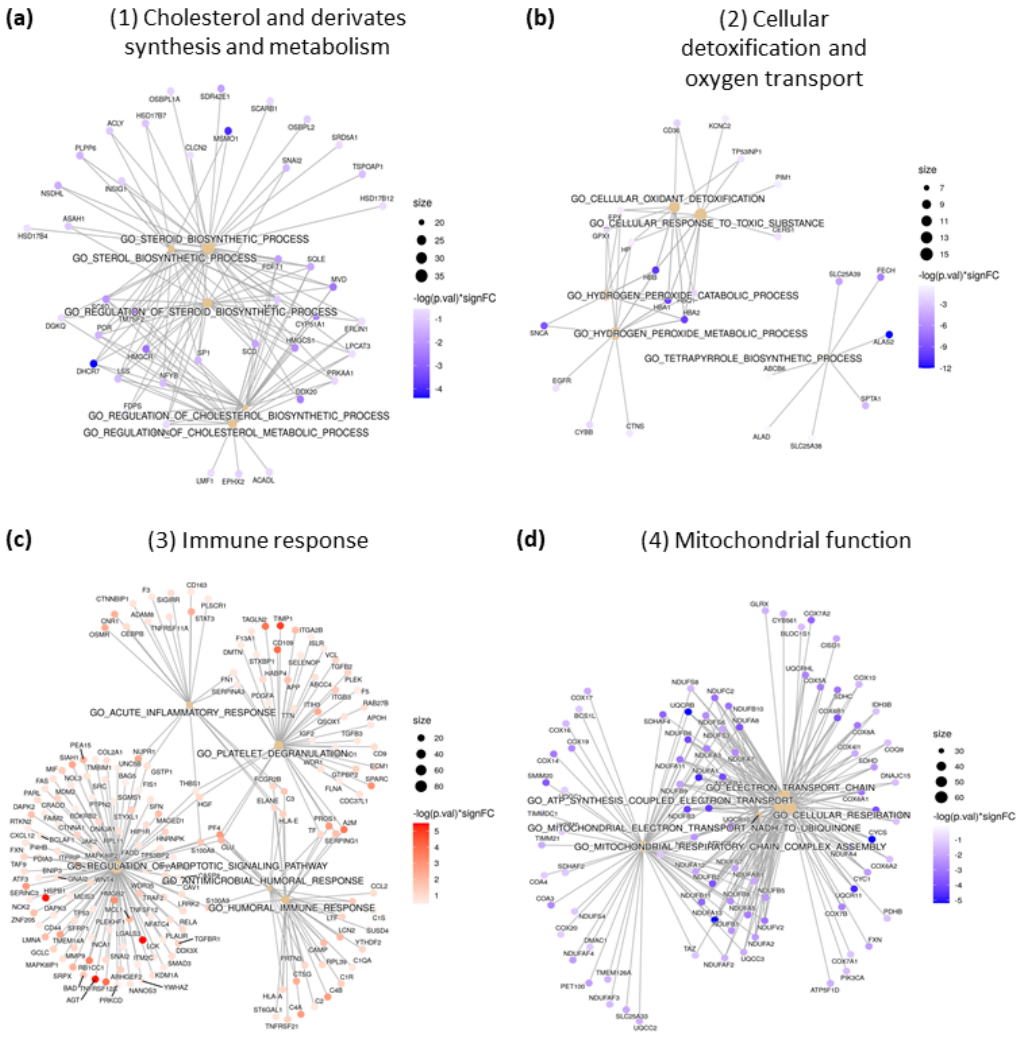

Figure 34. Relevant biological processes affected by VCR in astrocytes. Representative gene-concept networks with top 5 significantly enriched GO terms for the 4 functional clusters identified as significantly affected by VCR chemotherapy.

Supporting material

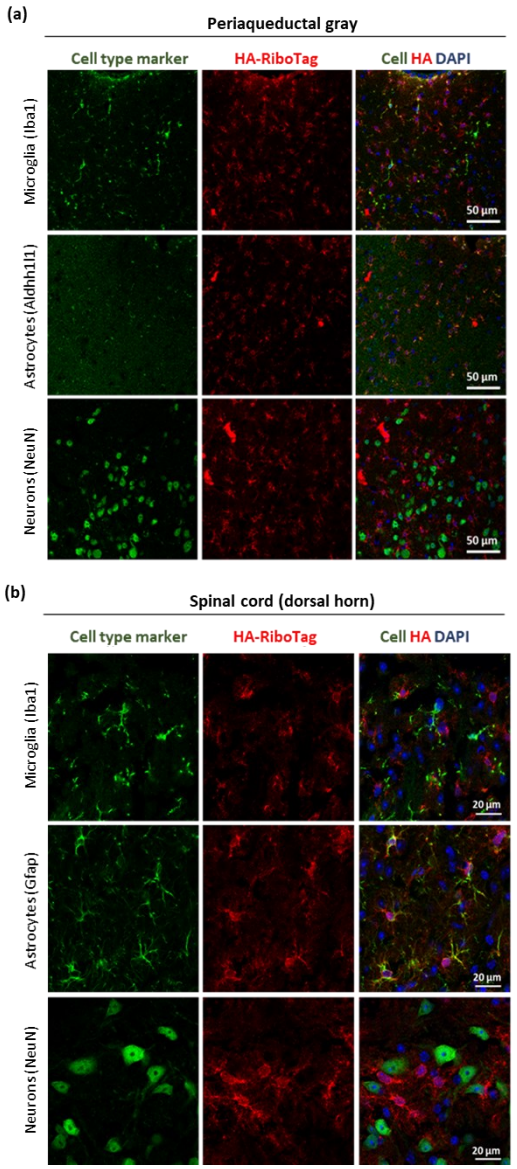

Supporting Figure 1. Anatomical validation of Astrocyte:RiboTag mouse line. Immunostaining for HA (red) and cell-specific markers (green), counterstained with DAPI (blue), to determine the cell-type expression of HA-tagged ribosomes in **(a)** the periaqueductal gray and **(b)** the dorsal spinal cord. Representative images showing strong co-expression between HA and Aldh1l1 or Gfap (Astrocytes), but no colocalization with Iba1 (microglia) or NeuN (neurons) (n= 2 x male/female mice).

Supporting Table 1. Detailed statistical evaluation for Figure 25.

Male	Statistic		Result
Figure 25 (a)	Repeated measures ANOVA	CIPN	F (1, 32) = 129.418; p < 0.001
		Treatment	F (1, 32) = 1.280; p = 0.266
		Day	F (17, 544) = 17.019; p < 0.001
		CIPN x Treatment	F (1, 32) = 1.413; p = 0.243
		CIPN x Day	F (17, 544) = 30.722; p < 0.001
		Treatment x Day	F (17, 544) = 1.968; p = 0.110
		CIPN x Treatment x Day	F (17, 544) = 0.771; p = 0.561
Figure 25 (c)	Two-way ANOVA	CIPN	F (1, 32) = 72.712; p < 0.001
		Treatment	F (1, 32) = 0.968; p = 0.333
		CIPN x Treatment	F (1, 32) = 1.156; p = 0.290

Female	Statistic		Result
Figure 25 (b)	Repeated measures ANOVA	CIPN	F (1, 32) = 26.867; p < 0.001
		Treatment	F (1, 32) = 0.021; p = 0.886
		Day	F (17, 544) = 2.613; p < 0.05
		CIPN x Treatment	F (1, 32) = 0.010; p = 0.921
		CIPN x Day	F (17, 544) = 9.685; p < 0.001
		Treatment x Day	F (17, 544) = 0.822; p = 0.543
		CIPN x Treatment x Day	F (17, 544) = 0.659; p = 0.666
Figure 25 (d)	Two -way ANOVA	CIPN	F (1, 32) = 26.646; p < 0.001
		Treatment	F (1, 32) = 0.014; p = 0.908
		CIPN x Treatment	F (1, 32) = 0.126; p = 0.725

Male vs Female	Statistic		Result
Figure 25 (a, b)	Repeated measures ANOVA	CIPN	F (1, 32) = 114.623; p <0.001
		Treatment	F (1, 32) = 0.290; p = 0.594
		Day	F (17, 544) = 11.615; p <0.001
		Sex	F (1, 32)= 24.296; p < 0.001
		CIPN x Treatment	F (1, 32) = 0.369; p = 0.548
		CIPN x Day	F (17, 544) = 31.771; p < 0.001
		CIPN x Sex	F (17, 544) = 6.357; p < 0.05
		Treatment x Day	F (1, 32) = 1.741; p = 0.136
		Treatment x Sex	F (1, 32) = 0.631; p = 0.433
		Day x Sex	F (17, 544) = 8.180; p < 0.001
		CIPN x Treatment x Day	F (17,544) = 1.070; p =0.377
		CIPN x Treatment x Sex	F (1, 32) = 0.626; p = 0.435
		CIPN x Day x Sex	F (17,544) = 5.703; p < 0.001
		Treatment x Day x Sex	F (17,544) = 0.990; p = 0.423
		CIPN x Treatment x Day x Sex	F (17, 544) = 0.240; p = 0.937

(continues)

Figure 25 (c, d)	Three -way ANOVA	CIPN	F (1, 32) = 88.648; p < 0.001
		Treatment	F (1, 32) = 0.572; p = 0.455
		Sex	F (1, 32) = 13.606; p < 0.001
		CIPN x Treatment	F (1, 32) = 0.966; p = 0.333
		CIPN x Sex	F (1, 32) = 5.871; p < 0.05
		Treatment x Sex	F (1, 32) = 0.395; p = 0.534
		CIPN x Treatment x Sex	F (1, 32) = 0.272; p = 0.605

Supporting Table 2. Detailed statistical evaluation for Figure 26.

MECHANICAL NOCICEPTION

Male	**Statistic**		**Result**
Figure 26 (a) Baseline mechanical thresholds	Kruskall-Wallis	Among 4 groups	H (3) = 0.856; p = 0.836
Figure 26 (a) Mechanical sensitivity PRE-treatment	Mixed Model	CIPN	F (1, 158.679) = 927.955; p < 0.001
		Treatment	F (1, 158.679) = 7.100; p < 0.01
		Day	F (5, 66.934) = 44.877; p < 0.001
		CIPN x Treatment	F (1, 158.679) = 30.560; p < 0.001
		CIPN x Day	F (5, 66.934) = 24.733; p < 0.001
		Treatment x Day	F (5, 66.934) = 1.300; p = 0.274
		CIPN x Treatment x Day	F (5, 66.934) = 2.107; p = 0.075
Figure 26 (a) Mechanical sensitivity POST-treatment	Mixed Model	CIPN	F (1, 171,006) = 781.413; p < 0.001
		Treatment	F (1, 171,006) = 18.841; p < 0.001
		Day	F (5, 60,443) = 42.573; p < 0.001
		CIPN x Treatment	F (1, 171,006) = 42.573; p < 0.001
		CIPN x Day	F (5, 60,443) = 22.723; p < 0.001
		Treatment x Day	F (5, 60,443) = 3.897; p < 0.01
		CIPN x Treatment x Day	F (5, 60,443) = 3.341; p < 0.01
Figure 26 (a) Acute effect of EST (POST vs PRE values)	Mixed Model	CIPN	F (1, 149.385) = 11.005; p < 0.01
		Treatment	F (1, 149.385) = 13.220; p < 0.001
		Day	F (5, 65.843) = 3.478; p < 0.05
		CIPN x Treatment	F (1, 149.385) = 8.216; p < 0.01
		CIPN x Day	F (5, 65.843) = 2.379; p = 0.061
		Treatment x Day	F (5, 65.843) = 4.091; p < 0.01
		CIPN x Treatment x Day	F (5, 65.843) = 1.928; p = 0.116

(continues)

Female	Statistic		Result
Figure 26 (b) Baseline mechanical thresholds	Kruskall-Wallis	Among 4 groups	H (3) = 1.183; p = 0.757
Figure 26 (b) Mechanical sensitivity PRE-treatment	Mixed Model	CIPN	F (1, 152.829) = 974.637; p < 0.001
		Treatment	F (1, 152.829) = 25.654; p < 0.001
		Day	F (5, 63.342) = 30.206; p < 0.001
		CIPN x Treatment	F (1, 152.829) = 14.159; p < 0.001
		CIPN x Day	F (5, 63.342) = 23.429; p < 0.001
		Treatment x Day	F (5, 63.342) = 5.490; p < 0.001
		CIPN x Treatment x Day	F (5, 63.342) = 3.825; p < 0.01
Figure 26 (b) Mechanical sensitivity POST-treatment	Mixed Model	CIPN	F (1, 150.404) = 940.469; p < 0.001
		Treatment	F (1, 150.404) = 50.422; p < 0.001
		Day	F (5, 63.556) = 30.226; p < 0.001
		CIPN x Treatment	F (1, 150.404) = 28.683; p < 0.001
		CIPN x Day	F (5, 63.556) = 23.420; p < 0.001
		Treatment x Day	F (5, 63.556) = 7.193; p < 0.001
		CIPN x Treatment x Day	F (5, 63.556) = 7.475; p < 0.001
Figure 26 (b) Acute effect of EST (POST vs PRE values)	Mixed Model	CIPN	F (1, 122.732) = 2.338;p = 0.129
		Treatment	F (1, 122.732) = 12.284; p < 0.001
		Day	F (5, 62.332) = 2.369; p = 0.062
		CIPN x Treatment	F (1, 122.732) = 7.445; p < 0.01
		CIPN x Day	F (5, 62.332) = 1.749; p = 0.150
		Treatment x Day	F (5, 62.332) = 0.687; p = 0.640
		CIPN x Treatment x Day	F (5, 62.332) = 2.086; p = 0.093

Male vs Female	Statistic		Result
Figure 26 (a vs b) Baseline mechanical thresholds	Kruskall-Wallis	Among 8 groups	H (7) = 4.810; p = 0. 683
Figure 26 (a vs b) Mechanical sensitivity PRE-treatment	Mixed Model	CIPN	F (1, 317.945) = 1902.459; p < 0.001
		Treatment	F (1, 317.945) = 29.945; p < 0.001
		Day	F (5, 122.384) = 69.241; p < 0.001
		Sex	F (1, 317.945) = 0.196; p = 0.658
		CIPN x Treatment	F (1, 317.945) = 43.096; p < 0.001
		CIPN x Day	F (5, 122.384) = 47.880; p < 0.001
		CIPN x Sex	F (1, 317.945) = 0.498; p = 0.481
		Treatment x Day	F (5, 122.384) = 5.621; p < 0.001
		Treatment x Sex	F (1, 317.945) = 2.954; p = 0.087
		Day x Sex	F (5, 122.384) = 2.882; p < 0.05
		CIPN x Treatment x Day	F (5, 122.384) = 5.288; p < 0.001
		CIPN x Treatment x Sex	F (1, 317.945) = 1.495; p = 0.222
		CIPN x Day x Sex	F (5, 122.384) = 0.328; p = 0.895
		Treatment x Day x Sex	F (5, 122.384) = 1.174; p = 0.326
		CIPN x Treatment x Day x Sex	F (5, 122.384) = 0.589; p = 0.708

(continues)

Figure 26 (a vs b) Mechanical sensitivity POST-treatment	Mixed Model	CIPN	F (1, 324.746) = 1715.193; p < 0.001
		Treatment	F (1, 324.746) = 64.928; p < 0.001
		Day	F (5, 116.823) = 68.202; p < 0.001
		Sex	F (1, 324.746) = 1.150; p = 0.284
		CIPN x Treatment	F (1, 324.746) = 73.677; p < 0.001
		CIPN x Day	F (5, 116.823) = 45.645; p < 0.001
		CIPN x Sex	F (1, 324.746) = 1.563 ; p = 0.212
		Treatment x Day	F (5, 116.823) = 10.204; p < 0.001
		Treatment x Sex	F (1, 324.746) = 3.317; p = 0.070
		Day x Sex	F (5, 116.823) = 2.432; p < 0.05
		CIPN x Treatment x Day	F (5, 116.823) = 9.679; p < 0.001
		CIPN x Treatment x Sex	F (1, 324.746) = 1.283; p = 0.258
		CIPN x Day x Sex	F (5, 116.823) = 0.135; p = 0.984
		Treatment x Day x Sex	F (5, 116.823) = 10.596; p = 0.703
		CIPN x Treatment x Day x Sex	F (5, 116.823) =0.576; p = 0.718

HEAT NOCICEPTION

Male	Statistic		Result
Figure 26 (c) Baseline heat thresholds	Two-way ANOVA	CIPN	F (1, 32) = 0.015; p = 0.903
		Treatment	F (1, 32) = 0.280; p = 0.600
		CIPN x Treatment	F (1, 32) = 0.296; p = 0.590
Figure 26 (c) Heat sensitivity 60 min after EST admin.	Mixed Model	CIPN	F (1, 187.482) =2141.830; p<0.001
		Treatment	F (1, 187.482) = 816.524; p < 0.001
		Day	F (5, 58.190) = 84.282; p < 0.001
		CIPN x Treatment	F (1, 187.482) = 799.856; p < 0.001
		CIPN x Day	F (5, 58.190) = 76.117; p < 0.001
		Treatment x Day	F (5, 58.190) = 63.115; p < 0.001
		CIPN x Treatment x Day	F (5, 58.190) = 61.999; p < 0.001

Female	Statistic		Result
Figure 26 (c) Baseline heat thresholds	Two-way ANOVA	CIPN	F (1, 32) = 0.243; p = 0.625
		Treatment	F (1, 32) = 0.596; p = 0.446
		CIPN x Treatment	F (1, 32) = 0.006; p = 0.939
Figure 26 (c) Heat sensitivity 60 min after EST admin.	Mixed Model	CIPN	F (1, 84.231) =1098.302; p < 0.001
		Treatment	F (1, 84.231) = 437.545; p < 0.001
		Day	F (5, 61.730) = 103.937; p < 0.001
		CIPN x Treatment	F (1, 84.231) = 103.937; p < 0.001
		CIPN x Day	F (5, 61.730) = 111.120; p < 0.001
		Treatment x Day	F (5, 61.730) = 74.376; p < 0.001
		CIPN x Treatment x Day	F (5, 61.730) = 71.309; p < 0.001

(continues)

Male vs Female	Statistic		Result
Figure 26 (c) Baseline heat thresholds	Three-way ANOVA	CIPN	F (1, 64) = 0.165; p = 0.686
		Treatment	F (1, 64) = 0.005; p = 0.941
		Sex	F (1, 64) =1.185; p = 0.281
		CIPN x Treatment	F (1, 64) = 0.223; p = 0.639
		CIPN x Sex	F (1, 64) = 0.046; p = 0.831
		Treatment x Sex	F (1, 64) = 0.805; p = 0.373
		CIPN x Treatment x Sex	F (1, 64) = 0.140; p = 0.709
Figure 26 (c) Heat sensitivity 60 min after EST admin.	Mixed Model	CIPN	F (1, 252.268) = 2965.226; p < 0.001
		Treatment	F (1, 252.268= 1154.861; p < 0.001
		Day	F (5, 135.306) = 183.391; p < 0.001
		Sex	F (1, 252.268) = 0.563; p = 0.454
		CIPN x Treatment	F (1, 252.268) = 1222.517; p < 0.001
		CIPN x Day	F (5, 135.306) = 178.251; p < 0.001
		CIPN x Sex	F (1, 252.268) = 3.388; p = 0.067
		Treatment x Day	F (5, 135.306) = 125.321; p < 0.001
		Treatment x Sex	F (1, 252.268) = 0.601; p = 0.439
		Day x Sex	F (5, 135.306) = 0.829; p = 0.531
		CIPN x Treatment x Day	F (5, 135.306) = 124.595; p < 0.001
		CIPN x Treatment x Sex	F (1, 252.268) = 0.317; p = 0.574
		CIPN x Day x Sex	F (5, 135.306) = 1.535; p = 0.183
		Treatment x Day x Sex	F (5, 135.306) = 0.478; p = 0.792
		CIPN x Treatment x Day x Sex	F (5, 135.306) = 0.319; p = 0.901

Supporting Table 3. Detailed statistical evaluation for Figure 27.

Male	Statistic			Result
Figure 27 (a) Analgesia (%) of EST in mechanical sensitivity	Repeated measures ANOVA	PRE	Day	F (4, 32) = 8.341; p < 0.001
		POST	Day	F (4, 32) = 13.016; p < 0.001
		Day		F (4, 32) = 12.342; p < 0.001
		PRE vs POST		F (1, 8) = 30.295; p < 0.001
		Day x PRE vs POST		F (4, 32) = 6.423; p < 0.001
Figure 27 (a) Analgesia (%) of EST in heat sensitivity	Repeated measures ANOVA	Day		F (4, 32) = 74.037; p < 0.001

Female	Statistic			Result
Figure 27 (b) Analgesia (%) of EST in mechanical sensitivity	Repeated measures ANOVA	PRE	Day	F (4, 32) = 23.962; p < 0.001
		POST	Day	F (4, 32) = 38.047; p < 0.001
		Day		F (4, 32) = 36.429; p < 0.001
		PRE vs POST		F (1, 8) = 33.174; p<0.001
		Day x PRE vs POST		F (4, 32) = 3.139; p<0.05

(continues)

Figure 27 (b) Analgesia (%) of EST in heat sensitivity	Repeated measures ANOVA	Day		F (4, 32) = 63.607; p<0.001

Male vs. Female	**Statistic**			**Result**
Figure 27 (a,b) Mechanical sensitivity	Repeated measures ANOVA	PRE values	Day	F (4, 32) = 29.189; p < 0.001
			Sex	F (1, 8) = 6,801; p = 0.135
			Day x Sex	F (4, 32) = 5.394; p < 0.05
		POST values	Day	F (4, 32) = 36.805; p < 0.001
			Sex	F (1, 8) = 30.295; p < 0.05
			Day x Sex	F (4, 32) = 5.212; p < 0.01
Heat sensitivity	Repeated measures ANOVA		Day	F (4, 32) = 125.748; p<0.001
			Sex	F (1, 8) = 0.659; p = 0.440
			Day x Sex	F (4, 32) = 2.054; p = 0.110

Supporting Table 4. Top 20 down- and upregulated genes in male and female astrocytes of each region by comparing VCR-vehicle to saline-vehicle groups receiving short-term chemotherapy (early). Overlapping genes between all regions are excluded.

MALE - Early											
DOWN (logFC < -1)						UP (logFC > 1)					
SS		PAG		SC		SS		PAG		SC	
Gene	logFC	Gene	logFC	Gene	logFC	Gene	logFC	Gene	logFC	Gene	logFC
Rassf6	-3,86	*Cpxm2*	-1,06	*Slc25a37*	-2,07*	*Pnma1*	3,36	*Hif3a*	1,01*	*Mir6236*	1,24*
Nrap	-4,22	*Snca*	-1,10	*Snca*	-1,78*	*Xkr4*	1,05	*Erdr1*	1,33*	*Sgk1*	1,31
Itih2	-1,16	*Slc25a37*	-1,06	*Gypa*	-5,37	*H2-Eb1*	1,24	*Mgp*	2,20*	*Mpl*	2,92
Vgll3	-3,96	*Lyn*	-1,23	*Gda*	-2,14	*Lefty1*	2,29	*Rbm47*	1,98*	*Hif3a*	1,14
Cyp26b1	-1,83	*Tpx2*	-1,22	*E2f2*	-2,05	*Cd53*	2,21	*Clic6*	1,90*	*P2ry2*	1,67
Col9a2	-1,06	*E2f2*	-2,12	*Spta1*	-4,51	*Zfp273*	1,05	*Map11*	1,03*	*Trp53rkb*	1,02
Nid1	-1,33	*Chrna7*	-1,50	*Epb41*	-1,08	*Rad51ap2*	2,38	*Epn3*	1,50*	*Myo1b*	1,11
Ankrd63	-1,43	*Trpc7*	-1,25	*Helz2*	-2,68	*Adap2*	1,57	*Cartpt*	1,23*	*Lingo3*	1,24
Myom1	-2,08	*Lrrc46*	-1,28	*Isg15*	-1,15	*Slco4a1*	1,70	*Enpp2*	1,36*	*Adh1*	1,01
Ly96	-1,28	*Mlxipl*	-1,05	*Th*	-3,26	*Klc3*	1,33	*Prmt8*	1,30	*Foxo6os*	1,89
Anxa3	-1,16	*Akr1c14*	-2,10	*H2-Eb1*	-1,31	*Cplx3*	1,15	*Poln*	2,40	*Palb2*	2,38
Alx4	-1,16	*Tcf19*	-1,87	*Rbp4*	-2,85	*Itga2b*	1,35	*Npffr1*	2,64	*Srd5a2*	3,43
Ctsk	-1,49	*Ascl1*	-1,04	*Cd74*	-1,34	*Elf4*	1,55	*Adamtsl2*	1,00	*Ifnlr1*	2,76
Mmp2	-1,47	*Hydin*	-1,20	*Tnfrsf1b*	-1,57	*Pus7l*	1,10	*Clic3*	3,00	*Pla2g2f*	3,27
Slc9a2	-1,21	*Adgrg6*	-1,31	*Fbxl7*	-1,06	*Cyp2f2*	1,51	*Ttr*	3,05	*Inmt*	2,53
Mns1	-1,01	*Lama4*	-1,59	*Cdh24*	-1,23	*Tnfsf10*	2,50	*Lepr*	2,80	*Acox2*	1,50
Nphs2	-1,56	*Bcl11b*	-1,04	*Itih2*	-1,26	*Chp2*	1,41	*Tshb*	2,10	*Slco5a1*	2,02
Mpzl3	-1,09	*Tacstd2*	-2,65	*Fcgr2b*	-1,16	*Uba1y*	2,05	*Tgfbi*	1,63	*Gabre*	2,47
Apoa2	-2,38	*H3f3aos*	-2,60	*Ccdc36*	-3,43	*H2-Aa*	1,44	*Prr32*	3,23	*Spin2c*	1,33
Spta1	-2,90	*Ppp1r17*	-2,84	*Igf2*	-2,56	*C3ar1*	2,39	*Cdkn1c*	1,10	*H2-T10*	1,92

FEMALE - Early											
DOWN (logFC < -1)						UP (logFC > 1)					
SS		PAG		SC		SS		PAG		SC	
Gene	logFC	Gene	logFC	Gene	logFC	Gene	logFC	Gene	logFC	Gene	logFC
F11r	-1,18*	*Slco1a4*	-1,28*	*mt-Nd4*	-1,25*	*Nrarp*	1,36*	*Nrarp*	1,21*	*Dapk3*	1,45*
Zic3	-1,28*	*Snca*	-1,40*	*mt-Cytb*	-1,16*	*Cav1*	1,14*	*Rhbdl1*	1,51*	*Arf6*	1,02*
Wfdc2	-2,88*	*S100a8*	-1,42*	*mt-Nd2*	-1,19*	*Prrx2*	1,17*	*Prokr2*	1,25*	*Igfbp6*	1,12*
Zfp618	-1,22	*Clec18a*	-3,35*	*mt-Tp*	-1,56*	*Pde1c*	1,30*	*Marveld3*	3,37	*Mir6236*	1,47*
H2-Ab1	-1,24	*S100a9*	-1,78	*mt-Nd6*	-1,16*	*Cebpb*	1,34*	*Ptx3*	1,20	*Mgp*	1,33*
Rbbp8	-1,04	*Ndufa4l2*	-2,32	*mt-Nd1*	-1,05*	*Actn2*	1,64*	*Cps1*	1,55	*Cfd*	3,64*
Arhgap30	-2,01	*Slc25a37*	-1,29	*Slc25a37*	-1,49*	*Epha6*	1,38*	*Pcdhb2*	1,88	*Ptgds*	1,94
Dsp	-3,04	*Acan*	-2,13	*Snca*	-1,34	*Pawr*	1,82*	*C2cd4d*	1,04	*Msln*	3,53
Cd52	-1,39	*Cldn5*	-1,52	*Isg15*	-1,50	*Srgn*	1,06	*Fancf*	1,06	*Cebpb*	1,80
Mir6240	-1,33	*Sox18*	-1,82	*mt-Tm*	-1,02	*Lgals12*	1,25	*Pcdhga3*	1,02	*Slc13a4*	1,82
Pde4c	-2,55	*Ttn*	-1,23	*Trim10*	-4,55	*Fam47e*	2,03	*Trpc4*	1,66	*Isyna1*	1,22
Cd24a	-1,36	*Gda*	-2,05	*Spata9*	-1,94	*Crhr2*	2,69	*Kdelr3*	1,16	*Ppp1r1c*	4,30
Gm7600	-1,42	*Gypa*	-3,90	*Spta1*	-5,20	*Fos*	1,11	*Wdr49*	1,53	*Tmem158*	1,31
S100a8	-1,04	*Tmem79*	-1,78	*Gda*	-1,80	*Lrrc46*	2,08	*Cavin2*	-1,03	*Npb*	1,09
Mmrn2	-1,69	*Vsig2*	-2,72	*mt-Atp6*	-1,28	*Rtp1*	1,22	*Irx3os*	-1,26	*Itih2*	1,18
Trim10	-3,27	*Sema3g*	-2,79	*Sash3*	-2,66	*Kif4*	2,46	*Enpp3*	-2,76	*Lor*	1,22
C5ar2	-2,74	*Pecam1*	-1,43	*Aldh1b1*	-1,02	*Tmem217*	2,27	*Adgrf5*	-1,25	*Anxa1*	1,26
Mterf1b	-1,34	*Nrgn*	-1,13	*E2f2*	-1,90	*Zfp92*	2,32	*Uox*	2,08	*S100a8*	1,30
Tgfbi	-1,66	*Cdh5*	-1,43	*Nox4*	-1,97	*Tac1*	1,71	*E2f2*	-1,76	*Igf2*	1,57
Nox1	-1,541893	*Spta1*	-3,41	*Helz2*	-1,63	*Glp2r*	2,54	*Igf2*	-1,26	*Htr1d*	2,44

Data from lists of differentially expressed genes (DEG) with $p < 0.05$ in astrocyte-specific RNAs from each region. The values are expressed as logFC between VCR-vehicle and saline-vehicle groups and ordered by significance level. Down, downregulated in VCR-vehicle; Up, upregulated in VCR-vehicle; SS, somatosensory cortical astrocytes; PAG, periaqueductal gray matter astrocytes; SC, spinal cord dorsal astrocytes.* adjusted $p < 0.05$.

Supporting Table 5. Top 20 down- and upregulated genes in male and female astrocytes of each region by comparing VCR-vehicle to saline-vehicle groups receiving chronic chemotherapy (late). Overlapping genes between all regions are excluded.

MALE - Late												
DOWN (logFC < -1)						UP (logFC > 1)					
SS		PAG		SC		SS		PAG		SC	
Gene	logFC	Gene	logFC	Gene	logFC	Gene	logFC	Gene	logFC	Gene	logFC
Plp1	-1,09*	*Enpp2*	-2,32*	*Ccl6*	-1,85	Apol11b	1,97	*Sstr2*	1,11	*Zan*	2,48
Cd74	-1,42*	*Spint2*	-2,07*	*Cep128*	-1,23	Slc4a1	1,67	*Slc26a8*	1,26	*Nlrc5*	1,35
Rassf10	-1,18	*Kcnj13*	-3,48*	*L3mbtl1*	-2,76	*Cyp26b1*	1,74	*Sh2d4a*	1,36	*Fam180a*	3,89
Tph2	-1,03	*Ecrg4*	-2,55*	*Ptchd1*	-2,37	*Rtp1*	1,39	*Hgf*	1,70	*Hsd17b2*	2,66
Rtn4rl2	-1,28	*Lbp*	-2,06*	*Fgf4*	-2,91	*Cenpk*	1,41	*Shisa8*	1,05	*Tex47*	2,15
Dock5	-1,00	*Rbm47*	-2,49*	*Samd7*	-2,35	*Ly6a*	1,08	*Irf7*	1,22	*Lrp8os2*	1,46
Hjv	-3,58	*Ttr*	-4,40*	*Dnhd1*	-1,68	*Nat8f2*	1,63	*Bnip5*	2,69	*Gpr156*	1,25
Tnnt3	-2,78	*Gng8*	-3,23*	*Ccr2*	-2,43	*Nuak2*	1,93	*Cdh23*	1,29	*Ankub1*	1,03
Tdgf1	-1,14	*Cgnl1*	-1,19*	*Itgb7*	-2,08	*Eno4*	1,72	*Tgif2*	1,26	*Terb1*	2,80
Ptpn22	-1,99	*Nwd2*	-1,77*	*Gstp2*	-2,36	*Tek*	1,10	*Slc36a2*	1,11	*Slc6a20a*	2,73
Sec14l5	-1,16	*Prlr*	-1,70*	*Col4a6*	-1,77	*Fmo2*	1,44	*Mrgprf*	2,08	*Polq*	1,84
Ugt8a	-1,49	*Elovl7*	-1,72*	*Sptssb*	-1,54	*Slc19a3*	2,68	*Tspear*	2,52	*Parvaos*	1,45
Stk32a	-2,68	*Kl*	-2,74*	*Rab26*	-1,33	*Nat2*	1,04	*Mirt1*	2,49	*Gm37345*	1,70
Atp10b	-2,47	*Tcea3*	-1,95*	*Satb2*	-3,13	*Haus5*	1,05	*Pcdha6*	1,97	*Alms1-ps2*	1,33
Cda	-3,24	*Car12*	-3,54*	*Pask*	-1,43	*Best3*	2,08	*Ccnf*	1,36	*Hic1*	2,33
Slc5a11	-1,40	*Ace*	-1,29*	*Zfp146*	-1,19	*Cabcoco1*	1,52	*Bbc3*	1,67	*Ifitm1*	2,95
Reln	-1,19	*Gm47494*	-2,55*	*Hoxc12*	-1,76	*Bcl6b*	2,83	*Slc6a3*	2,69	*Hsf2bp*	2,93
Hpgd	-1,58	*Mgp*	-1,65*	*Ms4a6b*	-2,36	*Zfp455*	1,22	*Havcr2*	2,81	*Tnfrsf13b*	2,66
Irf8	-1,35	*Krt8*	-2,38*	*Cnih3*	-1,66	*Cyp2f2*	1,50	*Apol11b*	1,22	*Igf2*	2,52
Rxfp2	-2,02	*Cd55*	-2,18*	*Lrguk*	-1,55	*Mrgprf*	1,44	*Ebf2*	1,54	*Slc9a3*	1,97

FEMALE - Late											
DOWN (logFC < -1)						UP (logFC > 1)					
SS		PAG		SC		SS		PAG		SC	
Gene	logFC	Gene	logFC	Gene	logFC	Gene	logFC	Gene	logFC	Gene	logFC
Sh3tc2	-3,52	*Opn4*	-3,45	*Pi4ka*	-1,30*	*Hp*	3,11	*En1*	1,02	*Ncoa4*	1,27*
Oprm1	-3,35	*Lamb3*	-2,31	*Unc13a*	-2,34*	*Itga2b*	1,41	*Mastl*	1,05	*Itgb4*	1,41*
Cacna1f	-3,02	*Cdhr3*	-1,36	*Trip11*	-1,24*	*F5*	1,54	*Casp12*	1,06	*Prg4*	3,12*
Fa2h	-1,57	*Lhcgr*	-1,28	*Tmcc3*	-1,13*	*Lcp1*	1,21	*Tmem63c*	1,07	*Enpp6*	1,71
Hs3st1	-1,20	*Pnpla3*	-1,16	*Sptb*	-1,86*	*Fancf*	1,46	*Dlk1*	1,23	*Myrf*	1,01
Car13	-2,16	*Dnajb3*	-1,12	*Mta3*	-1,49	*Thbs1*	1,59	*Erdr1*	1,48	*Tubb4a*	1,23
F11r	-1,17	*Oasl2*	-1,14	*Igkc*	-6,37	*Dll4*	2,48	*Il20rb*	1,66	*Ikzf1*	4,03
Capn12	-2,66	*Ttll10*	-2,13	*Mkks*	-1,30	*Cldn1*	1,55	*Dspp*	1,73	*Jpt2*	1,34
Tnni1	-2,06	*Tnfaip8l3*	-1,83	*Rxfp2*	-4,05	*Itgal*	1,39	*Gp5*	1,78	*Cd200*	1,56
Adamts10	-1,16	*Glis1*	-1,27	*Pcdhb12*	-2,55	*Cd52*	1,11	*Mybpc1*	1,83	*Pf4*	4,02
Col15a1	-2,23	*Shisa2*	-1,04	*Bud13*	-1,57	*Ptprc*	1,17	*Ltbp2*	1,84	*Ermn*	1,07
Adm	-2,22	*Sox7*	-1,75	*Panx2*	-1,09	*Alas2*	1,21	*Ctla2a*	1,86	*Cldn11*	1,33
Zpbp	-2,90	*Map2k3os*	-1,27	*Plin5*	-5,61	*Fbll1*	1,55	*Cbln3*	1,87	*Ippk*	1,14
Cox7b2	-1,69	*Ttll13*	-1,95	*Car3*	-1,09	*Acrbp*	1,57	*Fat2*	2,05	*Thbs1*	2,05
Atp2c2	-3,15	*Cyp4f18*	-1,69	*Slx4*	-1,45	*Zfp773*	1,77	*Tubb1*	2,46	*Anln*	1,12
Tec	-2,39	*Dlx4*	-2,72	*Rras*	-1,13	*H2-K2*	2,78	*Bcl2l15*	2,67	*Lsm12*	1,18
Steap1	-1,32	*Nhlh2*	-1,32	*Nog*	-1,51	*Ncf4*	2,92	*Ppbp*	2,82	*Trf*	1,21
Pcdhb13	-1,29	*Bche*	-1,57	*Cyp2e1*	-6,81	*Mfsd4b1*	2,95	*Pf4*	3,02	*Bin2*	3,04
Trf	-1,10	*Il21r*	-2,67	*Psme2b*	-1,79	*Ms4a4a*	2,80	*Cdkn3*	3,21	*Nacad*	1,16
Thbs2	-1,01	*Opn3*	-1,42	*Ap1ar*	-1,07	*S100a9*	1,37	*Lrmp*	3,55	*Fn1*	1,70

Data from lists of differentially expressed genes (DEG) with $p < 0.05$ in astrocyte-specific RNAs from each region. The values are expressed as logFC between VCR-vehicle and saline-vehicle groups and ordered by significance level. Down, downregulated in VCR-vehicle; Up, upregulated in VCR-vehicle; SS, somatosensory cortical astrocytes; PAG, periaqueductal gray matter astrocytes; SC, spinal cord dorsal astrocytes.* adjusted $p < 0.05$.

Supporting Table 6. Top 20 down- and upregulated genes in male and female astrocytes of each region by comparing VCR-EST to VCR-vehicle groups receiving short-term treatments (early).

MALE - Early												
DOWN (logFC < -1)						UP (logFC > 1)					
SS		PAG		SC		SS		PAG		SC	
Gene	logFC	Gene	logFC	Gene	logFC	Gene	logFC	Gene	logFC	Gene	logFC
Nxnl1	-1,41	*Slitrk4*	-1,12	*Skor1*	-2,99	*Fkbp5*	1,24*	*Piwil2*	3,62	*Tubb6*	1,06
Pik3r6	-2,09	*Rbm47*	-2,17	*Hipk4*	-1,05	*Gdpgp1*	1,03*	*Tpk1*	1,01	*Hspb1*	1,14
H2-Q6	-2,82	*Cdkn1c*	-1,61	*Btg3*	-1,99	*Cdkn1a*	1,22	*Akr1c14*	2,45	*Mpeg1*	1,28
Rhobtb1	-1,48	*Clgn*	-1,38	*Gabrg2*	-1,12	*Rnf39*	1,61	*Kcnk4*	1,91	*Tcim*	2,09
Wdr86	-1,31	*Drd2*	-1,67	*Rhov*	-1,48	*Rtp1*	1,05	*Hic1*	2,21	*Hsp25-ps1*	2,47
Krt18	-1,09	*Gpr27*	-1,20	*Rbm20*	-1,45	*Trpv4*	1,72	*Lyn*	1,06	*S100A11*	1,02
Samd9l	-1,52	*Rassf5*	-1,01	*Slc6a13*	-1,79	*Map3k6*	1,39	*Lama4*	1,81	*Timp1*	1,35
Tcaf2	-1,78	*Tmem169*	-1,18	*Abca8a*	-1,10	*Dnah3*	2,49	*Panct2*	2,64	*Fcgr2b*	1,51
Tlcd2	-1,85	*Dkkl1*	-3,29	*P3h2*	-1,22	*Setmar*	1,08	*Mmp19*	1,09	*Neurl3*	3,35
Tdrd6	-1,81	*Spint2*	-1,21	*Slc6a16*	-3,47	*Spag6*	1,35	*Klhl10*	1,27	*Cd52*	1,24
Mef2b	-1,13	*Cpne7*	-1,02	*Plcxd1*	-1,61	*Apoo2*	2,08	*Matn4*	1,01	*Plin4*	1,01
Sntn	-2,43	*Rasal3*	-2,95	*Lor*	-1,33	*Galnt6*	1,72	*Chrna6*	1,99	*Ccl6*	1,50
Cntf	-2,21	*Nts*	-2,11	*Spire2*	-1,02	*Casp1*	1,65	*Snora57*	2,08	*Cyp3a13*	2,35
Pde4c	-2,34	*Ldoc1*	-1,42	*Sema3e*	-1,62	*B3gnt5*	1,22	*Tcim*	1,64	*Itgb2*	1,39
Cxcr2	-2,09	*Cdh15*	-1,39	*Cfap47*	-1,60	*Gypc*	1,48	*Lcp2*	2,29	*Cdc20*	2,00
Tmem51os1	-1,42	*Necab2*	-1,29	*Doc2a*	-1,48	*Amd-ps7*	2,36	*Klhl40*	2,47	*Tfcp2l1*	2,12
Lefty1	-1,25	*Celf6*	-1,20	*Shf*	-1,21	*Sstr1*	1,45	*Sytl4*	1,26	*Acp5*	5,42
Slfn9	-1,28	*Rab3b*	-1,17	*Ppm1j*	-2,23	*Irf5*	1,59	*Lgals4*	1,60	*Cfp*	1,14
Sash3	-1,77	*Rasgrp3*	-1,04	*Bcl6b*	-3,48	*Kcne2*	1,49	*E2f2*	1,56	*Fblim1*	2,42
H2-Aa	-1,12	*Nhlh2*	-1,67	*Pde5a*	-1,70	*Lrrc23*	1,80	*Tlr4*	1,05	*Clcf1*	1,42

FEMALE - Early											
DOWN (logFC < -1)						UP (logFC > 1)					
SS		PAG		SC		SS		PAG		SC	
Gene	logFC	Gene	logFC	Gene	logFC	Gene	logFC	Gene	logFC	Gene	logFC
Medag	-1,25	*Apobec1*	-1,00	*Nrg2*	-1,34	*Steap1*	1,51	*Unc13a*	1,06	*Sgk1*	1,26
Olfr464	-3,31	*Gja5*	-1,69	*Pirt*	-4,82	*Ccna2*	1,12	*Sptb*	1,03	*Rnf43*	2,30
Klf5	-1,30	*Pcdhb2*	-1,78	*Isl2*	-3,75	*Il17rb*	1,14	*Clec18a*	3,45	*Ceacam1*	1,19
Grm8	-1,15	*Arhgap10*	-1,13	*Dsc3*	-2,24	*Pde4c*	2,61	*Aldob*	1,57	*Camk1g*	1,28
Prdm6	-1,31	*Rnf39*	-1,77	*Cdh23*	-1,85	*Cgas*	2,80	*Scube2*	2,01	*Helz2*	2,21
Bfsp1	-2,98	*Kdelr3*	-1,05	*Ryr1*	-1,82	*Card10*	1,38	*Fermt3*	1,30	*Ubxn10*	2,03
Crhr2	-2,20	*Fsip1*	-1,94	*Fxyd2*	-3,07	*Thbs1*	1,64	*Kcnu1*	2,10	*Uts2*	1,04
Bnip5	-2,01	*Brca1*	-1,18	*Retnla*	-3,58	*Oacyl*	1,29	*Actn2*	2,00	*Car7*	1,08
Pcdhga8	-1,32	*Tph2*	-2,06	*Acpp*	-3,52	*Wnt2*	1,98	*Cxadr*	1,03	*Mpeg1*	1,08
Tesk1	-1,01	*Siah3*	-1,42	*Tspan8*	-3,30	*Amigo3*	1,03	*Zwilch*	1,46	*Isg15*	1,09
Tcaf2	-2,29	*Notum*	-1,64	*Lrrn4*	-2,96	*Fbxw10*	2,05	*She*	2,31	*Fsbp*	1,10
Klhl35	-2,08	*Gramd1c*	-1,14	*Pbk*	-2,74	*H4c11*	1,68	*Ccno*	2,09	*Dbil5*	1,11
Spin2c	-1,21	*Gpr50*	-1,87	*Lncenc1*	-2,69	*Slc4a5*	1,60	*Foxc1*	2,10	*Gcfc2*	1,23
Nmbr	-2,76	*Oacyl*	-1,88	*Neurl3*	-2,64	*Gimap1*	2,19	*Rin1*	2,59	*Lgals4*	1,26
Mustn1	-2,40	*Psg16*	-1,01	*Erich5*	-2,64	*Olfr691*	2,16	*mt-Nd3*	3,26	*P2ry2*	1,34
Fgf10	-1,29	*Marchf3*	-1,64	*Msln*	-2,49	*Efhb*	1,71	*Gabra6*	1,05	*Car4*	1,41
Rell2	-1,08	*Kcnmb2*	-1,32	*Sertm1*	-2,48	*Tinagl1*	1,20	*Postn*	1,16	*Tnfrsf13c*	1,42
Gbp2	-1,15	*Klfc1*	-1,19	*Slamf9*	-2,47	*Parpbp*	2,40	*Tead4*	2,68	*Prrt2*	1,46
Marchf10	-2,14	*Tstd1*	-1,75	*Krt19*	-2,46	*Enkur*	1,26	*Lrrn4cl*	2,83	*Dyrk3*	1,53
Egln3	-1,29	*Slc11a1*	-1,51	*Gimap6*	-2,46	*Tnfsf13b*	2,12	*Cd248*	1,77	*Alx4*	1,55

Data from lists of differentially expressed genes (DEG) with $p < 0.05$ in astrocyte-specific RNAs from each region. The values are expressed as logFC between VCR-EST and VCR-vehicle groups and ordered by significance level. Down, downregulated in VCR-EST; Up, upregulated in VCR-EST; SS, somatosensory cortical astrocytes; PAG, periaqueductal gray matter astrocytes; SC, spinal cord dorsal astrocytes. * adjusted $p < 0.05$.

Supporting Table 7. Top 20 down- and upregulated genes in male and female astrocytes of each region by comparing VCR-EST to VCR-vehicle groups receiving chronic treatments (late). Overlapping genes between all regions are excluded.

MALE - Late												
DOWN (logFC < -1)						UP (logFC > 1)					
SS		PAG		SC		SS		PAG		SC	
Gene	logFC	Gene	logFC	Gene	logFC	Gene	logFC	Gene	logFC	Gene	logFC
Vat1l	-1,05	*Snca*	-1,14	*Snca*	-2,78*	*Ppbp*	1,93	*Dalir*	2,33	*Prmt6*	1,14
Clic6	-1,04	*Gda*	-1,46	*Rsad2*	-2,59*	*Itga2b*	1,26	*H2-T23*	1,25	*Rtkn2*	1,38
Epn3	-1,46	*Tnfsf10*	-3,21	*Epb41*	-1,95*	*Acta2*	1,03	*Atp2a3*	1,11	*Dennd3*	1,84
Calml4	-1,20	*Hfm1*	-1,77	*Gda*	-2,90*	*Pf4*	1,44	*Itga2b*	1,59	*Olfml3*	1,02
Cdh3	-1,23	*Evpl*	-1,06	*Isg20*	-2,44*	*Tnfrsf25*	1,90	*Arhgef33*	1,16	*Timp1*	1,28
Stc1	-1,62	*Ly86*	-1,78	*Spta1*	-3,09	*Pxdc1*	1,12	*Oasl2*	1,27	*Sema3d*	2,27
Olfr539	-2,76	*Ttc41*	-1,01	*Myo1g*	-3,02	*Itih2*	1,11	*Gipr*	2,32	*Cdkn1c*	1,01
Rassf6	-3,01	*Gja5*	-1,56	*Fabp4*	-3,68	*Spin4*	2,19	*Slc22a6*	1,42	*Rbm11*	1,57
Slc16a8	-1,56	*Insyn2a*	-1,09	*Spn*	-2,73	*Capn1*	1,09	*Mir6236*	1,07	*Dusp14*	1,45
Slc22a3	-2,83	*Kcnj12*	-1,29	*Slc4a1*	-2,39	*Srgn*	1,14	*Ppbp*	2,40	*Scrt1*	1,01
Krt8	-1,48	*Ccer2*	-1,80	*Gypa*	-2,30	*Ctla2a*	1,32	*Ppp1r17*	1,32	*Sspo*	2,54
Col8a1	-1,06	*Gabra6*	-1,14	*Hpn*	-2,59	*Tnnt3*	2,34	*Bhlhe22*	1,16	*Lrrc38*	2,90
Cfap61	-1,21	*Lalba*	-1,57	*Ctse*	-3,92	*Trpc7*	1,16	*Bst2*	1,11	*Pcdhac2*	1,33
Cd7	-2,61	*Glra4*	-2,44	*Cd300c2*	-3,31	*Doc2g*	1,60	*H1f10*	1,38	*Npffr1*	3,74
Pilra	-2,43	*Hvcn1*	-1,77	*Tnfrsf1b*	-1,82	*Cebpb*	1,18	*Cd248*	1,64	*Fam72a*	1,81
Htra4	-2,38	*Il17rb*	-1,07	*Pecam1*	-1,95	*H4c3*	1,69	*Thbd*	1,44	*Slc6a12*	3,15
Olfr316	-2,33	*Pitx2*	-2,36	*Ube2c*	-2,05	*Fam183b*	1,47	*Sema3f*	1,61	*Unc5a*	1,13
Best1	-2,23	*Mansc4*	-1,83	*Clec4a1*	-3,22	*Ndufs6b*	1,61	*Itgb3*	1,44	*Pcdhac1*	2,61
Aim2	-2,22	*Tent5a*	-1,17	*Sytl5*	-3,55	*Dnah3*	1,72	*Alox12*	2,02	*Oprk1*	1,36
Srpx2	-2,02	*Neurl1b*	-1,49	*Treml4*	-2,90	*Cyp11a1*	1,05	*Pf4*	2,13	*Sgk2*	1,72

FEMALE - Late											
DOWN (logFC < -1)						UP (logFC > 1)					
SS		PAG		SC		SS		PAG		SC	
Gene	logFC	Gene	logFC	Gene	logFC	Gene	logFC	Gene	logFC	Gene	logFC
Slc4a1	-2,42	*Cbln3*	-2,19	*Snca*	-1,52	*Sptb*	1,65*	*Msl3l2*	1,08	*C1qtnf4*	1,06
Otof	-1,35	*Gdf10*	-1,21	*Epb41*	-1,01	*Unc13a*	2,88*	*Sox21*	1,04	*Rasd2*	1,37
Itgb3	-2,17	*Dao*	-1,01	*Slc27a6*	-4,25	*Akap11*	1,00*	*Sox7*	2,94	*Notch4*	1,09
Treml4	-2,72	*Gabra6*	-2,39	*Pcdha3*	-3,76	*Pi4ka*	1,38*	*Mxra7*	1,08	*Olfm3*	1,37
Cd36	-2,04	*Abi3bp*	-1,13	*Lamb3*	-3,67	*Zfp532*	1,49*	*Nog*	1,16	*Hoxa13*	3,24
Bin2	-1,56	*Fat2*	-2,18	*Slc4a1*	-2,64	*Mta3*	1,97*	*Lhcgr*	1,19	*Mocs3*	1,19
Clec4a1	-2,29	*Casp12*	-1,54	*Bend4*	-1,75	*Birc6*	1,06*	*Phldb2*	1,18	*Slc4a9*	2,84
Pik3cd	-1,10	*Ctxn3*	-1,27	*Pi4kb*	-1,01	*Mir6236*	1,37*	*Atad5*	1,06	*Tbx3*	2,94
Itgb2	-1,35	*Cnpy1*	-1,46	*Isg20*	-1,85	*Slc22a2*	1,58	*Actn2*	2,62	*Shc2*	1,58
Gypa	-2,11	*Pcp2*	-2,49	*Pla2g3*	-1,31	*Cox7b2*	2,01	*Chst9*	2,94	*Mb*	3,62
Isg20	-1,67	*Mybpc1*	-2,38	*Gypa*	-1,93	*Spaar*	3,92	*Lhx2*	3,30	*Lor*	1,72
Samsn1	-2,58	*Msx2*	-1,45	*Lyl1*	-2,18	*Nlrc3*	2,85	*Igfbp7*	1,26	*Fosl2*	1,33
Hcls1	-1,81	*Ltbp2*	-2,06	*Hpx*	-2,97	*Gnmt*	1,59	*Rell2*	1,05	*Tcap*	3,67
Parvaos	-2,82	*Wdr49*	-2,31	*Slc34a3*	-1,78	*Tec*	2,38	*Scrt1*	1,09	*Rspo4*	4,70
Pf4	-1,27	*Cd70*	-1,86	*Pck1*	-4,08	*B3gnt9*	2,43	*Rhbdl1*	1,24	*Pcdhb19*	1,21
Ppbp	-2,04	*Slc10a4*	-2,35	*Ddc*	-1,39	*Nrtn*	1,14	*Chsy3*	1,50	*Greb1l*	1,08
Itgal	-1,41	*Dclk3*	-1,04	*Gda*	-1,37	*Sntn*	1,88	*Mill2*	1,78	*Mafa*	2,43
Kcnj8	-3,40	*Gabrd*	-1,15	*Hbq1b*	-2,48	*C1qtnf1*	1,55	*Avpr1a*	3,31	*Nr4a3*	1,22
Cybb	-1,24	*Ildr1*	-2,31	*Serpina3e-ps*	-4,35	*Zbtb8b*	2,02	*Thbd*	4,26	*Glra3*	1,23
Hmcn2	-1,92	*Pole*	-1,20	*Sema3e*	-1,58	*Sytl1*	1,91	*Serpinf2*	2,08	*Pdgfb*	1,69

Data from lists of differentially expressed genes (DEG) with $p < 0.05$ in astrocyte-specific RNAs from each region. The values are expressed as logFC between VCR-EST and VCR-vehicle groups and ordered by significance level. Down, downregulated in VCR-EST; Up, upregulated in VCR-EST; SS, somatosensory cortical astrocytes; PAG, periaqueductal gray matter astrocytes; SC, spinal cord dorsal astrocytes. * adjusted $p < 0.05$.

Supporting Table 8. Detailed statistical evaluation for Figure 32 b.

Male	Statistic		Result
Hbb	Two-way	CIPN	F (1, 8) = 26.641; p < 0.001
Early	ANOVA	Treatment	F (1, 8) = 0.328; p = 0.583
		CIPN x Treatment	F (1, 8) = 0.378; p = 0.556
		CIPN	F (1, 8) = 0.506; p = 0.497
Late		Treatment	F (1, 8) = 43.276; p < 0.001
		CIPN x Treatment	F (1, 8) = 54.277; p < 0.001
	Three-way	CIPN	F (1, 16) = 12.142; p < 0.01
	ANOVA	Treatment	F (1, 16) = 21.915; p < 0.001
		Time	F (1, 16) = 35.585; p < 0.001
Early vs Late		CIPN x Treatment	F (1, 16) = 18.344; p < 0.001
		CIPN x Time	F (1, 16) = 19.385; p < 0.001
		Treatment x Time	F (1, 16) = 14.491; p < 0.01
		CIPN x Treatment x Time	F (1, 16) = 27.279; p < 0.001
Hba	Two-way	CIPN	F (1, 8) = 23.793; p < 0.001
Early	ANOVA	Treatment	F (1, 8) = 0.322; p = 0.586
		CIPN x Treatment	F (1, 8) = 0.188; p = 0.676
		CIPN	F (1, 8) = 0.000; p = 0.986
Late		Treatment	F (1, 8) = 43.199; p < 0.001
		CIPN x Treatment	F (1, 8) = 59.489; p < 0.001
	Three-way	CIPN	F (1, 16) = 16.604; p < 0.001
	ANOVA	Treatment	F (1, 16) = 16.541; p < 0.001
		Time	F (1, 16) = 27.280; p < 0.001
Early vs Late		CIPN x Treatment	F (1, 16) = 14.838; p < 0.01
		CIPN x Time	F (1, 16) = 16.770; p < 0.001
		Treatment x Time	F (1, 16) = 9.714; p < 0.01
		CIPN x Treatment x Time	F (1, 16) = 20.959; p < 0.001
Alas2	Two-way	CIPN	F (1, 8) = 22.032; p < 0.01
Early	ANOVA	Treatment	F (1, 8) = 0.811; p = 0.394
		CIPN x Treatment	F (1, 8) = 0.649; p = 0.444
		CIPN	F (1, 8) = 20.688; p < 0.01
Late		Treatment	F (1, 8) = 77.464; p < 0.001
		CIPN x Treatment	F (1, 8) = 86.328; p < 0.001
	Three-way	CIPN	F (1, 16) = 0.059; p = 0.811
	ANOVA	Treatment	F (1, 16) = 45.415; p < 0.001
		Time	F (1, 16) = 61.552; p < 0.001
Early vs Late		CIPN x Treatment	F (1, 16) = 34.178; p < 0.001
		CIPN x Time	F (1, 16) = 42.719; p < 0.001
		Treatment x Time	F (1, 16) = 29.580; p < 0.001
		CIPN x Treatment x Time	F (1, 16) = 49.132; p < 0.001

(continues)

Female	Statistic		Result
Hbb	Two-way	CIPN	F (1, 8) = 95.711; p < 0.001
Early	ANOVA	Treatment	F (1, 8) = 4.272; p = 0.0.73
		CIPN x Treatment	F (1, 8) = 3,758; p = 0.0.89
		CIPN	F (1, 8) = 2.557; p = 0.149
Late		Treatment	F (1, 8) = 7.524; p < 0.05
		CIPN x Treatment	F (1, 8) = 4.623; p = 0.064
	Three-way	CIPN	F (1, 16) = 0.156; p = 0.698
	ANOVA	Treatment	F (1, 16) = 9.621; p < 0.01
		Time	F (1, 16) = 18.712; p < 0.001
Early vs Late		CIPN x Treatment	F (1, 16) = 2.951; p = 0.105
		CIPN x Time	F (1, 16) = 12.447; p < 0.01
		Treatment x Time	F (1, 16) = 5.166; p < 0.05
		CIPN x Treatment x Time	F (1, 16) = 6.226; p < 0.05
Hba	Two-way	CIPN	F (1, 8) = 71.253; p < 0.001
Early	ANOVA	Treatment	F (1, 8) = 2.988; p = 0.122
		CIPN x Treatment	F (1, 8) = 2.516; p = 0.151
		CIPN	F (1, 8) = 1.790; p = 0.218
Late		Treatment	F (1, 8) = 6.454; p < 0.05
		CIPN x Treatment	F (1, 8) = 5.472; p < 0.05
	Three-way	CIPN	F (1, 16) = 0.119; p = 0.735
	ANOVA	Treatment	F (1, 16) = 8.011; p < 0.05
		Time	F (1, 16) = 15.449; p < 0.01
Early vs Late		CIPN x Treatment	F (1, 16) = 3.930; p = 0.065
		CIPN x Time	F (1, 16) = 8.815; p < 0.01
		Treatment x Time	F (1, 16) = 4.630; p < 0.05
		CIPN x Treatment x Time	F (1, 16) = 6.787; p < 0.05
Alas2	Two-way	CIPN	F (1, 8) = 30.121; p < 0.001
Early	ANOVA	Treatment	F (1, 8) = 0.046; p = 0.836
		CIPN x Treatment	F (1, 8) = 0.620; p = 0.454
		CIPN	F (1, 8) = 4.065; p = 0.079
Late		Treatment	F (1, 8) = 6.405; p < 0.05
		CIPN x Treatment	F (1, 8) = 5.793; p < 0.05
	Three-way	CIPN	F (1, 16) = 0.242; p = 0.629
	ANOVA	Treatment	F (1, 16) = 6.236; p < 0.05
		Time	F (1, 16) = 14.157; p < 0.01
Early vs Late		CIPN x Treatment	F (1, 16) = 4.464; p = 0.051
		CIPN x Time	F (1, 16) = 11.536; p < 0.01
		Treatment x Time	F (1, 16) = 5.683; p < 0.05
		CIPN x Treatment x Time	F (1, 16) = 6.398; p < 0.05

(continues)

Male vs Female	Statistic		Result
Hbb	Three-way	CIPN	F (1, 16) = 68.932; p < 0.001
	ANOVA	Treatment	F (1, 16) = 1.612; p = 0.222
		Sex	F (1, 16) = 0.404; p = 0. 534
Early		CIPN x Treatment	F (1, 16) = 1.598; p = 0.224
		CIPN x Sex	F (1, 16) = 1.812; p = 0.197
		Treatment x Sex	F (1, 16) = 0.040; p = 0.844
		CIPN x Treatment x Sex	F (1, 16) = 0.013; p = 0.910
		CIPN	F (1, 16) = 3.063; p = 0.099
		Treatment	F (1, 16) = 27.231; p < 0.001
		Sex	F (1, 16) = 0.280; p = 0. 604
Late		CIPN x Treatment	F (1, 16) = 25.049; p < 0.001
		CIPN x Sex	F (1, 16) = 1.349; p = 0.263
		Treatment x Sex	F (1, 16) = 0.050; p = 0.826
		CIPN x Treatment x Sex	F (1, 16) = 1.187; p = 0.292
Hba	Three-way	CIPN	F (1, 16) = 57.077; p < 0.001
	ANOVA	Treatment	F (1, 16) = 1.308; p = 0.270
		Sex	F (1, 16) = 0.614; p = 0.445
Early		CIPN x Treatment	F (1, 16) = 0.937; p = 0.347
		CIPN x Sex	F (1, 16) = 2.453; p = 0.137
		Treatment x Sex	F (1, 16) = 0.007; p = 0. 935
		CIPN x Treatment x Sex	F (1, 16) = 0.025; p = 0.877
		CIPN	F (1, 16) = 1.616; p = 0.222
		Treatment	F (1, 16) = 20,629; p < 0.001
		Sex	F (1, 16) = 1.203; p = 0.289
Late		CIPN x Treatment	F (1, 16) = 22.306; p < 0.001
		CIPN x Sex	F (1, 16) = 1.585; p = 0.226
		Treatment x Sex	F (1, 16) = 0.069; p = 0.797
		CIPN x Treatment x Sex	F (1, 16) = 0.090; p = 0.769
Alas2	Three-way	CIPN	F (1, 16) = 47.587; p < 0.001
	ANOVA	Treatment	F (1, 16) = 0.767; p = 0.394
		Sex	F (1, 16) = 2.773; p = 0.115
Early		CIPN x Treatment	F (1, 16) = 1.213; p = 0.287
		CIPN x Sex	F (1, 16) = 1.084; p = 0.313
		Treatment x Sex	F (1, 16) = 0.419; p = 0.527
		CIPN x Treatment x Sex	F (1, 16) = 0.068; p = 0.797
		CIPN	F (1, 16) = 13.035; p < 0.01
		Treatment	F (1, 16) = 32.730; p < 0.001
		Sex	F (1, 16) = 0.001; p = 0.976
Late		CIPN x Treatment	F (1, 16) = 33.583; p < 0.001
		CIPN x Sex	F (1, 16) = 0.013; p = 0.912
		Treatment x Sex	F (1, 16) = 1.100; p = 0.310
		CIPN x Treatment x Sex	F (1, 16) = 1.827; p = 0. 195

Supplementary results

Characterization of Cx3cr1-CreERT2:RiboTag mouse line for microglia-specific transcriptomics: focus on the analgesic effects of a selective σ1R antagonist on CIPN

Supplementary results

Characterization of Cx3cr1-CreERT2:RiboTag mouse line for microglia-specific transcriptomics: focus on the analgesic effects of a selective σ1R antagonist on CIPN

This study was conducted in parallel to the ***Study 1*** by addressing the same approach and methodology unlike using male and female Cx3cr1-CreERT2:RiboTag mice (Haimon *et al.*, 2018) to investigate the specific transcriptomic alterations occurring in microglial population under neuropathic pain conditions induced by vincristine chemotherapy. The therapeutic effect of a σ1R antagonist in trial was also evaluated to elucidate its modulatory effects on microglial cells under this pathological condition. Here we present the results of the validation of the RiboTag approach on this mouse line and the behavioral characterization of the CIPN model to further proceed with cell-type specific transcriptomic analyses.

Anatomical validation of Microglia-RiboTag mouse line

To first validate the mouse line, two Cx3cr1-CreERT2:RiboTag mice per sex were sacrificed two weeks after exposure to tamoxifen (3 x 100 mg/Kg, i.p), and tissue samples (brain and SC) were dissected and prepared for immunofluorescence analysis. Immunostaining against the HA-epitope tag along with specific antibodies for microglia (Iba1), astrocytes (Aldh1l1 or Gfap), or neurons (NeuN), confirmed widespread expression of HA-tagged ribosomes in the CNS regions examined **(Figure 35 a)** which highly co-localized with Iba1-positive microglial cells **(Figure 35**¡Error! No se e ncuentra el origen de la referencia. **b)**, indicating an efficient and specific

recombination of Cre upon TAM exposure. No co-expression of the HA-tag was observed in neither Aldh1l1 or Gfap-positive astrocytes nor NeuN-positive neurons **(Figure 35**¡Error! No se encuentra el origen de la r eferencia. **b, SS; Supporting Figure 2, other regions).** In contrast, in non-TAM-treated mice we did not observe expression of HA-tagged ribosomes, which evidenced the suitability of the model for subsequent analysis.

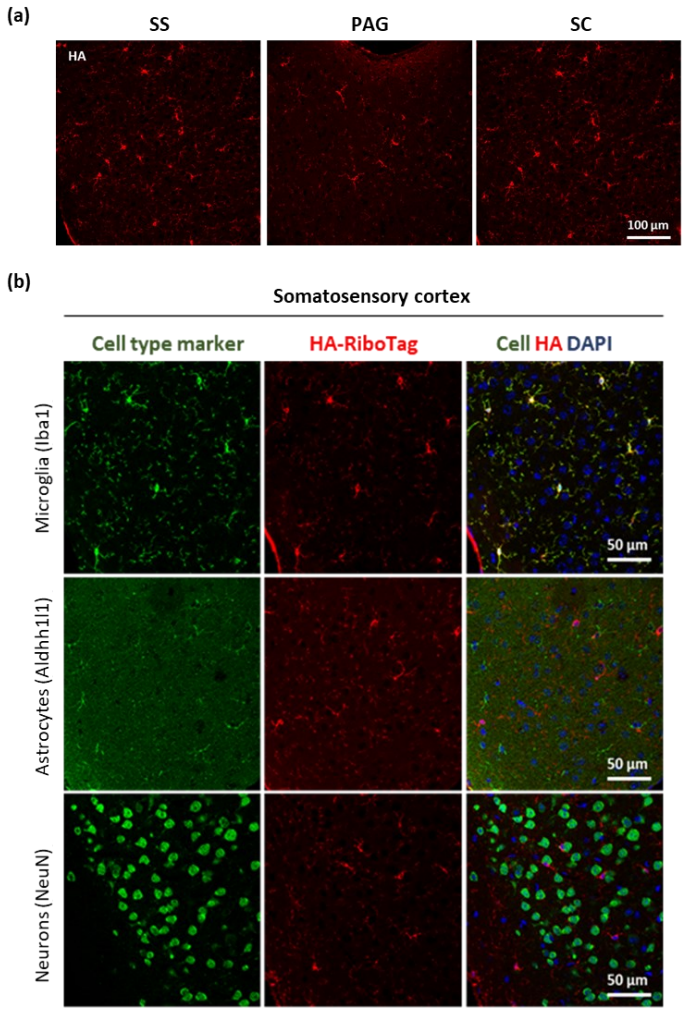

Figure 35. Anatomical validation of Microglia-RiboTag mouse line. (a) Representative images from HA immunostaining showing the efficient expression of the HA-tag in the various pain-related areas. **(b)** Double immunofluorescence

for HA (red) and cell-specific markers (green), counterstained with DAPI (blue), to determine the cell-type expression of HA-tagged ribosomes. Images showing strong co-expression between HA and Iba1 (microglia), but no colocalization with Aldh1l1 (astrocytes) or NeuN (neurons). Representative images from the somatosensory cortex (n= 2 x male/female mice). See supporting figure S1 for other regions.

Therapeutic efficacy of σ1R antagonist EST on the modulation of vincristine-induced nociceptive sensitivity: behavioral characterization on Microglia-RiboTag mouse line

Animal welfare

In line with the goal of minimizing any potential bias in nociceptive data, animals' body weight was measured daily to control health deterioration caused by any of the treatments provided. A gradual reduction in the body weight was observed in male and female animals treated with vincristine **(Figure 36 a,b).** Male mice showed a significantly higher weight loss than females ($p < 0.001$; **Figure 36**¡Error! No se encuentra el origen de la r eferencia. **c,d**). Nonetheless, no animal had to be excluded from the study for exceeding the ethical body-weight reduction limit (< 20%; Talbot *et al.*, 2020), and no significant modifications were observed in their general wellbeing throughout the experimental procedure. The exposure to EST drug did not produce significant changes in body weight within saline or VCR-treated groups in male mice, while in females it did produce slight but significant modifications ($p < 0.01$; **Figure 36 b**). However, no significant differences were observed between vehicle and EST-treated groups (saline or VCR) at the end of the study **(Figure 36**¡Error! No se encuentra e l origen de la referencia. **d).** Saline-treated mice did not display significant modifications in their body weight throughout the experimental sequence.

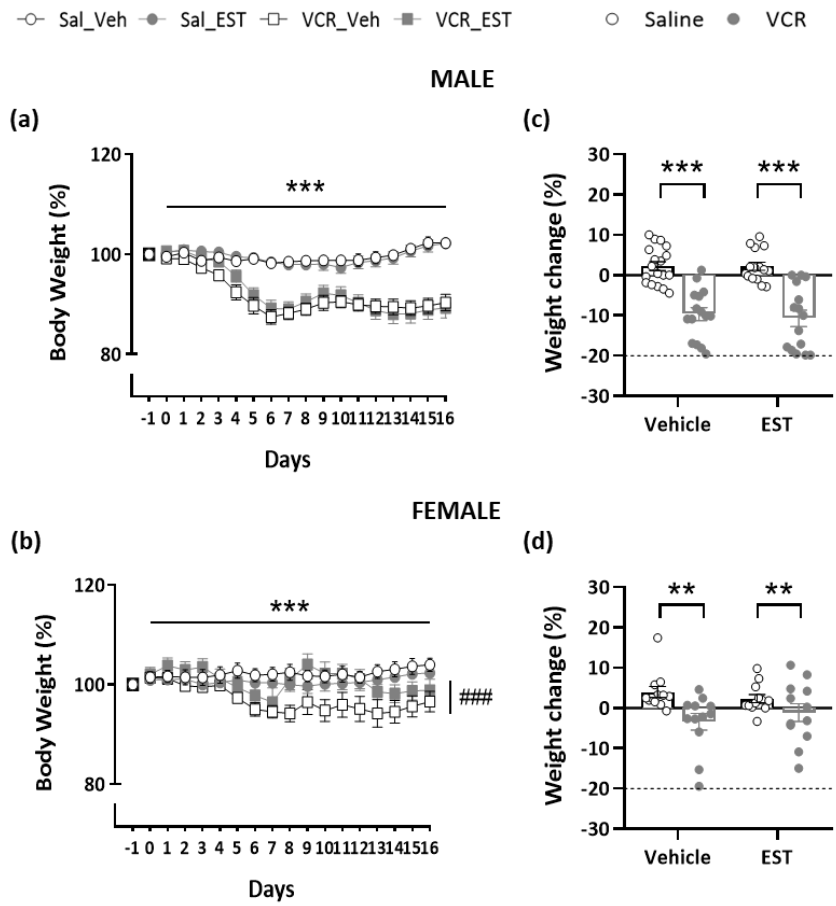

Figure 36. Effects of vincristine chemotherapy on the body weight of Microglia-RiboTag mice. Vincristine (0.5 mg/Kg i.p) caused substantial but not critical weight loss in both sexes. **(a,b)** Vincristine produced a progressive reduction in body weight in both sexes, especially in males. Repeated EST treatment did not produce significant weight changes in male mice but slight variations in female mice. **(c,d)** Total body weight reduction was significantly higher in male than female mice treated with vincristine. No animal had to be excluded from the study for exceeding ethical weight loss limits (< 20%; dot lines). Data are expressed as mean ± SEM: percentage of body weight relative to initial weight in naïve conditions (a,b); percentage of weight change at day 16 relative to initial weight. *** p<0.001 Sal vs. VCR. Mixed Model Analysis + Bonferroni (a,b); Kruskal-Wallis, Mann-Whitney U (c,d). Sal, saline; Veh, vehicle; VCR, vincristine; EST, σ1R antagonist. Detailed statistical analyses are shown in **Supporting Table 9**.

Effects of vincristine chemotherapy and EST treatment on nociception

Nociceptive sensitivity to mechanical stimuli was evaluated using the Von Frey test. Mechanical responses were evaluated before (PRE) and 30 minutes after (POST) the daily EST or vehicle administration to evaluate the long and short-term analgesic effects of the σ1R antagonist EST, respectively (**Figure 37 a,b**). All experimental groups had comparable baseline mechanical thresholds. Mechanical responses were unaffected by exposure to saline, and EST treatment had no effect on withdrawal thresholds in saline-treated mice **(Figure 37 a,b).** The antineoplastic treatment caused a significant and maintained reduction in withdrawal thresholds to mechanical stimulation compared to saline-treated mice in both sexes. Mechanical allodynia was observed following the initial dose of this drug and lasted the duration of the experimental sequence **(Figure 37**¡Error! No se encuentra el origen de la referencia. **a,b).** EST produced modest analgesic effects after acute administration, albeit not statistically significant **(Figure 37 a,b, *right panel*).** Repeated EST administration, on the contrary, resulted in a progressive recovery of mechanical thresholds in both sexes, especially in females, which showed a trend to recover baseline values at the end of the experimental protocol **(Figure 37 a,b, *left panel*).**

Once mechanical evaluations were completed, and approximately 60 minutes after vehicle or EST administration, sensitivity to thermal stimulation was assessed in the plantar test. Under basal conditions, all mice had comparable withdrawal latencies, albeit we observed a slight but significant effect of sex ($p < 0.05$), which is probably due to a higher number of males (n = 63) compared with females (n = 48). Exposure to saline did not modify heat sensitivity, and control saline mice responses

were unaffected by EST treatment **(Figure 37 c).** Heat hyperalgesia was induced in both male and female mice after a single dose of VCR and increased throughout this study. Repeated treatment with EST dramatically reduced this sensory alteration in both sexes, especially in females, which recovered baseline values at the end of the experiment **(Figure 37 c).**

These results are better understood by representing the percentage of induced analgesia on VCR-EST treated animals. Thus, we observed that repeated treatment with EST progressively increased the analgesic efficacy for both mechanical and heat sensitivity, reaching high efficacy at the end of the treatment in both sexes **(Figure 38 a).** In particular, EST exhibited almost total analgesic efficacy for heat sensitivity in both males (89.3 ± 5.2) and females (92 ± 3.7), with no significant differences between sexes. In contrast, the analgesic effect in mechanical sensitivity was lower, obtaining values of around 55% in males (55.0 ± 11.3; **Figure 38 a)** and around 72% in females (72.0 ± 19.6; **Figure 38 b**) (PRE values relative to baseline). In addition, acute EST administration was shown to have an enhancing effect on analgesic efficacy, as evidenced by significant higher levels of analgesia when compared to PRE values (supplementary figure 4. In this case, no differences were observed on mechanical analgesia between male and female mice.

Overall, these results indicate that persistent modulation of σ1R activity leads to functional changes that efficiently alleviate vincristine-induced mechanical allodynia and thermal hyperalgesia, with significantly higher effects in females.

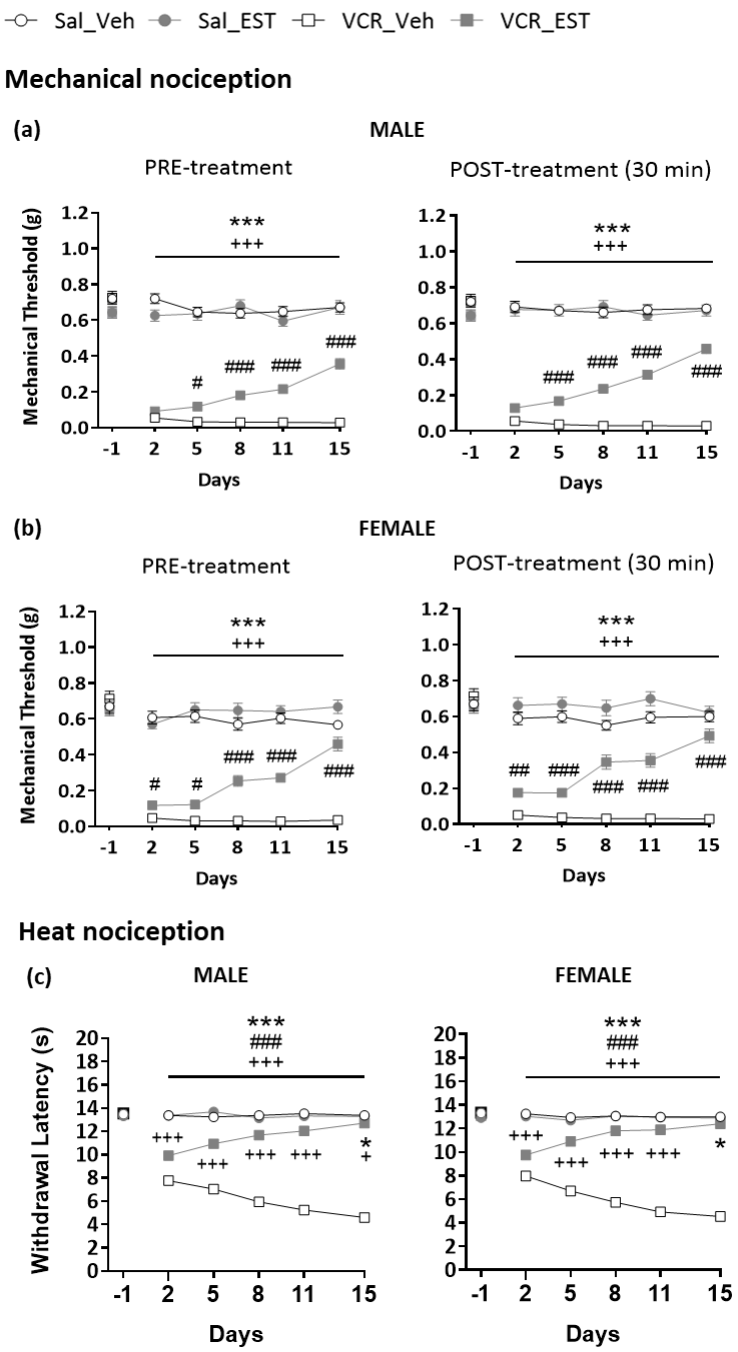

Figure 37. Effects of repeated and acute EST administration on mechanical and heat sensitivity in vincristine-induced neuropathy in Microglia-RiboTag mice. Von Frey and Hargreaves plantar test were used for mechanical and heat

thresholds determination, respectively**. (a, b)** Vincristine induced mechanical allodynia after a single injection (day 2) compared to saline-treated mice. Repeated treatment with σ1R antagonist EST produced a gradual increase of mechanical thresholds, especially in female. The acute administration of EST 25 mg/kg was inefficient in preventing mechanical hypersensitivity, as evidenced by no significant differences between PRE and POST mechanical values. No different mechanical nociceptive thresholds were observed between male and female mice. **(c)** Heat hyperalgesia was further verified by substantial differences in withdrawal latencies following a single dosage between saline and VCR-treated animals. Repeated EST administration resulted in a progressive normalization of heat sensitivity, with complete return of baseline levels in females. Data are expressed as mean ± SEM (Male: n = 15-18/ group; Female: n = 12/ group). ***p<0.001, * p<0.05 Sal vs VCR; # p<0.05, ## p<0.01, ### p<0.001 Veh vs EST; +++ p<0.001, + p<0.05 vs baseline (VCR-treated groups). Sal, saline; Veh, vehicle; VCR, vincristine; EST, σ1R antagonist. Kruskal-Wallis (baseline, a,b); Mixed Model Analysis + Bonferroni (a,b,c); Detailed statistical analyses are shown in **Supporting Table 10.**

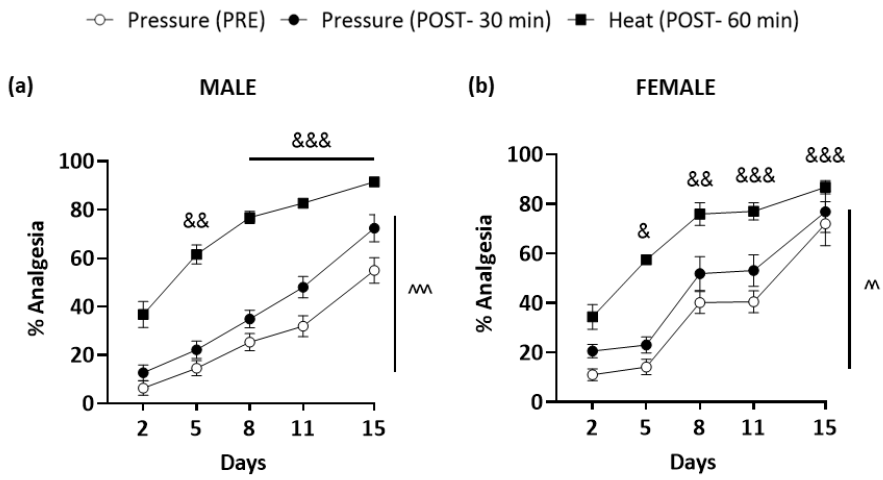

Figure 38. Analgesic efficacy of EST on vincristine-induced neuropathic pain in Microglia-RiboTag mice. (a) Repeated EST treatment produced different analgesic efficiency for mechanical and thermal sensitivity in both male **(a)** and female **(b)** mice. A total analgesic effect was obtained for heat sensitivity in both sexes. EST treatment exhibited subeffective antiallodynic effects in both male and female mice, with a trend to reach total analgesia at the end of the experiment in females. The acute administration of EST produced a slight increase of analgesic

effects on mechanical sensitivity. No significant differences were observed in analgesia between sexes. Data are expressed as mean ± SEM (n = 9/group). ^ p<0.05, ^^ p<0.01, ^^^ p<0.001 vs PRE; & p<0.05, && p<0.01, &&& p<0.001 vs Day 2. One or two-way repeated measures ANOVA + Bonferroni. Detailed statistical analyses are shown in Supporting Table 11.

Isolation and validation of microglial-enriched mRNA from diverse CNS regions for downstream analysis

After experimental protocol, microglia-enriched mRNA was isolated from multiple pain-related areas of the CNS - SS, PAG, and SC dorsal - by immunoprecipitation of HA-tagged polysomes. Validation of the isolated mRNA samples by qRT-PCR analysis revealed a huge enrichment of microglial marker *Cx3cr1* in immunoprecipitated samples (IP) compared to the input fraction (which comprises all mRNAs from the initial homogenate) and a de-enrichment of markers for astrocytes (*Aldh1l1),* oligodendrocytes *(Ugt8a)* and neurons *(Rbfox3)* **(Figure 39 a,b).** Samples exhibiting enrichment for any of the non-microglial markers were excluded for downstream analyses. Selected samples will be sequenced to identify the transcriptomic alterations occurring in microglial cells under vincristine-induced neuropathic pain conditions and the potential modulatory actions produced by the blockade of σ1R on microglia.

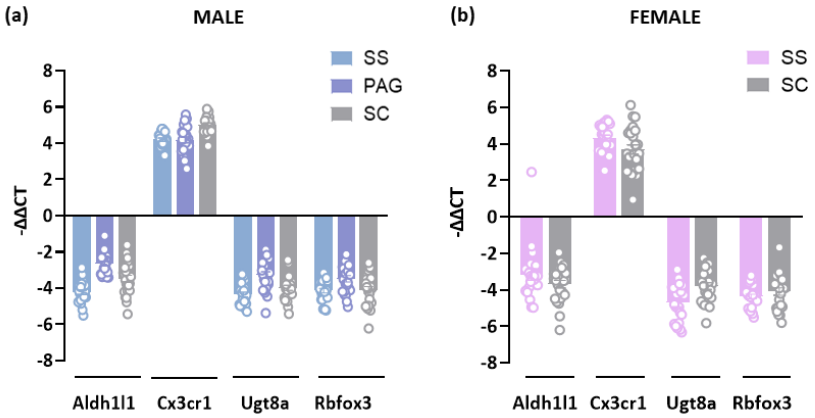

Figure 39. Isolation and validation of Microglia-RiboTag mice mRNAs. Validation by qRT-PCR (-ΔΔCt) of the enrichment of microglial markers (Cx3cr1) and de-enrichment of astrocyte (Aldh1l1), oligodendrocyte (Ugt8a) and neuronal (Rbfox3) markers after HA-immunoprecipitation from whole somatosensory cortices (SS), periaqueductal gray (PAG) and spinal cord dorsal horn (SC) extracts. Data are expressed as the fold change (mean ± SEM) comparing the immunoprecipitated samples vs. the input containing the mRNAs from all cellular types (n = 24 samples/ region/ sex). Male: all samples showed high microglial specificity and no contamination from other cell types; Female: One pool of SS was excluded for presenting astroglial contamination.

Supporting material

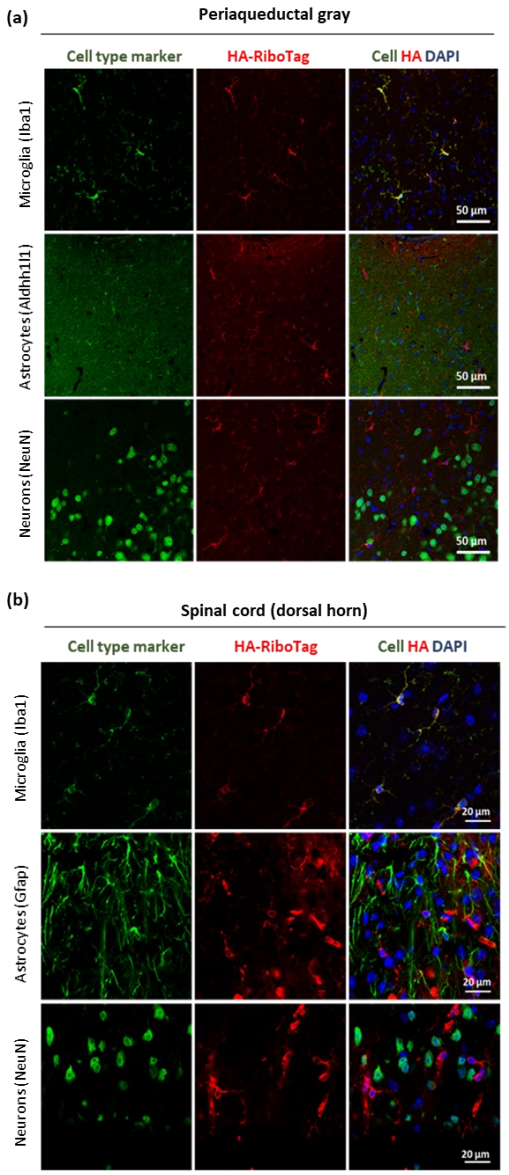

Supporting Figure 2. Anatomical validation of Aldh1l1-CreERT2:RiboTag mouse line. Immunostaining for HA (red) and cell-specific markers (green), counterstained with DAPI (blue), to determine the cell-type expression of HA-tagged ribosomes in **(a)** the periaqueductal gray and **(b)** the dorsal spinal cord. Representative images showing strong co-expression between HA and Aldh1l1 or Gfap (Astrocytes), but no colocalization with Iba1 (microglia) or NeuN (neurons) (n= 2 x male/female mice).

Supporting Table 9. Detailed statistical evaluation for Figure 36.

Male	Statistic		Result
Figure 36 (a)	Mixed Model	CIPN	F (1, 894.990) = 624.272; p < 0.001
		Treatment	F (1, 894.990) = 2.118; p = 0.146
		Day	F (16, 127.115) = 21.557; p < 0.001
		CIPN x Treatment	F (1, 894.990) = 2.477; p = 0.116
		CIPN x Day	F (16, 127.115) = 16.087; p < 0.001
		Treatment x Day	F (16, 127.115) = 0.757; p = 0.730
		CIPN x Treatment x Day	F (16, 127.115) = 0.234; p = 0.999
Figure 36 (c)	Kruskall-Wallis		H (3) = 34,710; p<0.001

Female	Statistic		Result
Figure 36 (b)	Mixed Model	CIPN	F (1, 684.780) = 46.849; p < 0.001
		Treatment	F (1, 684.780) = 9.484; p < 0.01
		Day	F (16, 95.907) = 1.919; p < 0.05
		CIPN x Treatment	F (1, 684.780) = 45.972; p < 0.001
		CIPN x Day	F (16, 95.907) = 3.111; p < 0.001
		Treatment x Day	F (16, 95.907) = 0.364; p = 0.987
		CIPN x Treatment x Day	F (16, 95.907) = 0.650; p = 0.835
Figure 36 (d)	Kruskall-Wallis		H (3) = 10,550; p<0.05

Male vs Female	Statistic		Result
Figure 36 (a, b)	Mixed Model	CIPN	F (1, 1594,320) = 439,643; p < 0.001
		Treatment	F (1, 1594,320) = 11,555; p < 0.001
		Day	F (16, 204,175) = 15,171; p < 0.001
		Sex	F (1, 1594,320)= 319,617; p < 0.001
		CIPN x Treatment	F (1, 1594,320) = 41,976; p < 0.001
		CIPN x Day	F (16, 204,175) = 14,805; p < 0.001
		CIPN x Sex	F (1, 1594,320) = 96,955; p < 0.001
		Treatment x Day	F (16, 204,175) = 0,378; p = 0.986
		Treatment x Sex	F (1, 1594,320) = 2,575; p = 0.109
		Day x Sex	F (16, 204,175) = 3,023; p < 0.001
		CIPN x Treatment x Day	F (16, 204,175) = 0,652; p = 0.838
		CIPN x Treatment x Sex	F (1, 1594,320) = 20,590; p < 0.001
		CIPN x Day x Sex	F (16, 204,175) = 1,471; p = 0.113
		Treatment x Day x Sex	F (16, 204,175) = 0,691; p = 0.801
		CIPN x Treatment x Day x Sex	F (16, 204,175) = 0,413; p = 0.978
Figure 36 (c, d)	Kruskall-Wallis		H (7) = 51,685; p < 0.001

Supporting Table 10. Detailed statistical evaluation for Figure 37

MECHANICAL NOCICEPTION

Male	Statistic		Result
Figure 37 (a) Baseline mechanical thresholds	Kruskall-Wallis	Among 4 groups	H (3) = 5.478; p = 0.140
Figure 37 (a) Mechanical sensitivity PRE-treatment	Mixed Model	CIPN	F (1, 333.337) = 1776.163; p < 0.001
		Treatment	F (1, 333.337) = 15.815; p < 0.01
		Day	F (5, 98.497) = 66.342; p < 0.001
		CIPN x Treatment	F (1, 333.337) = 48.721; p < 0.001
		CIPN x Day	F (5, 98.497) = 54.230; p < 0.001
		Treatment x Day	F (5, 98.497) = 9.828; p < 0.001
		CIPN x Treatment x Day	F (5, 98.497) = 4.453; p < 0.01
Figure 37 (a) Mechanical sensitivity POST-treatment	Mixed Model	CIPN	F (1, 332.174) = 1685.424; p < 0.001
		Treatment	F (1, 332.174) = 153.632; p < 0.001
		Day	F (5, 106.317) = 55.520; p < 0.001
		CIPN x Treatment	F (1, 332.174) = 78.477; p < 0.001
		CIPN x Day	F (5, 106.317) = 52.875; p < 0.001
		Treatment x Day	F (5, 106.317) = 12.565; p < 0.001
		CIPN x Treatment x Day	F (5, 106.317) = 9.671; p < 0.001
Figure 37 (a) Acute effect of EST (POST vs PRE values)	Mixed Model	CIPN	F (1, 287.527) = 3.645; p = 0.057
		Treatment	F (1, 287.527) = 32.379; p < 0.001
		Day	F (5, 107.147) = 1.987; p = 0.102
		CIPN x Treatment	F (1, 287.527) = 10.166; p < 0.01
		CIPN x Day	F (5, 107.147) = 1.067; p = 0.376
		Treatment x Day	F (5, 107.147) = 1.102; p = 0.359
		CIPN x Treatment x Day	F (5, 107.147) = 3.384; p < 0.05

Female	Statistic		Result
Figure 37 (b) Baseline mechanical thresholds	Kruskall-Wallis	Among 4 groups	H (3) =1.319; p = 0.725
Figure 37 (b) Mechanical sensitivity PRE-treatment	Mixed Model	CIPN	F (1, 227.598) = 1021.906; p < 0.001
		Treatment	F (1, 227.598) = 66.181; p < 0.001
		Day	F (5, 78.760) = 46.327; p < 0.001
		CIPN x Treatment	F (1, 227.598) = 29.230; p < 0.001
		CIPN x Day	F (5, 78.760) = 32.445; p < 0.001
		Treatment x Day	F (5, 78.760) = 11.923; p < 0.001
		CIPN x Treatment x Day	F (5, 78.760) = 3.793; p < 0.01
Figure 37 (b) Mechanical sensitivity POST-treatment	Mixed Model	CIPN	F (1, 244.724) = 804.115; p < 0.001
		Treatment	F (1, 244.724) = 111.100; p < 0.001
		Day	F (5, 63.556) = 37.554; p < 0.001
		CIPN x Treatment	F (1, 244.724) = 36.888; p < 0.001
		CIPN x Day	F (5, 63.556) = 30.295; p < 0.001
		Treatment x Day	F (5, 63.556) = 8.556; p < 0.001
		CIPN x Treatment x Day	F (5, 63.556) = 7.250; p < 0.001

(continues)

Figure 37 (b) Acute effect of EST (POST vs PRE values)	Mixed Model	CIPN	F (1, 199.278) = 5.057; p <0.05
		Treatment	F (1, 199.278) = 21.994; p < 0.001
		Day	F (5, 87.069) = 1.376; p = 0.249
		CIPN x Treatment	F (1, 199.278) = 2.712; p = 0.101
		CIPN x Day	F (5, 87.069) = 0.895; p = 0.471
		Treatment x Day	F (5, 87.069) = 3.506; p < 0.05
		CIPN x Treatment x Day	F (5, 87.069) = 2.421; p = 0.054

Male vs Female	**Statistic**		**Result**
Figure 37 (a vs b) Baseline mechanical thresholds	Kruskall-Wallis	Among 8 groups	H (7) = 8,375; p = 0.301
Figure 37 (a vs b) Mechanical sensitivity PRE-treatment	Mixed Model	CIPN	F (1, 505.680) = 3736.948; p < 0.001
		Treatment	F (1, 505.680) = 135.710; p < 0.001
		Day	F (4, 210.514) = 10.298; p < 0.001
		Sex	F (1, 505.680) = 0.683; p = 0.409
		CIPN x Treatment	F (1, 505.680) = 110.000; p < 0.001
		CIPN x Day	F (4, 210.514) = 8.303; p < 0.001
		CIPN x Sex	F (1, 505.680) = 15.509; p < 0.001
		Treatment x Day	F (4, 210.514) = 18.963; p < 0.001
		Treatment x Sex	F (1, 505.680) = 12.737; p < 0.001
		Day x Sex	F (4, 210.514) = 1.214; p = 0.306
		CIPN x Treatment x Day	F (4, 210.514) = 6.655; p < 0.001
		CIPN x Treatment x Sex	F (1, 505.680) = 0.148; p = 0.701
		CIPN x Day x Sex	F (4, 210.514) = 1.410; p = 0.232
		Treatment x Day x Sex	F (4, 210.514) = 0.514; p = 0.726
		CIPN x Treatment x Day x Sex	F (4, 210.514) = 0.165; p = 0.956
Figure 37 (a vs b) Mechanical sensitivity POST-treatment	Mixed Model	CIPN	F (1, 509.482) = 3186.224; p < 0.001
		Treatment	F (1, 509.482) = 266.763; p < 0.001
		Day	F (4, 196.662) = 9.700; p < 0.001
		Sex	F (1, 509.482) = 2.627; p = 0.106
		CIPN x Treatment	F (1, 509.482) = 153.227; p < 0.001
		CIPN x Day	F (4, 196.662) = 12.232; p < 0.001
		CIPN x Sex	F (1, 509.482) = 17.912; p < 0.001
		Treatment x Day	F (4, 196.662) = 11.994; p < 0.001
		Treatment x Sex	F (1, 509.482) = 13.339; p < 0.001
		Day x Sex	F (4, 196.662) = 0.326; p = 0.860
		CIPN x Treatment x Day	F (4, 196.662) = 15.433; p < 0.001
		CIPN x Treatment x Sex	F (1, 509.482) = 0.648; p = 0.421
		CIPN x Day x Sex	F (4, 196.662) = 1.019; p = 0.399
		Treatment x Day x Sex	F (4, 196.662) = 0.453; p = 0.770
		CIPN x Treatment x Day x Sex	F (4, 196.662) = 0.490; p = 0.743

HEAT NOCICEPTION

Male	Statistic		Result
Figure 37 (c) Baseline heat thresholds	Two-way ANOVA	CIPN	F (1, 59) = 0.473; p = 0.494
		Treatment	F (1, 59) = 0.325; p = 0.571
		CIPN x Treatment	F (1, 59) = 0.092; p = 0.763
Figure 37 (c) Heat sensitivity 60 min after EST admin.	Mixed Model	CIPN	F (1, 318.519) =2582.086; p < 0.001
		Treatment	F (1, 318.519) = 866.735; p < 0.001
		Day	F (5, 129.058) = 120.843; p < 0.001
		CIPN x Treatment	F (1, 318.519) = 896.989; p < 0.001
		CIPN x Day	F (5, 129.058) = 116.222; p < 0.001
		Treatment x Day	F (5, 129.058) = 75.474; p < 0.001
		CIPN x Treatment x Day	F (5, 129.058) = 79.147; p < 0.001

Female	Statistic		Result
Figure 37 (c) Baseline heat thresholds	Two-way ANOVA	CIPN	F (1, 44) = 0.299; p = 0.588
		Treatment	F (1, 44) = 3.709; p = 0.061
		CIPN x Treatment	F (1, 44) = 0.175; p = 0.678
Figure 37 (c) Heat sensitivity 60 min after EST admin.	Mixed Model	CIPN	F (1, 258.096) =2463.303; p < 0.001
		Treatment	F (1, 258.096) = 874.016; p < 0.001
		Day	F (5, 86.866) = 130.601; p < 0.001
		CIPN x Treatment	F (1, 258.096) = 1010.190; p < 0.001
		CIPN x Day	F (5, 86.866) = 114.922; p < 0.001
		Treatment x Day	F (5, 86.866) = 94.386; p < 0.001
		CIPN x Treatment x Day	F (5, 86.866) = 80.346; p < 0.001

Male vs Female	Statistic		Result
Figure 37 (c) Baseline heat thresholds	Three-way ANOVA	CIPN	F (1, 103) = 0.726; p = 0.396
		Treatment	F (1, 103) = 2.835; p = 0.095
		Sex	F (1, 103) = 5.507; p < 0.05
		CIPN x Treatment	F (1, 103) = 0.243; p = 0.623
		CIPN x Sex	F (1, 103) = 0.016; p = 0.900
		Treatment x Sex	F (1, 103) = 0.763; p = 0.384
		CIPN x Treatment x Sex	F (1, 103) = 0.004; p = 0.951
Figure 37 (c) Heat sensitivity 60 min after EST admin.	Mixed Model	CIPN	F (1, 482.070) = 5782.331; p < 0.001
		Treatment	F (1, 482.070) = 2040.460; p < 0.001
		Day	F (4, 229.341) = 2.161; p = 0.074
		Sex	F (1, 482.070) = 19.476; p < 0.001
		CIPN x Treatment	F (1, 482.070) = 2140.151; p < 0.001
		CIPN x Day	F (4, 229.341) = 1.754; p = 0.139
		CIPN x Sex	F (1, 482.070) = 4.861; p < 0.05
		Treatment x Day	F (4, 229.341) = 77.022; p < 0.001
		Treatment x Sex	F (1, 482.070) = 0.072; p = 0.789
		Day x Sex	F (4, 229.341) = 1.001; p = 0.480
		CIPN x Treatment x Day	F (4, 229.341) = 80.854; p < 0.001
		CIPN x Treatment x Sex	F (1, 482.070) = 0.337; p = 0.562
		CIPN x Day x Sex	F (4, 229.341) = 0.140; p = 0.967
		Treatment x Day x Sex	F (4, 229.341) = 0.853; p = 0.493
		CIPN x Treatment x Day x Sex	F (4, 229.341) = 0.750; p = 0.559

Supporting Table 11. Detailed statistical evaluation for Supplementary Figure 4

Male	Statistic			Result
Figure 37 (a) Analgesia (%) of EST in mechanical sensitivity	Repeated measures ANOVA	PRE	Day	F (4, 56) = 35.268; p < 0.001
		POST	Day	F (4, 56) = 51.058; p < 0.001
		PRE vs POST	Day	F (4, 56) = 60.681; p < 0.001
			PRE vs POST	F (1, 14) = 148.010; p < 0.001
			Day x PRE vs POST	F (4, 56) = 2.087; p = 0.135
Figure 37 (a) Analgesia (%) of EST in heat sensitivity	Repeated measures ANOVA		Day	F (4, 56) = 53.500; p < 0.001

Female	Statistic			Result
Figure 37 (a) Analgesia (%) of EST in mechanical sensitivity	Repeated measures ANOVA	PRE	Day	F (4, 56) = 29.556; p < 0.001
		POST	Day	F (4, 56) = 20.995; p < 0.001
		Day		F (4, 44) = 31,496; p < 0.001
		PRE vs POST		F (1, 11) =12.442; p < 0.01
		Day x PRE vs POST		F (4, 44) = 0.451; p = 0.669
Figure 37 (a) Analgesia (%) of EST in heat sensitivity	Repeated measures ANOVA	Day		F (4, 44) =32.052; p < 0.001

Male vs. Female	Statistic			Result
Figure 37 (a,b) Mechanical sensitivity	Repeated measures ANOVA	PRE values	Day	F (4, 44) = 41.165; p < 0.001
			Sex	F (1, 11) = 4.525; p = 0.057
			Day x Sex	F (4, 44) = 2.062; p = 102
		POST values	Day	F (4, 44) = 56,895; p < 0.001
			Sex	F (1, 11) = 1,265; p = 0.285
			Day x Sex	F (4, 44) = 0.922; p = 0.460
Heat sensitivity	Repeated measures ANOVA		Day	F (4, 44) = 68,701; p < 0.001
			Sex	F (1, 11) = 0,918; p = 0.359
			Day x Sex	F (4, 44) = 0.133; p = 0.894

Study 2

Molecular and functional heterogeneity of regional astrocytes in physiological state

STUDY 2

Molecular and functional heterogeneity of regional astrocytes in physiological state

Astrocytes were traditionally considered a homogeneous population of cells with limited morphology and the only function of providing support to neurons. However, astrocytes are now known to contribute to nearly every aspect of brain physiology and function (review by Khakh and Deneen, 2019), thus challenging this traditional view. Astrocytes serve a multitude of versatile and essential roles in providing metabolic and trophic support, regulating synaptogenesis and synaptic transmission, and maintaining blood-brain barrier integrity, as well as in responding to local neuropathology by mediating innate immune responses (Sofroniew and Vinters, 2010; Khakh and Sofroniew, 2015; Xin and Bonci, 2018). Consistent with this degree of functional diversity, recent evidence in RNA profiling indicates extensive heterogeneity of astrocytes across and within CNS regions, differing in morphology, molecular and functional properties, and response to disease (Cahoy *et al.*, 2008b; Morel *et al.*, 2017; Boisvert *et al.*, 2018; Lozzi *et al.*, 2020).

To increase insight into this field, we further investigated the unique molecular and functional astrocytic signature across three distinct CNS regions with an important role in the processing of the nociceptive information, namely the SS, PAG, and the dorsal horn of SC. To address this, we used RNA-seq analysis of mRNAs obtained from Astrocyte-RiboTag mice used in the Study 1. Particularly, we concentrated on datasets obtained from saline-vehicle control animals of both sexes, sacrificed early on the experimental protocol (day 3) to minimize any bias

introduced by the manipulation and administration of the compounds, and elucidate the astrocyte molecular profile on baseline conditions.

Uncovering astrocyte-specific gene expression signature between CNS regions

In order to assess the regional heterogeneity of astrocyte populations, we probed the transcriptome of the three regions of interest (SS, PAG, and SC) by using several bioinformatic techniques. First, we examined the overall variations of samples by PCA and clustering analysis. This analysis revealed a marked separation between IP and Input mRNAs, representing the primary source of variance (42%; **Figure 40 a**), thus validating the RiboTag approach. PCA also showed clear segregation of astrocyte populations (IP samples) based on their anatomical origin, with PAG and SC datasets closely grouped and SS exhibiting the greatest variation (14%; **Figure 40 a**). This regional clustering was further confirmed when the distribution of IP samples was analyzed separately. This analysis revealed that SS dataset displayed 25% of the overall variation (PC1), while PAG and SC have a 16% variability **(Figure 40 b),** suggesting that SS astrocytes mainly differ from those of the other two regions, which were found more similar. However, males and females cluster together within each CNS region examined, suggesting no relevant differences in astrocyte transcriptomic profiles between sexes **(Figure 40 a,b).** Still, data from both males and females were analyzed separately to investigate interregional differences within each sex, and together to elucidate whether there was any relevant intraregional difference between sexes. Since no significant differences were found between sexes for any analysis, all the results presented here are referred to male animals.

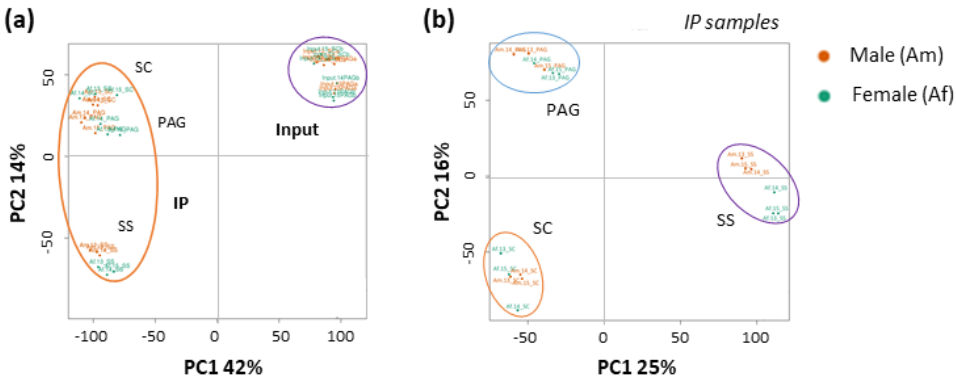

Figure 40. Astrocytes display regionally distinct translatome profiles. Principal component analysis of global gene expression of inputs and ribosome-bound (IP) mRNAs from SS, PAG, and SC of Aldh1l1-RiboTag male and female mice. **(a)** PCA revealed a primary aggregation by mRNA origin (42%; IP vs. Input), and then by anatomic region (14%). **(b)** Within astrocyte-specific mRNAs (IP), gene expression signatures significantly differ between CNS regions. Male and female samples always cluster together and show similar distribution. Each number corresponds to a pool of tissues from 3 mice (n = 3 replicates/ region/ sex). SS, somatosensory cortex; PAG, periaqueductal gray; SC, spinal cord dorsal horn.

To identify the astrocyte-specific gene expression profile in each region examined, we first compared immunoprecipitated samples (IP; ribosome-bound mRNAs) to their corresponding input fraction (containing mRNAs from all cell-types). By applying an adjusted p value (adj.p.val) of < 0.05 and filtering for a fold-change > 1.5, this analysis identified 2952, 2514 and 2778 astrocyte-enriched genes in the SS, PAG and SC, respectively, compared with inputs (**Figure 41 a**). Notably, many genes were similarly expressed across regions (**Figure 41 a**), revealing a conserved expression profile of robust astrocyte-specific genes throughout regions. Some of these genes include classical astrocytic markers *Slc1a2* and *Slc1a3,* encoding for glutamate transporters GLT1 and GLAST, respectively, *Slc6a11,* producing the GABA transporter GAT3, *Kcnj10,* encoding for the potassium channel Kir4.1, *Gja1,* which encodes for connexin 43*, Apoe,*

encoding for apolipoprotein E, and *Aldoc,* the enzyme aldolase C, among others. Moreover, this analysis also identified novel astrocytic markers across regions such as *Cst3,* which encodes for cystatin-C, *Plpp3,* encoding for phospholipid phosphatase 3, or *Ndrg2,* a member of N-myc downregulated gene family.

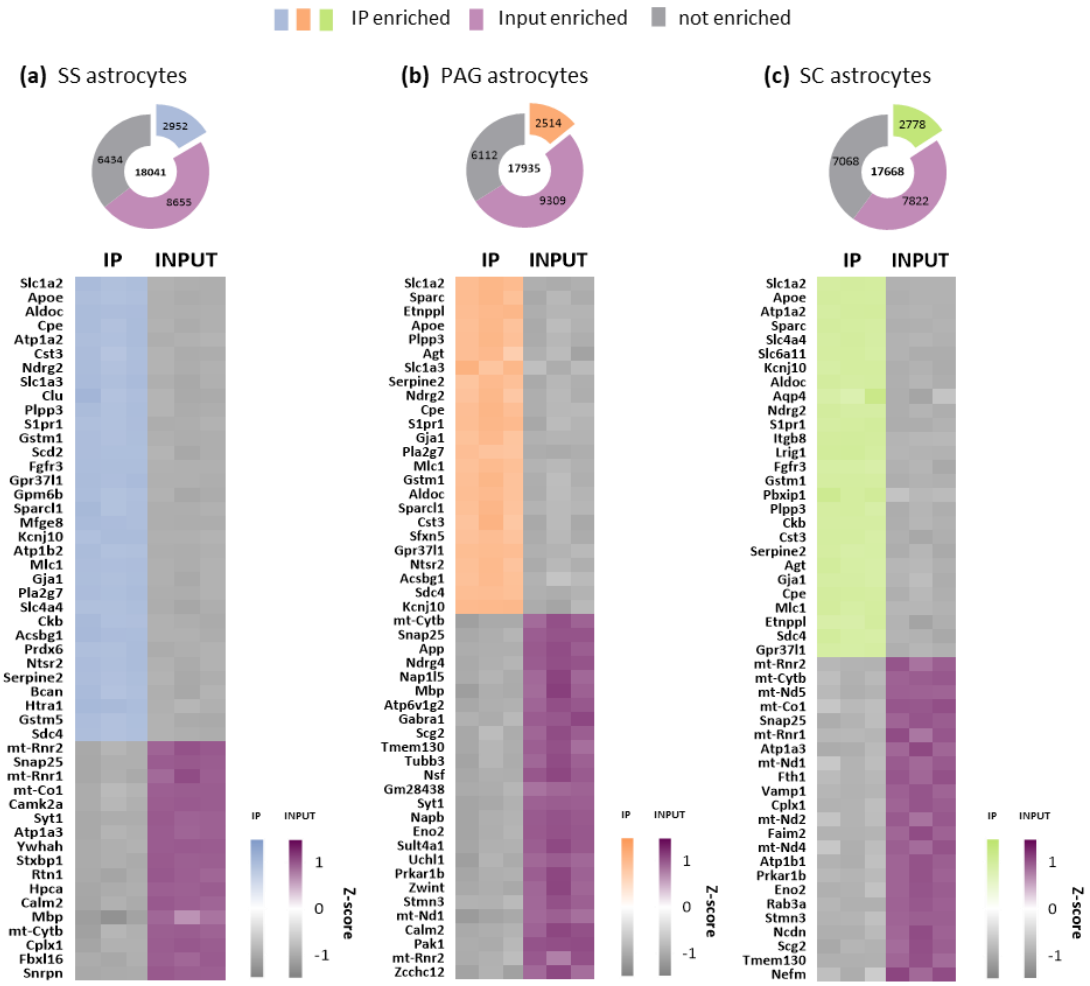

Figure 41. Translatome profile of astrocyte-enriched mRNAs from Astrocyte-RiboTag male mice. Doughnut charts showing the number of astrocyte-enriched genes (IP enriched) either in the **(a)** SS, **(b)** PAG, or the **(c)** SC, comparing IP mRNAs to the input fraction, and corresponding heatmaps of the top 50 genes most significantly enriched. Scaled expression values are color-coded according to the

legend. adj.p.val < 0.05. SS, somatosensory cortex; PAG, periaqueductal gray; SC, spinal cord dorsal horn. adj.p.val, FDR-adjusted p value.

Next, we computed Venn diagrams with all astrocyte-enriched genes to further characterize genes exclusively expressed on each region evaluated **(Figure 42 a).** This analysis supported previous observations from the PCA, showing that SS astrocytes had a greater number of exclusively expressed genes (746 genes) when compared to PAG (213 genes) and SC (464 genes) astrocytes **(Figure 42 a).** The representative top uniquely astrocyte-enriched genes in each region are shown in **Figure 42 b-d** and **Table 11.**

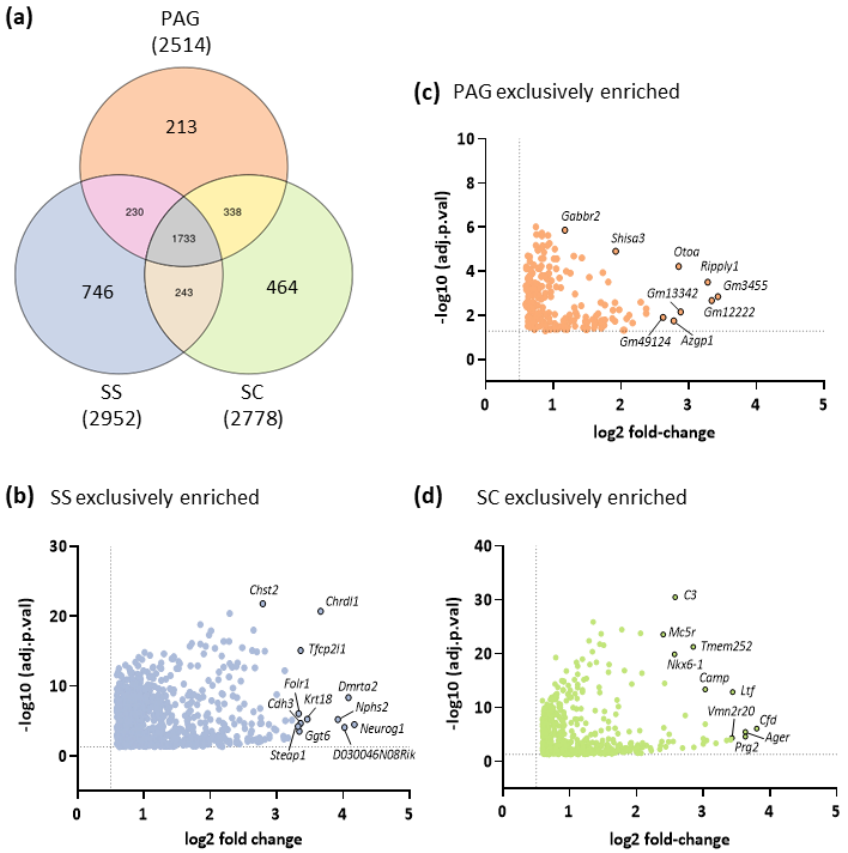

Figure 42. Characterization of the region-specific translatome profile of astrocyte-enriched mRNA. (a) Venn diagram representing overlap and exclusive

number of astrocyte-enriched genes between the three regions. **(b-d)** Volcano plots depicting astrocyte-specific genes (IP vs. Input filtered genes) that are exclusively enriched in SS **(b),** PAG **(c),** and SC **(d).** adj.p.val < 0.05 and FC > 1.5. adj.p.val, FDR-adjusted p value. SS, somatosensory cortex; PAG, periaqueductal gray; SC, spinal cord dorsal horn.

Table 11. Representative top 20 uniquely enriched genes (IP vs. Input) in astrocytes of CNS regions of interest from Astrocyte-RiboTag male mice.

SS			PAG			SC		
Gene	**logFC**	**adj.p.val**	**Gene**	**logFC**	**adj.p.val**	**Gene**	**logFC**	**adj.p.val**
Neurog1	4,17	3,35E-05	*Ripply1*	3,28	3,07E-04	*Cfd*	3,80	7,62E-07
Dmrta2	4,08	4,60E-09	*Otoa*	2,85	6,05E-05	*Ager*	3,63	3,31E-06
Nphs2	3,92	6,38E-06	*Azgp1*	2,78	1,77E-02	*Prg2*	3,63	2,34E-05
Chrdl1	3,66	1,96E-21	*Eya4*	2,29	2,52E-03	*Ltf*	3,44	1,24E-13
Krt18	3,46	5,59E-06	*Tmprss3*	2,08	1,40E-02	*Vmn2r20*	3,43	4,19E-05
Cdh3	3,36	2,21E-05	*Npm3-ps1*	2,05	4,54E-02	*Pkhd1*	3,19	4,05E-04
Tfcp2l1	3,36	7,42E-16	*Shisa3*	1,92	1,24E-05	*Trpm1*	3,05	1,22E-04
Ggt6	3,34	3,11E-04	*Cd70*	1,91	2,64E-03	*Camp*	3,03	3,71E-14
Folr1	3,33	9,13E-07	*Acox2*	1,87	1,40E-02	*Atp6v1e2*	3,00	5,62E-04
Steap1	3,32	5,87E-05	*Col2a1*	1,81	3,01E-04	*Mmp8*	3,00	5,55E-05
Sostdc1	3,23	7,98E-06	*Tectb*	1,76	1,59E-02	*Ctsg*	2,86	2,33E-03
Rnase13	3,17	2,65E-03	*Mybpc1*	1,73	1,14E-04	*Tmem252*	2,85	4,50E-22
Igfbpl1	3,13	9,09E-06	*H3c4*	1,71	1,70E-02	*Fabp4*	2,73	2,73E-09
Thbs4	3,12	5,65E-13	*Ppbp*	1,69	2,36E-02	*Treml1*	2,69	3,06E-03
Ear2	3,11	3,80E-03	*Phex*	1,66	8,41E-03	*C3*	2,58	3,43E-31
Hsd17b2	3,10	1,51E-03	*Uba1y*	1,60	3,68E-02	*Nkx6-1*	2,57	1,16E-20
Kl	3,00	1,71E-09	*Hk2*	1,53	1,86E-04	*Ly6a2*	2,55	1,85E-04
Prlr	2,96	1,31E-04	*Stc2*	1,50	2,03E-02	*Mpo*	2,49	8,61E-06
Slc16a8	2,89	1,08E-03	*Nat8f2*	1,49	4,35E-02	*Cdhr5*	2,48	2,12E-04
Draxin	2,88	3,09E-05	*Tnnt3*	1,48	1,18E-02	*Aqp6*	2,42	3,36E-15

Genes are ranked by logFC. adj.p.val, FDR-adjusted p value; logFC, log2 fold-change; SS, somatosensory cortex; PAG, periaqueductal gray; SC, spinal cord dorsal.

Identification of astrocytes' region-specific molecular and functional signature

We then expanded the analysis without prefiltering the IPs with the inputs, assuming adequate astrocyte-specificity, to identify the region-specific gene signatures. Toward this, we performed differential gene expression analysis by comparing one region to all two others to determine region-specific differentially expressed genes (DEGs). When PAG was analyzed, separate comparisons with either the SS or the SC were performed. The expression of each set of DEGs across regions is visualized in **(Figure 43 a,d,g,j,** to illustrate their specific expression on each region. Interestingly, the PAG showed higher DEGs when compared to SS than to SC, which further confirms that PAG and SC astrocytes are molecularly more related than SS astrocytes, as previously observed in the PCA **(Figure 40).** However, it is worth noting that SC displayed higher DEGs than SS when compared to each other region evaluated, and around 70% of those DEGs in SC were upregulated, which strongly suggests that the profile of astroglial translating mRNAs in SC greatly differ from that of supraspinal astrocytes. Visualized in **Figure 43 b,e,h,k** we show all significantly and differentially expressed genes (adj.p.val < 0.05 and FC > 1.5) in each region and identify some of the most relevant genes presented with logFC > 4. The representative top preferentially expressed genes in astrocytes of each region examined are listed in **Table 12**.

Region-specific astrocyte gene signature

Among the genes preferentially expressed in **SS astrocytes** we detected the transcription factors *Lhx2, Emx2, Foxg1* together with their interaction partners *Emx2os, Nr2e1, Fezf2* and *Dmrta2* **(Figure 43 b, Table 12).** Of note, all these genes play a crucial role in the early patterning and

development of the forebrain. Interestingly, we also found *Thbs4,* encoding thrombospondin 4, *Chrdl1,* producing chordin-like 1, and several potassium channels, such as Kir2.3 (*Kcnj4)* and Kv8.1 (*Kcnv1),* as genes with significantly increased expression in SS astrocytes **(Figure 43 b, Table 12)**. Similarly, in the **PAG** we also found several caudal forebrain and hindbrain specification factors such as *Otx1, Otx2, En1, En2, Irx1, Irx2, Irx3, Irx5, Pax3* and *Pax7,* forming a group of higher expressed genes linked to local control of PAG astrocytes **(Figure 43 e,h, Table 12)**. Of those, *Irx* genes are highly enriched in the PAG when compared with the SS (PAG vs SS), while *Otx* genes appeared as significantly increase in the comparison with the SC (PAG vs SC), indicating that these genes are critically linked to regional control of neural patterning and astrocyte specification in the PAG. Other interesting genes with preferential expression in the PAG include *Agt* and *Dao,* encoding for the enzymes angiotensinogen and D-amino acid oxidase, respectively, *Cd70* and *Gata3,* which are both involved in the immune response, especially T cells mediated immunity, *Gabra6,* a GABA-A receptor, *Cnpy1* and *Shisa3,* involved in the regulation of fibroblast growth factor (FGF) signaling, among other **(Figure 43 e,h, Table 12)**. Finally, in **SC astrocytes** we found a massive expression of *Hox* genes, together with their transcriptional regulator *Nkx6-1* **(Figure 43 k, Table 12),** indicating a clear involvement of these genes in positioning and specification of SC astrocytes. Of interest, we also found other relevant genes, such as *Mpz* and *Prx,* involved in myelination and axon ensheathment, *Cfd* and *C3,* which play an important role in the activation of the complement system, and *Ccl11,* encoding a chemokine critically involved in inflammatory process **(Figure 43 k, Table 12).**

Functional characterization of regional astrocyte heterogeneity

To gain a more comprehensive insight into the biological processes regulated by DEGs, we performed functional enrichment analysis on all DEGs obtained with each comparison **(Figure 43 c,f,l,l).** We found that astrocytes from each region participate in an array of different biological processes. For instance, DEGs in SS astrocytes were mainly associated with "dendrite development "and "synaptic plasticity and transmission" **(Figure 43 c),** whereas in the PAG, DEGs were enriched for "cilium/microtubule organization" and several "metabolic processes" **(Figure 43 f,i)**. On the other hand, two representative groups of processes were observed for SC astrocytes, namely "cellular respiration" and "immune response" **(Figure 43 l).**

Taken together, these results strongly support interregional heterogeneity in the transcriptome of astrocytes, revealing distinct molecular and functional profiles in astrocytes across CNS regions.

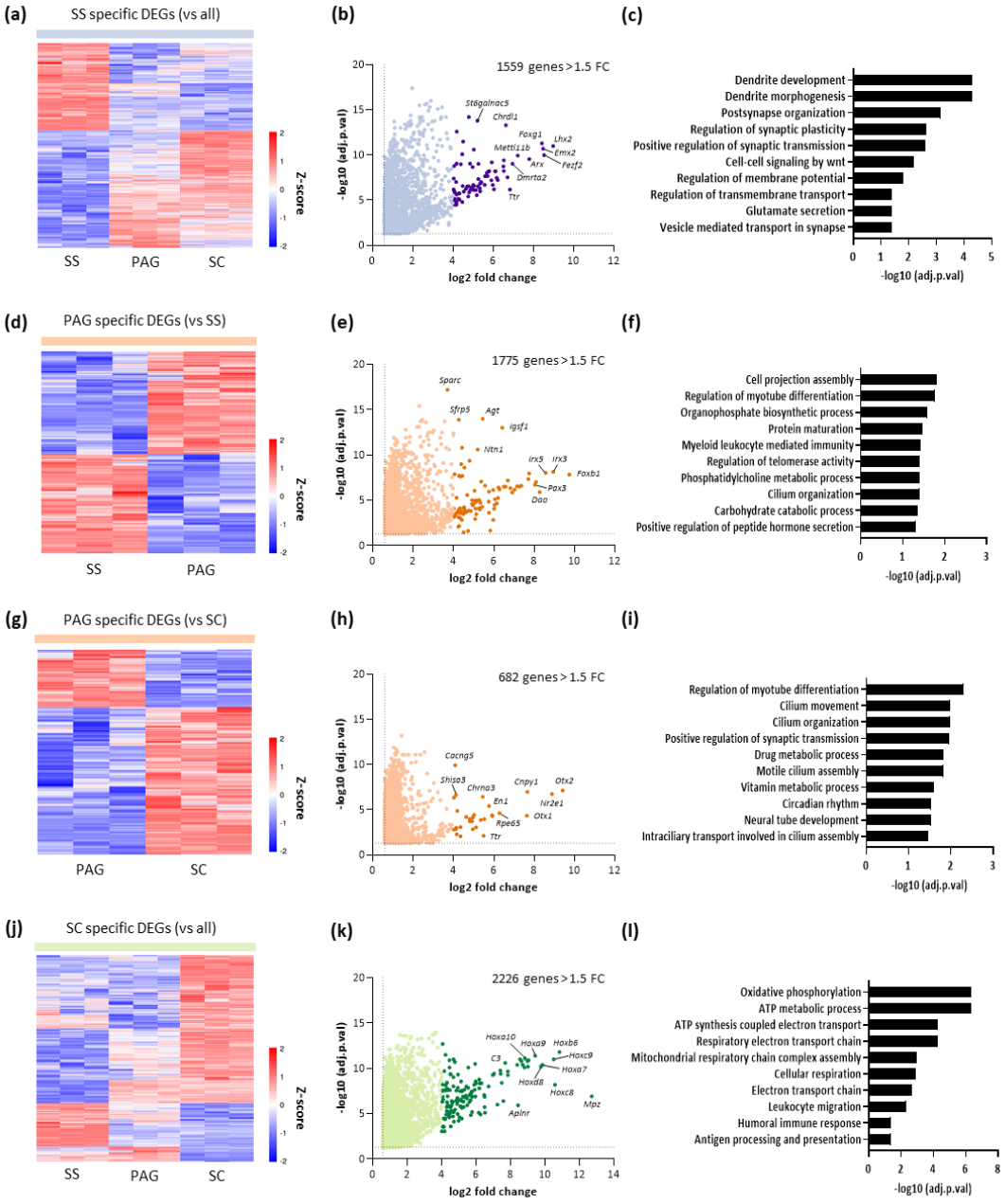

Figure 43. Identification of region-specific molecular and functional signature of astrocytes from male mice. Heatmaps showing unique gene expression signature of **(a)** SS, **(d,g)** PAG, and **(j)** SC. Each corresponding region's IP mRNA dataset was compared with either all two other regions or one another (in the case of the PAG) to obtain the region-specific molecular profile. adj.p.val < 0.05. Volcano plots

depicting specific DEGs in **(b)** SS, **(e,h)** PAG, and **(k)** SC IP samples. DEGs with logFC > 4 are colored darker. adj.p.val < 0.05 and fold-change > 1.5. Functional enrichment analysis of genes enriched in **(c)** SS, **(f,i)** PAG, and **(l)** SC. The top 10 GO terms are represented for each region. adj.p.val, FDR-adjusted p value. SS, somatosensory cortex; PAG, periaqueductal gray; SC, spinal cord dorsal horn.

Table 12. Top 50 preferentially expressed genes in SS, PAG, and SC astrocytes of male mice.

SS vs PAG+SC			PAG vs SS			PAG vs SC			SC vs SS+PAG		
Gene	logFC	adj.p.val	Gene	logFC	adj.p.val	Gene	logFC	adj.p.val	Gene	logFC	adj.p.val
Lhx2	8,98	1,06E-11	*Foxb1*	9,74	1,46E-08	*Otx2*	9,41	7,44E-08	*Mpz*	12,71	1,20E-07
Fezf2	8,53	9,85E-11	*Irx3*	8,94	7,44E-09	*Nr2e1*	8,88	1,83E-07	*Hoxb6*	10,83	1,58E-12
Emx2	8,48	2,17E-11	*Irx5*	8,57	9,52E-09	*Cnpy1*	7,66	1,04E-07	*Hoxc8*	10,57	6,47E-09
Foxg1	8,42	4,96E-12	*Dao*	8,27	1,24E-06	*Otx1*	7,63	4,34E-05	*Hoxc9*	10,50	9,49E-12
Arx	7,79	2,84E-10	*Pax3*	8,03	1,95E-07	*Rpe65*	6,28	2,31E-05	*Hoxa7*	9,84	3,62E-11
Mettl11b	7,22	1,14E-10	*Irx2*	7,75	1,06E-08	*Cd70*	5,93	5,07E-05	*Hoxd8*	9,76	5,69E-11
Dmrta2	6,96	9,21E-10	*Cnpy1*	7,71	4,55E-08	*Pcp2*	5,91	4,04E-05	*Hoxa9*	9,42	4,18E-12
Ttr	6,83	6,84E-07	*Shox2*	7,36	2,48E-07	*En1*	5,76	3,86E-06	*Hoxc10*	9,04	1,22E-11
Igfn1	6,71	2,94E-08	*Crnde*	7,27	3,00E-07	*Gabra6*	5,53	1,06E-04	*Hoxb8*	9,00	6,40E-11
Chrdl1	6,63	5,61E-14	*En1*	7,15	2,88E-07	*Ttr*	5,49	7,37E-03	*Hoxc6*	8,98	1,44E-11
Nr2e1	6,53	3,80E-10	*Irx1*	7,02	6,73E-07	*Chrna3*	5,45	3,51E-07	*Hoxa10*	8,83	8,73E-12
Tfcp2l1	6,51	1,81E-09	*Ebf3*	6,90	1,40E-06	*Fat2*	5,35	1,30E-04	*Hoxa5*	8,80	7,43E-11
Tbr1	6,23	5,83E-08	*Mab21l2*	6,82	4,51E-07	*Tph2*	5,12	8,92E-04	*Hoxb5*	8,70	3,62E-11
Kcnh3	6,11	6,03E-09	*Hotairm1*	6,69	6,44E-08	*Six3*	5,02	3,60E-05	*Hoxd9*	8,62	1,69E-11
Satb2	5,98	2,04E-07	*Nkx6-2*	6,49	3,13E-07	*Lhx9*	4,96	6,99E-05	*Hoxb7*	8,54	1,04E-11
Emx2os	5,93	6,38E-10	*Igsf1*	6,41	9,94E-14	*Cbln3*	4,95	1,44E-03	*Aplnr*	8,43	1,17E-06
Kcnv1	5,91	6,12E-08	*Lhx1os*	6,28	6,33E-07	*Ripply1*	4,92	1,84E-04	*Hoxd3os1*	8,38	3,77E-11
Rtp1	5,80	6,07E-09	*Pax7*	6,23	3,86E-07	*Mybpc1*	4,81	1,84E-04	*Hoxd10*	7,84	5,52E-10
Rpe65	5,77	6,50E-09	*Lhx1*	6,21	5,49E-06	*Chrnb4*	4,80	1,04E-04	*Hoxc5*	7,84	2,14E-10
Dlx1	5,72	2,14E-08	*Dgkk*	6,15	2,15E-05	*Barhl1*	4,63	6,00E-05	*C3*	7,68	2,69E-11
Krt12	5,60	2,24E-08	*Lhx9*	6,06	7,79E-06	*Six3os1*	4,35	8,09E-04	*Klk6*	7,58	3,96E-07
Dlx6os1	5,41	1,08E-07	*Gabra6*	6,04	3,19E-05	*Pcdh20*	4,35	8,46E-03	*Slc6a5*	7,48	3,94E-09
Emx1	5,39	9,68E-08	*Mybpc1*	6,01	8,59E-05	*Pax7*	4,18	1,32E-05	*Hoxb9*	7,42	3,91E-10
Dkkl1	5,35	1,46E-07	*Wif1*	5,97	1,44E-03	*Slc6a4*	4,16	5,26E-03	*Hoxc4*	7,40	1,71E-10
Mei1	5,34	4,81E-07	*Wnt8b*	5,97	7,20E-07	*Npsr1*	4,14	1,00E-03	*Prx*	7,23	9,95E-07
Vip	5,27	9,50E-10	*Aplnr*	5,82	2,20E-02	*Shisa3*	4,12	2,30E-07	*Hoxd4*	7,04	3,83E-10
Thbs4	5,24	2,91E-07	*Stk32a*	5,76	1,07E-06	*Ppp1r17*	4,11	1,44E-03	*Hoxb3os*	6,96	5,53E-10
St6galnac5	5,22	1,53E-14	*Ppp1r17*	5,76	2,34E-04	*Cacng5*	4,08	1,18E-10	*Dhh*	6,72	9,75E-09
Dlx2	5,19	2,76E-06	*Cbln1*	5,74	1,37E-05	*Cyp26b1*	4,02	4,54E-07	*Gm32122*	6,51	7,74E-06
Otx1	5,15	7,60E-07	*Chrna3*	5,56	2,45E-07	*Lhx2*	4,01	1,50E-03	*Gm53*	6,49	1,38E-07
Lypd6	5,04	2,74E-11	*Agt*	5,45	1,02E-14	*Emx2os*	3,90	4,82E-04	*Hoxc11*	6,49	1,84E-06
Kcnj4	5,04	7,55E-07	*Ripply1*	5,42	5,21E-05	*Tfap2d*	3,86	1,23E-03	*Nkx6-1*	6,47	8,67E-08
Egr3	4,98	2,10E-09	*Shisa3*	5,37	8,79E-08	*Otoa*	3,81	4,16E-04	*Hoxa3*	6,30	4,34E-09
Krt20	4,94	3,77E-07	*Lhx5*	5,33	1,84E-05	*Rhcg*	3,76	1,49E-03	*Cfd*	6,25	1,21E-05
Nphs1os	4,86	7,62E-07	*Ndst4*	5,31	1,02E-04	*Phex*	3,74	1,72E-03	*Hoxa2*	6,20	4,34E-09
Ddn	4,85	8,97E-10	*Otoa*	5,28	7,21E-05	*Emx2*	3,71	2,51E-03	*Gm11536*	6,18	1,63E-09
Nxf7	4,81	1,32E-06	*Irx3os*	5,27	9,30E-06	*Shox2*	3,65	7,78E-06	*Camp*	6,18	1,56E-08
Hapln1	4,79	5,66E-15	*Ntn1*	5,20	2,48E-11	*Gata3*	3,59	6,76E-04	*Fads2b*	6,15	7,67E-06
Robo3	4,78	2,90E-07	*Pax5*	5,19	1,03E-05	*Tal1*	3,52	8,45E-03	*Hoxb3*	5,98	4,64E-09
Stra6	4,76	3,90E-06	*Sspo*	5,13	3,50E-04	*Gm10421*	3,46	4,05E-03	*Ngp*	5,97	2,62E-09
Slc17a7	4,71	2,92E-07	*Tlr2*	5,08	1,72E-05	*Car8*	3,46	1,25E-03	*Hoxc13*	5,95	1,22E-07
Neurl1b	4,64	5,77E-07	*Pcp2*	5,08	1,09E-05	*Nup62cl*	3,45	1,73E-03	*Mc5r*	5,94	3,09E-11
Gm10115	4,54	1,12E-06	*Slc6a5*	5,07	1,14E-03	*Pax5*	3,44	3,19E-04	*Capn13*	5,91	2,30E-08
Nrgn	4,51	3,07E-12	*Wnt3*	5,04	8,65E-07	*Krt18*	3,43	3,54E-03	*Pmp2*	5,88	6,49E-09
Rin1	4,48	2,68E-07	*Pax8*	4,97	3,49E-05	*Gm3455*	3,38	2,01E-03	*Hoxaas2*	5,76	1,31E-07
Chp2	4,47	1,61E-05	*En2*	4,92	2,49E-05	*Tmprss3*	3,38	6,64E-03	*Calca*	5,76	6,35E-06
Hgf	4,46	8,32E-11	*Pdlim3*	4,85	1,52E-04	*Neurod1*	3,36	5,51E-04	*Haglr*	5,74	3,47E-08
Ptk2b	4,39	1,03E-09	*Galnt10*	4,79	4,29E-10	*En2*	3,35	5,04E-04	*Hoxa11*	5,71	5,14E-08
Ighg2c	4,33	8,65E-06	*Pou4f1*	4,76	1,32E-04	*Ocln*	3,35	8,59E-07	*Fabp4*	5,69	1,42E-05
Sp5	4,32	1,79E-06	*Klk6*	4,72	2,36E-02	*Barhl2*	3,29	1,83E-03	*Ccl11*	5,68	5,88E-08

Genes are ranked by logFC. adj.p.val, FDR-adjusted p value; logFC, log2 fold-change; SS, somatosensory cortex; PAG, periaqueductal gray; SC, spinal cord dorsal.

Regional diversity of classical astrocyte homeostatic functions

Next, we investigated whether astrocytes from distinct CNS regions have differential expression of genes involved in major astrocyte functions, such as synaptic transmission and neural homeostasis, synapse modification, immune process, and cholesterol metabolism **(Figure 5).**

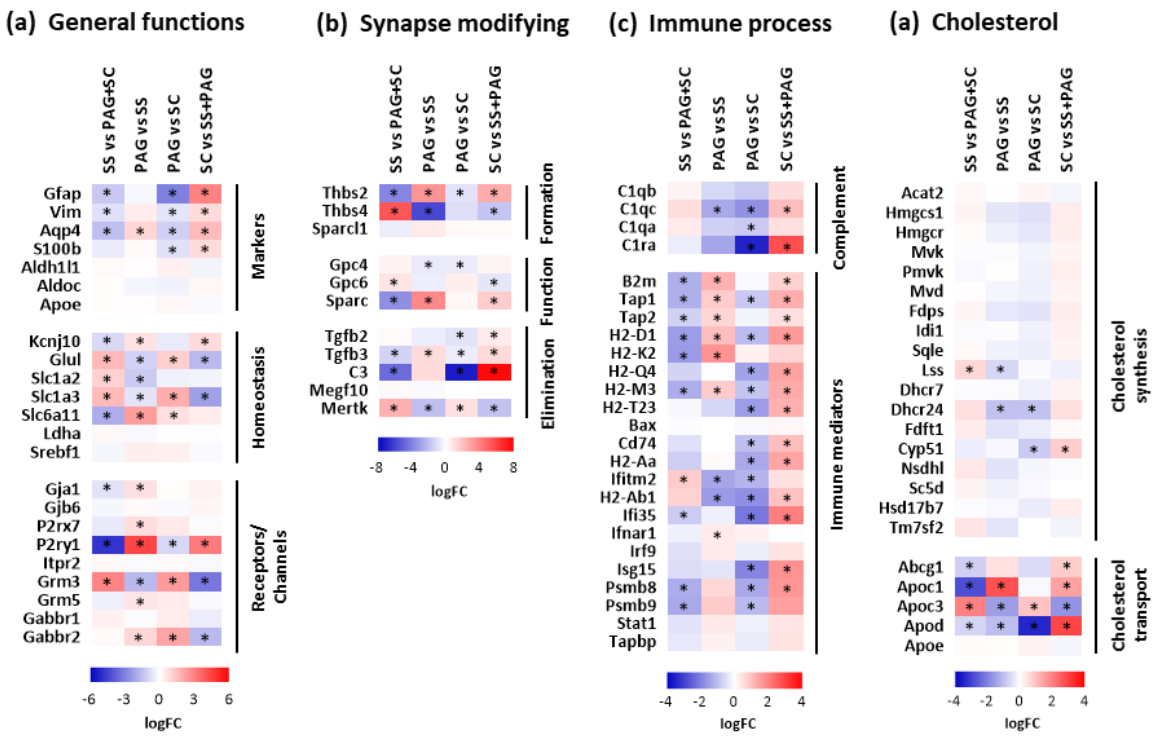

Figure 44. Regional differences between astrocytes in physiological conditions. Comparison of expression of genes that are important for astrocyte identity and function: (a) astrocyte markers, h some genes of the complement system and immune mediators, homeostasis and neurotransmitter receptors, (b) synapse formation, function and elimination, (c) immune system, and (d) enzymes for cholesterol synthesis and cholesterol transport proteins. * significantly different expression with adj.p.val < 0.05 and FC > 1.5. SS, somatosensory cortex; PAG, periaqueductal gray; SC, spinal cord dorsal; logFC, log2 fold-change. adj.p.val, FDR-adjusted p value.

First, we examined the expression of genes considered conventional **astrocytic markers**, including cytoskeletal proteins GFAP (*Gfap)* and vimentin (*Vim),* the water channel *Aqp4,* the cytosolic markers *S100b, Aldh1l1,* and *Aldoc,* and the lipoprotein *Apoe.* Of these, *Gfap*, *Vim,* and *S100b* were significantly increased in SC astrocytes, particularly *Gfap* (8-fold) **(Figure 44 a).** In addition, *Aqp4* was also expressed with significantly higher levels (3-fold) in the SC, following an anterior to posterior increasing expression gradient **(Figure 44 a).**

Astrocytes also express numerous **channels and neurotransmitter receptors**, regulating synaptic transmission and homeostasis (Khakh and Sofroniew, 2015). Examination of genes related to these functions revealed a significantly higher expression of glutamate synaptic transmission genes in SS astrocytes, following an anteroposterior expression gradient **(Figure 44 a).** These genes include the glutamate transporters *Slc1a2* (GLT) and *Slc1a3* (GLAST), the enzyme glutamine synthase *Glul,* and the metabotropic glutamate receptor *Grm3.* Conversely, metabotropic glutamate receptor *Grm5* expression was higher in the PAG, where we also found significantly increased expression of GABA transporter *Slc6a11* (GAT3), GABA-B receptor *Gabbr2,* and purinergic receptor *P2rx7* **(Figure 44 a).** Finally, SC astrocytes showed a significantly increased expression of potassium channel *Kcnj10* (Kir4.1) and purinergic receptor *P2ry1* **(Figure 44 a).** Hence, this analysis showed that the genes related to astrocytes' general functions are differentially expressed across CNS regions, which demonstrate their high pleiotropism in response and functional diversity.

Then, we asked whether genes expressed by astrocytes that regulate synapses during development were differentially expressed in these

regions. We examined the expression levels of genes with a well-known role in **synaptogenesis**, like thrombospondins (*Thbs*) and Hevin (*Sparcl1)* **(Figure 44 b)**. Interestingly, thrombospondins showed opposite expression between cortical regions, with a 10-fold increase of *Thbs2* in the PAG and a 54-fold higher expression of *Thbs4* in the SS (PAG vs SS). Notably, *Thbs4* expression was higher in SS astrocytes (38-fold) than in the other regions examined, while *Thbs2* was significantly increased in SC astrocytes compared to cortical regions. Examination of astrocytic regulators of **synaptic function** revealed a significant 13-fold increase of synaptic inhibitor *Sparc* in the PAG compared to the SS, with a higher expression in SC astrocytes than in supraspinal regions. In contrast, Glypicans 4 and 6 *(Gpc)* levels were significantly higher in SS astrocytes **(Figure 44 b).** Finally, analyzing **synapse elimination inducers**, we found a significantly 200-fold increase of complement factor *C3* in SC astrocytes, which also expressed significantly increased levels of transforming growth factor beta (TGF-β) genes *Tgfb2* and *6.* Of note, TGF-β release by astrocytes is known to induce complement factor C1q expression, along with C3, in unwanted synapses, tagging them for phagocytosis by microglia. Astrocyte-mediated synapse elimination is dependent on phagocytic receptors MEGF10 and MERTK. Critically, *Mertk* expression was significantly higher in SS astrocytes, while *Megf10* was similarly expressed across regions **(Figure 44 b).**

Regarding the critical role of astrocytes in **immune defense**, we also investigated the expression of some genes of the complement system and main regulators of innate immune response **(Figure 44 c)**. Notably, most genes examined were significantly higher in SC astrocytes with a 2-7-fold increase, especially C1ra (7-fold). Additionally, most genes of the major histocompatibility complex (MHC) class I showed significantly higher expression in PAG than SS, thus indicating an anteroposterior increasing

expression gradient from the SS to the SC. Hence, these findings show that astrocytes from the SC are highly specialized in general immune defense processes, followed by PAG astrocytes, which also showed minor contribution.

Astrocytes are a major source of lipid synthesis in the brain and provide neurons with cholesterol, essential for presynaptic vesicle formation. Analysis of genes involved in cholesterol synthesis revealed similar expression across CNS regions, whereas cholesterol transport genes were differentially expressed between regions **(Figure 44 d).** Critically, lipoproteins *Apoc 1* and *3* showed opposite anteroposterior expression, with *Apoc1* being significantly higher in the SC (3-fold) and *Apoc3* in the SS (4-fold). In addition, SC astrocytes also have increased mRNAs for *Abcg1* and *Apod.* These results suggest that astrocytes from distinct regions differ in their capacity for cholesterol transport but not for synthesis.

Overall, these results further demonstrate astrocyte diversity across CNS even regarding classical homeostatic functions, which may be relevant to consider during pathologic conditions producing dysfunction in these regions, such as in neuropathic pain.

DISCUSSION

The overall purpose of this Doctoral Thesis was to identify novel therapeutic targets for the treatment of CIPN by exploring the specific contribution of glial cells on this pathology and in the analgesic effects of a new σ1R antagonist. Using a mouse model of neuropathic pain induced by vincristine chemotherapy combined with a cell-specific transcriptomic approach, we determined gene expression changes occurring exclusively in glial cells (astrocytes, by now) during this pathology, and investigated the molecular and functional heterogeneity of this cellular population across relevant pain-related areas of the CNS.

Effect of σ1R blockade on the nociceptive manifestations of vincristine-induced neuropathic pain

Although CIPN is one of the major causes of treatment cessation in patients receiving vincristine, there are no effective treatments to control or prevent the development of this neuropathy (Starobova and Vetter, 2017; Cavaletti *et al.*, 2019). Considering that the blockade of σ1R has shown promising results in alleviating chemotherapy-induced neuropathic pain with different antineoplastic agents and species (Nieto *et al.*, 2012, 2014; Gris *et al.*, 2016a; Bruna *et al.*, 2018; Paniagua *et al.*, 2019), here we aimed to test the efficacy of a new selective σ1R antagonist on reducing the symptoms of this neuropathy.

Patients undergoing chemotherapy treatment with vincristine experience severe sensory disturbances, such as altered responses to light touch or pinprick and increased sensitivity to temperature. These symptoms were well replicated in our murine model of CIPN, with vincristine producing rapid and maintained mechanical allodynia and thermal hyperalgesia. Notably, mechanical allodynia was previously described in several studies using a similar dose and schedule (Old *et al.*, 2014; Starobova *et al.*, 2019),

whereas the cause of thermal hyperalgesia was not ascertained or reported as with no changes in the majority of studies. Nonehteless, the presence of both sensory alterations further validates the model and suggests that peripheral neural damage induced by VCR in our conditions was severe.

Unlike in other neuropathies, the onset of neuropathic pain in cancer patients receiving chemotherapy is readily identifiable and preventive treatment can be given. Under this premise, the efficacy of σ1R antagonist EST was tested on this model using a preventive protocol of administration. Importantly, EST did not modify the mechanical or heat sensitivity of saline-treated (control) animals. This suggests that the blockade of σ1Rs is not affecting sensory transmission and perception during physiological conditions. In agreement, responses of σ1R KO mice to mechanical and thermal stimuli were shown to be indistinguishable from those of WT mice in absence of sensitization (de la Puente *et al.*, 2009; Entrena *et al.*, 2009; Nieto *et al.*, 2012, 2014). This is consistent with the σ1Rs' chaperone activity, which increases affinity for their targets only under pathological circumstances when they are conformationally unstable requiring σ1R chaperone support (Hayashi and Su, 2007; Su *et al.*, 2010). Therefore, since σ1Rs have a natural chaperone's modulatory role, the implications of their stimulation may only be manifested when another biological system is first triggered.

Under **vincristine-induced sensitization**, in our experimental conditions, results demonstrated that the repeated treatment with EST promoted a gradual recovery of mechanical and thermal sensitivity without inducing the development of analgesic tolerance. As noted, the improvement in these sensory alterations was gradual, meaning that EST was not able to

prevent the development of the neuropathy from the beginning of the induction. These findings are consistent with those observed in a previous study performed using a similar experimental design to ours with co-administration of oxaliplatin and σ1R antagonist S1RA (Gris *et al.*, 2016a), in which S1RA progressively reduced cold allodynia. On the contrary, other studies demonstrated a preventive effect of S1RA on the development of painful neuropathy in different models of CIPN. Particularly relevant is the case of the co-administration of paclitaxel and S1RA, which prevented the development of paclitaxel-induced cold and mechanical allodynia at least until 3 weeks after first paclitaxel administration (Nieto *et al.*, 2012). Similarly, rats given cisplatin or vincristine concomitantly with S1RA not only did not develop sensorial neuropathic symptoms but even increased the threshold above control values (Paniagua *et al.*, 2019), suggesting that S1RA behaves as an analgesic drug. Interestingly though, our studies show that EST produced greater efficacy in alleviating thermal hyperalgesia than mechanical allodynia, for which it is probably necessary a longer treatment to completely recover baseline levels.

On the other hand, the acute effect of EST was also investigated. In our conditions, EST did not show acute antiallodynic effects on any testing day. It is important to note that only one dose and time-point was tested. Indeed, EST showed greater efficacy relieving thermal hyperalgesia than mechanical allodynia, which may be probably due to this difference in the time-point of testing in each modality of pain (30 min post-administration for mechanical allodynia vs around 60 min after EST administration for thermal hyperalgesia). Testing the compound at higher doses may reveal relevant acute analgesic effects and for longer periods of time. In support of this suggestion, previous studies with the σ1R antagonist S1RA in CIPN models showed important acute analgesic effects in a dose-dependent

manner (Nieto *et al.*, 2012; Gris *et al.*, 2016a), reaching the maximum of inhibition at 90 min after the administration of the compound (Nieto *et al.*, 2012). Hence, future studies may be directed to address these issues.

Overall, our results suggest that repeated treatment with EST may result in neurophysiological modifications in different areas of the CNS involved in the processing of the nociceptive signalling, resulting in the alleviation of vincristine-induced neuropathy symptoms . However, our data indicate a reduced efficiency of EST compared with other σ1R antagonists with similar properties, such as S1RA (Nieto *et al.*, 2012, 2014; Gris *et al.*, 2016a; Bruna *et al.*, 2018; Paniagua *et al.*, 2019). It is worth mentioning that new administration protocols may be studied with this new σ1R antagonist. For instance, a future approach would be to assess the effects of prolonged treatment with EST, but also to evaluate its long-lasting effects once administration schedules are completed.

On the other hand, it is important to notice that CIPN has been mainly studied in male rodents or mixed-sex groups (Gadgil *et al.*, 2019), despite the fact of existing huge evidence highlighting a higher prevalence of chronic pain disorders in females (Mogil, 2012), including CIPN (Diouf *et al.*, 2015). Considering this, the present work included both sexes to evaluate not only a new therapeutic compound to attenuate chemotherapy-induced neuropathic symptoms but also to evaluate possible gender-related differences. In our conditions, we did not observe major sex-specific variations neither on vincristine-induced sensory alterations nor on the effects of EST treatment on these disturbances but for a mild analgesic effect in females. Some previous studies also evaluated the effect of σ1R inhibition on pain modulation in animals of both sexes, obtaining similar results to ours (Entrena *et al.*, 2009; Bravo-

Caparrós *et al.*, 2019). It should be noted that although sexual dimorphism can be manifested as a difference in pain sensitivity, this is not always the case, since molecular differences between sexes have been detected despite male and female sensitivity to the painful stimulus being similar (González-Cano *et al.*, 2020).

Astrocyte-specific transcriptomic alterations contributing to vincristine-induced neuropathy

In recent years, it has become increasingly clear that vincristine-induced neuropathy is not simply a consequence of the known pharmacological action of this compound but a complex symptomatology involving significant neuro-glial interactions. Accordingly, vincristine was shown to induce infiltration of circulating monocytes and activation of macrophages into peripheral nerves and DRGs (Kiguchi *et al.*, 2008a; Old *et al.*, 2014), contributing to the triggering and maintenance of the neuropathy. Supporting these findings, vincristine treatment induced a striking upregulation of genes related to immune cell recruitment and inflammatory process in DRGs (Starobova *et al.*, 2020). However, relatively little is known about the contribution of glial cells in the CNS in response to vincristine-induced neuropathy. Hence, we carried out cell-type specific transcriptomic analysis of relevant areas of the CNS for pain transmission and processing axis with the objective to address this issue. It should be noted that only astrocyte transcriptome was finally analyzed due to technical and temporary restrictions, with the perspective to document microglial alterations to obtain more solid conclusions.

Here, we provide a detailed transcriptional characterization of astrocytes during CIPN progression. Our astrocyte gene expression datasets showed clear regional heterogeneity of astrocytes, in agreement with previous

studies (Chai *et al.*, 2017; Itoh *et al.*, 2017; John Lin *et al.*, 2017; Boisvert *et al.*, 2018; Borggrewe *et al.*, 2021), and robust cell-type specificity supported by other microarray and RNA-seq profiles of astrocytes from the adult brain (Cahoy *et al.*, 2008a; Doyle *et al.*, 2008; Zhang *et al.*, 2014). However, since we did not restrict our differential expression analysis to genes exclusively enriched in astrocytes compared with the whole-tissue input, small contamination from other cell types cannot be excluded. Moreover, the RiboTag approach limits the analysis to ribosome-associated mRNAs, thus being more likely to be actively translated into proteins, providing an image of the translational status of the cells (Sanz *et al.*, 2009), which is particularly important during pathological conditions. Finally, as with all large datasets, these results should be interpreted with caution until further experimental validations of genes and processes described in this study are done. Interestingly, our findings indicate that vincristine is primarily affecting to four main biological systems in astrocytes, with little variation between the regions examined or sexes, suggesting that vincristine is inducing a widespread alteration of astrocyte functions along the CNS pain-related axis that may contribute on the whole to the development and maintenance of the neuropathy.

One major and unexpected finding of our analysis was that vincristine caused predominantly a downregulation of genes with a known role in **heme biosynthesis and function** early during treatment. Some of these genes included *Hba-a1/a2* and *Hbb-bt/bs,* which encode the adult alfa and beta chain of hemoglobin (Hb), respectively, *Alas2,* encoding an erythroid enzyme that catalyzes the first step of heme biosynthesis, Slc4a1(AE1), which encodes band 3, an erythrocyte membrane protein, and Gypa, which encodes Glycophorin A, an erythroid protein that interacts with AE1, among other genes. While the known functions of these genes are

primarily erythrocyte-specific, pleiotropic functions yet to be discovered for these genes could be important in other cells. For instance, Hb chains have been detected in a wide variety of nonerythroid cells such as epithelial cells of different origins (Saha *et al.*, 2014), endometrial cells, neurons (Schelshorn *et al.*, 2008; Biagioli *et al.*, 2009; Jellen *et al.*, 2013; Russo *et al.*, 2013) and glial cells, including astrocytes and oligodendrocytes (Biagioli *et al.*, 2009), in agreement with our results.

Interestingly, Biagioli *et al.*, 2009 revealed that Hb expression occurs in dopaminergic neurons of the *substantia nigra* where it plays an important functional role there. Specifically, they found that Hb regulates genes involved in oxygen homeostasis and iron metabolism, and suggested that Hb may act as an oxygen reservoir and transport molecule to provide a homeostatic mechanism in anoxic and hypoxic conditions, which is particularly important for neurons since they have an obligate demand to sustained energy (Biagioli *et al.*, 2009). In line with these findings, altered Hb levels have been observed in neurodegenerative diseases post-mortem brains, with decreased expression levels in neurons of Alzheimer's and Parkinson's disease brains (Biagioli *et al.*, 2009; Ferrer *et al.*, 2011). Extending this model to other Hb-expressing cells such as astrocytes, its widespread distribution, and proximity to neurons may constitute a network of oxygen-storage cells, providing much-needed relief to nearby neurons during hypoxic conditions (Biagioli *et al.*, 2009). In this regard, Hb levels have been reported to be decreased in aged astrocytes, indicating that this oxygen-supply capacity of astrocytes may decrease with age (Orre *et al.*, 2014). Taken together, these results suggest that Hb may play a role in the normal physiology of the brain and neurodegenerative diseases.

Extrapolating this rationale to our model, here we showed that vincristine is inducing a decrease or loss of this capacity in astrocytes and, presumably, a strong hypoxic situation, together contributing to neuron damage. It is postulated that hypoxia may in turn stimulate Hb expression through the production of erythropoietin (EPO), thus improving the oxygenation (Schelshorn *et al.*, 2008). This could explain the increase of Hb levels during chronic exposure to vincristine compared to saline, as evidenced in the qRT-PCR validation of RNAseq results. However, while appropriate levels of Hb may be neuroprotective, supraphysiological levels of Hb may be harmful (Chang *et al.*, 2017; Ma *et al.*, 2019), although this remains to be explained.

Additionally, vincristine may also be producing a huge heme deficiency, which is indirectly inferred by a significant decrease in the expression of *Alas2* early during chemotherapy. In fact, the reduction of free heme may also be the reason for the decrease of Hb since heme is known to be a strong activator of globin-chain transcription (Richter *et al.*, 2009). Similarly to Hb, the expression levels of this enzyme (and consequently, heme) increased with longer exposure to vincristine. Considering that EPO stimulates heme synthesis (Noguchi *et al.*, 2007), and hypoxia induces the production of EPO, as previously mentioned (Schelshorn *et al.*, 2008), our results suggest that vincristine is inducing strong hypoxia and anemia in a positive feedback loop, causing astrocytic dysfunction and contributing to the initiation of the neuropathology. Nonetheless, more research is needed to shed light on these issues, opening an area of research that calls for further attention. Altogether, the present study not only confirmed the expression of Hb in astrocytes, clearing some discrepancies in this matter (Schelshorn *et al.*, 2008; Biagioli *et al.*, 2009) but, to the best of our

knowledge, this is the first study to describe alterations in heme functionality associated with the development of neuropathic pain.

Alternatively, vincristine treatment also caused significant **mitochondrial dysfunction**, as revealed in the GSEA analysis, in line with accumulating evidence reporting that this alteration is both caused and contributor to CIPN (Canta *et al.*, 2015), although it has not been reported before to occur in astrocytes. Specifically, it is recognized that vincristine alters mitochondrial Ca^{2+} homeostasis, which consequently increases exocytosis of neurotransmitters and production of ROS (Canta *et al.*, 2015; Starobova and Vetter, 2017; Triarico *et al.*, 2021), leading to impaired neuronal excitability and glial function. In this regard, a large number of studies proved that oxidative stress is involved in the pathophysiology of CIPN. Indeed, a recent study showed that vincristine treatment led to a significant increase in ROS production, H_2O_2 levels, and NADPH oxidase activity in spinal cord samples of mice, with subsequent activation of glial cells and increased inflammatory cytokine levels (Chen *et al.*, 2020). Contrary to this study, although we did observe altered mitochondrial function, and presumably ROS accumulation and oxidative stress due to decreased antioxidant systems such as GPx, this alteration did not induce astrocyte reactivity, as described above, but dysfunction.

Connected to the mitochondrial altered functionality may be the decreased Hb levels discussed before. Hb chains are predominantly located in the inner mitochondrial membrane of neurons (Shephard *et al.*, 2014), and have been involved in the control of mitochondrial function in normal and pathological conditions, especially by regulating cellular respiration and redox system (Biagioli *et al.*, 2009; Richter *et al.*, 2009; Brown *et al.*, 2016). Interestingly, a decline of mitochondrial Hb levels was

reported in aged mouse and human brains (Shephard *et al.*, 2014), indicating that Hb plays a protective role against oxidative stress, a feature associated with aging (Beckman and Ames, 1998). Therefore, apart from the direct action that vincristine may be exerting to mitochondrial homeostasis, the loss of the antioxidant protection of Hb may be another mechanism contributing to the mitochondrial dysfunction observed in our model. In that case, this alteration would be expected to occur in parallel to the Hb deficiency, which is especially relevant during the induction of CIPN; however, it is predominantly observed with long-term exposure to vincristine, where Hb levels were recovered. Hence, we speculate that the rapid decrease of Hb from the very beginning of chemotherapy led to a progressive increase of the oxidative conditions, accumulation of respiratory chain alterations, and finally to mitochondrial failure. Nevertheless, further research is required to validate this hypothesis and reveal the extent of mitochondrial damage and its implication for astrocytic function.

Our study of the astrocyte transcriptome during CIPN surprisingly also pointed to changes in **cholesterol homeostasis** associated with the development of the neuropathology Specifically, the GSEA analysis revealed an enrichment of cholesterol synthesis-related pathways in astrocytes during the early exposure to vincristine, and a switch to downregulation of these processes in the chronic stage of the neuropathy. The brain is one of the organs with higher cholesterol content in the body, with cholesterol playing an important role in membrane fluidity, vesicle formation, and therefore, in synaptic transmission. Because peripheral cholesterol does not cross the blood-brain barrier, cholesterol in the brain must be synthesized *de novo* (Pfrieger and Ungerer, 2011). In the adult brain, astrocytes are a major source of cholesterol synthesis, which is

delivered to neurons and oligodendrocytes, where it is required for neurotransmission, synaptogenesis, and myelination (Mauch *et al.*, 2001; Saher and Stumpf, 2015). Interestingly, reduced cholesterol synthesis in astrocytes has been reported in several studies using animal models of multiple sclerosis (Itoh *et al.*, 2017; Borggrewe *et al.*, 2021) and aging (Boisvert *et al.*, 2018). These data suggest that decreased cholesterol levels in astrocytes may lead to reduced cholesterol transport to neurons and oligodendrocytes, thereby limiting dendritic elaboration, presynaptic function, and myelin formation, and finally producing a disruptive neuronal transmission. Accordingly, our results indicate that vincristine is altering cholesterol production in astrocytes, thus compromising both astrocyte function and correct neuronal transmission. As mentioned, this alteration was more pronounced during late chemotherapy while, in contrast, an increased cholesterol production was observed during CIPN induction. One possible explanation could be that astrocytes rapidly respond to the strong neurotoxicity caused by vincristine by supplying neurons and oligodendrocytes of cholesterol to prevent further damage. Supporting this idea there is the enrichment of steroid (neurosteroid) synthesis processes, in parallel to cholesterol, at this initial time-point. Another purpose of *de novo* synthesis of cholesterol in astrocytes is neurosteroid production, which is known to be a neuroprotective response to neural injury (Melcangi *et al.*, 2007; Luchetti *et al.*, 2011). However, with longer exposure to vincristine, astrocytes became dysfunctional and loss this supportive capacity. Further validation of this hypothesis is now warranted since it may involve a new therapeutic target to prevent or palliate CIPN.

Finally, DE analysis but mainly GSEA also identified a mild implication of **immune responses** among the mechanisms induced by the chemotherapy

treatment. We observed an early downregulation of immune-related genes, including interferon-inducible genes *Rsad2, Isg20,* or *Isg15,* and many GO biological processes involved in the regulation of the innate immune response. Critically, females but not males showed a mild enrichment of these processes mainly in the SC with prolonged chemotherapy. However, no common markers of astrocyte reactivity were detected in any stage nor sex examined, indicating no astrocyte activation. These results were somehow surprising since growing studies confirmed that vincristine induces the activation of both astrocytes and microglia in the spinal cord (Kiguchi *et al.*, 2008b; Shen *et al.*, 2015; Zhou *et al.*, 2018; Chen *et al.*, 2020), thereby producing a neuroinflammatory response that contributes to the sensitization process that leads to neuropathic pain. Indeed, astrocytes are suggested to have a major involvement in CIPN compared to microglia (Zhang *et al.*, 2012; Robinson *et al.*, 2014). However, there are also other studies reporting no changes in astrocyte number and activation following chemotherapy (Kim *et al.*, 2015; Makker *et al.*, 2017). Considering the many discrepancies, further studies may be needed to shed light on this issue; however, it should be considered that astrocytes activation may be a contributing factor but not a critical mechanism for the development of CIPN.

Taken together, vincristine seems to be directly or indirectly affecting astrocyte homeostatic functions especially involved in oxygen and cholesterol supply to neurons, antioxidant protection, and general mitochondrial function. Thus, we propose that astrocyte dysfunction rather than the classical activated state contribute to the initiation and progression of CIPN, although these are not mutually exclusive events. Indeed, a loss of homeostatic signature genes may be also a hallmark of

reactive astrocytes and should be considered when studying this population in a given disease.

Effects of σ1R blockade on the astrocyte transcriptomic profile during vincristine-induced neuropathy

σ1R are considered to play a key role in neuroglial communication during chronic pain by modulating the activity of microglia and astrocyte, as revealed in several studies using a variety of pain models (Ruiz-Cantero *et al.*, 2021). However, the modulation of glial cells actions by σ1R in neuropathic pain induced by antineoplastics has not been studied to date. We investigated whether the blockade of σ1R by EST had direct or indirect modulatory effects in the astrocyte transcriptomic profile in our CIPN model.

The transcriptional analysis showed minor changes in gene expression profiles between EST and vehicle groups of vincristine-injected animals, suggesting that the analgesic effects observed *in vivo* are mainly due to σ1R modulation of sensitization processes through other systems. One possible explanation could be little expression or absence of σ1Rs in astrocytes on the regions examined. Interestingly, while the evidence for the location of σ1Rs in peripheral sensory neurons is clear, there is no consensus on their exact location in the CNS, with some studies showing a neuronal-exclusive expression of this receptor (Alonso *et al.*, 2000), others have detected it in astrocytes but not neurons (Moon *et al.*, 2014), and others in both cell types (Ruscher *et al.*, 2011). Histological validation, for instance, with co-staining of σ1R and an astrocyte-specific marker would be needed to cast light into this possibility. Alternatively, one major finding was that EST treatment produced a significant effect in astrocyte transcriptome related to heme synthesis and function during the late

period. Surprisingly, *Hbb, Hba,* and *Alas2*, among other related genes, were significantly downregulated in the VCR-EST group, in contrast to the VCR-vehicle group at that time-point, as previously described. These results further support the clear involvement of this system in the pathological mechanisms of CIPN, as proposed here, and suggest that σ1Rs have a role in its modulation. It was somehow unexpected but not surprising, since it has been postulated that σ1Rs play pivotal roles in regulating mitochondrial homeostasis and function (Nguyen *et al.*, 2015; Weng *et al.*, 2017), and Hb and heme synthesis all occur in the mitochondria. In this regard, activation of σ1Rs through agonists promoted neuronal survival and restored neuronal functions in neurodegenerative diseases via multiple mechanisms, including the blockade of lipid peroxidation and attenuation of ROS production, suggesting a key role of σ1Rs in neuroprotection (Ruscher *et al.*, 2011; Nguyen *et al.*, 2015, 2017; Ruscher and Wieloch, 2015). Since EST is a σ1R antagonist, the blockade of these receptors may not be beneficial in reversing vincristine-induced damage in this case.

Interestingly, the downregulation of these genes was more prominent in the SC, and especially in males; in fact, validation of the RNAseq results showed that females treated with EST increase expression to control levels, indicating sexual dimorphism in the role of σ1R modulation of these genes. This result may explain, at least in part, the improved analgesic efficacy of EST in females compared to males. Overall, although the exact modulatory connections between σ1Rs and astrocyte functional alterations induced by antineoplastics remain to be totally clarified, we encourage further investigation of its involvement in Hb and heme-related functions in this and other pathologies.

Astrocyte heterogeneity in physiological conditions

Accumulating evidence from bulk and single-cell RNA-Seq data suggest that astrocytes exhibit significant functional and molecular heterogeneity, especially in a region-dependent manner (Chai *et al.*, 2017; Itoh *et al.*, 2017; Morel *et al.*, 2017; Boisvert *et al.*, 2018; Batiuk *et al.*, 2020; Bayraktar *et al.*, 2020; Borggrewe *et al.*, 2021). Here, we further extent insight into astrocyte molecular diversity, with a focus on regions of the pain axis in a physiological setting. Notably, no characterization of astrocyte transcriptome profile from PAG has been reported before, and only a few studies did so on the other two regions examined here, namely the SS (Boisvert *et al.*, 2018; Bayraktar *et al.*, 2020) and the SC (Borggrewe *et al.*, 2021), adding value to this study. Our dataset analysis revealed astrocyte clustering transcriptomically based on anatomical region, in agreement with the literature. Interestingly, SS astrocytes displayed the greatest variation in gene expression and the higher number of uniquely expressed genes compared with PAG and SC astrocytes, which clustered closer. These observations suggest intriguing possibilities, including functional links between these astrocyte populations. Conversely, males and females shared similar gene expression patterns across regions. It was perhaps disappointing since sex differences in the number, differentiation, and function of astrocytes have been associated with sex differences in the structure and function of neuronal circuits (Arias *et al.*, 2009; Santos-Galindo *et al.*, 2011). However, the lack of sex-dimorphic molecular signature in physiological conditions does not exclude the generation of sex differences in the responses to pathological insults.

Transcriptional analysis of DEGs across regions further revealed region-specific astrocyte signatures that translate to spatially distinct functional

differences. One explanation for this diversity is that astrocytes are developmentally pre-ordained, where molecularly distinct subpopulations of astrocytes are specified, and each subtype migrates to different locations where they maintain region-specific heterogeneity into adulthood (Tsai *et al.*, 2012; Morel *et al.*, 2017). Supporting this hypothesis, our data suggest that astrocytes retain signatures of early regional specification. Specifically, we found a combinatorial code involving differential expression of transcriptional factors that seem to specify astrocyte positional identity. For instance, we regard the expression of the transcription factors *Lhx2, Emx2,* and *Foxg1* in SS astrocytes, which are long known to be crucial for the specification of cortical neural progenitors (Bulchand *et al.*, 2001; Molyneaux *et al.*, 2007), and have been recently also identified to be involved in astrocyte specification and maturation in the mouse cortex (Lattke *et al.*, 2021; Welle *et al.*, 2021). Similarly, PAG astrocytes showed a strong and predominant expression of other regulators of the early brain or neural development such as *Otx1-2, En1-2, Irx1-5, Pax3/7* (Lecaudey *et al.*, 2005; Agoston *et al.*, 2012), recently also identified in astrocytes (Welle *et al.*, 2021), and SC astrocytes massively expressed a variety of *Hox* genes together with their transcription factor *Nkx6-1,* which are all documented to be implicated in dorsoventral patterning of the spinal cord and hindbrain, as well as in positioning of SC astrocytes (Hochstim *et al.*, 2008; Di Bonito *et al.*, 2013; Lozzi *et al.*, 2020; Borggrewe *et al.*, 2021). Therefore, these findings extend previous observations and further suggest that transcription follows a rostrocaudal axis.

Alternatively, another hypothesis suggests that astrocytes undergo molecular reorganization upon terminal migration to become specialized for interacting with neighboring neurons in their specific region (Molofsky

et al., 2014; Chai *et al.*, 2017). Our results also showed consistency with this interpretation. For instance, we observed a functional adaptation of SS astrocytes to synaptic plasticity and transmission-related processes, reflected also with preferential expression of neurotransmitter receptors, transporters, and enzymes, especially related to glutamatergic signaling, but also synapse modifying proteins, indicative of a continued role for astrocytes in adult synaptogenesis (Theodosis *et al.*, 2008) but also in supporting the main role of this region in processing and integration of sensory information (Kim *et al.*, 2016). On the other hand, SC astrocytes were enriched in genes involved in astrocyte activation and immune response, which may contribute to greater respond to pathological insults, considering that SC is the main gateway of nociceptive transmission. Finally, PAG astrocytes showed an intermediate gene expression profile reflective of their anatomical position between the SS and the SC, with a mixed functional pattern involving synaptic transmission elements, in this case, more related to GABA signaling, indicative of its contribution to descending pain modulation, and immune-related processes. Interestingly, we also observed that gene expression generally followed a rostrocaudal gradient of expression, as noted previously in this study and other studies (Morel *et al.*, 2017; Boisvert *et al.*, 2018; Borggrewe *et al.*, 2021). Therefore, our results indicate that astrocyte heterogeneity is specified in conjunction with developmental patterning and later regional circuitry requirements. Overall, we extended current knowledge on astrocyte molecular and functional diversity that can help to better understand their role in pain-related disorders, in this case, but potentially in other neurological diseases.

In conclusion, the present Thesis has characterized the role of astrocytes in the pathophysiology of neuropathic pain induced by chemotherapy and provided a comprehensive transcriptional blueprint of interregional astrocyte features both during CIPN and physiological conditions. We have proposed common mechanisms by which antineoplastic agents may affect the astrocytic function and in turn, contribute to CIPN initiation and progression. Although it must be still clarified, may represent novel approaches to treat this disease. Alternatively, this Thesis has also demonstrated the therapeutic potential of a new σ1R antagonist compound on improving the nociceptive manifestations induced by vincristine treatment. However, the transcriptomic data suggest that this behavioral analgesic effect may constitute a modulatory effect of σ1R blockade on other cell types but astrocytes, although further research is needed to clarify this issue. Overall, our results provide proof of concept that unbiased bioinformatics analyses of the molecular signature of gene expression during disease in a cell-specific and region-specific manner can provide unique insights.

CONCLUSIONS

The main conclusions of the work presented in this Thesis can be summarized as follows:

1. The chemotherapeutic treatment with vincristine produces a rapid onset of sensory disturbances in mice, replicating common symptoms observed in clinics and thus, validating the model to test new therapeutic compounds to treat or prevent this pathology.
2. Repeated exposure to σ1R antagonist EST, starting one day before the first exposure to vincristine does not prevent the development of the neuropathy but promotes a gradual normalization of mechanical and thermal sensitivity, with a slight enhanced efficacy in females.
3. Acute administration of EST 25 mg/Kg does not produce significant alleviation of vincristine-induced mechanical hypersensitivity. New doses of this compound should be tested to conclude this effect.
4. The RiboTag approach in combination with the inducible Cre-transgenic mice used allows for successfully isolate cell-type specific mRNAs (astrocytes and microglia) and profile their transcriptome.
5. Vincristine treatment induces a widespread dysfunction of astrocytes by altering four main biological processes involved in (1) oxygen supply and antioxidant protection, (2) mitochondrial function, (3) cholesterol homeostasis, and (4) immune response. These alterations are both cause and contributing factors to the development and progression of CIPN.
6. The blockade of σ1R does not produce relevant changes in vincristine-induced transcriptomic alterations in astrocytes,

suggesting that the analgesic effects of EST are independent of the modulation of astrocytic functions.

7. However, σ1Rs do seem to play a role in the modulation of hemoglobin and heme synthesis and function in astrocytes, since EST prolongs the downregulation of this system induced by VCR, especially in males. This suggests a sexual dimorphism in the role of σ1Rs as modulators of this system in astrocytes, although further investigation is required to confirm this interpretation.
8. Astrocytes exhibit regional heterogeneity in physiological conditions, specified in conjunction with developmental patterning and later regional circuitry requirements.
9. Our results depict a clear different functional specialization of astrocytes in the pain-related regions examined, suggesting that they may have a different region-specific during pathological pain conditions.
10. We provide new insights to better understand the complexity of CIPN and we suggest the targeting of astrocytes as a promising therapeutic strategy for the management of chemotherapy-induced chronic pain conditions.

REFERENCES

Ab Aziz, C. B. and Ahmad, A. H. (2006) The role of the thalamus in modulating pain, *Malaysian Journal of Medical Sciences*. School of Medical Sciences, Universiti Sains Malaysia, 13(2), pp. 11–18.

Abbott, C. A. *et al.* (2011) Prevalence and characteristics of painful diabetic neuropathy in a large community-based diabetic population in the U.K., *Diabetes Care*, 34(10), pp. 2220–2224.

Adamsky, A. *et al.* (2018) Astrocytic Activation Generates De Novo Neuronal Potentiation and Memory Enhancement, *Cell*. Cell, 174(1), pp. 59-71.e14.

Agoston, Z. *et al.* (2012) Genetic and physical interaction of Meis2, Pax3 and Pax7 during dorsal midbrain development, *BMC Developmental Biology*. BioMed Central, 12(1), pp. 1–12.

Aida, T. *et al.* (2015) Astroglial glutamate transporter deficiency increases synaptic excitability and leads to pathological repetitive behaviors in mice, *Neuropsychopharmacology : official publication of the American College of Neuropsychopharmacology*. Neuropsychopharmacology, 40(7), pp. 1569–1579.

Alliot, F., Godin, I. and Pessac, B. (1999) Microglia derive from progenitors, originating from the yolk sac, and which proliferate in the brain, *Developmental Brain Research*. Elsevier, 117(2), pp. 145–152.

Almansa, C. and Vela, J. (2014) Selective sigma-1 receptor antagonists for the treatment of pain, *Future medicinal chemistry*. Future Med Chem, 6(10), pp. 1179–1199.

Alonso, G. *et al.* (2000) Immunocytochemical localization of the sigma(1) receptor in the adult rat central nervous system, *Neuroscience*. Neuroscience, 97(1), pp. 155–170.

Anderson, M. A. *et al.* (2016) Astrocyte scar formation aids central nervous system axon regeneration., *Nature*. Nature Publishing Group, 532(7598), pp. 195–200.

Apfel, S. C., Arezzo, J. C., Lewis, M. E. and Kessler, J. A. (1993) The Use of Insulin-like Growth Factor I in the Prevention of Vincristine Neuropathy in Mice, *Annals of the New York Academy of Sciences*, 692(1).

Apkarian, a. V. *et al.* (2004) Chronic pain patients are impaired on an emotional decision-making task, *Pain*, 108, pp. 129–136.

Araque, A., Parpura, V., Sanzgiri, R. and Haydon, P. (1999) Tripartite synapses: glia, the unacknowledged partner, *Trends in neurosciences*. Trends Neurosci, 22(5), pp. 208–215.

Areti, A., Yerra, V. G., Naidu, V. G. M. and Kumar, A. (2014) Oxidative stress and nerve damage: Role in chemotherapy induced peripheral neuropathy, *Redox Biology*.

Argyriou, A. A., Bruna, J., Marmiroli, P. and Cavaletti, G. (2012) Chemotherapy-induced peripheral neurotoxicity (CIPN): An update, *Critical Reviews in Oncology/Hematology*. Elsevier, pp. 51–77.

Arias, C. *et al.* (2009) Sex and estrous cycle-dependent differences in glial fibrillary acidic protein immunoreactivity in the adult rat hippocampus, *Hormones and Behavior*, 55(1), pp. 257–263.

Attal, N. *et al.* (2010) EFNS guidelines on the pharmacological treatment of neuropathic pain: 2010 revision, *European Journal of Neurology*. Wiley/Blackwell (10.1111), 17(9), pp. 1113-e88.

Attal, N. *et al.* (2011) The specific disease burden of neuropathic pain: Results of a French nationwide survey, *Pain*, 152(12), pp. 2836–2843.

Attal, N. (2019) Pharmacological treatments of neuropathic pain: The latest recommendations, *Revue Neurologique*. Elsevier Masson SAS, pp. 46–50.

Aydar, E., CP, P., VA, K. and MB, J. (2002) The sigma receptor as a ligand-regulated auxiliary potassium channel subunit, *Neuron*. Neuron, 34(3), pp. 399–410.

Bachstetter, A. *et al.* (2011) Fractalkine and CX 3 CR1 regulate hippocampal neurogenesis in adult and aged rats, *Neurobiology of aging*. Neurobiol Aging, 32(11), pp. 2030–2044.

Banach, M., Juranek, J. K. and Zygulska, A. L. (2017) Chemotherapy-induced neuropathies—a growing problem for patients and health care providers, *Brain and Behavior*. John Wiley and Sons Ltd, 7(1).

Bangaru, M. L. *et al.* (2013) Sigma-1 Receptor Expression in Sensory Neurons and the Effect of Painful Peripheral Nerve Injury, *Molecular Pain*. Mol Pain, 9(1), pp. 1744-8069-9–47.

Baron, R., Binder, A. and Wasner, G. (2010) *Neuropathic pain: diagnosis, pathophysiological mechanisms, and treatment*, *Lancet Neurol*.

Le Bars, D., Dickenson, A. H. and Besson, J. M. (1979) Diffuse noxious inhibitory controls (DNIC). I. Effects on dorsal horn convergent neurones in the rat, *Pain*. No longer published by Elsevier, 6(3), pp. 283–304.

Barton, D. L. *et al.* (2011) A double-blind, placebo-controlled trial of a topical treatment for chemotherapy-induced peripheral neuropathy: NCCTG trial N06CA, *Supportive Care in Cancer*, 19(6).

Basbaum, A. I., Bautista, D. M., Scherrer, G. and Julius, D. (2009) Cellular and Molecular Mechanisms of Pain, *Cell*.

Bates, D. *et al.* (2019) A Comprehensive Algorithm for Management of Neuropathic Pain, *Pain Medicine*, 20(Supplement_1), pp. S2–S12.

Batiuk, M. Y. *et al.* (2020) Identification of region-specific astrocyte subtypes at single cell resolution, *Nature Communications 2020 11:1*. Nature Publishing Group, 11(1), pp. 1–15.

Bayraktar, O. A., Fuentealba, L. C., Alvarez-Buylla, A. and Rowitch, D. H. (2015) Astrocyte development and heterogeneity, *Cold Spring Harbor Perspectives in Biology*. Cold Spring Harbor Laboratory Press, 7(1).

Bayraktar, O. A. *et al.* (2020) Astrocyte layers in the mammalian cerebral cortex revealed by a single-cell in situ transcriptomic map, *Nature Neuroscience*. Nature Publishing Group, 23(4), pp. 500–509.

Beckman, K. B. and Ames, B. N. (1998) The Free Radical Theory of Aging Matures, *Physiological Reviews*, 78(2), pp. 547–581.

Benjamini, Y. and Hochberg, Y. (1995) Controlling the False Discovery Rate: A Practical and Powerful Approach to Multiple Testing, *Journal of the Royal Statistical Society. Series B (Methodological)*. [Royal Statistical Society, Wiley], 57(1), pp. 289–300. Available at: http://www.jstor.org/stable/2346101.

Bennett, M. I. *et al.* (2019) The IASP classification of chronic pain for ICD-11: Chronic cancer-related pain, *Pain*. Lippincott Williams and Wilkins, pp. 38–44.

Bennett, M. L. *et al.* (2016) New tools for studying microglia in the mouse and human CNS., *Proceedings of the National Academy of Sciences of the United States of America*, 113(12), pp. E1738-46.

Biagioli, M. *et al.* (2009) Unexpected expression of α- and β-globin in mesencephalic dopaminergic neurons and glial cells, *Proceedings of the National Academy of Sciences*. National Academy of Sciences, 106(36), pp. 15454–15459.

Biber, K., Neumann, H., Inoue, K. and Boddeke, H. (2007) Neuronal 'On' and 'Off' signals control microglia, *Trends in neurosciences*. Trends Neurosci, 30(11), pp. 596–602.

Blais, V. and Rivest, S. (2004) Effects of TNF-alpha and IFN-gamma on nitric oxide-induced neurotoxicity in the mouse brain, *Journal of immunology (Baltimore, Md. : 1950)*. J Immunol, 172(11), pp. 7043–7052.

Blaszczyk, L. *et al.* (2018) Sequential alteration of microglia and astrocytes in the rat thalamus following spinal nerve ligation, *Journal of Neuroinflammation 2018 15:1*. BioMed Central, 15(1), pp. 1–23.

Boisvert, M. M., Erikson, G. A., Shokhirev, M. N. and Allen, N. J. (2018) The Aging Astrocyte Transcriptome from Multiple Regions of the Mouse Brain, *Cell Reports*. Elsevier B.V., 22(1), pp. 269–285.

Di Bonito, M., Glover, J. C. and Studer, M. (2013) Hox genes and region-specific sensorimotor circuit formation in the hindbrain and spinal cord, *Developmental Dynamics*. John Wiley & Sons, Ltd, 242(12), pp. 1348–1368.

Borggrewe, M. *et al.* (2021) Regionally diverse astrocyte subtypes and their heterogeneous response to EAE, *GLIA*. John Wiley & Sons, Ltd, 69(5), pp. 1140–1154.

Bouhassira, D. *et al.* (2008) Prevalence of chronic pain with neuropathic characteristics in the general population., *Pain*, 136(3), pp. 380–387.

Bouhassira, D. and Attal, N. (2018) Emerging therapies for neuropathic pain: new molecules or new indications for old treatments?, *Pain*, 159(3), pp. 576–582.

Bouhassira, D. and Attal, N. (2019) The multiple challenges of neuropathic pain, *Neuroscience Letters*. Elsevier Ireland Ltd, pp. 6–10.

Boyette-Davis, J. A. *et al.* (2013) Persistent chemoneuropathy in patients receiving the plant alkaloids paclitaxel and vincristine, *Cancer chemotherapy and pharmacology*. NIH Public Access, 71(3), p. 619.

Boyette-Davis, J. A., Hou, S., Abdi, S. and Dougherty, P. M. (2018) An updated understanding of the mechanisms involved in chemotherapy-induced neuropathy, *Pain Management*. Future Medicine Ltd., pp. 363–375.

Bravo-Caparrós, I. *et al.* (2019) Sigma-1 Receptor Inhibition Reduces Neuropathic Pain Induced by Partial Sciatic Nerve Transection in Mice by Opioid-Dependent and -Independent Mechanisms, *Frontiers in Pharmacology*. Frontiers Media SA, 10(JUN), p. 613.

Bravo-Caparrós, I. *et al.* (2020) Sigma-1 receptors control neuropathic pain and macrophage infiltration into the dorsal root ganglion after peripheral nerve injury, *The FASEB Journal*. John Wiley & Sons, Ltd, 34(4), pp. 5951–5966.

Breivik, H., Eisenberg, E., O'Brien, T. and OPENMinds (2013) The individual and societal burden of chronic pain in Europe: the case for strategic prioritisation and action to improve knowledge and availability of appropriate care., *BMC public health*. BioMed Central, 13, p. 1229.

Le Bricon, T., Gugins, S., Cynober, L. and Baracos, V. (1995) Negative impact of cancer chemotherapy on protein metabolism in healthy and tumor-bearing rats, *Metabolism: clinical and experimental*. Metabolism, 44(10), pp. 1340–1348.

Bridges, D., Thompson, S. W. and Rice, A. S. (2001) Mechanisms of neuropathic pain., *British journal of anaesthesia*, 87(1), pp. 12–26.

Brown, N. *et al.* (2016) Neuronal Hemoglobin Expression and Its Relevance to Multiple Sclerosis Neuropathology, *Journal of Molecular Neuroscience 2016 59:1*. Springer, 59(1), pp. 1–17.

Bruna, J. *et al.* (2018) Efficacy of a Novel Sigma-1 Receptor Antagonist for Oxaliplatin-Induced Neuropathy: A Randomized, Double-Blind, Placebo-Controlled Phase IIa Clinical Trial, *Neurotherapeutics*, 15(1).

Bruttger, J. *et al.* (2015) Genetic Cell Ablation Reveals Clusters of Local Self-Renewing Microglia in the Mammalian Central Nervous System, *Immunity*. Immunity, 43(1), pp. 92–106.

Bulchand, S., Grove, E. A., Porter, F. D. and Tole, S. (2001) LIM-homeodomain gene Lhx2 regulates the formation of the cortical hem, *Mechanisms of Development*. Elsevier, 100(2), pp. 165–175.

Burgos, E. *et al.* (2012) Cannabinoid agonist WIN 55,212-2 prevents the development of paclitaxel-induced peripheral neuropathy in rats. Possible involvement of spinal glial cells, *European Journal of Pharmacology*. Elsevier, 682(1–3), pp. 62–72.

Bushnell, M. C., Čeko, M. and Low, L. A. (2013) Cognitive and emotional control of pain and its disruption in chronic pain, *Nature Reviews Neuroscience*.

Bushong, E. A., Martone, M. E., Jones, Y. Z. and Ellisman, M. H. (2002) Protoplasmic astrocytes in CA1 stratum radiatum occupy separate anatomical domains, *The Journal of neuroscience : the official journal of the Society for Neuroscience*. J Neurosci, 22(1), pp. 183–192.

Butovsky, O. and Weiner, H. L. (2018) Microglial signatures and their role in health and disease, *Nature Reviews Neuroscience 2018 19:10*. Nature Publishing Group, 19(10), pp. 622–635.

Buttgereit, A. *et al.* (2016) Sall1 is a transcriptional regulator defining microglia identity and function, *Nature Immunology 2016 17:12*. Nature Publishing Group, 17(12), pp. 1397–1406.

Cahoy, J. D. *et al.* (2008a) A transcriptome database for astrocytes, neurons, and oligodendrocytes: A new resource for understanding brain development and function, *Journal of Neuroscience*, 28(1), pp. 264–278.

Cahoy, J. D. *et al.* (2008b) A transcriptome database for astrocytes, neurons, and oligodendrocytes: A new resource for understanding brain development and function, *Journal of Neuroscience*, 28(1), pp. 264–278.

Canta, A., Pozzi, E. and Carozzi, V. (2015) Mitochondrial Dysfunction in Chemotherapy-Induced Peripheral Neuropathy (CIPN), *Toxics*, 3(2), pp. 198–223.

Cao, X. *et al.* (2013) Astrocyte-derived ATP modulates depressive-like behaviors, *Nature medicine*. Nat Med, 19(6), pp. 773–777.

Carcolé, M. *et al.* (2019a) Blockade of the Sigma-1 receptor relieves cognitive and emotional impairments associated to chronic osteoarthritis pain, *Frontiers in Pharmacology*, 10(MAY), pp. 1–15.

Carcolé, M. *et al.* (2019b) Sigma-1 receptor modulates neuroinflammation associated with mechanical hypersensitivity and opioid tolerance in a mouse model of osteoarthritis pain, *British Journal of Pharmacology*, 176(20), pp. 3939–3955.

Carozzi, V. A., Canta, A. and Chiorazzi, A. (2015) Chemotherapy-induced peripheral neuropathy: What do we know about mechanisms?, *Neuroscience Letters*. Elsevier Ireland Ltd, 596, pp. 90–107.

Castany, S. *et al.* (2018) Critical role of sigma-1 receptors in central neuropathic pain-related behaviours after mild spinal cord injury in mice, *Scientific Reports*. Nature Publishing Group, 8(1).

Castany, S. *et al.* (2019) Repeated Sigma-1 Receptor Antagonist MR309 Administration Modulates Central Neuropathic Pain Development After Spinal Cord Injury in Mice, *Frontiers in Pharmacology*. Frontiers Media SA, 10(MAR).

Cavaletti, G. and Marmiroli, P. (2010) Chemotherapy-induced peripheral neurotoxicity, *Nature Reviews Neurology*. Nature Publishing Group, pp. 657–666.

Cavaletti, G. and Marmiroli, P. (2015) Chemotherapy-induced peripheral neurotoxicity, *Current Opinion in Neurology*. Lippincott Williams and Wilkins, pp. 500–507.

Cavaletti, G. *et al.* (2019) Chemotherapy-induced peripheral neurotoxicity: A multifaceted, still unsolved issue, *Journal of the Peripheral Nervous System*. John Wiley & Sons, Ltd, 24(S2), pp. S6–S12.

Cendán, C. *et al.* (2005) Formalin-induced pain is reduced in sigma(1) receptor knockout mice, *European journal of pharmacology*. Eur J Pharmacol, 511(1), pp. 73–74.

Ceolin, L. et al. *et al.* (2017) Cell Type-Specific mRNA Dysregulation in Hippocampal CA1 Pyramidal Neurons of the Fragile X Syndrome Mouse Model, *Frontiers in Molecular Neuroscience*.

Cervero, F. and Laird, J. (1991) One Pain or Many Pains?, *Physiology*. American Physiological Society, 6(6), pp. 268–273.

Di Cesare Mannelli, L. *et al.* (2014) Glial role in oxaliplatin-induced neuropathic pain, *Experimental Neurology*. Academic Press, 261, pp. 22–33.

Chai, H. *et al.* (2017) Neural Circuit-Specialized Astrocytes: Transcriptomic, Proteomic, Morphological, and Functional Evidence, *Neuron*, 95(3), pp. 531-549.e9.

Chang, X. *et al.* (2017) RNA-seq analysis of amygdala tissue reveals characteristic expression profiles in schizophrenia, *Translational Psychiatry 2017 7:8*. Nature Publishing Group, 7(8), pp. e1203–e1203.

Chaplan, S. R. *et al.* (1994) Quantitative assessment of tactile allodynia in the rat paw, *Journal of Neuroscience Methods*, 53(1), pp. 55–63.

Chappell-Maor, L. *et al.* (2019) Comparative analysis of CreER transgenic mice for the study of brain macrophages – a case study, *bioRxiv*. Cold Spring Harbor Laboratory, p. 725218.

Chen, G. *et al.* (2018) Sex-Dependent Glial Signaling in Pathological Pain: Distinct Roles of Spinal Microglia and Astrocytes, *Neuroscience Bulletin*.

Chen, Q. and Heinricher, M. M. (2019) Descending Control Mechanisms and Chronic Pain., *Current rheumatology reports*. Current Medicine Group LLC 1, 21(5), p. 13.

Chen, X. J., Wang, L. and Song, X. Y. (2020) Mitoquinone alleviates vincristine-induced neuropathic pain through inhibiting oxidative stress and apoptosis via the improvement of mitochondrial dysfunction, *Biomedicine & Pharmacotherapy*. Elsevier Masson, 125, p. 110003.

Chien, C. and Pasternak, G. (1993) Functional antagonism of morphine analgesia by (+)-pentazocine: evidence for an anti-opioid sigma 1 system, *European journal of pharmacology*. Eur J Pharmacol, 250(1).

Choi, S.-R. *et al.* (2016) Astrocyte sigma-1 receptors modulate connexin 43 expression leading to the induction of below-level mechanical allodynia in spinal cord injured mice, *Neuropharmacology*. Pergamon, 111, pp. 34–46.

Chucair-Elliott, A. J. *et al.* (2020) Inducible cell-specific mouse models for paired epigenetic and transcriptomic studies of microglia and astroglia., *Communications biology*. Springer US, 3(1), p. 693.

Chung, W.-S. *et al.* (2013) Astrocytes mediate synapse elimination through MEGF10 and MERTK pathways, *Nature 2013 504:7480*. Nature Publishing Group, 504(7480), pp. 394–400.

Chung, W., Allen, N. and Eroglu, C. (2015) Astrocytes control synapse formation, function, and elimination, *Cold Spring Harb. Perspect. Biol.* Cold Spring Harbor Laboratory Press, 6(9), p. a020370.

Clarke, L. E. *et al.* (2018) Normal aging induces A1-like astrocyte reactivity, *Proceedings of the National Academy of Sciences*. National Academy of Sciences, 115(8), pp. E1896–E1905.

Cobos, E. *et al.* (2008) Pharmacology and therapeutic potential of sigma(1) receptor ligands, *Current neuropharmacology*. Curr Neuropharmacol, 6(4), pp. 344–366.

Colleoni, M. and Sacerdote, P. (2010) Murine models of human neuropathic pain, *Biochimica et Biophysica Acta - Molecular Basis of Disease*. Elsevier B.V., 1802(10), pp. 924–933.

Colloca, L. *et al.* (2017) Neuropathic pain, *Nature Reviews Disease Primers*. Elsevier, 3(1), p. 17002.

Costigan, M., Scholz, J. and Woolf, C. J. (2009) Neuropathic pain: A maladaptive response of the nervous system to damage, *Annual Review of Neuroscience*. NIH Public Access, pp. 1–32.

Cousins, M. J. *et al.* (2010) Upcoming Issues Diagnosis and Classifi cation of Neuropathic Pain Epidemiology and Impact of Neuropathic Pain The Nature and Management of Neuropathic Pain, *PAIN: Clinical updates*, 18(7).

D'Mello, R. and Dickenson, A. H. (2008) Spinal cord mechanisms of pain., *British journal of anaesthesia*, 101(1), pp. 8–16.

Davis, M. P. (2015) Sigma-1 receptors and animal studies centered on pain and analgesia, *Expert Opinion on Drug Discovery*.

Deijk, A.-L. F. van *et al.* (2017) Astrocyte lipid metabolism is critical for synapse development and function in vivo, *Glia*. John Wiley & Sons, Ltd, 65(4), pp. 670–682.

Dekkers, M. and Barde, Y. (2013) Developmental biology. Programmed cell death in neuronal development, *Science (New York, N.Y.)*. Science, 340(6128), pp. 39–41.

Demant, D. T. *et al.* (2015) Pain relief with lidocaine 5% patch in localized peripheral neuropathic pain in relation to pain phenotype: A randomised, double-blind, and placebo-controlled, phenotype panel study, *Pain*. Lippincott Williams and Wilkins, 156(11), pp. 2234–2244.

Denk, F., McMahon, S. B. and Tracey, I. (2014) Pain vulnerability: A neurobiological perspective, *Nature Neuroscience*. Nat Neurosci, pp. 192–200.

Dentesano, G. *et al.* (2014) CD200R1 and CD200 expression are regulated by PPAR-γ in activated glial cells, *Glia*. Glia, 62(6), pp. 982–998.

Descalzi, G. *et al.* (2017) Neuropathic pain promotes adaptive changes in gene expression in brain networks involved in stress and depression, *Science Signaling*, 10(471), p. eaaj1549.

Descoeur, J. *et al.* (2011) Oxaliplatin-induced cold hypersensitivity is due to remodelling of ion channel expression in nociceptors, *EMBO Molecular Medicine*, 3(5).

Díaz, J. L. *et al.* (2012) Synthesis and Biological Evaluation of the 1-Arylpyrazole Class of σ 1 Receptor Antagonists: Identification of 4-{2-[5-Methyl-1-(naphthalen-2-yl)-1 H -pyrazol-3-yloxy]ethyl}morpholine (S1RA, E-52862), *Journal of Medicinal Chemistry*. J Med Chem, 55(19), pp. 8211–8224.

Diouf, B. *et al.* (2015) Association of an Inherited Genetic Variant With Vincristine-Related Peripheral Neuropathy in Children With Acute Lymphoblastic Leukemia, *JAMA*, 313(8), pp. 815–823.

Dixon, W. J. (1965) The Up-and-Down Method for Small Samples, *Journal of the American Statistical Association*, 60(312), pp. 967–978.

Doan, L., Manders, T. and Wang, J. (2015) Neuroplasticity underlying the comorbidity of pain and depression., *Neural plasticity*. Hindawi Publishing Corporation, 2015, p. 504691.

Dobin, A. *et al.* (2013) STAR: ultrafast universal RNA-seq aligner, *Bioinformatics (Oxford, England)*. Bioinformatics, 29(1), pp. 15–21.

Doyle, J. *et al.* (2008) Application of a translational profiling approach for the comparative analysis of CNS cell types, *Cell*. Cell, 135(4), pp. 749–762.

Dubin, A. E. and Patapoutian, A. (2010) Nociceptors: the sensors of the pain pathway., *The Journal of clinical investigation*. American Society for Clinical Investigation, 120(11), pp. 3760–72.

Duggett, N. A. *et al.* (2016) Oxidative stress in the development, maintenance and resolution of paclitaxel-induced painful neuropathy, *Neuroscience*, 333.

Entrena, J. *et al.* (2009) Sigma-1 receptors are essential for capsaicin-induced mechanical hypersensitivity: studies with selective sigma-1 ligands and sigma-1 knockout mice, *Pain*. Pain, 143(3), pp. 252–261.

Escartin, C. *et al.* (2021) Reactive astrocyte nomenclature, definitions, and future directions., *Nature neuroscience*.

Etkin, A., Egner, T. and Kalisch, R. (2011) Emotional processing in anterior cingulate and medial prefrontal cortex, *Trends in Cognitive Sciences*. Elsevier, 15(2), pp. 85–93.

Evans, S., Fishman, B., Spielman, L. and Haley, A. (2003) Randomized trial of cognitive behavior therapy versus supportive psychotherapy for HIV-related peripheral neuropathic pain., *Psychosomatics*, 44(1), pp. 44–50.

Fallon, M. T. and Colvin, L. (2013) Neuropathic pain in cancer, *British Journal of Anaesthesia*. Oxford University Press, 111(1), pp. 105–111.

Ferrer, I. *et al.* (2011) Neuronal Hemoglobin is Reduced in Alzheimer's Disease, Argyrophilic Grain Disease, Parkinson's Disease, and Dementia with Lewy Bodies, *Journal of Alzheimer's Disease*. IOS Press, 23(3), pp. 537–550.

Finnerup, N. B. *et al.* (2015) Pharmacotherapy for neuropathic pain in adults: a systematic review and meta-analysis., *The Lancet. Neurology*. Lancet Publishing Group, 14(2), pp. 162–73.

Flatters, S. J. L., Xiao, W. H. and Bennett, G. J. (2006) Acetyl-L-carnitine prevents and reduces paclitaxel-induced painful peripheral neuropathy, *Neuroscience Letters*, 397(3).

Flatters, S. J. L. and Bennett, G. J. (2006) Studies of peripheral sensory nerves in paclitaxel-induced painful peripheral neuropathy: Evidence for mitochondrial dysfunction, *Pain*, 122(3), pp. 245–257.

Flatters, S. J. L., Dougherty, P. M. and Colvin, L. A. (2017) Clinical and preclinical perspectives on Chemotherapy-Induced Peripheral Neuropathy (CIPN): A narrative review, *British Journal of Anaesthesia*. Oxford University Press, pp. 737–749.

Foley, J. C., McIver, S. R. and Haydon, P. G. (2011) Gliotransmission modulates baseline mechanical nociception, *Molecular Pain*. SAGE Publications, 7, p. 93.

Fontanilla, D. *et al.* (2009) The hallucinogen N,N-dimethyltryptamine (DMT) is an endogenous sigma-1 receptor regulator, *Science*, 323(5916), pp. 934–937.

Freitas-Andrade, M. and Naus, C. (2016) Astrocytes in neuroprotection and neurodegeneration: The role of connexin43 and pannexin1, *Neuroscience*. Neuroscience, 323, pp. 207–221.

Fumagalli, G. *et al.* (2021) Neuroinflammatory Process Involved in Different Preclinical Models of Chemotherapy-Induced Peripheral Neuropathy, *Frontiers in Immunology*, 11(February), pp. 1–24.

Gadgil, S. *et al.* (2019) A systematic summary and comparison of animal models for chemotherapy induced (peripheral) neuropathy (CIPN), *PLoS ONE*. Public Library of Science, 14(8).

Gao, V. *et al.* (2016) Astrocytic β2-adrenergic receptors mediate hippocampal long-term memory consolidation, *Proceedings of the National Academy of Sciences of the United States of America*. Proc Natl Acad Sci U S A, 113(30), pp. 8526–8531.

Ghelardini, C. *et al.* (2010) Effects of a new potent analog of tocainide on hNav1.7 sodium channels and in vivo neuropathic pain models, *Neuroscience*, 169(2).

Ghoreishi, Z. *et al.* (2012) Omega-3 fatty acids are protective against paclitaxel-induced peripheral neuropathy: A randomized double-blind placebo controlled trial, *BMC Cancer*, 12.

Giaume, C. *et al.* (2010) Astroglial networks: a step further in neuroglial and gliovascular interactions, *Nature Reviews Neuroscience 2010 11:2*. Nature Publishing Group, 11(2), pp. 87–99.

Ginhoux, F. *et al.* (2010) Fate Mapping Analysis Reveals That Adult Microglia Derive from Primitive Macrophages, *Science*. American Association for the Advancement of Science, 330(6005), pp. 841–845.

Glare, P. A. *et al.* (2014) Pain in cancer survivors, *Journal of Clinical Oncology*. American Society of Clinical Oncology, pp. 1739–1747.

Gold, M. S. and Gebhart, G. F. (2010) Nociceptor sensitization in pain pathogenesis, *Nature Medicine*. NIH Public Access, 16(11), pp. 1248–1257.

Goldmann, T. *et al.* (2013) A new type of microglia gene targeting shows TAK1 to be pivotal in CNS autoimmune inflammation, *Nature neuroscience*. Nat Neurosci, 16(11), pp. 1618–1626.

Golgi, C. (1870) Sulla sostanza connettiva del cervello (nevroglia), *Rendiconti del R Instituto Lombardo di Scienze e Lettere*, 3: 275–277.

Golgi, C. (1903) Opera Omnia, *Milano: Hoepli*.

Gonçalves, L. *et al.* (2008) Neuropathic pain is associated with depressive behaviour and induces neuroplasticity in the amygdala of the rat, *Experimental Neurology*. Academic Press, 213(1), pp. 48–56.

González-Cano, R. *et al.* (2020) The search for translational pain outcomes to refine analgesic development: Where did we come from and where are we going?, *Neuroscience & Biobehavioral Reviews*. Pergamon, 113, pp. 238–261.

Gordon, G. R. J., Mulligan, S. J. and MacVicar, B. A. (2007) Astrocyte control of the cerebrovasculature, *Glia*. Glia, 55(12), pp. 1214–1221.

Gosselin, D. *et al.* (2017) An environment-dependent transcriptional network specifies human microglia identity, *Science*. American Association for the Advancement of Science, 356(6344), pp. 1248–1259.

Grace, P. M., Hutchinson, M. R., Maier, S. F. and Watkins, L. R. (2014) Pathological pain and the neuroimmune interface., *Nat. Rev. Immunol.* Nature Publishing Group, 14(4), pp. 217–231.

Gris, G. *et al.* (2014) S1RA, a selective sigma-1 receptor antagonist, inhibits inflammatory pain in the carrageenan and complete Freund's adjuvant models in mice, *Behavioural Pharmacology*. Behav Pharmacol, 25(3), pp. 226–235.

Gris, G. *et al.* (2016a) The selective sigma-1 receptor antagonist E-52862 attenuates neuropathic pain of different aetiology in rats, *Scientific reports*. Sci Rep, 6.

Gris, G. *et al.* (2016b) The selective sigma-1 receptor antagonist E-52862 attenuates neuropathic pain of different aetiology in rats OPEN, *Nature Publishing Group*.

Groh, A., Krieger, P., Mease, R. A. and Henderson, L. (2018) Acute and Chronic Pain Processing in the Thalamocortical System of Humans and Animal Models, *Neuroscience*. Elsevier Ltd, pp. 58–71.

Haimon, Z. *et al.* (2018) Re-evaluating microglia expression profiles using RiboTag and cell isolation strategies, *Nature Immunology*, 19(6), pp. 636–644.

Hamby, M. E. *et al.* (2012) Inflammatory Mediators Alter the Astrocyte Transcriptome and Calcium Signaling Elicited by Multiple G-Protein-Coupled Receptors, *The Journal of Neuroscience*. Society for Neuroscience, 32(42), p. 14489.

Hammond, T. R. *et al.* (2019) Single-Cell RNA Sequencing of Microglia throughout the Mouse Lifespan and in the Injured Brain Reveals Complex Cell-State Changes, *Immunity*. Cell Press, 50(1), pp. 253-271.e6.

Hansen, N. *et al.* (2011) Serotonin transporter deficiency protects mice from mechanical allodynia and heat hyperalgesia in vincristine neuropathy, *Neuroscience letters*. Neurosci Lett, 495(2), pp. 93–97.

Hargreaves, K. *et al.* (1988) A new and sensitive method for measuring thermal nociception in cutaneous hyperalgesia, *Pain*, 32(1).

Hasnie, F. S. *et al.* (2007) Further characterization of a rat model of varicella zoster virus-associated pain: Relationship between mechanical hypersensitivity and anxiety-related behavior, and the influence of analgesic drugs, *Neuroscience*. Pergamon, 144(4), pp. 1495–1508.

Hayashi, T. and Su, T. (2007) Sigma-1 receptor chaperones at the ER-mitochondrion interface regulate Ca(2+) signaling and cell survival, *Cell*. Cell, 131(3), pp. 596–610.

Hayashi, T. *et al.* (2011) Targeting ligand-operated chaperone sigma-1 receptors in the treatment of neuropsychiatric disorders, *Expert opinion on therapeutic targets*. Expert Opin Ther Targets, 15(5), pp. 557–577.

Van Hecke, O. *et al.* (2014) Neuropathic pain in the general population: A systematic review of epidemiological studies, *Pain*. Elsevier B.V., pp. 654–662.

Heiman, M. *et al.* (2008) A Translational Profiling Approach for the Molecular Characterization of CNS Cell Types, *Cell*. Cell Press, 135(4), pp. 738–748.

Heiman, M. *et al.* (2014) Cell type-specific mRNA purification by translating ribosome affinity purification (TRAP), *Nature Protocols*.

Hellewell, S. *et al.* (1994) Rat liver and kidney contain high densities of sigma 1 and sigma 2 receptors: characterization by ligand binding and photoaffinity labeling, *European journal of pharmacology*. Eur J Pharmacol, 268(1), pp. 9–18.

Herculano-Houzel, S. (2014) The glia/neuron ratio: how it varies uniformly across brain structures and species and what that means for brain physiology and evolution, *Glia*. Glia, 62(9), pp. 1377–1391.

Hershman, D. L. *et al.* (2013) Randomized double-blind placebo-controlled trial of acetyl-L-carnitine for the prevention of taxane-induced neuropathy in women undergoing adjuvant breast cancer therapy, *Journal of Clinical Oncology*, 31(20).

Hertz, L. and Chen, Y. (2016) Importance of astrocytes for potassium ion (K +) homeostasis in brain and glial effects of K + and its transporters on learning, *Neuroscience and biobehavioral reviews*. Neurosci Biobehav Rev, 71, pp. 484–505.

Hickman, S. E. *et al.* (2013) The microglial sensome revealed by direct RNA sequencing, *Nature Neuroscience 2013 16:12*. Nature Publishing Group, 16(12), pp. 1896–1905.

Hochstim, C. *et al.* (2008) Identification of Positionally Distinct Astrocyte Subtypes whose Identities Are Specified by a Homeodomain Code, *Cell*. Elsevier B.V., 133(3), pp. 510–522.

Hui, K. F. *et al.* (2013) Bortezomib and SAHA synergistically induce ROS-driven caspase-dependent apoptosis of nasopharyngeal carcinoma and block replication of epstein-barr virus, *Molecular Cancer Therapeutics*, 12(5).

Ibrahim, E. Y. and Ehrlich, B. E. (2020) Prevention of chemotherapy-induced peripheral neuropathy: A review of recent findings, *Critical Reviews in Oncology/Hematology*. Elsevier Ireland Ltd, p. 102831.

Inoue, K. (2019) Role of the P2X4 receptor in neuropathic pain, *Current Opinion in Pharmacology*. Elsevier Ltd, 47, pp. 33–39.

Itoh, N. *et al.* (2017) Cell-specific and region-specific transcriptomics in the multiple sclerosis model: Focus on astrocytes, *Proceedings of the National Academy of Sciences of the United States of America*. National Academy of Sciences, 115(2), pp. E302–E309.

Janes, K. *et al.* (2013) Bioenergetic deficits in peripheral nerve sensory axons during chemotherapy-induced neuropathic pain resulting from peroxynitrite-mediated post-translational nitration of mitochondrial superoxide dismutase, *Pain*, 154(11).

Janes, K. *et al.* (2014) A3 adenosine receptor agonist prevents the development of paclitaxel-induced neuropathic pain by modulating spinal glial-restricted redox-dependent signaling pathways, *Pain*, 155(12).

Jellen, L. C. *et al.* (2013) Iron deficiency alters expression of dopamine-related genes in the ventral midbrain in mice, *Neuroscience*. NIH Public Access, 0, p. 13.

Jensen, T. S. *et al.* (2011) A new definition of neuropathic pain, *Pain*. Elsevier B.V., pp. 2204–2205.

Ji, R.-R. *et al.* (2018) Neuroinflammation and Central Sensitization in Chronic and Widespread Pain, *Anesthesiology*. American Society of Anesthesiologists, 129(2), pp. 343–366.

Ji, R.-R., Donnelly, C. R. and Nedergaard, M. (2019) Astrocytes in chronic pain and itch, *Nature Reviews Neuroscience*, 20(11), pp. 667–685.

Ji, R. R., Berta, T. and Nedergaard, M. (2013) Glia and pain: Is chronic pain a gliopathy?, in *Pain*.

John Lin, C.-C. *et al.* (2017) Identification of diverse astrocyte populations and their malignant analogs, *Nature Neuroscience*, 20(3), pp. 396–405.

Jung, S. *et al.* (2000) Analysis of Fractalkine Receptor CX 3 CR1 Function by Targeted Deletion and Green Fluorescent Protein Reporter Gene Insertion , *Molecular and Cellular Biology*. American Society for Microbiology, 20(11), pp. 4106–4114.

Kaiser, T. and Feng, G. (2019) Tmem119-EGFP and Tmem119-CreERT2 Transgenic Mice for Labeling and Manipulating Microglia, *eNeuro*. Society for Neuroscience, 6(4).

Kawasaki, Y., Zhang, L., Cheng, J. and Ji, R. (2008) Cytokine mechanisms of central sensitization: distinct and overlapping role of interleukin-1beta, interleukin-6, and tumor necrosis factor-alpha in regulating synaptic and neuronal activity in the superficial spinal cord, *The Journal of neuroscience : the official journal of the Society for Neuroscience*. J Neurosci, 28(20), pp. 5189–5194.

Kettenmann, H., Hanisch, U., Noda, M. and Verkhratsky, A. (2011) Physiology of microglia, *Physiological reviews*. Physiol Rev, 91(2), pp. 461–553.

Khakh, B. S. and Sofroniew, M. V (2015) Diversity of astrocyte functions and phenotypes in neural circuits, *Nature Neuroscience 2015 18:7*. Nature Publishing Group, 18(7), pp. 942–952.

Khakh, B. S. and Deneen, B. (2019) The Emerging Nature of Astrocyte Diversity, *https://doi.org/10.1146/annurev-neuro-070918-050443*. Annual Reviews, 42, pp. 187–207.

Kierdorf, K. and Prinz, M. (2017) Microglia in steady state, *The Journal of clinical investigation*. J Clin Invest, 127(9), pp. 3201–3209.

Kiguchi, N. *et al.* (2008a) The critical role of invading peripheral macrophage-derived interleukin-6 in vincristine-induced mechanical allodynia in mice., *European journal of pharmacology*. Elsevier, 592(1–3), pp. 87–92.

Kiguchi, N., Maeda, T., Kobayashi, Y. and Kishioka, S. (2008b) Up-regulation of tumor necrosis factor-alpha in spinal cord contributes to vincristine-induced mechanical allodynia in mice., *Neuroscience letters*. Elsevier, 445(2), pp. 140–3.

Kim, B. S. *et al.* (2018) Efficacy and safety of oxycodone/naloxone as add-on therapy to gabapentin or pregabalin for the management of chemotherapy-induced peripheral neuropathy in Korea, *Asia-Pacific Journal of Clinical Oncology*, 14(5).

Kim, F. *et al.* (2010) Sigma 1 receptor modulation of G-protein-coupled receptor signaling: potentiation of opioid transduction independent from receptor binding, *Molecular pharmacology*. Mol Pharmacol, 77(4), pp. 695–703.

Kim, S. K. *et al.* (2016) Cortical astrocytes rewire somatosensory cortical circuits for peripheral neuropathic pain, *Journal of Clinical Investigation*, 126(5), pp. 1983–1997.

Kim, S. T. *et al.* (2015) Protective effects of phosphatidylcholine on oxaliplatin-induced neuropathy in rats, *Life Sciences*, 130, pp. 81–87.

King, K. M. *et al.* (2017) Single and combined effects of Δ9-tetrahydrocannabinol and cannabidiol in a mouse model of chemotherapy-induced neuropathic pain, *British Journal of Pharmacology*, 174(17).

Kiyoshi and Zhou, M. (2019) Astrocyte syncytium: a functional reticular system in the brain, *Neural Regeneration Research*. Medknow Publications and Media Pvt. Ltd., 14(4), p. 595.

Kleckner, I. R. *et al.* (2018) Effects of exercise during chemotherapy on chemotherapy-induced peripheral neuropathy: a multicenter, randomized controlled trial, *Supportive Care in Cancer*, 26(4).

Kofler, J. and Wiley, C. (2011) Microglia: key innate immune cells of the brain, *Toxicologic pathology*. Toxicol Pathol, 39(1), pp. 103–114.

Kol, A. *et al.* (2020) Astrocytes contribute to remote memory formation by modulating hippocampal–cortical communication during learning, *Nature Neuroscience 2020 23:10*. Nature Publishing Group, 23(10), pp. 1229–1239.

Kosek, E. *et al.* (2016) Do we need a third mechanistic descriptor for chronic pain states?, *PAIN*, 157(7).

Kottschade, L. A. *et al.* (2011) The use of vitamin E for the prevention of chemotherapy-induced peripheral neuropathy: Results of a randomized phase III clinical trial, *Supportive Care in Cancer*, 19(11).

Kriegstein, A. and Alvarez-Buylla, A. (2009) The glial nature of embryonic and adult neural stem cells, *Annual review of neuroscience*. Annu Rev Neurosci, 32, pp. 149–184.

Kumar, A., Kaur, H. and Singh, A. (2018) Neuropathic Pain models caused by damage to central or peripheral nervous system, *Pharmacological Reports*. Institute of Pharmacology, Polish Academy of Sciences, 70(2), pp. 206–216.

de la Puente, B. *et al.* (2009) Sigma-1 receptors regulate activity-induced spinal sensitization and neuropathic pain after peripheral nerve injury, *Pain*. Pain, 145(3), pp. 294–303.

Langley, P. C., Van Litsenburg, C., Cappelleri, J. C. and Carroll, D. (2013) The burden associated with neuropathic pain in Western Europe., *Journal of medical economics*, 16(1), pp. 85–95.

Latremoliere, A. and Woolf, C. J. (2009) Central sensitization: a generator of pain hypersensitivity by central neural plasticity., *The journal of pain : official journal of the American Pain Society*, 10(9), pp. 895–926.

Lattke, M. *et al.* (2021) Extensive transcriptional and chromatin changes underlie astrocyte maturation in vivo and in culture, *Nature Communications*. Nature Publishing Group, 12(1).

Lawson, L. J., Perry, V. H., Dri, P. and Gordon, S. (1990) Heterogeneity in the distribution and morphology of microglia in the normal adult mouse brain, *Neuroscience*. Pergamon, 39(1), pp. 151–170.

Lecaudey, V. *et al.* (2005) Expression of the zebrafish Iroquois genes during early nervous system formation and patterning, *Journal of Comparative Neurology*. John Wiley & Sons, Ltd, 492(3), pp. 289–302.

Lee, J. H. and Kim, W. (2020) The role of satellite glial cells, astrocytes, and microglia in oxaliplatin-induced neuropathic pain, *Biomedicines*. MDPI AG.

Lees, J. G. *et al.* (2017) Immune-mediated processes implicated in chemotherapy-induced peripheral neuropathy, *European Journal of Cancer*. Elsevier Ltd, pp. 22–29.

Leite-Almeida, H. *et al.* (2009) The impact of age on emotional and cognitive behaviours triggered by experimental neuropathy in rats., *Pain*, 144(1–2), pp. 57–65.

Li, Y. *et al.* (2017) Dorsal root ganglion neurons become hyperexcitable and increase expression of voltage-gated T-type calcium channels (Cav3.2) in paclitaxel-induced peripheral neuropathy, *Pain*, 158(3).

Li, Y. *et al.* (2018) Drg voltage-gated sodium channel 1.7 is upregulated in paclitaxel-induced neuropathy in rats and in humans with neuropathic pain, *Journal of Neuroscience*, 38(5).

Liao, Y., Smyth, G. and Shi, W. (2014) featureCounts: an efficient general purpose program for assigning sequence reads to genomic features, *Bioinformatics (Oxford, England)*. Bioinformatics, 30(7), pp. 923–930.

Liu, D. *et al.* (2014) Medial prefrontal activity during delay period contributes to learning of a working memory task., *Science (New York, N.Y.)*, 346(6208), pp. 458–63.

Liu, M. G. and Chen, J. (2014) Preclinical research on pain comorbidity with affective disorders and cognitive deficits: Challenges and perspectives, *Progress in Neurobiology*.

Liu, X. J. *et al.* (2014) Nociceptive neurons regulate innate and adaptive immunity and neuropathic pain through MyD88 adapter, *Cell Research*. Nature Publishing Group, pp. 1374–1377.

Lolignier, S., Eijkelkamp, N. and Wood, J. N. (2015a) Mechanical allodynia., *Pflugers Archiv : European journal of physiology*, 467(1), pp. 133–9.

Lolignier, S. *et al.* (2015b) The Nav1.9 Channel Is a Key Determinant of Cold Pain Sensation and Cold Allodynia, *Cell Reports*, 11(7).

Loprinzi, C. L. *et al.* (2020) Prevention and Management of Chemotherapy-Induced Peripheral Neuropathy in Survivors of Adult Cancers: ASCO Guideline Update., *Journal of clinical oncology : official journal of the*

American Society of Clinical Oncology. American Society of Clinical Oncology, 38(28), pp. 3325–3348.

Lovatt, D. *et al.* (2007) The transcriptome and metabolic gene signature of protoplasmic astrocytes in the adult murine cortex, *The Journal of neuroscience : the official journal of the Society for Neuroscience*. J Neurosci, 27(45), pp. 12255–12266.

Lozzi, B. *et al.* (2020) Regionally Distinct Astrocytes Display Unique Transcription Factor Profiles in the Adult Brain, *Frontiers in Neuroscience*. Frontiers Media S.A., 14.

Luchetti, S., Huitinga, I. and Swaab, D. F. (2011) Neurosteroid and GABA-A receptor alterations in Alzheimer's disease, Parkinson's disease and multiple sclerosis, *Neuroscience*. Pergamon, 191, pp. 6–21.

Ma, K. *et al.* (2019) Identification of key genes, pathways and miRNA/mRNA regulatory networks of CUMS-induced depression in nucleus accumbens by integrated bioinformatics analysis, *Neuropsychiatric Disease and Treatment*. Dove Press, 15, pp. 685–700.

Magnowska, M. *et al.* (2018) Effectiveness of gabapentin pharmacotherapy in chemotherapy-induced peripheral neuropathy, *Ginekologia Polska*, 89(4).

Makar, T. K. *et al.* (1994) Vitamin E, Ascorbate, Glutathione, Glutathicne Disulfide, and Enzymes of Glutathione Metabolism in Cultures of Chick Astrocytes and Neurons: Evidence that Astrocytes Play an Important Role in Antioxidative Processes in the Brain, *Journal of Neurochemistry*. John Wiley & Sons, Ltd, 62(1), pp. 45–53.

Makker, P. G. S. *et al.* (2017) Characterisation of Immune and Neuroinflammatory Changes Associated with Chemotherapy-Induced Peripheral Neuropathy, *PLOS ONE*. Edited by M. Costigan. Public Library of Science, 12(1), p. e0170814.

Mapplebeck, J., Beggs, S. and Salter, M. (2017) Molecules in pain and sex: a developing story, *Molecular brain*. Mol Brain, 10(1).

Martínez-Navarro, M. *et al.* (2020) Mu and delta opioid receptors play opposite nociceptive and behavioural roles on nerve-injured mice, *British Journal of Pharmacology*, 177(5), pp. 1187–1205.

Masuda, T., Sankowski, R., Staszewski, O. and Prinz, M. (2020a) Microglia Heterogeneity in the Single-Cell Era, *Cell Reports*, 30(5), pp. 1271–1281.

Masuda, T. *et al.* (2020b) Novel Hexb-based tools for studying microglia in the CNS., *Nature immunology*. Nature Publishing Group, 21(7), pp. 802–815.

Matcovitch-Natan, O. *et al.* (2016) Microglia development follows a stepwise program to regulate brain homeostasis, *Science*. American Association for the Advancement of Science, 353(6301).

Matute, C., Domercq, M. and Sánchez-Gómez, M. V. (2006) Glutamate-mediated glial injury: Mechanisms and clinical importance, *GLIA*.

Mauch, D. H. *et al.* (2001) CNS Synaptogenesis Promoted by Glia-Derived Cholesterol, *Science*. Science, 294(5545), pp. 1354–1357.

Maurice, T., Urani, A., Phan, V. and Romieu, P. (2001) The interaction between neuroactive steroids and the sigma1 receptor function: behavioral consequences and therapeutic opportunities, *Brain research. Brain research reviews*. Brain Res Brain Res Rev, 37(1–3), pp. 116–132.

Maurice, T. and Su, T. (2009) The pharmacology of sigma-1 receptors, *Pharmacology & therapeutics*. Pharmacol Ther, 124(2), pp. 195–206.

McCann, D., Weissman, A. and Su, T. (1994) Sigma-1 and sigma-2 sites in rat brain: comparison of regional, ontogenetic, and subcellular patterns, *Synapse (New York, N.Y.)*. Synapse, 17(3), pp. 182–189.

McCarberg, B. and Peppin, J. (2019) Pain Pathways and Nervous System Plasticity: Learning and Memory in Pain., *Pain medicine (Malden, Mass.)*.

Melcangi, R. C., Garcia-Segura, L. M. and Mensah-Nyagan, A. G. (2007) Neuroactive steroids: State of the art and new perspectives, *Cellular and Molecular Life Sciences*, 65(5), p. 777.

Melzack, R. and Wall, P. D. (1965) Pain mechanisms: a new theory., *Science (New York, N.Y.)*, 150(3699), pp. 971–9.

Merlos, M. *et al.* (2017) Pharmacological Modulation of the Sigma 1 Receptor and the Treatment of Pain, *Advances in experimental medicine and biology*. Adv Exp Med Biol, 964, pp. 85–107.

Merskey H, Bogduk N, Merskey, H. and Bogduk, N. (1994) Classification of chronic pain, *IASP Press: Seattle*. 2nd. ed. Seattle.

Meunier, J. and Hayashi, T. (2010) Sigma-1 receptors regulate Bcl-2 expression by reactive oxygen species-dependent transcriptional regulation of nuclear factor kappaB, *The Journal of pharmacology and experimental therapeutics*. J Pharmacol Exp Ther, 332(2), pp. 388–397.

Milla, P. *et al.* (2009) Administration of reduced glutathione in FOLFOX4 adjuvant treatment for colorectal cancer: effect on oxaliplatin pharmacokinetics, Pt-DNA adduct formation, and neurotoxicity., *Anti-cancer drugs*, 20(5).

Milligan, E. D. and Watkins, L. R. (2009) Pathological and protective roles of glia in chronic pain, *Nature Reviews Neuroscience*, 10(1), pp. 23–36.

Mogil, J. (2012) Sex differences in pain and pain inhibition: multiple explanations of a controversial phenomenon, *Nature reviews. Neuroscience*. Nat Rev Neurosci, 13(12), pp. 859–866.

Molofsky, A. V. *et al.* (2014) Astrocyte-encoded positional cues maintain sensorimotor circuit integrity, *Nature 2014 509:7499*. Nature Publishing Group, 509(7499), pp. 189–194.

Molofsky, A. V. and Deneen, B. (2015) Astrocyte development: A Guide for the Perplexed, *Glia*. John Wiley & Sons, Ltd, 63(8), pp. 1320–1329.

Molyneaux, B. J., Arlotta, P., Menezes, J. R. L. and Macklis, J. D. (2007) Neuronal subtype specification in the cerebral cortex, *Nature Reviews Neuroscience 2007 8:6*. Nature Publishing Group, 8(6), pp. 427–437.

Moon, J. Y. *et al.* (2014) σ1 receptors activate astrocytes via p38 MAPK phosphorylation leading to the development of mechanical allodynia in a mouse model of neuropathic pain, *British Journal of Pharmacology*, 171(24), pp. 5881–5897.

Morel, L. *et al.* (2017) Molecular and functional properties of regional astrocytes in the adult brain, *Journal of Neuroscience*. Society for Neuroscience, 37(36), pp. 8706–8717.

Moriarty, O., McGuire, B. E. and Finn, D. P. (2011) The effect of pain on cognitive function: A review of clinical and preclinical research, *Progress in Neurobiology*. Elsevier Ltd, 93(3), pp. 385–404.

Muñoz, M. and Esteve, R. (2005) Reports of memory functioning by patients with chronic pain., *The Clinical journal of pain*, 21(4), pp. 287–91.

Nadal, X., Porta, C. La, Bura, S. A. and Maldonado, R. (2013) Involvement of the opioid and cannabinoid systems in pain control: New insights from knockout studies, *European Journal of Pharmacology*, 716, pp. 142–157.

Nair, A. B. and Jacob, S. (2016) A simple practice guide for dose conversion between animals and human, *Journal of Basic and Clinical Pharmacy*. Wolters Kluwer -- Medknow Publications, 7(2), p. 27.

Namaka, M. *et al.* (2009) A treatment algorithm for neuropathic pain: an update., *The Consultant pharmacist : the journal of the American Society of Consultant Pharmacists*, 24(12), pp. 885–902.

Nguyen, L. *et al.* (2015) Role of sigma-1 receptors in neurodegenerative diseases, *Journal of Pharmacological Sciences*. Elsevier, 127(1), pp. 17–29.

Nguyen, L. *et al.* (2017) Sigma-1 Receptors and Neurodegenerative Diseases: Towards a Hypothesis of Sigma-1 Receptors as Amplifiers of Neurodegeneration and Neuroprotection, *Advances in Experimental Medicine and Biology*. Springer, Cham, 964, pp. 133–152.

Nicholas, M. *et al.* (2019) The IASP classification of chronic pain for ICD-11: chronic primary pain., *Pain*, 160(1), pp. 28–37.

Nicolson, S. E., Caplan, J. P., Williams, D. E. and Stern, T. A. (2009) Comorbid pain, depression, and anxiety: Multifaceted pathology allows for multifaceted treatment, *Harvard Review of Psychiatry*, pp. 407–420.

Nieto, F. R. *et al.* (2012) Role of sigma-1 receptors in paclitaxel-induced neuropathic pain in mice, *Journal of Pain*. Elsevier, 13(11), pp. 1107–1121.

Nieto, F. R. *et al.* (2014) Genetic inactivation and pharmacological blockade of sigma-1 receptors prevent paclitaxel-induced sensory-nerve mitochondrial abnormalities and neuropathic pain in mice, *Molecular Pain*. SAGE Publications, 10(1), p. 11.

Nieweg, K., Schaller, H. and Pfrieger, F. W. (2009) Marked differences in cholesterol synthesis between neurons and glial cells from postnatal rats, *Journal of Neurochemistry*. John Wiley & Sons, Ltd, 109(1), pp. 125–134.

Nimmerjahn, A., Kirchhoff, F. and Helmchen, F. (2005) Resting microglial cells are highly dynamic surveillants of brain parenchyma in vivo, *Science (New York, N.Y.)*. Science, 308(5726), pp. 1314–1318.

Nishiyama, A. *et al.* (2016) Lineage, fate, and fate potential of NG2-glia, *Brain Research*. Elsevier, 1638, pp. 116–128.

Noguchi, C. T., Asavaritikrai, P., Teng, R. and Jia, Y. (2007) Role of erythropoietin in the brain, *Critical reviews in oncology/hematology*. NIH Public Access, 64(2), p. 159.

Northington, F. J. *et al.* (1998) Regional and cellular expression of glial (GLT1) and neuronal (EAAC1) glutamate transporter proteins in ovine fetal brain, *Neuroscience*. Pergamon, 85(4), pp. 1183–1193.

Oberheim, N. A. *et al.* (2009) Uniquely hominid features of adult human astrocytes, *The Journal of neuroscience : the official journal of the Society for Neuroscience*. J Neurosci, 29(10), pp. 3276–3287.

Oe, Y. *et al.* (2016) Glycogen distribution in the microwave-fixed mouse brain reveals heterogeneous astrocytic patterns, *Glia*. John Wiley & Sons, Ltd, 64(9), pp. 1532–1545.

Old, E. A. *et al.* (2014) Monocytes expressing CX3CR1 orchestrate the development of vincristine-induced pain, *Journal of Clinical Investigation*.

Olney, K. *et al.* (2020) Reference genome and transcriptome informed by the sex chromosome complement of the sample increase ability to detect sex differences in gene expression from RNA-Seq data, *Biology of sex differences*. Biol Sex Differ, 11(1).

Orban, P. C., Chui, D. and Marth, J. D. (1992) Tissue- and site-specific DNA recombination in transgenic mice., *Proceedings of the National Academy of Sciences of the United States of America*. National Academy of Sciences, 89(15), p. 6861.

Orihuela, R., McPherson, C. A. and Harry, G. J. (2016) Microglial M1/M2 polarization and metabolic states, *British Journal of Pharmacology*. John Wiley & Sons, Ltd, 173(4), pp. 649–665.

Orre, M. *et al.* (2014) Acute isolation and transcriptome characterization of cortical astrocytes and microglia from young and aged mice, *Neurobiology of Aging*. Neurobiol Aging, 35(1), pp. 1–14.

Ossipov, M. H., Morimura, K. and Porreca, F. (2014) Descending pain modulation and chronification of pain, *Current Opinion in Supportive and Palliative Care*. Lippincott Williams and Wilkins, pp. 143–151.

Pacini, A. *et al.* (2016) The α9α10 nicotinic receptor antagonist α-conotoxin RgIA prevents neuropathic pain induced by oxaliplatin treatment, *Experimental Neurology*, 282.

Pal, A. *et al.* (2007) Identification of regions of the sigma-1 receptor ligand binding site using a novel photoprobe, *Molecular pharmacology*. Mol Pharmacol, 72(4), pp. 921–933.

Pal, A. *et al.* (2008) Juxtaposition of the steroid binding domain-like I and II regions constitutes a ligand binding site in the sigma-1 receptor, *The Journal of biological chemistry*. J Biol Chem, 283(28), pp. 19646–19656.

Palacios, G. *et al.* (2004) Immunohistochemical localization of the sigma1 receptor in Schwann cells of rat sciatic nerve, *Brain Research*. Elsevier, 1007(1–2), pp. 65–70.

Paniagua, N. *et al.* (2019) May a sigma-1 antagonist improve neuropathic signs induced by cisplatin and vincristine in rats?, *European Journal of Pain*. John Wiley & Sons, Ltd, 23(3), pp. 603–620.

Parkhurst, C. *et al.* (2013) Microglia promote learning-dependent synapse formation through brain-derived neurotrophic factor, *Cell*. Cell, 155(7), pp. 1596–1609.

Patel, R. and Dickenson, A. H. (2016) Mechanisms of the gabapentinoids and α 2 δ-1 calcium channel subunit in neuropathic pain., *Pharmacology research & perspectives*. Wiley-Blackwell, 4(2), p. e00205.

Patestas, M. A. and Gartner, L. P. (2016) *A textbook of neuroanatomy*, *Wiley-Blackwell*.

Pfrieger, F. W. and Ungerer, N. (2011) Cholesterol metabolism in neurons and astrocytes, *Progress in Lipid Research*. Pergamon, 50(4), pp. 357–371.

Pinho-Ribeiro, F. A., Verri, W. A. and Chiu, I. M. (2017) Nociceptor Sensory Neuron–Immune Interactions in Pain and Inflammation, *Trends in Immunology*. Elsevier, 38(1), pp. 5–19.

van der Poel, M. *et al.* (2019) Transcriptional profiling of human microglia reveals grey–white matter heterogeneity and multiple sclerosis-associated changes, *Nature Communications 2019 10:1*. Nature Publishing Group, 10(1), pp. 1–13.

La Porta, C., Lara-Mayorga, I. M., Negrete, R. and Maldonado, R. (2016) Effects of pregabalin on the nociceptive, emotional and cognitive manifestations of neuropathic pain in mice, *European Journal of Pain (United Kingdom)*.

Price, T. J. and Ray, P. R. (2019) Recent advances toward understanding the mysteries of the acute to chronic pain transition, *Current Opinion in Physiology*. Elsevier Ltd, pp. 42–50.

Prinz, M. and Priller, J. (2014) Microglia and brain macrophages in the molecular age: from origin to neuropsychiatric disease., *Nature reviews. Neuroscience*, 15(5), pp. 300–12.

Prinz, M., Jung, S. and Priller, J. (2019) Microglia Biology: One Century of Evolving Concepts, *Cell*. Cell Press, 179(2), pp. 292–311.

Przewlocki, R. *et al.* (1992) Gene expression and localization of opioid peptides in immune cells of inflamed tissue: Functional role in antinociception, *Neuroscience*. Pergamon, 48(2), pp. 491–500.

Qin, B. *et al.* (2020) Notch activation enhances microglial CX3CR1/P38 MAPK pathway in rats model of vincristine-induced peripheral neuropathy, *Neuroscience Letters*, 715(November 2019), pp. 1–6.

Raja, S. N. *et al.* (2020) The revised International Association for the Study of Pain definition of pain: concepts, challenges, and compromises, *Pain*. NLM (Medline), pp. 1976–1982.

Ramachandran, S. *et al.* (2009) The sigma1 receptor interacts with N-alkyl amines and endogenous sphingolipids, *European journal of pharmacology*. Eur J Pharmacol, 609(1–3), pp. 19–26.

Ramón y Cajal, S. (1895) Algunas conjeturas sobre el mechanismoanatomico de la ideacion, asociacion y atencion, *Imprenta y Libreria de Nicolas Moya*.

Richter, F. *et al.* (2009) Neurons express hemoglobin α- and β-chains in rat and human brains, *Journal of Comparative Neurology*. John Wiley & Sons, Ltd, 515(5), pp. 538–547.

Del Rio-Hortega, P. (1919) El tercer elemento de los centros nerviosos. I. La microglia en estado normal. II. Intervencíon de la microglia en los procesos patológicos. III. Naturaleza probable de la microglia, *Bol de la Soc esp de biol*, 9:69–120.

Ritchie, M. *et al.* (2015) limma powers differential expression analyses for RNA-sequencing and microarray studies, *Nucleic acids research*. Nucleic Acids Res, 43(7), p. e47.

Robinson, C. R., Zhang, H. and Dougherty, P. M. (2014) Astrocytes, but not microglia, are activated in oxaliplatin and bortezomib-induced peripheral neuropathy in the rat, *Neuroscience*. Elsevier Ltd, 274, pp. 308–317.

Robinson, C. R. and Dougherty, P. M. (2015) Spinal astrocyte gap junction and glutamate transporter expression contributes to a rat model of bortezomib-induced peripheral neuropathy, *Neuroscience*, 285.

Robinson, M. and Oshlack, A. (2010) A scaling normalization method for differential expression analysis of RNA-seq data, *Genome biology*. Genome Biol, 11(3).

Robinson, M., McCarthy, D. and Smyth, G. (2010) edgeR: a Bioconductor package for differential expression analysis of digital gene expression data, *Bioinformatics (Oxford, England)*. Bioinformatics, 26(1), pp. 139–140.

Robinson, S. R. (2001) Changes in the cellular distribution of glutamine synthetase in Alzheimer's disease, *Journal of Neuroscience Research*. John Wiley & Sons, Ltd, 66(5), pp. 972–980.

Roman, F. *et al.* (1989) Neuropeptide Y and peptide YY interact with rat brain sigma and PCP binding sites, *European journal of pharmacology*. Eur J Pharmacol, 174(2–3), pp. 301–302.

Romero-Sandoval, E. A., Asbill, S., Paige, C. A. and Byrd-Glover, K. (2015) Peripherally Restricted Cannabinoids for the Treatment of Pain, *Pharmacotherapy*, 35(10).

Romero, L. *et al.* (2012) Pharmacological properties of S1RA, a new sigma-1 receptor antagonist that inhibits neuropathic pain and activity-induced spinal sensitization, *British journal of pharmacology*. Br J Pharmacol, 166(8), pp. 2289–2306.

Ruan, C. *et al.* (2020) A novel Tmem119-tdTomato reporter mouse model for studying microglia in the central nervous system, *Brain, Behavior, and Immunity*. Academic Press, 83, pp. 180–191.

Ruiz-Cantero, M. C. *et al.* (2021) Sigma-1 receptor: A drug target for the modulation of neuroimmune and neuroglial interactions during chronic pain, *Pharmacological Research*. Academic Press.

Ruiz-Medina, J., Baulies, A., Bura, S. A. and Valverde, O. (2013) Paclitaxel-induced neuropathic pain is age dependent and devolves on glial response, *European Journal of Pain*. John Wiley & Sons, Ltd, 17(1), pp. 75–85.

Ruscher, K. *et al.* (2011) The sigma-1 receptor enhances brain plasticity and functional recovery after experimental stroke, *Brain*, 134(3), pp. 732–746.

Ruscher, K. and Wieloch, T. (2015) The involvement of the sigma-1 receptor in neurodegeneration and neurorestoration, *Journal of Pharmacological Sciences*. Elsevier, 127(1), pp. 30–35.

Russo, R. *et al.* (2013) Hemoglobin is present as a canonical α2β2 tetramer in dopaminergic neurons, *Biochimica et Biophysica Acta (BBA) - Proteins and Proteomics*. Elsevier, 1834(9), pp. 1939–1943.

Rymo, S. *et al.* (2011) A two-way communication between microglial cells and angiogenic sprouts regulates angiogenesis in aortic ring cultures, *PloS one*. PLoS One, 6(1).

Saha, D. *et al.* (2014) Hemoglobin Expression in Nonerythroid Cells: Novel or Ubiquitous?, *International Journal of Inflammation*. Hindawi Limited, 2014.

Saher, G. and Stumpf, S. K. (2015) Cholesterol in myelin biogenesis and hypomyelinating disorders, *Biochimica et Biophysica Acta (BBA) - Molecular and Cell Biology of Lipids*. Elsevier, 1851(8), pp. 1083–1094.

Saika, F. *et al.* (2009) Suppressive effect of imipramine on vincristine-induced mechanical allodynia in mice, *Biological and Pharmaceutical Bulletin*, 32(7).

Sałat, K. (2020) Chemotherapy-induced peripheral neuropathy: part 1—current state of knowledge and perspectives for pharmacotherapy, *Pharmacological Reports*. Springer, pp. 486–507.

Salter, M. W. and Stevens, B. (2017) Microglia emerge as central players in brain disease, *Nature Medicine 2017 23:9*. Nature Publishing Group, 23(9), pp. 1018–1027.

Samovilova, N. and Vinogradov, V. (1992) Subcellular distribution of (+)-[3H]SKF 10,047 binding sites in rat liver, *European journal of pharmacology*. Eur J Pharmacol, 225(1), pp. 69–74.

Sánchez-Blázquez, P. *et al.* (2014) The calcium-sensitive Sigma-1 receptor prevents cannabinoids from provoking glutamate NMDA receptor hypofunction: implications in antinociception and psychotic diseases, *The International Journal of Neuropsychopharmacology*. Int J Neuropsychopharmacol, 17(12), pp. 1943–1955.

Sánchez-Fernández, C. *et al.* (2013) Potentiation of morphine-induced mechanical antinociception by σ1 receptor inhibition: Role of peripheral σ1 receptors, *Neuropharmacology*. Neuropharmacology, 70, pp. 348–358.

Sánchez-Fernández, C., Entrena, J. M., Baeyens, J. M. and Cobos, E. J. (2017) Sigma-1 Receptor Antagonists: A New Class of Neuromodulatory Analgesics, *Advances in Experimental Medicine and Biology*. Springer, Cham, 964, pp. 109–132.

Santos-Galindo, M., Acaz-Fonseca, E., Bellini, M. J. and Garcia-Segura, L. M. (2011) Sex differences in the inflammatory response of primary astrocytes to lipopolysaccharide, *Biology of Sex Differences*. BioMed Central, 2(1), p. 7.

Sanz, E. *et al.* (2009) Cell-type-specific isolation of ribosome-associated mRNA from complex tissues, *Proceedings of the National Academy of Sciences of the United States of America*, 106(33), pp. 13939–13944.

Sanz, E. *et al.* (2019) RiboTag: Ribosomal Tagging Strategy to Analyze Cell-Type-Specific mRNA Expression In Vivo, *Current Protocols in Neuroscience*, 88(1), pp. 139–148.

Schafer, D. *et al.* (2012) Microglia sculpt postnatal neural circuits in an activity and complement-dependent manner, *Neuron*. Neuron, 74(4), pp. 691–705.

Schaible, H. G. (2007) Peripheral and central mechanisms of pain generation., *Handbook of experimental pharmacology*. Berlin, Heidelberg: Springer Berlin Heidelberg, 177(177), pp. 3–28.

Schelshorn, D. W. *et al.* (2008) Expression of Hemoglobin in Rodent Neurons:, *http://dx.doi.org/10.1038/jcbfm.2008.152*. SAGE PublicationsSage UK: London, England, 29(3), pp. 585–595.

Schloss, J. M. *et al.* (2017) A randomised, placebo-controlled trial assessing the efficacy of an oral B group vitamin in preventing the development of chemotherapy-induced peripheral neuropathy (CIPN), *Supportive Care in Cancer*, 25(1).

Scholz, J. and Woolf, C. J. (2002) Can we conquer pain?, *Nature Neuroscience*, 5(11s), pp. 1062–1067.

Scholz, J. and Woolf, C. J. (2007) The neuropathic pain triad: Neurons, immune cells and glia, *Nature Neuroscience*.

Scholz, J. *et al.* (2019) The IASP classification of chronic pain for ICD-11: Chronic neuropathic pain, *Pain*. Lippincott Williams and Wilkins, pp. 53–59.

Schütz, S. G. and Robinson-Papp, J. (2013) HIV-related neuropathy: current perspectives., *HIV/AIDS (Auckland, N.Z.)*. Dove Press, 5, pp. 243–51.

Seifert, G., Schilling, K. and Steinhäuser, C. (2006) Astrocyte dysfunction in neurological disorders: a molecular perspective, *Nature reviews. Neuroscience*. Nat Rev Neurosci, 7(3), pp. 194–206.

Seretny, M. *et al.* (2014) Incidence, prevalence, and predictors of chemotherapy-induced peripheral neuropathy: A systematic review and meta-analysis, *Pain*, 155(12), pp. 2461–2470.

Serra Catafau, J. (2007) Tratado de dolor neuropático, *Editorial Médica Panamericana*.

Shen, Y. *et al.* (2015) Exogenous induction of HO-1 alleviates vincristine-induced neuropathic pain by reducing spinal glial activation in mice, *Neurobiology of Disease*. Elsevier Inc., 79, pp. 100–110.

Shephard, F. *et al.* (2014) A mitochondrial location for haemoglobins—Dynamic distribution in ageing and Parkinson's disease, *Mitochondrion*. Elsevier, 14(1), pp. 64–72.

Sheridan, G. and Murphy, K. (2013) Neuron-glia crosstalk in health and disease: fractalkine and CX3CR1 take centre stage, *Open biology*. Open Biol, 3(12).

Shin, S. M. *et al.* (2020) Sigma-1 receptor activity in primary sensory neurons is a critical driver of neuropathic pain, *Gene Therapy 2020*. Nature Publishing Group, pp. 1–15.

Sierra, A. *et al.* (2010) Microglia shape adult hippocampal neurogenesis through apoptosis-coupled phagocytosis, *Cell stem cell*. Cell Stem Cell, 7(4), pp. 483–495.

Siracusa, R., Fusco, R. and Cuzzocrea, S. (2019) Astrocytes: Role and Functions in Brain Pathologies, 10.

Sisignano, M., Baron, R., Scholich, K. and Geisslinger, G. (2014) Mechanism-based treatment for chemotherapy-induced peripheral neuropathic pain, *Nature Reviews Neurology*. Nature Publishing Group, 10(12), pp. 694–707.

Smith, E. M. L. *et al.* (2013) Effect of duloxetine on pain, function, and quality of life among patients with chemotherapy-induced painful peripheral neuropathy: A randomized clinical trial, *JAMA - Journal of the American Medical Association*, 309(13).

Smith, S. B., Crager, S. E. and Mogil, J. S. (2004) Paclitaxel-induced neuropathic hypersensitivity in mice: Responses in 10 inbred mouse strains, in *Life Sciences*.

Sofroniew, M. (2009) Molecular dissection of reactive astrogliosis and glial scar formation, *Trends in neurosciences*. Trends Neurosci, 32(12), pp. 638–647.

Sofroniew, M. and Vinters, H. (2010) Astrocytes: biology and pathology, *Acta Neuropathol.*, 119(1), pp. 7–35.

Sofroniew, M. (2014) Astrogliosis, *Cold Spring Harbor perspectives in biology*. Cold Spring Harb Perspect Biol, 7(2).

Sofroniew, M. V. (2012) Transgenic Techniques for Cell Ablation or Molecular Deletion to Investigate Functions of Astrocytes and Other GFAP-Expressing Cell Types, *Methods in Molecular Biology*. Humana Press, 814, pp. 531–544.

Sorge, R. *et al.* (2011) Spinal cord Toll-like receptor 4 mediates inflammatory and neuropathic hypersensitivity in male but not female mice, *The Journal of neuroscience : the official journal of the Society for Neuroscience*. J Neurosci, 31(43), pp. 15450–15454.

Sorge, R. *et al.* (2012) Genetically determined P2X7 receptor pore formation regulates variability in chronic pain sensitivity, *Nature medicine*. Nat Med, 18(4), pp. 595–599.

Sorge, R. E. *et al.* (2015) Different immune cells mediate mechanical pain hypersensitivity in male and female mice, *Nature Neuroscience*, 18(8), pp. 1081–1083.

Srinivasan, R. *et al.* (2016) New Transgenic Mouse Lines for Selectively Targeting Astrocytes and Studying Calcium Signals in Astrocyte Processes In Situ and In Vivo., *Neuron*, 92(6), pp. 1181–1195.

Starobova, H. and Vetter, I. (2017) Pathophysiology of chemotherapy-induced peripheral neuropathy, *Frontiers in Molecular Neuroscience*, 10(May), pp. 1–21.

Starobova, H. *et al.* (2019) Minocycline Prevents the Development of Mechanical Allodynia in Mouse Models of Vincristine-Induced Peripheral Neuropathy, *Frontiers in Neuroscience*. Frontiers, 0(JUN), p. 653.

Starobova, H. *et al.* (2020) Inflammatory and Neuropathic Gene Expression Signatures of Chemotherapy-Induced Neuropathy Induced by Vincristine, Cisplatin, and Oxaliplatin in C57BL/6J Mice, *The Journal of Pain*. Elsevier Inc., 21(1–2), pp. 182–194.

Steiner, J. *et al.* (2007) Evidence for a wide extra-astrocytic distribution of S100B in human brain, *BMC Neuroscience 2007 8:1*. BioMed Central, 8(1), pp. 1–10.

Stratoulias, V., Venero, J. L., Tremblay, M.-È. and Joseph, B. (2019) Microglial subtypes: diversity within the microglial community, *The EMBO Journal*. John Wiley & Sons, Ltd, 38(17), p. e101997.

Su, T.-P. *et al.* (2010) The sigma-1 receptor chaperone as an inter-organelle signaling modulator, *Trends in Pharmacological Sciences*. Trends Pharmacol Sci, 31(12), pp. 557–566.

Su, T., London, E. and Jaffe, J. (1988) Steroid binding at sigma receptors suggests a link between endocrine, nervous, and immune systems, *Science (New York, N.Y.)*. Science, 240(4849), pp. 219–221.

Su, TP, Su, TC, Nakamura, Y. and Tsai, S. (2016) The Sigma-1 Receptor as a Pluripotent Modulator in Living Systems, *Trends in pharmacological sciences*. Trends Pharmacol Sci, 37(4), pp. 262–278.

Subramanian, A. *et al.* (2005) Gene set enrichment analysis: a knowledge-based approach for interpreting genome-wide expression profiles, *Proceedings of the National Academy of Sciences of the United States of America*. Proc Natl Acad Sci U S A, 102(43), pp. 15545–15550.

Sun, S. *et al.* (2015) Translational profiling identifies a cascade of damage initiated in motor neurons and spreading to glia in mutant SOD1-mediated ALS, *Proceedings of the National Academy of Sciences*. National Academy of Sciences, 112(50), pp. E6993–E7002.

Sung, B., Lim, G. and Mao, J. (2003) Altered expression and uptake activity of spinal glutamate transporters after nerve injury contribute to the pathogenesis of neuropathic pain in rats, *The Journal of neuroscience : the official journal of the Society for Neuroscience*. J Neurosci, 23(7), pp. 2899–2910.

Tabata, H. (2015) Diverse subtypes of astrocytes and their development during corticogenesis, *Frontiers in Neuroscience*. Frontiers, 9(APR), p. 114.

Talbot, K., Madden, V. J., Jones, S. L. and Moseley, G. L. (2019) The sensory and affective components of pain: are they differentially modifiable dimensions or inseparable aspects of a unitary experience? A systematic review, *British Journal of Anaesthesia*. Elsevier Ltd, pp. e263–e272.

Talbot, S. *et al.* (2020) Defining body-weight reduction as a humane endpoint: a critical appraisal, *Laboratory animals*. Lab Anim, 54(1), pp. 99–110.

Tan, L. L. and Kuner, R. (2021) Neocortical circuits in pain and pain relief, *Nature Reviews Neuroscience*. Nat Rev Neurosci.

Taves, S. *et al.* (2016) Spinal inhibition of p38 MAP kinase reduces inflammatory and neuropathic pain in male but not female mice: Sex-dependent microglial signaling in the spinal cord, *Brain, Behavior, and Immunity*. Elsevier Inc., 55, pp. 70–81.

Tay, T. L., Carrier, M. and Tremblay, M. È. (2019) Neuroglia in Neurodegenerative diseases, *Advances in Experimental Medicine and Biology*. Springer New York LLC, 1175, pp. 129–148.

Theodosis, D. T., Poulain, D. A. and Oliet, S. H. R. (2008) Activity-Dependent

Structural and Functional Plasticity of Astrocyte-Neuron Interactions, *Physiological Reviews*. American Physiological Society, 88(3), pp. 983–1008.

Thibault, K. *et al.* (2008) Serotonin 5-HT2A receptor involvement and Fos expression at the spinal level in vincristine-induced neuropathy in the rat, *Pain*, 140(2).

Thibault, K. *et al.* (2012) Cortical effect of oxaliplatin associated with sustained neuropathic pain: Exacerbation of cortical activity and down-regulation of potassium channel expression in somatosensory cortex, *Pain*, 153(8).

Thompson, J. M. and Neugebauer, V. (2019) Cortico-limbic pain mechanisms., *Neuroscience letters*, 702, pp. 15–23.

Toma, W. *et al.* (2017) Effects of paclitaxel on the development of neuropathy and affective behaviors in the mouse, *Neuropharmacology*, 117(1), pp. 305–315.

Torrance, N. *et al.* (2013) Neuropathic pain in the community: more under-treated than refractory?, *Pain*. Elsevier, 154(5), pp. 690–9.

Toyama, S. *et al.* (2014) Characterization of acute and chronic neuropathies induced by oxaliplatin in mice and differential effects of a novel mitochondria-targeted antioxidant on the neuropathies, *Anesthesiology*, 120(2).

Tozaki-Saitoh, H. and Tsuda, M. (2019) Microglia-neuron interactions in the models of neuropathic pain, *Biochemical Pharmacology*. Elsevier, 169(July), p. 113614.

Treede, R.-D. *et al.* (2008) Neuropathic pain: Redefinition and a grading system for clinical and research purposes, *Neurology*, 70(18), pp. 1630–1635.

Treede, R. D. (2018) The International Association for the Study of Pain definition of pain: As valid in 2018 as in 1979, but in need of regularly updated footnotes, *Pain Reports*. Lippincott Williams and Wilkins.

Treede, R. D. *et al.* (2019) Chronic pain as a symptom or a disease: The IASP Classification of Chronic Pain for the International Classification of Diseases (ICD-11), *Pain*. Lippincott Williams and Wilkins, pp. 19–27.

Tremblay, M. *et al.* (2011) The role of microglia in the healthy brain, *The Journal of neuroscience : the official journal of the Society for Neuroscience*. J Neurosci, 31(45), pp. 16064–16069.

Triarico, S. *et al.* (2021) Vincristine-induced peripheral neuropathy (Vipn) in pediatric tumors: Mechanisms, risk factors, strategies of prevention and treatment, *International Journal of Molecular Sciences*, 22(8).

Tsai, H.-H. *et al.* (2012) Regional Astrocyte Allocation Regulates CNS Synaptogenesis and Repair, *Science*. American Association for the Advancement of Science, 337(6092), pp. 358–362.

Tsuda, M. and Inoue, K. (2016) Neuron-microglia interaction by purinergic signaling in neuropathic pain following neurodegeneration, *Neuropharmacology*. Neuropharmacology, 104, pp. 76–81.

Ueno, M. *et al.* (2013) Layer V cortical neurons require microglial support for survival during postnatal development, *Nature neuroscience*. Nat Neurosci, 16(5), pp. 543–551.

Uhelski, M. L., Khasabova, I. A. and Simone, D. A. (2015) Inhibition of anandamide hydrolysis attenuates nociceptor sensitization in a murine model of chemotherapy-induced peripheral neuropathy, *Journal of Neurophysiology*, 113(5).

Ullian, E., Sapperstein, S., Christopherson, K. and Barres, B. (2001) Control of synapse number by glia, *Science (New York, N.Y.)*. Science, 291(5504), pp. 657–661.

Ulmann, L. *et al.* (2008) Up-regulation of P2X4 receptors in spinal microglia after peripheral nerve injury mediates BDNF release and neuropathic pain, *The Journal of neuroscience : the official journal of the Society for Neuroscience*. J Neurosci, 28(44), pp. 11263–11268.

Usoskin, D. *et al.* (2015) Unbiased classification of sensory neuron types by large-scale single-cell RNA sequencing., *Nature neuroscience*, 18(1), pp. 145–53.

Vacca, V. *et al.* (2014) Higher pain perception and lack of recovery from neuropathic pain in females: a behavioural, immunohistochemical, and proteomic investigation on sex-related differences in mice, *Pain*. Pain, 155(2), pp. 388–402.

Velasco, R. and Bruna, J. (2010) Chemotherapy-induced peripheral neuropathy: an unresolved issue, *Neurologia (Barcelona, Spain)*. Neurologia, 25(2), pp. 116–31. Available at: https://pubmed.ncbi.nlm.nih.gov/20487712/ (Accessed: 15 October 2021).

Verkhratsky, A. and Butt, A. (2013) Glial physiology and pathophysiology., *Wiley-Blackwell, Chichester*, p. p 560.

Verkhratsky, A. and Nedergaard, M. (2018) Physiology of Astroglia, *Physiological reviews*. Physiol Rev, 98(1), pp. 239–389.

Virchow, R. (1856) Gesammelte Abhandlungen zyr wissenschaftlischen Medizin. Frankfurt, Germany: Verlag von Meidinger Sohn & Comp, 1856, p. 1024, *Verlag von Meidinger Sohn & Comp*, p. 1024.

Volterra, A. and Meldolesi, J. (2005) Astrocytes, from brain glue to communication elements: the revolution continues, *Nature reviews. Neuroscience*. Nat Rev Neurosci, 6(8), pp. 626–640.

Wake, H. *et al.* (2009) Resting microglia directly monitor the functional state of synapses in vivo and determine the fate of ischemic terminals, *The Journal of neuroscience : the official journal of the Society for Neuroscience*. J Neurosci, 29(13), pp. 3974–3980.

Waller, R. *et al.* (2016) Gene expression profiling of the astrocyte transcriptome in multiple sclerosis normal appearing white matter reveals a neuroprotective role, *Journal of Neuroimmunology*. Elsevier, 299, pp. 139–146.

Wang, J. *et al.* (2011) A Single Subanesthetic Dose of Ketamine Relieves Depression-like Behaviors Induced by Neuropathic Pain in Rats, *Anesthesiology*. The American Society of Anesthesiologists, 115(4), pp. 812–821.

Watkins, L. R. *et al.* (2006) Handbook of Clinical Neurology, in Cervero, F. and Jensen, T. S. B. T.-H. of C. N. (eds) *Cervero, F.; Jensen, TS., editors. Elsevier*. Elsevier, pp. 309–323.

Welle, A. *et al.* (2021) Epigenetic control of region-specific transcriptional programs in mouse cerebellar and cortical astrocytes, *Glia*. John Wiley & Sons, Ltd, 69(9), pp. 2160–2177.

Weng, T.-Y., Tsai, S.-Y. A. and Su, T.-P. (2017) Roles of sigma-1 receptors on mitochondrial functions relevant to neurodegenerative diseases, *Journal of Biomedical Science 2017 24:1*. BioMed Central, 24(1), pp. 1–14.

Westbom, C. *et al.* (2015) Inflammasome Modulation by Chemotherapeutics in Malignant Mesothelioma, *PLOS ONE*. Public Library of Science, 10(12), p. e0145404.

Winchenbach, J. *et al.* (2016) Inducible targeting of CNS astrocytes in Aldh1l1-CreERT2 BAC transgenic mice, *F1000Research*. F1000Res, 5.

Wlodarczyk, A. *et al.* (2017) A novel microglial subset plays a key role in myelinogenesis in developing brain, *The EMBO journal*. EMBO J, 36(22), pp. 3292–3308.

Woolf, C. J. and Mannion, R. J. (1999) Neuropathic pain: Aetiology, symptoms, mechanisms, and management, *Lancet*.

Woolf, C. J. (2011) Central sensitization: Implications for the diagnosis and treatment of pain, *Pain*. NIH Public Access, p. S2.

Xin, W. and Bonci, A. (2018) Functional astrocyte heterogeneity and implications for their role in shaping neurotransmission, *Frontiers in Cellular Neuroscience*. Frontiers Media S.A.

Yam, M. F. *et al.* (2018) General pathways of pain sensation and the major neurotransmitters involved in pain regulation, *International Journal of Molecular Sciences*, 19(8).

Yang, Y. *et al.* (2011) Molecular comparison of GLT1+ and ALDH1L1+ astrocytes in vivo in astroglial reporter mice, *Glia*. John Wiley & Sons, Ltd, 59(2), pp. 200–207.

Yarnitsky, D. (2015) Role of endogenous pain modulation in chronic pain mechanisms and treatment, *Pain*. Lippincott Williams and Wilkins, pp. S24–S31.

Yona, S. *et al.* (2013) Fate mapping reveals origins and dynamics of monocytes and tissue macrophages under homeostasis, *Immunity*. Immunity, 38(1), pp. 79–91.

Yu, G., Wang, L., Han, Y. and He, Q. (2012) clusterProfiler: an R package for comparing biological themes among gene clusters, *Omics : a journal of integrative biology*. OMICS, 16(5), pp. 284–287.

Zajaczkowską, R. *et al.* (2019) Mechanisms of chemotherapy-induced peripheral neuropathy, *International Journal of Molecular Sciences*, 20(6).

Zamanian, J. L. *et al.* (2012) Genomic Analysis of Reactive Astrogliosis, *Journal of Neuroscience*. Society for Neuroscience, 32(18), pp. 6391–6410.

Zamanillo, D., Portillo-Salido, E., Vela, J. and and Romero, L. (2012) Sigma-1 receptor chaperone: Pharmacology and therapeutic prespectives, in Botana, L. and Loza, M. (eds) *Therapeutic Targets: Modulation, Inhibition, and Activation*. John Wiley & Sons, Inc, pp. 225–278.

Zamanillo, D., Romero, L., Merlos, M. and Vela, J. M. (2013) Sigma 1 receptor: A new therapeutic target for pain, *European Journal of Pharmacology*. Eur J Pharmacol, 716(1–3), pp. 78–93.

Zhang, H. and Dougherty, P. M. (2014) Enhanced excitability of primary sensory neurons and altered gene expression of neuronal ion channels in dorsal root ganglion in paclitaxel-induced peripheral neuropathy, *Anesthesiology*, 120(6).

Zhang, H. *et al.* (2016) Dorsal Root Ganglion Infiltration by Macrophages Contributes to Paclitaxel Chemotherapy-Induced Peripheral Neuropathy, *Journal of Pain*. Churchill Livingstone Inc., 17(7), pp. 775–786.

Zhang, Haijun, Yoon, S. Y., Zhang, Hongmei and Dougherty, P. M. (2012) Evidence that spinal astrocytes but not microglia contribute to the pathogenesis of paclitaxel-induced painful neuropathy, *Journal of Pain*. Elsevier, 13(3), pp. 293–303.

Zhang, Y. *et al.* (2014) An RNA-Sequencing Transcriptome and Splicing Database of Glia, Neurons, and Vascular Cells of the Cerebral Cortex, *Journal of Neuroscience*.

Zheng, F. Y., Xiao, W.-H. and Bennett, G. J. (2011) The response of spinal microglia to chemotherapy-evoked painful peripheral neuropathies is distinct from that evoked by traumatic nerve injuries, *Neuroscience*, 176(1), pp. 447–454.

Zheng, H., Xiao, W. H. and Bennett, G. J. (2011) Functional deficits in peripheral nerve mitochondria in rats with paclitaxel- and oxaliplatin-evoked painful peripheral neuropathy, *Experimental Neurology*, 232(2).

Zheng, H., Xiao, W. H. and Bennett, G. J. (2012) Mitotoxicity and bortezomib-induced chronic painful peripheral neuropathy, *Experimental Neurology*, 238(2).

Zhou, L. *et al.* (2018) Levo-corydalmine alleviates vincristine-induced neuropathic pain in mice by inhibiting an NF-kappa B-dependent CXCL1/CXCR2 signaling pathway, *Neuropharmacology*. Elsevier Ltd, 135, pp. 34–47.

Zimmermann, M. (1986) Ethical considerations in relation to pain in animal experimentation, *Acta Physiologica Scandinavica*, 128(SUPPL. 554), pp. 221–233.